ASSESSMENT OF THE CAPABILITIES OF TWO POLAR sPC-SAFT TERMS THROUGH APPLICATION TO MEASURED KETONE-ALKANE PHASE EQUILIBRIA DATA

by

Jamie Theo Cripwell

Thesis presented in partial fulfilment
of the requirements for the Degree

of

MASTER IN ENGINEERING
CHEMICAL ENGINEERING

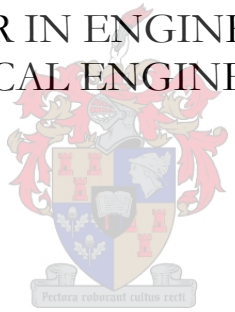

in the Faculty of Engineering
at Stellenbosch University

Supervisor
Prof A.J. Burger

Co-Supervisor
Dr C.E. Schwarz

April 2014

Declaration

By submitting this thesis electronically, I declare that the entirety of the work contained therein is my own, original work, that I am the sole author thereof (save to the extent explicitly otherwise stated), that reproduction and publication thereof by Stellenbosch University will not infringe any third party rights and that I have not previously in its entirety or in part submitted it for obtaining any qualification.

Jamie Theo Cripwell — 21/02/2013

…… ……..

Signature — Date

Abstract

Thermodynamic models have been investigated extensively since Johannes van der Waals first devised a mathematical relation capable of predicting both vapour and liquid phases for a mixture at equilibrium. With the advent of modern computing power, these equations of state have gone from their humble empirical beginnings to the comprehensive and fundamentally derived models we have today. One such physically sound model is the Statistical Associating Fluid Theory (SAFT) family of equations, derived from the molecular perturbation theories of the 1980's. The relative youth of this thermodynamic framework has meant that much work has gone into modification and optimisation of the model recently. The variants of particular interest to this work are the simplified perturbed chain SAFT equations with the Jog & Chapman (sPC-SAFT$_{JC}$) and Gross & Vrabec (sPC-SAFT$_{GV}$) polar terms.

Each of the polar terms supports one adjustable polar parameter that relates to the quantity of polar segments in the reference fluid but not necessarily its position in the carbon chain. The strength of polar interactions is known to decrease as the functional group moves away from the terminal methyl group and the effects of steric hindrance increase. **Thus, in question here is whether the models can account for the change in polar interactions associated with the changing position of the polar group, by only adjusting the values of the existing pure component parameters; that is, in lieu of a position specific parameter.** The carbonyl group in ketone molecules is one such polar group, and it is this homologous series that is the focus of this study.

The decrease in polar interactions as the carbonyl group in a ketone molecule shifts centrally is apparent from the lower boiling points of the isomers where the polar group is central as compared to those where the functional group is nearer the terminal methyl group. The effect of this functional group shift on binary phase behaviour has not previously been assessed for any system however, as the lack of experimental data attests. Thus, experiments had to be conducted to generate phase equilibrium data for systems comprising each structural isomer of a mid-length ketone with a common second component with no functionality. This limitation was imposed to isolate the cause of experimentally observed phenomena to the shifting polar group alone. The generated data could then be appropriately modelled using the polar sPC-SAFT variants and the capabilities of each model, as outlined above, assessed.

To this end, isobaric binary vapour-liquid equilibrium data were measured for 2-, 3- & 4-heptanone with three separate normal alkanes of similar length (n-octane, n-nonane & n-decane) at 40kPa. The apparatus used was a dynamic Gillespie VLE still with temperature and pressure accuracies of 0.03°C and 1.6mbar respectively. Equipment verification was achieved through the reproduction of experimental data for the ethanol/1-butanol system at 1.013bar. The vapour and liquid samples for all nine systems were analysed by gas chromatography with a maximum compositional error of ±0.022 mole fraction. All reported data were found to be thermodynamically consistent using both the L/W and McDermott-Ellis consistency tests.

When paired with a common n-alkane, all three structural heptanone isomers displayed similar qualitative trends in phase behaviour. Minimum boiling azeotropes were measured in all nine systems; in the high alkane region for n-octane systems (~98 mole%), the equal concentration region for n-nonane systems (34 mole% to 53 mole%) and in the very dilute n-alkane region for n-decane systems (~3 mole%). The n-nonane systems in particular highlighted the effect of shifting functional group, with completely separate phase envelopes away from the pure alkane composition space evident in a particularly small temperature range.

Modelling was performed using in-house developed software, with pure component parameters generated for each system using five different regression procedures. The first was traditional fitting of the segment diameter (σ), segment number (m), segment energy (ε/k) and the respective polar parameter (x_p, n_p) to DIPPR correlations of pure component saturated vapour pressure, liquid density and the heat of vaporisation. The latter four procedures included the fixing of the polar parameter according to functional group correlations and the three instances of including the binary VLE data set for each of the three alkanes considered in this work. When applied to the nine binary ketone-alkane systems measured in this work, excellent predictions of the experimental data were in evidence in most cases and only small binary interaction parameters were necessary to correlate the data where pure predictions were poor.

The performance of the parameter sets based on the fixing of the polar parameter and the inclusion of VLE data were consistent and of a high quality for both models, with near identical parameters generated in all four cases for each of the nine systems. The parameter sets generated in this fashion were shown to be applicable not only to the systems measured in this work, but also successfully predicted the independently measured experimental data of the n-hexane/4-heptanone system. It was thus concluded that either of these regression alternatives are viable for the generation of accurate component parameters, and the choice of VLE data set included is trivial.

The pure predictions of the sPC-SAFT$_{GV}$ model were generally better than its sPC-SAFT$_{JC}$ counterpart, particularly in the case of the traditionally regressed parameter sets. sPC-SAFT$_{GV}$ displayed constant qualitative agreement with the experimental data for each of the heptanone isomers with a given n-alkane. The quality of the predictions of sPC-SAFT$_{JC,}$ however, worsened significantly as the polar interactions diminished from 2- to 4-heptanone, with no predictions even possible for the least polar isomer. This was attributed to the different perturbation theories used in the development of these terms, but a more detailed study would be necessary to confirm this.

This work thus shows an apparent inability of the sPC-SAFT$_{JC}$ equation of state to account for the decreasing polar interactions associated with the carbonyl group in a ketone molecule shifting centrally, while sPC-SAFT$_{GV}$ produces qualitatively good fits for all three isomers. These flaws can be overcome through the incorporation of VLE data in the regression procedure if such data is available, or otherwise through the use of group specific correlations for fixing the polar parameter value.

Opsomming

Sedert Johannes van der Waals die eerste wiskundige verhouding ontwikkel het wat beide die damp- en vloeibare fases van 'n mengsel by ewewig kon voorspel, is die veld van termodinamiese modellering al deeglik ondersoek. Na die koms van die moderne rekenaars het hierdie vergelykings van hul nederige empiriese wortels gegroei tot die omvattende, fundamentele modelle wat ons vandag het. Een so 'n fundamenteel gebaseerde familie van vergelykings is die '*Statistical Associating Fluid Theory*' (SAFT) modelle, wat afgelei is vanaf molekulêre versteuringsteorieë, ontwikkel in die 1980s. Hierdie relatiewe jong modelle het in die afgelope ruk aansienlike aanpassing en optimering ondervind. Modelvariante van besondere belang tot hierdie werk, is die vereenvoudigde versteurde ketting of '*simplified perturbed chain*' SAFT vergelykings, met Jog & Chapman (sPC- SAFT$_{JC}$) en Gross & Vrabec (sPC- SAFT$_{GV}$) polêre terme.

In die sPC-SAFT toestandsvergelyking word elkeen van die polêre terme ondersteun deur een polêre veranderlike. Hierdie veranderlike is afhanklik van die aantal polêre segmente in die verwysingsvloeistof, maar nie noodwendig hul posisie in die koolstofketting nie. Daarteen is dit bekend dat die polêre interaksies tussen molekules swakker word soos die polêre groep wegbeweeg van die terminale metielgroep, en steriese hindernis 'n groter rol begin speel. **Dus is die vraag of die model die verandering in die polêre interaksie, as gevolg van veranderende posisie van die polêre groep, kan voorspel deur in plek van 'n posisie afhanklike parameter, slegs 'n aanpassing van die polêre waardes van die suiwer komponente te maak.** Die karbonielgroep in ketoon molekules is een so 'n polêre groep, en 'n homoloë reeks ketone word in hierdie studie ondersoek.

Die afname in die polêre interaksie soos wat die karbonielgroep in 'n ketoon molekule weg skuif vanaf die terminale metiel groep is sigbaar deur die afname in kookpunt van die verskillende isomere. Hierdie effek van die funksionele groepsposisie op binêre fasegedrag is nog nie voorheen vir enige stelsels geëvalueer nie en geen eksperimentele data is vrylik beskikbaar nie. Om hierdie tekortkoming in die literatuur aan te spreek, is eksperimentele fase ewewig data gemeet. 'n Reeks stelsels is ondersoek wat elk bestaan uit 'n struktuurisomeer van 'n mid-lengte ketoon en 'n tweede komponent met geen funksionele bydrae. Eksperimente is so opgestel om die effek van die skuiwende polêre groep op die fasegedrag te isoleer en kwalitatief te ondersoek. Die gegenereerde data is dan gemodelleer met behulp van die polêre sPC- SAFT variante, soos hierbo gespesifiseer, en die vermoëns van elke model is beoordeel.

Isobariese binêre fase ewewig data is by 40kPa gemeet vir damp-vloeistof stelsels bestaande uit 2, 3 & 4 heptanoon, gemeng met drie verskillende normaal alkane van vergelykbare kettinglengte (n-oktaan, n-nonaan & n-dekaan). Die apparaat wat gebruik was is 'n dinamiese Gillespie VLE eenheid met temperatuur- en drukakkuraatheid van 0,03°C en 1.6mbar, onderskeidelik. Die akkuraatheid van die toerusting is bevestig deur eksperimentele data vir 'n etanol/1-butanol stelsel by 1.013bar te reproduseer. Die damp en vloeibare monsters vir al nege stelsels is ontleed deur gaschromatografie met 'n maksimum

komposisionele fout van ± 0,022 (molfraksie). Alle data is as termodinamies konsekwent gevind deur van beide die L/W en McDermott-Ellis konsekwentheidstoetse gebruik te maak.

Mengsels van die drie strukturele isomere van heptanoon met 'n gemene n-alkaan het tydens eksperimente soortgelyke kwalitatiewe tendense in fasegedrag getoon. Gedurende eksperimente is die lae kookpunt asiotrope gemeet vir al nege stelsels. Die asiotrope verskyn in die hoë alkaan konsentrasies (~98 mol%) vir n-oktaan stelsels, medium konsentrasies (34 mol% tot 53 mol%) vir n-nonaan stelsels en baie verdunde konsentrasies (~ 3 mol%) vir n-dekaan stelsels. Die n-nonaan stelsels beeld veral die effek van die verskuiwing van die funksionele groep uit, met diskrete fasegrense wat duidelik apart staan van die suiwer alkaan ruimte, binne 'n klein temperatuurverskil.

Modellering van die stelsels is uitgevoer met behulp van sagteware wat in-huis ontwikkel is. Suiwer komponent data is gegenereer vir elke stelsel deur van vyf verskillende regressie prosedures gebruik te maak. Die eerste is die tradisionele passing van die segment deursnee (σ), segment nommer (m), segment energie (ϵ/k) en die onderskeie polêre parameters (x_p, n_p) op DIPPR korrelasies van die suiwer komponent versadigde dampdruk, vloeistof digtheid en die hitte van verdamping. Die oorblywende vier prosedures sluit in die bepaling van die polêre parameter deur funksionelegroep korrelasies, en drie gevalle waar die binêre VLE data vir elk van die drie alkane ingesluit is. Deur hierdie prosedures op die modellering van die nege binêre ketoon/alkaan stelsels toe te pas, is uitstekende passings van die eksperimentele data verkry met slegs baie klein binêre interaksie parameters nodig waar voorspellings minder akkuraat was.

Die prestasie van die parameter stelle, gebaseer op die bepaling van die polêre parameter en die insluiting van VLE data, is konsekwent en van 'n hoë gehalte vir albei modelle, met 'n byna identiese parameters gegenereer in al vier gevalle vir elk van die nege stelsels. Die parameter stelle wat op hierdie metode gegenereer is, is nie net toepaslik gevind op eksperimentele data gemeet in hierdie werk nie, maar ook op onafhanklike data vir die n-heksaan/4-heptanoon stelsel. Daar is tot die gevolgtrekking gekom dat beide van die regressie alternatiewe lewensvatbaar is vir die generasie van akkurate suiwer komponent parameters, en dat die insluiting van die VLE data triviaal is.

Die suiwer sPC - $SAFT_{GV}$ voorspelling was oor die algemeen beter as die suiwer sPC- $SAFT_{JC}$ model met die voorspelling van data, veral in die geval van passings gedoen met parameters verkry vanaf tradisionele regressie metodes. sPC- $SAFT_{GV}$ het 'n voortdurende, kwalitatiewe ooreenkoms met eksperimentele data getoon vir elk van die nege stelsels. Daarteen het voorspellings deur sPC- $SAFT_{JC}$ beduidend verswak soos die polêre interaksies afgeneem het vanaf 2- na 4- heptanoon, met geen akkurate voorspelling moontlik vir die minste polêre isomeer nie. Die verskynsel kan toegeskryf word aan die verskil in versteuringsteorieë wat gebruik word in die ontwikkeling van die onderskeie toestandsvergelykings, maar 'n meer in-diepte ondersoek is nodig om hierdie teorie te bevestig.

Hierdie werk toon dus 'n skynbare onvermoë van die sPC - $SAFT_{JC}$ toestandsvergelyking om die verandering in polêre interaksie, as gevolg van die veranderende posisie van die polêre groep, vir die karbonielgroep in 'n ketoon te voorspel, terwyl die sPC-$SAFT_{GV}$

toestandsvergelyking goeie kwalitatiewe passings vir al drie isomere bied. Hierdie tekortkominge kan oorkom word deur VLE data, indien beskikbaar, in die regressie prosedure in te sluit, of deur die gebruik van groep spesifieke korrelasies vir die aanpassing van die polêre parameter.

Acknowledgements

This work is based on the research supported in part by the National Research Foundation of South Africa (Grant specific unique reference number (UID) 83966) and Sasol Technology (Pty) Ltd. The authors acknowledge that opinions, findings and conclusions or recommendations expressed in any publication generated by the supported research are that of the authors, and that the sponsors accepts no liability whatsoever in this regard.

The author would like to express his personal thanks to the following people for their contributions, both big and small, to the completion of this work:

- Prof. A.J. Burger, not only for helping bring me to Stellenbosch in the first place, but for all the valuable guidance given so freely.
- Dr C.E. Schwarz for all the insight you gave to the work and helping me look at different aspects from angles I would not have thought to consider. All your time and effort is truly appreciated.
- Dr A.J. de Villiers for always making yourself available for a quick consult and all your work in writing and modifying the software used in this work.
- Mrs. H. Botha and Mrs. L. Simmers for your assistance with the GC and all things analytical.
- Mr Herman Franken for selflessly donating his time to compensate for my poor Afrikaans and help with the writing of the Opsomming.
- My colleagues in Postgrad Office C416 for sharing in my highs and lows and not letting me get too absorbed in the work. Long may the informal coffee breaks and after work beers continue.
- To my parents Jonathan and Lesley who supported me in your own unique ways; dad for being my voice of reason and always willing to listen and mom for loving me unconditionally and reminding me there is always someone thinking of me.
- To my fiancée Rose for embarking on this adventure with me and being at my side each step of the way. We would never have dreamt we'd be here five years ago and I wouldn't change a minute of it.
- Finally, to the Lord who has always watched over me and made my life and work the blessing it is, thank you.

Nomenclature & Abbreviations

Symbol	Description
A	Helmholtz free energy
a	Attractive force parameter
b	Co-volume parameter
D	Parameter in L/W consistency test
D_{ij}	Constants for dispersion term (Equation 2.21)
d	Temperature dependent segment diameter
f	Fugacity
G	Gibbs free energy
$\underline{G}$	Molar Gibbs free energy
g_{ij}	Radial distribution function
H	Enthalpy
$\underline{H}$	Molar Enthalpy
ΔH^{vap}	Heat of vaporisation
k	Boltzmann constant
k_{ij}	Binary interaction parameter for dispersion energy
L	Parameter in L/W consistency test
M_W	Molecular mass
m	Segment number
N	Number of moles
N_{Av}	Avogadro's number
n_p	Number of polar segments
n_μ	Number of dipoles
OF	Objective function
P	Pressure
P^{vap}	Vapour pressure
P^{sat}	Vapour pressure
R	Ideal gas constant
r	Distance between molecules
r^*_{ij}	Reduced radial distance between molecules i & j
ΔS	Parameter in L/W consistency test
ΔS^{vap}	Entropy of vaporisation
T	Temperature
T^{bub}	Mixture bubble temperature
T^{vap}	Boiling temperature
u	Segment potential energy (Lennard-Jones)

Symbol	Description
u(123)	Function of angles and distances between three interacting polar molecules
$\tilde{u}(r)$	Reduced potential function
V	Volume
$\underline{V}$	Molar volume
v^0	Temperature dependent segment volume
v^{00}	Temperature independent segment volume
W	Parameter in L/W consistency test
w	Parameter in L/W consistency test
x	Liquid phase mole fraction
x_p	Fraction of polar segments
y	Vapour phase mole fraction
Z	Compressibility factor
z	Mole fraction in a given mixture
β	B constant from Antoine equation
γ	Activity coefficient
δ	C constant from Antoine equation
ε	Segment potential energy (square well)
ζ_n	Function of molar density and temperature dependent segment diameter (Equation 2.12)
η	Segment packing fraction
θ	Representative and distinct phase
λ	Representative and distinct phase
μ	Dipole moment
$\mu^{\alpha/\beta}$	Chemical potential of component α/β
ξ	Binary interaction parameter for dispersion energy
ρ	Molar density
ρ^{sat}	Saturated liquid density
ρ^*	Polar reduced density
σ	Segment diameter
τ	Packing factor for spherical particles

Superscript	Description
AB	Association sites A & B
assoc	Association contribution
chain	Chain contribution
disp	Dispersion contribution
hs	Hard sphere contribution
L	Liquid phase
polar	Polar contribution
res	Residual property
seg	Segment contribution

Abbreviation	Description
EOS	Equation of State
SAFT	Statistical Associating Fluid Theory
$SAFT_{Ch}$	Statistical Associating Fluid Theory as developed by the research group of Chapman
$SAFT_{HR}$	Statistical Associating Fluid Theory as developed by Huang & Radosz
p-SAFT	Polar Statistical Associating Fluid Theory (SAFT with Jog & Chapman Polar Term)
PC-SAFT	Perturbed Chain Statistical Associating Fluid Theory
sPC-SAFT	Simplified Perturbed Chain Statistical Associating Fluid Theory
$sPC\text{-}SAFT_{GV}$	Simplified Perturbed Chain Statistical Associating Fluid Theory with Gross & Vrabec Polar Term
$sPC\text{-}SAFT_{JC}$	Simplified Perturbed Chain Statistical Associating Fluid Theory with Jog & Chapman Polar Term

Table of Contents

Abstract i

Opsomming iii

Acknowledgements vi

Nomenclature & Abbreviations vii

Table of Contents x

CHAPTER 1 Introduction 1

1.1. Phase Equilibrium and Thermodynamic Models 1

1.1.1. Phase Equilibrium Fundamentals 1

1.1.2. Thermodynamic Models 2

1.1.3. Role of Phase Equilibrium Data 3

1.1.4. State of the Art Thermodynamic Modelling: The SAFT Family of EOSs 3

1.2. Problem Identification 4

1.3. Study Objectives 5

1.4. Thesis Overview 6

CHAPTER 2 Statistical Associating Fluid Theory (SAFT) 7

2.1. Origins of SAFT 7

2.1.1. Chapman's Reference Fluid 8

2.1.2. Chapman's Equation of State 10

2.1.3. Chapman's Model Results 12

2.2. SAFT of Huang and Radosz 12

2.2.1. Huang and Radosz's Reference Fluid 13

2.2.2. Huang and Radosz's Equation of State 14

2.2.3. Huang & Radosz's Model Results 15

2.3. Perturbed Chain SAFT 16

2.3.1. Gross & Sadowski's Reference Fluid 17

2.3.2. Gross & Sadowski's Equation of State 18
2.3.3. Gross & Sadowski's Model Results 20
2.4. Simplified PC-SAFT 20
2.4.1. The First Modification 21
2.4.2. The Second Modification 22
2.4.3. sPC-SAFT Model Results 22
2.5. Polar PC-SAFT 23
2.5.1. Jog and Chapman's Polar Contribution 23
2.5.2. Gross and Vrabec's Polar Contribution 27
2.5.3. Major Shortcoming of Polar Terms 30
2.5.4. Polar sPC-SAFT & Study Highlights 30
2.5.5. Application of Polar SAFT Models to Ketone-n-Alkane Mixtures 31

CHAPTER 3 Low Pressure Phase Equilibria 32
3.1. Low Pressure Phase Behaviour 32
3.2. Existing Ketone-n-Alkane VLE Data 33
3.3. Phase Equilibria Measurement 35
3.3.1. Othmer Dynamic Still 35
3.3.2. Gillespie Dynamic Still 37
3.4. Experimental Rationale 38
3.5. Thermodynamic Consistency 39
3.5.1. McDermott-Ellis Consistency Test 39
3.5.2. L/W Consistency Test 40
3.5.3. Summary of Thermodynamic Consistency 43

CHAPTER 4 Materials & Methods 44
4.1. Materials 44
4.2. Apparatus 44
4.2.1. Unit Description 44

4.2.2. System Modification 46
4.3. Experimental Procedure 46
4.3.1. Preliminaries 46
4.3.2. Still Preparation 47
4.3.3. Experimental Runs 48
4.3.4. Draining and Washing 49
4.3.5. Analysis 49
4.4. Compositional Error Analysis 50
4.4.1. Experimental Effects 50
4.4.2. Analysis Effects 53
4.4.3. Summary 53

CHAPTER 5 Experimental Results 54
5.1. Verification 54
5.2. n-Octane Systems 57
5.2.1. n-Octane/2-Heptanone 59
5.2.2. n-Octane/3-Heptanone 60
5.2.3. n-Octane/4-Heptanone 61
5.3. n-Nonane Systems 62
5.3.1. n-Nonane/2-Heptanone 64
5.3.2. n-Nonane/3-Heptanone 65
5.3.3. n-Nonane/4-Heptanone 66
5.4. n-Decane Systems 67
5.4.1. n-Decane/2-Heptanone 69
5.4.2. n-Decane/3-Heptanone 70
5.4.3. n-Decane/4-Heptanone 71
5.5. Experimental Summary 72

CHAPTER 6 Thermodynamic Modelling Results 73

6.1. Regression Method 73
6.1.1. Regression Obstacles 73
6.1.2. Regression Algorithm 75
6.1.3. Regression Alternatives 76
6.2. Regressed Parameters 77
6.3. VLE Prediction Results 80
6.3.1. n-Octane Systems 84
6.3.2. n-Nonane Systems 91
6.3.3. n-Decane Systems 98
6.3.4. Independent System: n-Hexane – 4-Heptanone 104
6.3.5. Prediction Results Highlights 106

CHAPTER 7 Conclusions & Recommendations 113
7.1. Conclusions 113
7.2. Recommendations 115

References 116

Appendix A Detailed Methodology 123
A.1. Detailed Operating Procedure 123
A.1.1. Preliminaries 124
A.1.2. Experimental Runs 127
A.1.3. Draining & Washing 128
A.2. System Hydraulic Modifications 129
Appendix B Certificates of Calibration 131
Appendix C GC Calibration Curves & Error Analysis Results 135
C.1. GC Calibration Curves 135
C.2. Error Analysis 144
Appendix D Experimental Results 149

Appendix E Thermodynamic Consistency Testing Results 169

Appendix F Thermodynamic Modelling Extensive Results..... 180

Chapter 1 Introduction

Thermodynamic principles are the foundation of industrial processes and define the limit of what is possible. Exhibiting the largest economic investment of any element of a chemical plant, nowhere is the fundamental understanding of thermodynamic properties and interactions more important than in the design of separation units. Distillation has been the primary choice in the refinement of chemical products for the better part of the last century and will remain so until viable alternatives can be implemented on an industrial scale. Until such time however, it is of vital importance to optimise the design of these units and the best place to start is at the beginning.

1.1. Phase Equilibrium and Thermodynamic Models

Phase equilibrium is the underlying thermodynamic principle in most separation processes, with vapour-liquid equilibrium the driving force behind distillation. Thus in order to optimise the design of industrial separation processes, it is important to start with thermodynamic fundamentals; we need a sound understanding of the thermodynamic properties and molecular interactions at the heart of phase equilibria.

1.1.1. Phase Equilibrium Fundamentals

For a mixture of components, the criterion for phase equilibrium is the equality of fugacities for each component in each phase (Sandler, 2006):

$$f_i^L(T,P,\underline{x}) = f_i^V\left(T,P,\underline{y}\right) \tag{1.1}$$

Conceptually, the fugacity of a component within a given phase can be thought of as the tendency of that component to escape that phase. To give a physical meaning to the fugacity of a species, it can be considered as the pressure of an ideal gas exhibiting the same properties of the real fluid at the temperature and composition of interest (Sandler, 2006).

The fugacity is not itself a fundamental fluid property, but rather derived from the chemical potential of the species. Thus the true thermal equilibrium conditions from which Equation 1.1 was derived are the equality of temperature, pressure and chemical potential of each species (i) in each phase (θ,λ):

$$\begin{aligned} T^\theta &= T^\lambda \\ P^\theta &= P^\lambda \\ {\mu_i}^\theta &= {\mu_i}^\lambda \end{aligned} \tag{1.2}$$

The fugacity is calculated from the physical properties and the composition of the system according to Sandler (2006):

$$\ln\frac{f_i}{z_i P} = \frac{1}{RT}\int_{\underline{V}=\infty}^{\underline{V}=\frac{ZRT}{P}}\left[\frac{RT}{\underline{V}} - N\left(\frac{\partial P}{\partial N_i}\right)_{T,V,N_{j\neq i}}\right]d\underline{V} - \ln\frac{P\underline{V}}{RT} \tag{1.3}$$

Here, the latter term represents the ideal gas contribution, or equivalently, the pressure the component of interest would be at if it behaved as an ideal gas. As most substances are not ideal and deviations from ideality exist in many systems, the former term of Equation 1.3 is included to account for these deviations. This integral term represents the departure function and is the means by which non-ideal behaviour, including polar forces and association effects, are accounted for in a real fluid. The description of real fluid behaviour is achieved through the use of equations of state, which embody our fundamental and theoretical understanding of fluid behaviour at a molecular level.

1.1.2. Thermodynamic Models

The partial derivative in Equation 1.3 is determined through the incorporation of an appropriate pressure explicit equation of state, at which point the fugacity of the component may be calculated and equilibrium properties of the fluid mixture may be determined by the equality criterion of Equation 1.1. The first pressure explicit equation of state capable of predicting two phase equilibria was that proposed by Johannes van der Waals (van der Waals, 1873):

$$P = \frac{RT}{\underline{V} - b} - \frac{a}{\underline{V}^2} \tag{1.4}$$

This model has been expanded upon extensively to allow for its applicability to more and more complex systems, with the likes of the Soave-Rieldich-Kwong (SRK) (Soave, 1972) and Peng-Robinson (Peng & Robinson, 1976) equations of state incorporating additional aspects of temperature and volume dependence that still find applicability to some systems today (Wei & Sadus, 2000). These original equations of state were only applicable to non-polar mixtures, but the sheer magnitude of work in the field of equation of state development over the past 50 years has allowed for the incorporation of polar, chain and association effects among others in more and more complicated revisions of the original semi-empirical van der Waals equation.

While such semi-empirical equations have gained a reputation for reliable correlation of phase equilibria data, apparent from their extensive use in the design of industrial equipment, their limited or, in some cases, lack of a theoretical basis has limited the performance of such models to the availability of reliable data against which their constants can be regressed (Cotterman *et al.*, 1986). Furthermore, when one considers the strong non-ideality of many industrially relevant mixtures and the subsequent development of azeotropic and extractive distillation techniques employed to overcome these deviations (Steinhauser & White, 1949), the importance of highly accurate and representative data for the development of equally accurate thermodynamic models becomes evident.

1.1.3. Role of Phase Equilibrium Data

The importance of accurate phase equilibrium data to the success of a thermodynamic model cannot be overstated; without appropriate experimental data to fit model parameters to, thermodynamic models would be nothing more than sheer guesswork. More importantly, phase equilibrium data serve as a rigorous verification of the applicability of a thermodynamic model, the physical reality that the theory strives to imitate and it sets the benchmark for the success or failure of a model.

The measurement of phase equilibrium data has evolved in much the same way that its modelling counterpart has. From the humble beginnings of the pot still for batch experiments, equilibrium stills have advanced to the point where a large amount of data can be generated in a relatively short period of time with a high degree of representation of all phases involved.

1.1.4. State of the Art Thermodynamic Modelling: The SAFT Family of EOSs

The dramatic increase in performance of the personal computer and subsequent development of hydrogen bonding and polar interaction theories have resulted in more comprehensive and fundamentally sound fluid theories and equations of state being produced in recent years. These more comprehensive models have largely been classified into three classes, namely chemical, quasi-chemical and perturbation theories (Economou & Donahue, 1991). The focus of the first two categories was the prediction of solvation and association effects associated with hydrogen bonding molecules, while the latter were developed for the explicit accountability of polar interactions. The focus of this study is the performance of thermodynamic models in systems exhibiting strong polar forces, and so our attention will be focused on the development of thermodynamic models based on perturbation theory.

One such model framework is the Statistical Associating Fluid Theory (SAFT), originally developed from first-order perturbation theory based on the work of Wertheim (Wertheim, 1984a, b, 1986a, and b). The theory considers a reference fluid of spherical segments to which the intermolecular forces of dispersion, association and polar attraction are applied using distinct mathematical functions with a sound theoretical basis.

The SAFT family of equations of state collectively consider the residual Helmoholtz free energy of a system as the sum of contributions based on different intermolecular interactions.

$$A^{res} = A^{seg} + A^{chain} + A^{assoc} + A^{polar} \tag{1.5}$$

These intermolecular interactions are those considered to exist between the segments of the reference fluid of the model, namely:

- the repulsive and dispersive effects of individual segments (A^{seg})
- the effects of chain formation between segments (A^{chain}); and
- the effects of association between segments (A^{assoc})

- polar effects from molecular dipoles and quadrupoles (A^{polar})

The general formalism presented in Equation 1.5 has been elaborated extensively since its inception in the 1980's and extensive reviews of its applicability are available in the literature (Müller & Gubbins, 2001, Economou, 2002). In particular, recent works have allowed for the explicit accountability of polar effects through the addition of an equivalent contribution to the residual Helmoholtz energy (A^{polar}). This model development will be the focus of Chapter 2. In the context of this investigation, it is favourable to define a pressure explicit equation of state in terms of the Helmholtz energy for application of SAFT to phase equilibria. This is made possible using the following thermodynamic identity (Michelsen & Mollerup, 2007):

$$A^{res} = -\int_{\underline{V}=\infty}^{\underline{V}=\frac{ZRT}{P}} \left[P - \frac{RT}{\underline{V}}\right] d\underline{V} \tag{1.6}$$

Employing this relation, and switching the order of differentiation and integration, in the equation for the fugacity (Equation 1.3), allows calculation of f_i in terms of the residual Helmholtz energy according to:

$$\ln \frac{f_i}{z_i P} = \frac{N}{RT}\left(\frac{\partial A^{res}}{\partial N_i}\right)_{T,V,N_{j\neq i}} - \ln \frac{P\underline{V}}{RT} \tag{1.7}$$

This final relation is an important result for the characterisation of phase equilibria in the context of the Statistical Association Fluid Theory.

1.2. Problem Identification

The polar SAFT variants considered in this work account for polarity in similar ways but by means of different perturbation theories, as will be detailed in Chapter 2. Each model considers a polar mixture to be appropriately represented by four adjustable pure component parameters, only one of which represents the polar contribution. In both cases, this polar parameter accounts for the presence of polar segments, but not explicitly for their position within the chain. This is not an important consideration for smaller molecules as only one polar isomer exists for chain lengths smaller than C_4. As the chain length increases however, the number of polar structural isomers possible within a homolgous group (here, ketones) increases and the nature of the polar interactions change; steric hindrance effects are increased and the magnitude of the polar interactions decrease as the polar functional group shifts centrally.

Thus, of interest here is whether the considered polar SAFT models, with their existing parameter sets, can appropriately account for this changing magnitude of polar forces when predicting binary phase behaviour. To test this, the effect of the shifting functional group needs to be isolated; specifically, the models need to be fit to VLE data for a series of polar structural isomers with the same second component, bereft of any functionality. To this end, normal alkanes provide the most suitable partner to the ketone structural isomers. To date, there is very little VLE data for the mid-length ketones with

normal alkanes and no instances of all structural isomers of a given polar molecule with a common second component in the open literature.

1.3. Study Objectives

The general focus of the current investigation is the measurement of the isobaric phase equilibria for the industrially relevant binary mixtures of medium length ketones (C_7) and alkanes (C_8 – C_{10}) and thermodynamic modelling of the equilibria within the framework of the Statistical Associating Fluid Theory.

Particular attention is paid to the effect of the shifting carbonyl group through structural isomerism of the ketone on the binary phase equilibria of each isomer with a common secondary component. To isolate the effects of the changing polar interactions with the functional group shift, the second component in question is chosen as a non-polar normal alkane of similar length, with three such cases considered (n-octane, n-nonane and n-decane). With reference to Table 1.1, the change in phase behaviour in moving from left to right in a column is of interest experimentally, while from a modelling point of view, consistency in qualitative trend and ability of the thermodynamic models to accurately correlate each row in a given column are the focus.

Table 1.1: Molecular representation of binary VLE systems considered in this work. 3 dimensional molecular representations drawn using ACD ChemSketch Freeware.

	2-Heptanone 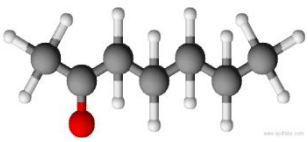	**3-Heptanone** 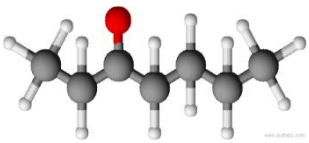	**4-Heptanone** 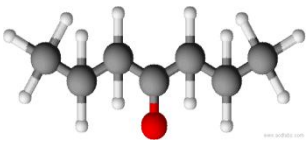
n-Octane 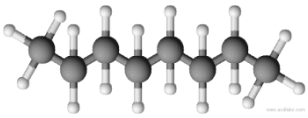	n-Octane/2-Heptanone	n-Octane/3-Heptanone	n-Octane/4-Heptanone
n-Nonane 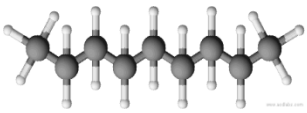	n-Nonane/2-Heptanone	n-Nonane/3-Heptanone	n-Nonane/4-Heptanone
n-Decane 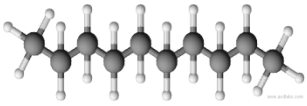	n-Decane/2-Heptanone	n-Decane/3-Heptanone	n-Decane/4-Heptanone

The equations of state of interest in this work are the two polar variants of the Simplified Perturbed Chain Statistical Associating Fluid Theory (sPC-SAFT) based on the works of Jog & Chapman ($sPC\text{-}SAFT_{JC}$) and that of Gross & Vrabec ($sPC\text{-}SAFT_{GV}$). Both thermodynamic models are fit to

experimental data and the quality of the predictions of each model assessed. The decreasing polar interactions as a result of increased steric hindrance expected in the experimental data is not explicitly accounted for by either model, thus, in particular, the ability of each model to deal with the effect of the shifting functional group is assessed.

Thus, to summarise, the objectives of this work are:

(i.) To produce isobaric vapour-liquid equilibrium data for the nine binary systems comprising one structural isomer of heptanone with one n-alkane from n-octane, n-nonane and n-decane, with particular attention paid to any and all azeotropic conditions arising in these systems.

(ii.) To generate pure component parameters for all components considered and assess their applicability with respect to their correlation of pure component properties.

(iii.) To model the experimentally measured phase equilibria for all nine systems for both polar sPC-SAFT variants, by means of pure predictions if possible, or by correlation if not.

(iv.) To assess the ability of both sPC-SAFT$_{JC}$ and sPC-SAFT$_{GV}$ to successfully model the changes in phase behaviour associated with the shifting carbonyl group and identify any bias in either model towards the successful prediction of VLE in one column of Table 1.1 over the other two.

(v.) To assess the impact of different regression procedures on the resulting parameter sets and the performance of these different parameter sets for a given model.

1.4. Thesis Overview

A detailed literature study of the development of the SAFT family of EOSs is provided in Chapter 2. The fundamentals of low pressure phase equilibrium are discussed in Chapter 3, including how phase equilibrium data is measured and how the conformance of measured data to thermodynamic principles can be tested. Chemically similar systems, independently measured and available in the open literature are presented and, subsequently, the experimental rationale is defined. Chapter 4 details the materials, methods and apparatus used in the experimental phase of the Masters study. Verification of the experimental setup is provided in Chapter 5, followed by the VLE data measured for the nine combinations of n-octane, n-nonane and n-decane with 2-, 3- & 4-heptanone. Chapter 6 addresses the modelling aspects of the work, with challenges in the regression procedure highlighted and means of navigating them provided. The regressed parameters for each model and the various regression procedures for each component are provided, before these parameter sets are used for the prediction of the phase behaviour observed experimentally. The performance of both polar sPC-SAFT models and highlights of the study are discussed at the end of Chapter 6 before the work is summarised with conclusions drawn and recommendations made in Chapter 7.

Chapter 2 Statistical Associating Fluid Theory (SAFT)

Many equations of state that find extensive use in industry today can have their origins traced back to the original van der Waals equation (Equation 1.4.). While the modifications incorporated to distinguish these EOS's have resulted in successful application to a variety of systems, the family of equations derived from the original van der Waals equation will always be limited by the nature of the spherical molecule reference fluid (Wei & Sadus, 2000).

Such a representation, by its very nature, cannot account for the non-spherical nature of many industrially relevant compounds. The obvious shortcoming of such a reference fluid, from Figure 2.1, is the overestimation of molecular volumes which influence the degree of repulsive and dispersive interactions between such molecules. Furthermore, such a reference fluid cannot account for major sources of nonideal behaviour including the effects of association and strong polar interaction. As has been mentioned previously, the improvement of computer processing power and the advances made in the fields of statistical mechanics and molecular fluid theory have resulted in a number of more fundamentally sound equations of state being developed, able to account for such effects. One such equation of state, and the focus of this investigation, is the Statistical Associating Fluid Theory.

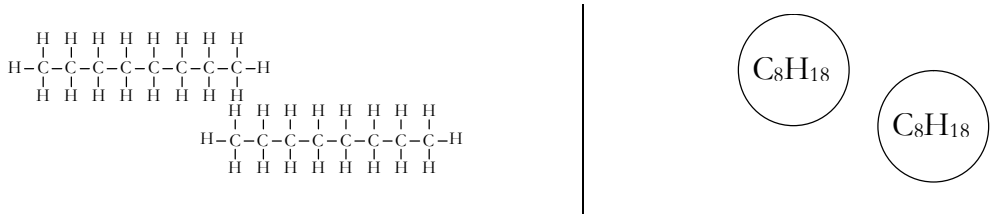

Figure 2.1: Representation of two n-octane molecules using the hard sphere reference fluid of van der Waals type EOS's

The development of the SAFT framework is presented and discussed to the point of its use in this work, namely the polar variants of the simplified Perturbed Chain SAFT (sPC-SAFT), in the sections that follow.

2.1. Origins of SAFT

The Statistical Associating Fluid Theory, or SAFT, has its origins in the molecular theory of associating fluids, particularly the statistical mechanical perturbation theories developed in the 1970's and 1980's. These theories provide a fundamental understanding of the relationship between molecular interactions and the bulk fluid behaviour and, as such, result in models with greater predictive capacity.

The original SAFT model, here termed $SAFT_{Ch}$, was developed by the research group of Chapman in two separate papers (Chapman *et al.*, 1989, 1990), and makes use of the perturbation theories published by Wertheim in a series of papers between 1984 and 1986 (Wertheim, 1984a,b, 1986a,b). In

Wertheim's works, a simplified expression for the residual Helmholtz energy of a mixture was derived as a series of integrals in the molecular distribution functions and association potential. The residual Helmholtz energy is an ideal starting point for the derivation of molecular based equations of state due to the fact that the expressions necessary for phase equilibria calculations (i.e. P and μ) are easily determinable by appropriate differentiation (von Solms *et al.*, 2003). Chapman *et al.,* (1990) made use of Wertheim's first-order perturbation theory to produce an equation of state model for associating fluids.

2.1.1. Chapman's Reference Fluid

As with EOS's based on the original van der Waals equation, a reference fluid is used to model real fluid behaviour in the proposed model. Unlike the simple hard-sphere reference fluid used in these van der Waals type EOS's however, Chapman *et al.* (1989, 1990) used a reference fluid incorporating both the chain length (or molecular shape) and molecular association. In this way, the major effects of both non-spherical shape and molecular association, previously unaccounted for by the van der Waals EOSs, are fundamentally incorporated into a new, more predictive, thermodynamic model.

The reference fluid is given to comprise a mixture of spheres with a Lennard-Jones potential of magnitude ε, characterised by a segment diameter, σ. Onto these spheres, Chapman and co-workers imposed two types of bonds; namely covalent-like bonds for chain formation and association bonds to account for intermolecular attraction (Chapman *et al.*, 1990). Each such chain is formed from a fluid of m spheres or segments, characterising its chain length. These are the three pure component parameters necessary for the modelling of non-associating pure fluid, detailed in Figure 2.2.

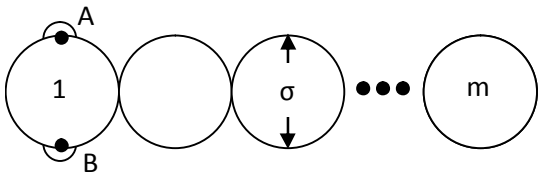

Figure 2.2: Model of chain molecule comprising m segments of characteristic diameter σ, with two association sites A and B. Figure redrawn and adapted from (Chapman et al., 1990)

Extension to non-associating mixtures of Lennard-Jones spheres is achieved using van der Waals one-fluid theory, where the parameters of a hypothetical pure fluid f with the same residual properties as the real fluid of interest are derived (Chapman *et al.*, 1990). These hypothetical properties are found according to Equations 2.1 and 2.2, using the mixing rules of Equations 2.3 and 2.4:

$$\sigma_f{}^3 = \frac{\sum_i \sum_j x_i x_j m_i m_j \sigma_{ij}{}^3}{(\sum_i x_i m_i)^2} \tag{2.1}$$

$$\epsilon_f \sigma_f{}^3 = \frac{\sum_i \sum_j x_i x_j m_i m_j \sigma_{ij}{}^3 \epsilon_{ij}}{(\sum_i x_i m_i)^2} \tag{2.2}$$

$$\epsilon_{ij} = \xi_{ij} \left(\epsilon_{ii} \epsilon_{jj}\right)^{1/2} \tag{2.3}$$

$$\sigma_{ij} = \frac{(\sigma_{ii} + \sigma_{jj})}{2} \tag{2.4}$$

Sites for potential association on a given spherical molecule or segment within a chain are labelled as shown in Figure 2.2, with a number of restrictions applied to the association mechanism by the nature of the first order perturbation theory used (Chapman *et al.*, 1990). Firstly, association between two sites is only possible when both the distance between molecules and their orientation is favourable, with the degree of association characterised by the bond strength, ε^{AB}. Second, the activity of one association site is independent of bonding at any other site on the same molecule. Also, associated molecules in the reference fluid are allowed to form branched or chain-like clusters but may not form rings and the association strength is independent of this orientation. Finally, three approximations on steric hindrance are imposed (Wertheim, 1984a, b):

i. If two molecules are close enough such that site *A* on molecule *i* associates with site *B* on molecule *j*, the repulsive cores of these molecules prevent any third molecule *k* from getting close enough to form association bonds at either *A* or *B*
ii. Single sites cannot form multiple bonds
iii. Two molecules cannot share more than one bond

The abovementioned mechanisms, disallowed by Wertheim's steric hindrance postulates, are illustrated in Figure 2.3.

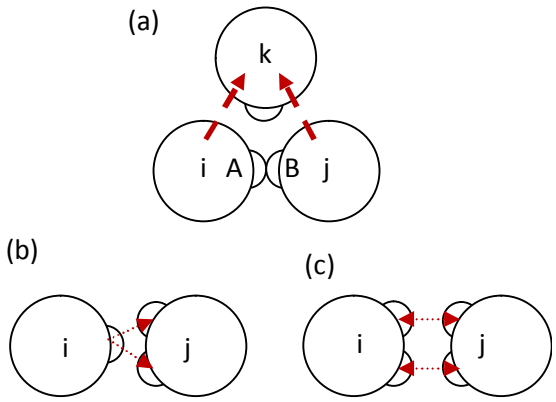

Figure 2.3: Steric hindrance approximations; (a) Repulsion of cores prevent multiple molecules bonding at one site. (b) One site cannot form multiple bonds. (c) No double bonds may exist. Figure redrawn and adapted from (Chapman et al., 1990)

The bond strength is quantified using a square-well potential and defined using two pure component parameters; namely the association energy, ε^{AB}, and the association volume, κ^{AB}. The former is a measure of the depth of the square well while the latter can be related to its width, r^{AB}, as represented in Figure 2.4.

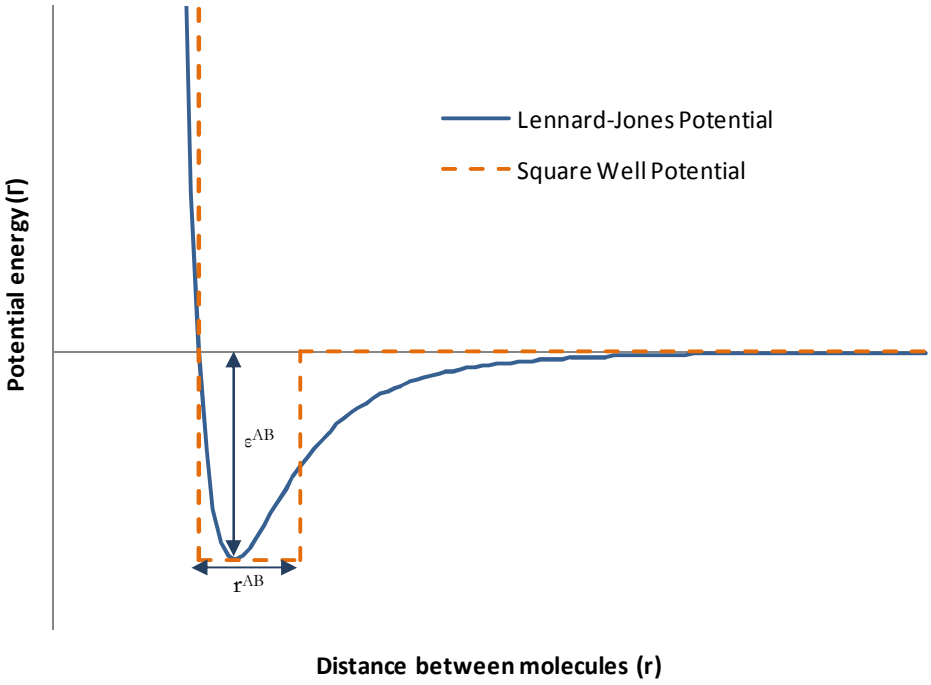

Figure 2.4: Representative plots of both Lennard-Jones (for reference fluid segments) and Square-Well (for association bond strength) potentials

With the reference fluid well defined, the temperature independent parameters necessary for the description of a pure fluid or mixture, comprising either associating or non-associating components may be summarised: for pure, non-associating components one needs the segment diameter (σ), Lennard-Jones interaction energy (ε/k) and the number of segments in the chain (m). Association effects are incorporated by specifying two further parameters; namely the association energy (ε^{AB}) and volume (κ^{AB}). The pure component parameters are traditionally fit to pure component vapour pressure and liquid density data, while the association parameters are fit to bulk phase equilibria (Chapman *et al.*, 1990). The specification of the necessary model parameters necessitates definition of the structure of the equation of state itself.

2.1.2. Chapman's Equation of State

As previously mentioned, the SAFT EOS is defined in terms of the residual Helmholtz energy as per Equation 2.5 (Economou, 2002, Chapman *et al.*, 1990):

$$A^{res} = A^{seg} + A^{chain} + A^{assoc} \tag{2.5}$$

The A^{seg} term accounts for the inter-segment interactions, the A^{chain} term accounts for covalent bonding between the fluid segments while the final A^{assoc} term accounts for association and hydrogen bonding effects. In the absence of hydrogen bonding, that is, for non-asscoiating systems, the association term is equal to zero. Because the work performed here considers polar, non-associating systems, the presence of the last term in each model is acknowledged but its subsequent development is ignored in this work.

Segment Term

The segment term accounts for the contribution to the residual Helmholtz energy of those segments which do not associate. These segments were considered by Chapman *et al.* as hard spheres interacting with a Lennard-Jones potential and was further divided into the contribution of the hard spheres and the dispersive effects. The hard sphere term (Equation 2.7) used was that proposed by Carnahan and Starling (1969) as a function of the segment packing fraction (Equation 2.8) and is applicable to both pure fluids and mixtures. This reduced density may be extended to mixtures using van der Waals one-fluid theory mixing rules, replacing the segment number by the summation term in Equation 2.13. The segment diameter (d) in Equation 2.8 is the temperature dependent diameter, a generic function of the pure component parameters σ, ε/k and m (Chapman *et al.*, 1989).

$$A_0{}^{seg} = A_0{}^{hs} + A_0{}^{disp} \tag{2.6}$$

$$\frac{A_0{}^{hs}}{RT} = \frac{4\eta - 3\eta^2}{(1-\eta)^2} \tag{2.7}$$

$$\eta = \frac{\pi N_{Av}}{6}\rho d^3 m \tag{2.8}$$

The dispersion contribution is determined from molecular simulation data for the reference fluid considered (here, Lennard-Jones spheres) and thus a number of expressions are possible, with Chapman and co-workers making use of the empirical correlation determined by Cotterman *et al.,* (1986).

Chain Term

The contribution of covalent bond formation to a^{res} is given in Equation 2.9 (Chapman *et al.*, 1990) and was developed by considering segments with infinitely small bonding sites with bonds of infinite strength:

$$\frac{A^{chain}}{RT} = \sum_i x_i(1-m_i)\ln\left(g_{ii}(d_{ii})^{hs}\right) \tag{2.9}$$

In Equation 2.9, g_{ii} is the segment radial distribution function, here evaluated at the point of tangential contact of identical segments. It is approximated as the radial distribution function for mixtures proposed by Reed and Gubbins (1973) for hard spheres; this in keeping with approximating the reference fluid segments as hard spheres. The derived expression is given for generic mixtures in Equation 2.10 and for mixtures of like spheres, as required in Equation 2.9, in Equation 2.11.

$$g_{ij}(d_{ij})^{seg} \approx g_{ij}(d_{ij})^{hs} = \frac{1}{1-\zeta_3} + \frac{3d_{ii}d_{jj}}{d_{ii}+d_{jj}}\frac{\zeta_2}{(1-\zeta_3)^2} + 2\left[\frac{d_{ii}d_{jj}}{d_{ii}+d_{jj}}\right]^2 \frac{{\zeta_2}^2}{(1-\zeta_3)^3} \tag{2.10}$$

$$g_{ii}(d_{ii})^{seg} \approx g_{ii}(d_{ii})^{hs} = \frac{1}{1-\zeta_3} + \frac{3d_{ii}}{2}\frac{\zeta_2}{(1-\zeta_3)^2} + 2\left[\frac{d_{ii}}{2}\right]^2 \frac{{\zeta_2}^2}{(1-\zeta_3)^3} \tag{2.11}$$

Here, the d_{ij} term is simply the arithmetic mean of the temperature dependent diameter of each component, and the parameter ζ_n is a function of the molecular molar density and the temperature dependent molecular diameter according to:

$$\zeta_{n=0,1,2,3} = \frac{\pi N_{Av}}{6}\rho \sum_i x_i m_i {d_{ii}}^n \tag{2.12}$$

It is noted that this parameter reduces to the segment packing fraction (Equation 2.8) for $n = 3$.

2.1.3. Chapman's Model Results

The proposed model was fitted to reliable molecular simulation data of independent parties and found to be in excellent agreement for both associating and non-associating, single-site and two-site pure fluids and mixtures, in terms of both compressibility factors and excess enthalpies. The model was further fitted to alkanes up to C_8 and benzene as well as two self-associating compounds (methanol and acetic acid). The segment number was approximated to be equal to the carbon number while the segment diameters and interaction energies, as well as association energies and volumes for the associating compounds, were regressed from vapour pressure and liquid density data. These models were then used to predict pure component vapour pressure data and good agreement with independently determined data was in evidence.

2.2. SAFT of Huang and Radosz

The SAFT model developed by Chapman and co-workers was later modified by Huang and Radosz in two separate papers; first to pure components (Huang & Radosz, 1990) and later extended to mixtures (Huang & Radosz, 1991). The core of the model was kept intact with a number of changes made to the reference fluid, association mechanisms as well as contributions to the EOS itself. They went further to derive pure component parameters of over 100 real fluids and showed that these parameters could be derived for other hydrocarbon molecules based only on molecular structure and molar mass. The model derived by Huang and Radosz is referred to here as $SAFT_{HR}$ as distinct from $SAFT_{Ch}$ discussed previously.

2.2.1. Huang and Radosz's Reference Fluid

Like Chapman and co-workers, Huang and Radosz considered a reference fluid of spherical segments on which covalent, chain forming bonds and site specific association bonds were imposed. The primary difference however was that the segments in the new reference fluid interacted with a square-well potential rather than the Lennard-Jones potential used by Chapman *et al.* (Huang & Radosz, 1990). Thus, while the magnitude of square-well segment-segment interactions may be considered similar or indeed the same as that for Lennard-Jones interactions, they are based on different potential functions. As such, Huang and Radosz redefined their segment energy (u_0/k) to represent the well depth, although their parameter is interchangeable with that of Chapman *et al.*:

$$\frac{u^o}{k}(square-well\ seg\ potential) \approx \frac{\epsilon}{k}(L-J\ seg\ potential) \tag{2.13}$$

Further, where Chapman and co-workers considered the segment diameter as a pure component parameter, Huang and Radosz considered a characteristic segment volume to be more representative. This volume could be determined by manipulating the segment packing fraction equation (Equation 2.8) to yield the temperature dependent segment volume:

$$v^o = \frac{\pi N_{Av}}{6\tau} d^3 \tag{2.14}$$

The corresponding temperature independent segment volume is the second pure component parameter in $SAFT_{HR}$ and is similarly defined in terms of the temperature independent segment diameter:

$$v^{oo} = \frac{\pi N_{Av}}{6\tau} \sigma^3 \tag{2.15}$$

Huang and Radosz defined the temperature dependence of both the segment diameter and the segment volume on expressions derived by Chen and Kreglewski (1977), who solved the Barker Henderson integral equation (Barker & Henderson, 1967) for the segment diameter considering a square-well fluid. These temperature dependencies are given in Equations 2.16 and 2.17, where the aforementioned square-well potential parameter is in evidence:

$$d = \sigma\left[1 - 0.12exp\left(\frac{-3u^o}{kT}\right)\right] \tag{2.16}$$

$$v^o = v^{oo}\left[1 - 0.12exp\left(\frac{-3u^o}{kT}\right)\right]^3 \tag{2.17}$$

Finally, the altered dispersion contribution to the residual Helmholtz energy (discussed in Section 2.2.2) requires description of the temperature dependence of square-well potential:

$$u = u^o\left[1 + \frac{e}{kT}\right] \tag{2.18}$$

Here, the parameter ϵ/k is a component specific constant related to the critical temperature and acentric factor (Chen & Kreglewski, 1977). Huang and Radosz chose to set this parameter constant at a value of 10 considering its applicability was to segments rather than molecules.

2.2.2. Huang and Radosz's Equation of State

Like $SAFT_{Ch}$, $SAFT_{HR}$ is presented in terms of contributions to the residual Helmholtz energy accounting for hard sphere interactions, dispersion interactions, chain formation and association. Where some of the original terms were maintained, others were altered and these differences arehighlighted below.

Segment Term

As before, the segment contribution to a^{res} is divided into a hard sphere contribution and a mean field term. The former, for pure components, is that proposed by Carnahan and Starling (1969) as given in Equation 2.7. The equation was extended to mixtures (Huang & Radosz, 1991), where $SAFT_{HR}$ employs the hard sphere term derived from the work of Mansoori and co-workers for mixtures of hard spheres(Mansoori *et al.*, 1971) given by Equation 2.19:

$$\frac{A^{hs}}{RT} = \frac{6}{\pi\rho}\left[\frac{\zeta_2{}^3 + 3\zeta_1\zeta_2\zeta_3 - 3\zeta_1\zeta_2\zeta_3{}^2}{\zeta_3(1-\zeta_3)^2} - \left(\zeta_0 - \frac{\zeta_2{}^3}{\zeta_3{}^2}\right)\ln(1-\zeta_3)\right] \tag{2.19}$$

where ζ_n is the same parameter used by Chapman *et al.* (1990) in Equation 2.12. For pure components, Equation 2.19 reduces to the form given below, where a_o^{hs} is the Carnahan-Starling (Carnahan & Starling, 1969) hard sphere term as required.

$$\frac{A^{hs}}{RT} = m\frac{A_0{}^{hs}}{RT} \tag{2.20}$$

For pure components (Huang & Radosz, 1990), the dispersion term is in the form of a power series, derived by Alder and co-workers (Alder *et al.*, 1972) from molecular dynamics data for a square-well fluid, with this a_0^{disp} term given in Equation 2.21:

$$\frac{A_0{}^{disp}}{RT} = \sum_i \sum_j D_{ij}\left(\frac{u}{kT}\right)^i \left(\frac{\eta}{\tau}\right)^j \tag{2.21}$$

Here, the D_{ij} terms are universal constants, fitted to independent, reliable PVT, internal energy and second virial coefficient data for argon (Chen & Kreglewski, 1977). It is this dispersion term that distinguishes $SAFT_{HR}$ from $SAFT_{Ch}$, discerning the Lennard-Jones empirical mean-field contribution from its square-well counterpart in Equation 2.21 above. A limitation of the use of this dispersion contribution however is its inability to account for the nonspherical shape of molecules (Gross & Sadowski, 2001). Extension to mixtures is once again achieved by employing van der Waals mixing rules, with the only binary interaction parameter employed by the model found in the mixing rule for the dispersion energy.

Chain Term

The chain terms employed in $SAFT_{HR}$ for both pure components (Huang & Radosz, 1990) and for mixtures (Huang & Radosz, 1991) are identical to those employed by $SAFT_{Ch}$. For a pure fluid of hard spheres, use is made of the Carnahan-Starling approximation (Carnahan & Starling, 1969) as per Equations 2.9, while for mixtures, the pair correlation function for segment mixtures (Equations 2.10 and 2.11) are used.

2.2.3. Huang & Radosz's Model Results

Huang and Radosz regressed their model against vapour pressure and saturated liquid density data for over 100 real fluids, ranging from normal alkanes to polynuclear aromatic compounds and strongly associating compounds (Huang & Radosz, 1990) and over sixty binary mixtures of the aforementioned molecules (Huang & Radosz, 1991). Excellent agreement was found between the data and the model predictions, with deviations well within the range considered acceptable for a three-parameter EOS.

An important difference between the parameter fitting here and that for $SAFT_{Ch}$ is that, in $SAFT_{HR}$, all three pure component parameters were fitted (Huang & Radosz, 1990), where Chapman and co-workers approximated the number of segments as being equal to the carbon number in the chain (Chapman *et al.*, 1989). This is an important observation as the segment number was found to be systematically smaller than the carbon number by Huang and Radosz, for n-alkanes larger than methane, with $m = 1$ in this case. This shows that the approximation of long chain alkanes as tangentially connected spherical segments proposed by $SAFT_{Ch}$ is unrealistic, with a chain of overlapping spherical segments appearing to be a more accurate representation. A similar trend was found for $m < C_i$ in other homologous series of organic compounds.

Using the pure component parameters fit to the real fluid data, Huang and Radosz found that the parameters for pure component, non-associating fluids were well behaved functions of the molecular mass for molecules in the same homologous series (Huang & Radosz, 1990). While initially proposed to allow for the determination of model parameters for polymer fluids, where limited or no vapour pressure or liquid density data is available for use in parameter regression, these functions may similarly be used as a first approximation for parameters of components in a homologous series for which parameters have not been determined.

Finally, the VLE for a number of binary mixtures was well correlated using the derived equation of state, both in terms of qualitative fit to the experimental data and necessitating only small (generally <0.05) binary interaction parameters (Huang & Radosz, 1991). Such successful model fits were easily comparable to existing empirical and activity coefficient models, highlighted by the incorporation of some SAFT terms into existing models and EOS's such as UNIQUAC and cubic equations (Müller & Gubbins, 2001).

The SAFT formalism of Huang and Radosz is widely considered the original or founding contribution to subsequent developments of the EOS (Economou, 2002) and was, industrially, the most extensively adopted form (Gross & Sadowski, 2001) for the better part of a decade before the next significant contribution to the EOS was made.

2.3. Perturbed Chain SAFT

While a number of modifications to $SAFT_{HR}$ were made over the following 10 years (a comprehensive review of these modifications is given by Müller and Gubbins (Müller & Gubbins, 2001)) the next significant contribution to the development of the model was that of Joachim Gross and Gabriele Sadowski in a series of papers between 2000 and 2002 (Gross & Sadowski, 2000, 2001, 2002). The fundamental difference between this form and those that came before was the formation of a chain reference from spherical segments, and then the application of dispersion forces to the resulting chains. This differs from previous versions where the dispersion forces were applied to the spherical fluid segments, followed by chain formation as represented in Figure 2.5. The use of this hard chain reference fluid lead to the modification being referred to as the perturbed-chain SAFT model or, more generally and from this point forth, PC-SAFT.

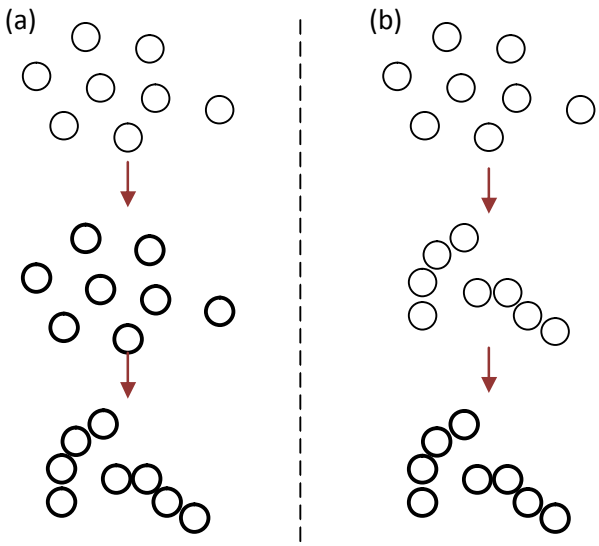

Figure 2.5: Reference fluid formulation in (a) SAFT$_{Ch}$ & SAFT$_{HR}$ and (b) PC-SAFT. Thicker borders represent application of dispersion forces

2.3.1. Gross & Sadowski's Reference Fluid

In the first of their works, Gross and Sadowski developed a fluid theory for chain molecules, different from the hard spheres fluids considered by Chapman *et al.* and Huang and Radosz. This was achieved by applying the second order perturbation theory of Barker and Henderson (Barker & Henderson, 1967a, b) to a hard chain reference fluid. The molecules considered by Gross and Sadowski were hard chains composed of approximately spherical segments that interact with a modified square well potential (Chen & Kreglewski, 1977) detailed in Equation 2.22 and graphically presented in Figure 2.6. This modified potential is used to account for the soft repulsion effects exhibited by real fluids at radial distances smaller than the segment diameter (Gross & Sadowski, 2001).

$$u(r) = \begin{cases} \infty & r < (\sigma - s_1) \\ 3\epsilon & (\sigma - s_1) \leq r < \sigma \\ -\epsilon & \sigma \leq r < \lambda\sigma \\ 0 & r \geq \lambda\sigma \end{cases} \tag{2.22}$$

The use of such a reference fluid gives rise to the specification of three pure component parameters for non-associating molecules identical to those used in SAFT$_{Ch}$ and SAFT$_{HR}$, namely the temperature independent segment diameter (σ), the square-well potential depth, or interaction energy, (ϵ/k) and the segment number (m).

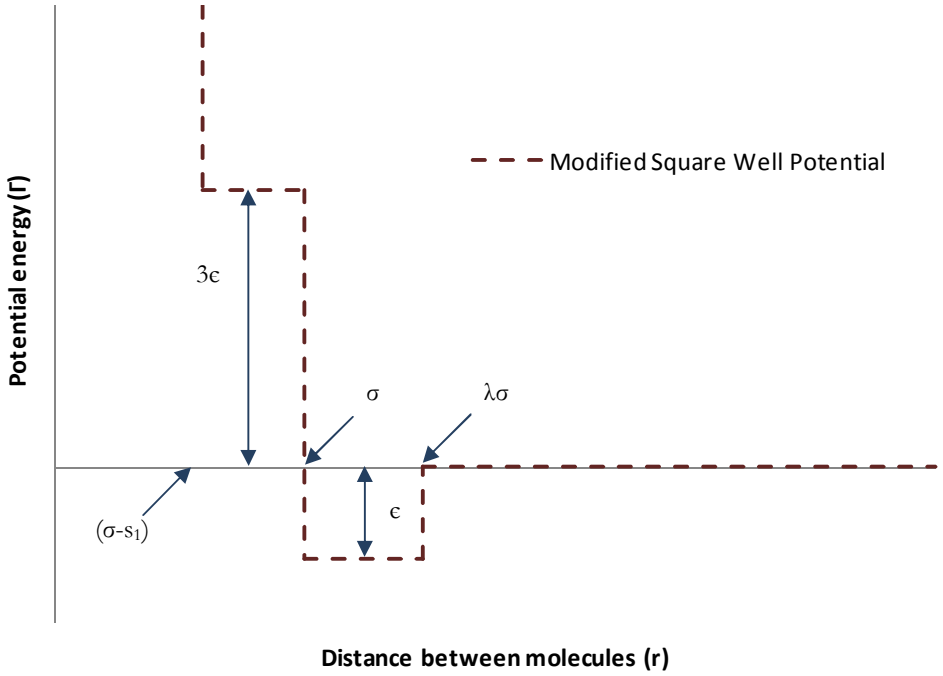

Figure 2.6: Modified square-well potential used for interaction of hard sphere chains. Figure adapted from that presented in (Chen & Kreglewski, 1977)

In keeping with the postulates of Barker and Henderson's perturbation theory, the effective collision diameter of the chain segments exhibiting soft repulsion may be calculated from the following integral (Gross & Sadowski, 2001):

$$d(T) = \int_0^{\sigma} \left[1 - exp\left(-\frac{u(r)}{kT}\right)\right] dr \tag{2.23}$$

Which, for the modified square-well potential defined in Equation 2.22, may be integrated to yield the temperature dependent segment diameter given by Equation 2.16 with a simple nomenclature change:

$$d_i(T) = \sigma_i \left[1 - 0.12exp\left(-\frac{3\epsilon_i}{kT}\right)\right] \tag{2.16a}$$

The equality of Equations 2.16 and 2.16a show that $SAFT_{HR}$ and PC-SAFT can be seen to have identical reference fluids (Gross & Sadowski, 2001).

2.3.2. Gross & Sadowski's Equation of State

Where $SAFT_{Ch}$ and $SAFT_{HR}$ are presented as residual Helmholtz energy expansions, Gross and Sadowski present PC-SAFT in terms of compressibility factors, comprising ideal, hard chain and dispersion contributions:

$$Z = 1 + Z^{hc} + Z^{disp} \tag{2.24}$$

To account for this change in model presentation, the reference fluid equation of state developed by Chapman and co-workers is given in the same form and, as the reference fluids are identical, used as the hard chain contribution in PC-SAFT:

$$Z^{hc} = \bar{m}Z^{hs} - \sum_i x_i(m_i - 1)\rho \frac{\partial \ln g_{ii}^{hs}}{\partial \rho} \tag{2.25}$$

$$\bar{m} = \sum_i x_i m_i \tag{2.26}$$

The segment radial distribution function is the same as presented in Equation 2.10 while the residual contribution of the hard sphere fluid to the compressibility factor (Z^{hs}) is an expression derived by Boublik (1992):

$$Z^{hs} = \frac{\zeta_3}{1-\zeta_3} + \frac{3\zeta_1\zeta_2}{\zeta_0(1-\zeta_3)^2} + \frac{3\zeta_2{}^3 - \zeta_3\zeta_2{}^3}{\zeta_0(1-\zeta_3)^3} \tag{2.27}$$

and the parameter ζ_n defined as previously in Equation 2.12.

PC-SAFT differs from $SAFT_{Ch}$ and $SAFT_{HR}$ through the use of the second order perturbation theory of Barker and Henderson (Barker & Henderson, 1967a, b) to describe the dispersion effects of the chain interactions. The theory is given as a sum of the first and second order contributions in the Helmholtz free energy according to Equation 2.28., with these first and second order contributions described in terms of an average inter-chain segment-segment radial distribution function and any potential function (e.g. square-well, Lennard-Jones) by (Gross & Sadowski, 2001):

$$\frac{A^{disp}}{kTN} = \frac{A_1}{kTN} + \frac{A_2}{kTN} \tag{2.28}$$

$$\frac{A_1}{kTN} = -2\pi\rho m^2 \left(\frac{\epsilon}{kT}\right)\sigma^3 \int_1^\infty \tilde{u}(r)^2 g^{hc}\left(m; r\frac{\sigma}{d}\right) x^2 dx \tag{2.29}$$

$$\frac{A_2}{kTN} = -\pi\rho m \left(1 + Z^{hc} + \rho\frac{\partial Z^{hc}}{\partial\rho}\right)^{-1} m^2 \left(\frac{\epsilon}{kT}\right)^2 \times \sigma^3 \frac{\partial}{\partial\rho}\left[\rho \int_1^\infty \tilde{u}(r)^2 g^{hc}\left(m; r\frac{\sigma}{d}\right) x^2 dx\right] \tag{2.30}$$

Here, $g^{hc}(m;r\sigma/d)$ is the aforementioned average radial distribution function, while r and $\tilde{u}(r)$ are the radial distance and reduced potential respectively. While analytical functions for the average inter-chain segment-segment radial distribution function do exist, Gross and Sadowski proposed the use of approximations for the integrals in Equations 2.29 and 2.30 to avoid unnecessarily tedious calculation of A_1 and A_2. These integrals were replaced by power series in the segment packing fraction whose coefficients are functions of the segment number and greatly reduce computational intensity of the model at no great cost in accuracy.

As with previous modifications, the PC-SAFT EOS is readily extended to mixtures by applying appropriate one-fluid mixing rules, with molecular simulation data for chain mixtures indicating that no significant errors are introduced by their application (Gross & Sadowski, 2000). Application of the van der Waals one-fluid mixing rules to the dispersion terms yields (Gross & Sadowski, 2001):

$$\frac{A_1}{kTN} = -2\pi\rho I_1(\eta,\bar{m})\sum_i\sum_j x_i x_j m_i m_j \left(\frac{\epsilon_{ij}}{kT}\right)\sigma_{ij}{}^3 \tag{2.31}$$

$$\frac{A_2}{kTN} = -\pi\rho\bar{m}\left(1 + Z^{hc} + \rho\frac{\partial Z^{hc}}{\partial\rho}\right)^{-1} I_2(\eta,\bar{m})\sum_i\sum_j x_i x_j m_i m_j \left(\frac{\epsilon_{ij}}{kT}\right)^2 \sigma_{ij}{}^3 \tag{2.32}$$

Parameters for unlike segments are determined from Berthelot-Lorentz combining rules, with all parameters defined as previously and extended to mixtures: It is this change in the description of the dispersion term and its application to the hard chain reference fluid which distinguishes PC-SAFT from the previous forms. As with $SAFT_{Ch}$ and $SAFT_{HR}$, however, PC-SAFT also only introduces a single binary interaction parameter in the dispersion term.

2.3.3. Gross & Sadowski's Model Results

Application of PC-SAFT to vapour pressure and liquid density data, and comparison with similar predictions made using $SAFT_{HR}$, show systematic deviations occur for the latter as a function of temperature, with much improved predictions in evidence for the former. Gross and Sadowski postulated that this could be attributed to their new dispersion term; namely that the non-spherical shape of molecules and thus molecular shape effects are now accounted for, resulting in improved predictive capacity (Gross & Sadowski, 2001). Similar results were obtained for both pure component and mixture VLE data with systematic improvement of correlations for PC-SAFT in evidence compared to those of $SAFT_{HR}$ in terms of both a smaller binary interaction parameter and greater qualitative agreement with experimental data.

Like Huang and Radosz before them, Gross and Sadowski used the pure component parameters they derived for over 70 pure, non-associating components to illustrate that these parameters were well behaved functions of the molecular mass and can be correlated to obtain parameters for components where no such data are available. The reader is directed to the appendices of the original work for a more detailed assessment of these correlations (Gross & Sadowski, 2001).

2.4. Simplified PC-SAFT

In 2003, von Solms and co-workers (von Solms *et al.*, 2003) proposed two simplifications to the PC-SAFT EOS with the view of reducing the model complexity. They argued that their reasoning was twofold; namely to produce a simpler EOS that was more likely to be adopted industrially and in process

simulation packages, but more specifically, to increase computational speed when using the model. These aims were to be met by merely adjusting the existing model, making no new contribution to the model itself, without a significant loss of accuracy. The resulting model was termed simplified PC-SAFT or sPC-SAFT as it is referred to here.

The proposed simplifications considered the hard chain contribution to the total Helmholtz free energy of the fluid, not just the residual component, which may be written as:

$$\frac{A^{hc}}{kTN} = \bar{m}\frac{A^{hs}}{kTN} - \sum_i x_i(m_i - 1)\ln g_{ii}^{hs} \tag{2.33}$$

As previously given by Huang and Radosz, the hard sphere term is given by Equation 2.19:

$$\frac{A^{hs}}{RT} = \frac{6}{\pi\rho}\left[\frac{{\zeta_2}^3 + 3\zeta_1\zeta_2\zeta_3 - 3\zeta_1\zeta_2{\zeta_3}^2}{\zeta_3(1-\zeta_3)^2} - \left(\zeta_0 - \frac{{\zeta_2}^3}{{\zeta_3}^2}\right)\ln(1-\zeta_3)\right] \tag{2.19}$$

and the radial distribution function remains that derived by Carnahan and Starling (Carnahan & Starling, 1969):

$$g_{ij}(d_{ij})^{hs} = \frac{1}{1-\zeta_3} + \frac{3d_{ii}d_{jj}}{d_{ii}+d_{jj}}\frac{\zeta_2}{(1-\zeta_3)^2} + 2\left[\frac{d_{ii}d_{jj}}{d_{ii}+d_{jj}}\right]^2\frac{{\zeta_2}^2}{(1-\zeta_3)^3} \tag{2.10}$$

with the temperature dependent segment diameter that of Chen and Kreglewski (Chen & Kreglewski, 1977):

$$d_i(T) = \sigma_i\left[1 - 0.12exp\left(-\frac{3\epsilon_i}{kT}\right)\right] \tag{2.16a}$$

2.4.1. The First Modification

The first approximation proposed by von Solms and co-workers involved the relation for the segment diameter: it was assumed that all segments in the mixture had the same diameter, under the constraint that the segment packing fraction (i.e. η) using this universal segment diameter is equal to that of the original mixture of different sized spheres (von Solms *et al.*, 2003). Under this assumption, the new average diameter is given by:

$$d = \left(\frac{\sum_i x_i m_i {d_i}^3}{\sum_i x_i m_i}\right)^{1/3} \tag{2.34}$$

According to the authors, the justification of this approximation is the similarity of experimentally determined segment diameters for a wide range of molecules, previously published under the PC-SAFT formalism (Gross & Sadowski, 2001). Defining the segment diameter in this way allows the ζ_n terms to be recalculated using Equation 2.12 and simplifies the hard sphere radial distribution function of Equation 2.10 to a simple relation in the segment packing fraction (von Solms *et al.*, 2003):

$$g(d)^{hs} = \frac{1 - \frac{\eta}{2}}{(1-\eta)^3} \tag{2.35}$$

The radial distribution function thus determined is inherently composition independent and results in significant simplification of the EOS.

2.4.2. The Second Modification

The second modification is a direct consequence of the first and allows simplification of the hard sphere contribution to the residual Helmholtz free energy. Substituting the average diameter defined in Equation 2.35 into the A^{hs} term results in the Carnahan-Starling approximation, formerly used for pure components in $SAFT_{Ch}$ and $SAFT_{HR}$ and now assumed applicable to mixtures under sPC-SAFT (von Solms *et al.*, 2003):

$$\frac{A^{hs}}{NkT} = \frac{4\eta - 3\eta^2}{(1-\eta)^2} \tag{2.7a}$$

The modifications thus did not change the fundamental nature of the PC-SAFT equations, but simply reduced the computational intensity of the EOS. An important result of this is that the pure component parameters of both PC-SAFT and sPC-SAFT (namely σ, ε/k and m) are identical.

2.4.3. sPC-SAFT Model Results

One or both of the modifications may be implemented under sPC-SAFT, with use of the second modification yielding a larger deviation from the predictions of the original PC-SAFT due to the significant simplification inherent in this approximation. Both modifications were compared with the predictions of PC-SAFT for both pure components and mixtures, considering both non-associating and associating compounds, with no significant disparity between the models in evidence. The model was even shown to produce good qualitative agreement for pure predictions of strongly non-ideal alcohol-alkane systems, indicative of the applicability of the model despite the significance of the inherent simplifications (von Solms *et al.*, 2003).

In a later publication by the same research group (von Solms *et al.*, 2006), the capabilities and limitations of the sPC-SAFT EOS were assessed, in which a number of important points were highlighted:

- PC-SAFT and sPC-SAFT were both found to produce highly satisfactory and comparable results for alcohol-alkane systems and high pressure polymer and co-polymer systems.
- Application to aqueous systems of alcohols and alkanes have yielded mixed results in the few studies in which the SAFT variants had been applied, in particular due to the uncertainty in choice of the "correct" association scheme for water.
- Application of SAFT variants to polar systems produces highly unsatisfactory results in the original SAFT framework, where polar interactions were simply incorporated into the dispersion term instead of being explicitly accounted for.

The second and third points have been the focus of the subsequent development of SAFT, generally within the (s)PC-SAFT frameworks. The former has been assessed by a number of research groups, but is not the primary focus of this work. The reader is directed to the works of the research groups of Grenner (Grenner *et al.*, 2007), Al-Saifi (Al-Saifi *et al.*, 2008) and de Villiers (de Villiers *et al.*, 2011) among others for a detailed assessment of the treatment of aqueous systems using SAFT variants. It is the latter that is more pertinent to the application of ketone-alkane systems assessed in this work.

2.5. Polar PC-SAFT

Neither $SAFT_{Ch}$ nor $SAFT_{HR}$ accounted for polar interactions explicitly, allowing rather for these effects to be incorporated into the dispersion effects. When applied to polar fluids, this oversimplification results in a much larger attraction energy (ϵ or u) between molecules of the pure fluid than is actually the case (Jog *et al.*, 2001). In looking at the interaction energy accountability in the EOS, the impact of this generalisation becomes clearer:

$$\epsilon_{ij} = (1 - k_{ij})\sqrt{\epsilon_{ii}\epsilon_{jj}} \tag{2.36}$$

If the interaction energy of polar molecule i is larger than reality, the geometric mean is excessive and a much larger binary interaction parameter is required to produce any sort of realistic correlation to experimental data. As such the predictive capability of the model is reduced and the inability of $SAFT_{Ch}$ and $SAFT_{HR}$ to account for polar effects is highlighted. Attempts to specifically account for polar interactions in EOS's had been previously considered however. In these works (Kraska & Gubbins, 1996a,b; Xu *et al.*, 1998) dipolar molecules are regarded as spherical molecules of volume equal to that of the chain molecule they are representing, with an ideal dipole at the centre of the molecule. The diameter of such molecule is given by:

$$d_{molecule} = \left(m{d_{segment}}^3\right)^{\frac{1}{3}} \tag{2.37}$$

where $d_{segment}$ is the diameter of an equal-sized segment in a chain of m such segments.

Such treatment is adequate when considering that the reduced influence of polar interaction with increasing molecular size and distance between the dipoles is accounted for (Jog *et al.*, 2001). However, as with the dispersion effects of $SAFT_{Ch}$ and $SAFT_{HR}$ before PC-SAFT was developed, molecular shape was unaccounted for in the polar contribution. It was from this starting point that representative polar contributions were subsequently formulated.

2.5.1. Jog and Chapman's Polar Contribution

The first significant contribution towards the development of a polar term for inclusion in the SAFT framework came from the same research group who developed the original SAFT equation. The work of Jog, Chapman and co-workers was presented in two papers; first applied to molecular simulation data (Jog & Chapman, 1999) before being extended to real fluids (Jog *et al.*, 2001), where significant

improvement was made in correlating the phase behaviour of polar fluids and their mixtures compared to the predictions of the original SAFT EOS's. The model was in fact so successful that, for some systems, pure predictions of VLE produced excellent agreement with experimental data.

Polar Term in SAFT Framework: p-SAFT

In the original work, Jog and Chapman pointed out the fact that, beside the fact that the nonsphericity of molecules is not accounted for by the previous attempts at accounting for polarity (an approach they dubbed the "molecular sphere approach" (Jog & Chapman, 1999)), the reduced effect of polarity with increasing chain length is over exaggerated and multiple dipoles cannot be accounted for. These effects are illustrated graphically in Figure 2.7.

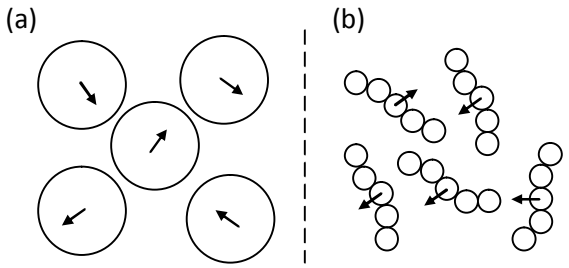

Figure 2.7: Graphic representation of (a) Molecular sphere approach and (b) Segment approach of Jog & Chapman. Figure redrawn and adapted from (Jog et al., 2001)

As is readily apparent from the figure, the molecular sphere approach limits the degree of closeness chain molecules can achieve and thus the effect of reduced polar effects is exaggerated. Jog and Chapman sought to remedy this effect by developing the so-called "segment approach" where the molecules are considered as chains of tangential spherical segments, where the dipole moment is assumed perpendicular to the molecular axis in all cases (Jog & Chapman, 1999). In this way, the distance of closest approach of dipoles is better represented and the location and number of dipoles on a molecule of a real fluid can be characterised. The molecular sphere approach was shown to underestimate the effects of dipolar interaction by a factor equal in magnitude to the segment number (m), highlighting the magnitude of error introduced by using this approach, particularly for long chains (Jog *et al.*, 2001).

The contributions to the residual Helmholtz free energy for real fluids were later illustrated, making use of the u-expansion from perturbation theory. The u-expansion however is only applicable to mixtures of polar spheres and so its application to chain molecules requires manipulation of the theoretical fluid. This involves dissolving the bonds in the chain and subsequently applying the u-expansion to the resulting mixture of polar and non-polar spheres (Jog *et al.*, 2001). To account for the fact that this mixture does not only comprise polar segments, Jog and Chapman defined a new pure component parameter, x_p, to account for the fraction of dipolar segments in a molecule. Thus, in the case of a single dipolar segment, as in the case of ketones, this parameter should be equal to m^{-1} (Jog & Chapman, 1999).

The u-expansion is an infinite power series where the second and third terms are explicitly accounted for and all higher order terms are estimated using the Padé approximant proposed by Rushbrooke and co-workers (Rushbrooke *et al.*, 1973). The expansion for A^{res}, including the new polar contribution, may thus be written as (Jog & Chapman, 1999):

$$A^{res} = A^{hs} + A^{disp} + A^{polar} + A^{chain} + A^{assoc} \tag{2.38}$$

where the original $SAFT_{HR}$ terms, including the Chen and Kreglewski (Chen & Kreglewski, 1977) dispersion term, are used for the other terms, unaffected by the additional polar term (Jog & Chapman, 1999), which is defined by:

$$A^{polar} = \frac{A_2}{1 - \frac{A_3}{A_2}} \tag{2.39}$$

For a mixture of pure components, Jog and Chapman presented the second and third order contributions as integrals over the two- and three-body correlation functions for the reference (hard sphere) fluid (Jog & Chapman, 1999):

$$\frac{A_2}{kTN} = -\frac{2}{9}\frac{\pi\rho}{(kT)^2}\frac{\mu^4}{\sigma^3}x_p^2.I_2(\rho^*) \tag{2.40}$$

$$\frac{A_3}{kTN} = \frac{5}{162}\frac{\pi^2\rho^2}{(kT)^3}\frac{\mu^6}{\sigma^3}x_p^3.I_3(\rho^*) \tag{2.41}$$

where μ is the pure component dipole moment, x_p is the fraction of dipolar segments in a molecule defined earlier and the reduced density (designated the "polar reduced density", ρ^*, not to be confused with the segment packing fraction, η, defined earlier) is given by:

$$\rho^* = \rho m \sigma^3 \tag{2.42}$$

The integrals are defined by:

$$I_2(\rho^*) = \frac{3\sigma^3}{4\pi}\int g_{HS}(r,\rho^*).\frac{1}{r^6}d\boldsymbol{r} \tag{2.43}$$

$$I_3(\rho^*) = \frac{3\sigma^3}{5\pi^2}\int g_{HS}(123,\rho^*).u(123).d\boldsymbol{r_2}d\boldsymbol{r_3} \tag{2.44}$$

where $u(123)$ is a function of the angles and distances between the three interacting molecules. Rushbrooke and co-workers (Rushbrooke *et al.*, 1973), however, showed that these integrals may be readily approximated as simple functions of the polar reduced density:

$$I_2(\rho^*) = \frac{1 - 0.3618\rho^* - 0.3205\rho^{*2} + 0.1078\rho^{*3}}{(1 - 0.5236\rho^*)^2} \tag{2.45}$$

$$I_3(\rho^*) = \frac{1 + 0.62378\rho^* - 0.11658{\rho^*}^2}{1 - 0.59056\rho^* + 0.20059{\rho^*}^2} \tag{2.46}$$

The formalism may be extended to a mixture of polar fluids, where the second and third order contributions are given by (Jog *et al.*, 2001):

$$\frac{A_2}{kTN} = -\frac{2}{9}\frac{\pi\rho}{(kT)^2}\sum_i\sum_j x_i x_j m_i m_j x_{pi} x_{pj}\frac{{\mu_i}^2{\mu_j}^2}{{d_{ij}}^3}.I_{2,ij} \tag{2.47}$$

$$\frac{A_3}{kTN} = \frac{5}{162}\frac{\pi^2\rho^2}{(kT)^3}\sum_i\sum_j\sum_k x_i x_j x_k m_i m_j m_k x_{pi} x_{pj} x_{pk}\frac{{\mu_i}^2{\mu_j}^2{\mu_k}^2}{d_{ij}d_{jk}d_{ik}}.I_{3,ijk} \tag{2.48}$$

Here, the $I_{2,ij}$ and $I_{3,ijk}$ terms are calculation intensive integrals over the two- and three-body correlation functions for the reference (hard sphere) fluid, given by (Jog *et al.*, 2001):

$$I_{2,ij} = \frac{3{d_{ij}}^3}{4\pi}\int g_{HS_{ij}}(r,\rho^*)\frac{1}{r^6}dr = 3\int_1^\infty g_{HS_{ij}}(r_{ij}^*,\rho^*).\frac{1}{{r_{ij}}^4}dr_{ij}^* \tag{2.49}$$

$$\begin{aligned} I_{3,ijk} = \frac{192\pi}{5}\sqrt{\frac{14\pi}{5}}\int_0^\infty dr_{12}^*{r_{12}^*}^{-2}\int_0^\infty dr_{13}^*{r_{13}^*}^{-2} \\ \times\int_{\left(\frac{\sigma_{ij}}{\sigma_{jk}}\right)r_{12}^*-\left(\frac{\sigma_{ij}}{\sigma_{jk}}\right)r_{13}^*}^{\left(\frac{\sigma_{ij}}{\sigma_{jk}}\right)r_{12}^*+\left(\frac{\sigma_{ij}}{\sigma_{jk}}\right)r_{13}^*} dr_{23}^*{r_{23}^*}^{-2}\,g_{ijk}(r_{12}^*,r_{13}^*,r_{23}^*) \\ \times\psi_{222(\alpha_1,\alpha_2,\alpha_3)} \end{aligned} \tag{2.50}$$

Where the reduced radial distance is defined by:

$${r_{ij}}^* = \frac{r_{ij}}{d_{ij}} \tag{2.51}$$

However, to simplify these integrals, it was assumed that, in reduced form, the integrals are independent of component at a given density (Jog *et al.*, 2001), for which the mixture integrals reduce to their pure fluid integrals, as defined in Equations 2.45and 2.46 previously, according to:

$$I_{2,ij} = I_2\left(\rho{d_f}^3\right) \tag{2.52}$$

$$I_{3,ijk} = I_3\left(\rho{d_f}^3\right) \tag{2.53}$$

$${d_f}^3 = \sum_i X_i m_i {d_{ii}}^3 \tag{2.54}$$

The extension of the SAFT equations to accommodate polar components by Chapman's research group was thus concluded. The above variant, having been developed at the same time as PC-SAFT, is used within the SAFT framework and is often referred to, as will be the case from this point on, as polar-SAFT or simply p-SAFT.

As previously highlighted, the fraction of polar segments in a chain is ideally meant to be equal to the inverse of the segment number. For pure fluids however, the parameter is left adjustable as the view of a chain of tangentially joined segments (the aforementioned ideal case) has been shown to be an oversimplified model (Jog *et al.*, 2001). It was, however, shown by the authors that, for a given homologous series (e.g. 2-alkanones), the product mx_p is a constant and thus this relation may be used for the determination of component parameters if those of a compound in the same homologous series have previously been measured (Jog *et al.*, 2001).

p-SAFT thus requires the regression of four pure component parameters for the description of phase equilibria, namely; the segment volume (v^{00}), segment interaction energy (u^0/k), segment number (m) and x_p without the introduction of any additional binary interaction parameters on top of that used in the dispersion contribution (Jog *et al.*, 2001).

Extension of Polar Term to PC-SAFT Framework: PC-SAFT$_{JC}$

In their later work, Chapman's research group acknowledged the increasing influence of other SAFT variants and, as such, concluded that their polar term could easily be incorporated by other chain fluid equations of state (Jog *et al.*, 2001). Tumakaka and Sadowski (Tumakaka & Sadowski, 2004) extended this polar term to the PC-SAFT formalism without any further modification. Thus, although no new contribution was made by their work per se, it was the first instance of an explicit polar term being incorporated into the PC-SAFT equation of state, and the resulting model is thus often referred to as perturbed chain polar-SAFT (PCP-SAFT). Here however, use is made of the abbreviation PC-SAFT$_{JC}$ to acknowledge the original contribution of Jog and Chapman.

As with the original work for PC-SAFT, the PCP-SAFT$_{JC}$ equation of state is presented as a series of compressibility factors, with the newly incorporated polar term:

$$Z = 1 + Z^{hc} + Z^{disp} + Z^{assoc} + Z^{polar} \tag{2.55}$$

Here again, the original three pure component parameters of the PC-SAFT equation (σ, m and ϵ/k) are required in addition to the fraction of polar segments in a chain (x_p), with no additional binary interaction parameters introduced.

2.5.2. Gross and Vrabec's Polar Contribution

The research group responsible for the development of the PC-SAFT model later developed their own polar interaction contribution. The basis of their derivation was in two previous works. The first was the work of Gubbins and Twu (Gubbins & Twu, 1978), (Twu & Gubbins , 1978), who developed

expressions accounting for dipolar and quadrupolar forces between molecules interacting with a Lennard-Jones potential, based on third order perturbation theory. The second was that of Saager and Fischer (Saager & Fischer, 1992), who performed molecular simulations to fit empirical expressions for the dipolar and quadrupolar effects in a two-centre Lennard-Jones (2CLJ) plus point di-/quadru-pole fluid. This molecular model is different to the tangent sphere model in Wertheim's Thermodynamic Perturbation Theory of first order (TPT1), on which the SAFT equation of state was originally developed.

Gross and Vrabec (Gross & Vrabec, 2006) aimed to produce an equation of state contribution for the dipolar interactions of chain molecules. Based on third order perturbation theory in the Padé approximant, with model constants fitted to simulation data of pure 2CLJ plus point dipole fluids, it was intended to be applied in the PC-SAFT framework. The model was thus referred to, as is the case here, as perturbed-chain polar-SAFT or PC-SAFT$_{GV}$.

Polar Term in PC-SAFT Framework: PC-SAFT$_{GV}$

The fact that different perturbation theories were used for the description of the reference fluid meant that Gross & Vrabec had to reconcile the fundamental differences between these molecular models so that an appropriate polar term could be generated. The difference lies in the reference fluid description, where TPT1 considers chains of *m* tangentially joined segments, while the 2CLJ fluid instead considers molecular centres to be separated by a molecular elongation, *L* (Gross, 2005), which allows for segment overlapping, as detailed in Figure 2.8.

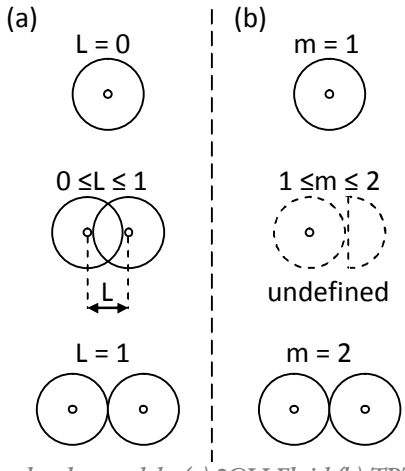

Figure 2.8 Fundamental differences in molecular models. (a) 2CLJ Fluid (b) TPT1 Fluid. Figure redrawn and adapted from (Gross, 2005)

Thus, reconciliation involved the generation of appropriate correlations to relate 2CLJ molecular simulation results to the equivalent TPT1 representation. The reader is directed to the original work for a more in-depth analysis of this conversion procedure, but the resulting pure component parameter conversions allow the phase-equilibrium properties of a 2CLJ fluid to be accurately calculated by considering it as a tangent-sphere fluid and applying first order perturbation theory, including SAFT (Gross & Vrabec, 2006). This is an important result for the development of Gross and Vrabec's polar term.

Similar to the work of Jog and Chapman, Gross and Vrabec presented the dipolar interaction contribution using third order perturbation theory presented in the Padé approximant (Gross & Vrabec, 2006):

$$\frac{A^{DD}}{kTN} = \frac{\frac{A_2}{kTN}}{1 - \frac{A_3}{A_2}} \tag{2.56}$$

The second and third order perturbation terms can be written using the expressions of Boublik (Boublik, 1992):

$$\frac{A_2}{kTN} = -\pi\rho \sum_i \sum_j x_i x_j \frac{\epsilon_{ii}}{kT}\frac{\epsilon_{jj}}{kT}\frac{{\sigma_{ii}}^3 {\sigma_{jj}}^3}{{\sigma_{ij}}^3} n_{\mu,i} n_{\mu,j} {\mu^*_i}^2 {\mu^*_j}^2 . {J_{2,ij}}^{DD} \tag{2.57}$$

$$\frac{A_3}{kTN} = -\frac{4}{3}\pi^2\rho^2 \sum_i \sum_j \sum_k x_i x_j x_k \frac{\epsilon_{ii}}{kT}\frac{\epsilon_{jj}}{kT}\frac{\epsilon_{kk}}{kT}\frac{{\sigma_{ii}}^3 {\sigma_{jj}}^3 {\sigma_{kk}}^3}{\sigma_{ij}\sigma_{jk}\sigma_{ik}} \times n_{\mu,i} n_{\mu,j} n_{\mu,k} {\mu^*_i}^2 {\mu^*_j}^2 {\mu^*_k}^2 . {J_{3,ijk}}^{DD} \tag{2.58}$$

where Berthelot-Lorentz combining rules are used for σ_{ij} and ϵ_{ij}, and the reduced dipole moment is defined by:

$${\mu^*_i}^2 = \frac{{\mu_i}^2}{m_i \epsilon_{ii} {\sigma_{ii}}^3} \tag{2.59}$$

Similarly to Jog and Chapman, a new parameter is defined in Equations 2.57 and 2.58, namely the number of dipoles on a given molecule, $n_{\mu,i}$ (Gross & Vrabec, 2006). Unlike Jog and Chapman however, this pure component parameter was not left adjustable. For low molecular weight compounds including ketones, $n_{\mu,i}$ was originally equal to unity and can be changed to accommodate molecules exhibiting multiple dipoles.

The ${J_{2,ij}}^{DD}$ and ${J_{3,ijk}}^{DD}$ terms are integrals over the two- and three-body correlation functions for the reference fluid and are assumed to be simple power functions in the segment packing fraction, η, and the interaction energy (Gross & Vrabec, 2006), where the $a_{n,ij}$, $b_{n,ij}$ and $c_{n,ij}$ constants are defined in a similar fashion to those used in the original PC-SAFT derivation, using expressions proposed by Liu and Hu (Liu & Hu, 1996).

$${J_{2,ij}}^{DD} = \sum_{n=0}^{4} \left(a_{n,ij} + b_{n,ij}\frac{\epsilon_{ij}}{kT}\right)\eta^n \tag{2.60}$$

$${J_{3,ijk}}^{DD} = \sum_{n=0}^{4} c_{n,ijk}\,\eta^n \tag{2.61}$$

It is in the determination of the *a,b* and *c* constants of Equations 2.60 and 2.61 above that the conversion relation between the 2CLJ reference fluid and the tangent-sphere fluid is important. Having used a 2CLJ reference fluid, these constants had to be regressed to molecular simulation data of a pure 2CLJ fluid (Gross & Vrabec, 2006). Thus, the constants are fitted to a 2CLJ reference fluid in terms of L^* but converted to the TPT1 framework through the correlations developed between m and L^*. The polar contribution of Equation 2.56 is thus readily incorporated into the PC-SAFT formalism, here PC-SAFT$_{GV}$.

2.5.3. Major Shortcoming of Polar Terms

The primary shortcoming of the polar terms developed by both Jog & Chapman and Gross & Vrabec is the incorporation of a constant effective dipole moment for polar components. Reported dipole moments are typically measured for the gas phase under vacuum, although this value is by no means constant and is phase dependent. The use of a constant, typically gas phase dipole moment thus introduces an unquantifiable error into predictions that is typically compensated for by adjusting the remaining pure component parameters.

The changing dipole moment associated with the polar carbonyl group shifting centrally is the primary reflection of the decreased polar interactions of different structural isomers. It will thus be interesting to see whether the reported dipole moments and component parameters adjusted to compensate for resulting polar discrepancies will be sufficient to predict the phase equilibria data to be measured in this work, or if this shortcoming of the polar terms will be highlighted in the modelling procedure.

The nature of the considered dipole moment is by no means the only shortcoming of the polar PC-SAFT terms, although the other major drawbacks highlighted in the literature are concerned with the combined effects of polar and association effects in systems exhibiting both phenomena and in the prediction of phase behaviour in aqueous systems; problems which will not be encountered in the ketone-alkane systems investigated in this work. The reader is referred to the works of Al-Saifi (Al-Saifi *et al.*, 2008) and de Villiers (de Villiers *et al.,* 2011) for a more comprehensive discussion of these aspects of the Jog & Chapman and Gross & Vrabec polar terms.

2.5.4. Polar sPC-SAFT & Study Highlights

As has been discussed previously, the modification of PC-SAFT to the simplified version of von Solms and co-workers was seamless, with equally good predictions achieved at lower computational intensity. Until only recently however, the polar terms generated by Jog & Chapman and Gross & Vrabec had not been incorporated into the sPC-SAFT framework. The structure of the SAFT type models is conducive to the incorporation of the different terms into the model variants as each term is simply the contribution to the residual Helmholtz energy of the type of molecular interaction under consideration. Thus, de Villiers *et al.* (2011) were the first authors to consider incorporating both polar terms into the sPC-SAFT formalism. Extensive application of the resulting model found to yield excellent predictions of the VLE of the polar systems considered. It is this model that is the focus of this study.

2.5.5. Application of Polar SAFT Models to Ketone-n-Alkane Mixtures

The previous applications of the various polar SAFT models to experimental ketone-n-alkane systems are presented in Table 2.1. As the most strongly polar and extensively studied alkanone, binary mixtures of acetone with various hydrocarbons are the most extensively studied in the literature, with the instances of application to larger ketone molecules being very limited.

Table 2.1: Previous applications of polar SAFT variants to ketone-n-alkne mixtures

SAFT Variant	Binary System	Reference
p-SAFT	Acetone/n-Pentane Acetone/n-Hexane Acetone/n-Decane Acetone/n-Dodecane	(Jog *et al.*, 2001)
	2-Butanone/n-Heptane 3-Pentanone/n-Heptane	(Sauer & Chapman, 2003)
PC-SAFT$_{JC}$	Acetone/n-Pentane Acetone/n-Hexane Acetone/n-Decane Acetone/n-Dodecane	(Tumakaka & Sadowski, 2004)
PC-SAFT$_{GV}$	Acetone/Ethane Acetone/n-Butane Acetone/n-Pentane Acetone/n-Decane	(Gross & Vrabec, 2006)
PC-SAFT$_{GV}$ (induced polarisation)	3-Pentanone/n-Heptane Acetone/n-Heptane	(Kleiner & Gross, 2006)
sPC-SAFT (both polar variants)	Acetone/n-Pentane Acetone/n-Hexane Acetone/n-Heptane Acetone/n-Octane 2-Butanone/n-Hexane 2-Butanone/n-Heptane 3-Pentanone/n-Heptane	(de Villiers *et al.*, 2011)

Further, as no instances of ketones larger than C_5 have been considered, the effect of a shifting carbonyl group on the polar interactions and, thus, phase equilibria for a given unbranched ketone has not been assessed. From the relevant pure component vapour pressures, we can tell that polar interactions are diminished as a carbonyl group shifts from the terminal end of the chain centrally, but the effect of these diminished polar effects has not been investigated for a binary mixture and, thus, the ability of the polar SAFT models to accurately predict these effects are unknown.

The aforementioned is the aim of this investigation, but, as no appropriate binary VLE data are available, before the performance of the polar sPC-SAFT models can be assessed in this regard, the relevant binary VLE data need to be generated experimentally. The means by which this is achieved is the subject of the next chapter.

Chapter 3 Low Pressure Phase Equilibria

The accurate measurement of phase equilibria and interpretation of experimentally observed phenomena are of vital importance to the testing and development of accurate thermodynamic models. In the absence of previously measured data available in the open literature, it is necessary to generate and interpret such data oneself. In this Chapter, the more practical aspects of vapour-liquid equilibrium are assessed, including the types of phase behaviour expected at low pressures, the availability of existing data and the means by which reliable and thermodynamically sound data can be generated.

3.1. Low Pressure Phase Behaviour

Experimentally witnessed phase behaviour conducted at low pressures can be classified into two categories; namely zeotropic behaviour and azeotropic behaviour.

Azeotropic behaviour, derived from the Greek words *a* meaning "non", *zeo* meaning "boil" and *tropos* meaning "change", describes systems where the equilibrium vapour and liquid phase compositions are identical at a given combination of temperature and pressure. On a molecular level, azeotropes are found in systems where the liquid phase intermolecular attractions between like molecules and those between unlike molecules are very much unequal (Smith *et al.,* 2005). Physically, such intermolecular behaviour is often, but not always, found in systems of molecules exhibiting different functionality or when the pure component vapour boiling points are close together. Only when the difference in magnitude between like and unlike intermolecular forces is great enough to produce an extreme in the mixture temperature under isobaric conditions, or a similar extreme in the pressure under isothermal conditions, will an azeotrope form (Malesiński, 1965). Azeotropes are of particular interest industrially as they represent the largest degree to which a mixture may be separated by partial vaporisation, the inherent operating principle of traditional distillation columns.

Azeotropes can further be divided into homoazeotropes and heteroazeotropes depending on whether or not the azeotropic liquid phase is homogenous or heterogenous respectively (Malesiński, 1965). Heteroazeotropes are formed when the attraction between like molecules are so strong as to prevent complete liquid miscibility, resulting two liquid phases of varying composition (Smith *et al.*, 2005). Homoazeotropes are more common than heteroazeotropes, with the latter generally found in systems containing water (Malesiński, 1965). As the ketone-alkane systems of this study are not expected to exhibit liquid immiscibility, the focus of this work will be the presence of homoazeotropes, the phase behaviour of which is typified in Figure 3.1a.

The definition of zeotropic behaviour is simply the behaviour exhibited by systems where no azeotrope is present (Malesiński, 1965). Such behaviour is witnessed experimentally in systems exhibiting near-ideal behaviour, or more generally, systems of components exhibiting similar functionality and large differences in boiling point under isobaric conditions, or vapour pressure under isothermal conditions.

The equilibrium vapour and liquid compositions are never equal in zeotropic mixtures and the extremes in temperature and pressure are the pure component boiling points and vapour pressures for isobaric and isothermal conditions respectively. Typical zeotropic behaviour is presented in Figures 3.1b. & c.

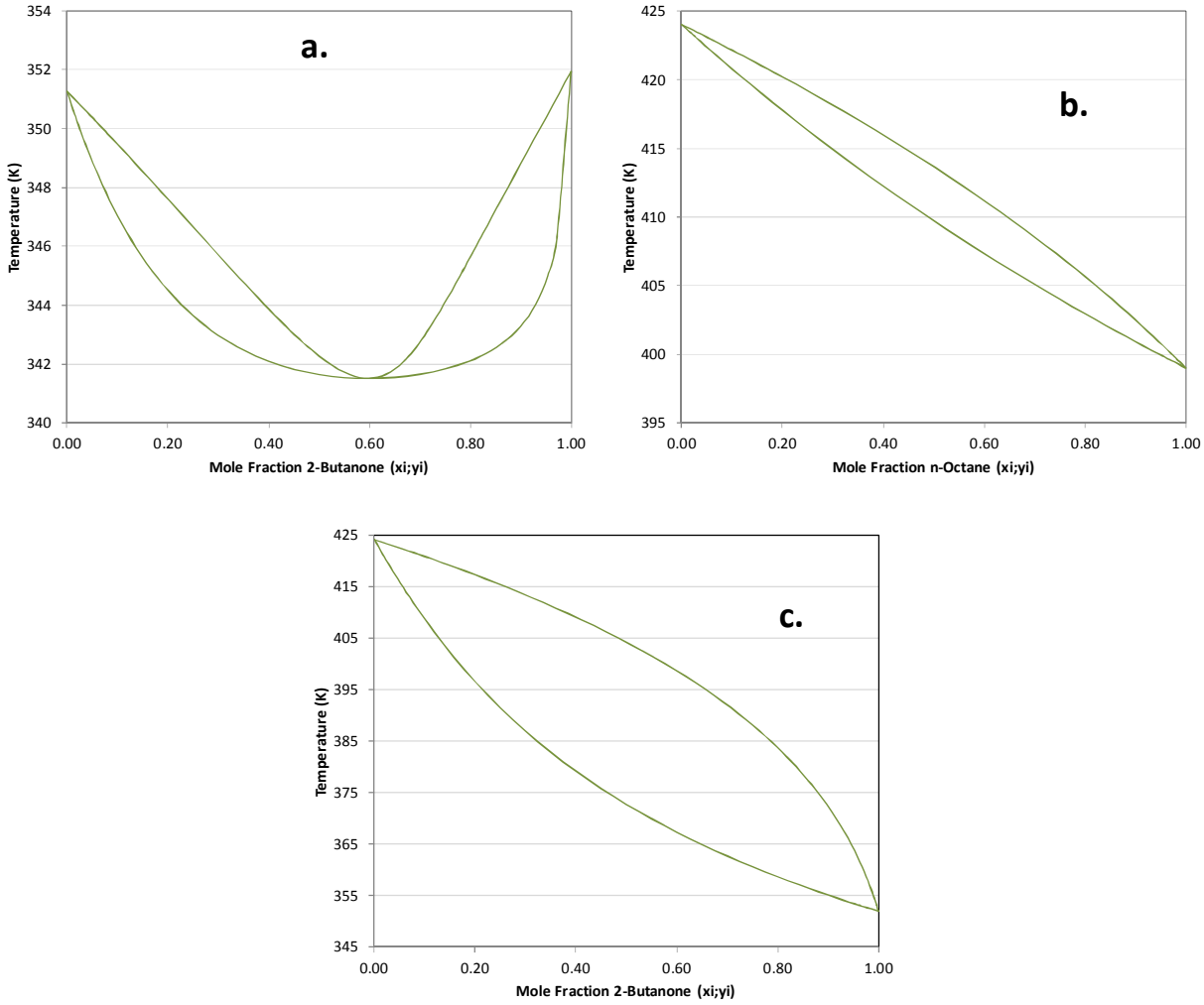

Figure 3.1: Typical low pressure phase behaviour in binary mixtures. (a.) Azeotropic behaviour in highly non-ideal chemically dissimilar 2-butanone/ethanol system (b.) Zeotropic behaviour in (ideal) n-octane/n-nonane. (c.) Zeotropic behaviour in chemically similar non-ideal mixture (2-butanone/2-heptanone).

3.2. Existing Ketone-n-Alkane VLE Data

Table 3.1 details all existing vapour-liquid equilibrium measurements for binary systems of ketones larger than acetone with n-alkanes previously measured and available in the open literature and highlights the phase behaviour apparent in these systems.

Table 3.1: Compilation of available binary VLE data for ketone/alkane systems from butanone to heptanone

Alkanone	Alkane	Zeotropic/ Azeotropic	Isobaric/ Isothermal	Pressure/ Temperature	Reference
Butanone	Hexane	Azeotropic	Isothermal	60°C	(Hanson & van Winkle, 1967)
		Azeotropic	Isothermal	65°C	(Maripuri & Ratcliff, 1972)
		Azeotropic	Isobaric	760mm Hg	(Gmehling *et al.*, 1993)
	Heptane	Azeotropic	Isobaric	760mm Hg	(Steinhauser & White, 1949)
		Azeotropic	Isobaric	760mm Hg	(Aristovich *et al.*, 1965)
		Azeotropic	Isothermal	45°C	(Takeo *et al.*, 1979)
		Azeotropic	Isobaric	705.6mm Hg	(Wisniak *et al.*, 1998)
	Octane	Zeotropic	Isothermal	65°C	(Maripuri & Ratcliff, 1972)
		Zeotropic	Isobaric	760mm Hg	(Gmehling *et al.*, 1993)
		Zeotropic	Isothermal	40°C	(Gmehling *et al.*, 1993)
	Decane	Zeotropic	Isothermal	70°C	(Gmehling *et al.*, 1993)
		Zeotropic	Isothermal	65°C	(Gmehling & Onken, 2004)
		Zeotropic	Isothermal	25, 60 & 90°C	(Pierotti *et al.*, 1959)
2-Pentanone	Heptane	Azeotropic	Isothermal	90°C	(Scheller & Rao, 1973)
3-Pentanone	Hexane	Azeotropic	Isothermal	65°C	(Maripuri & Ratcliff, 1972)
		Azeotropic	Isothermal	10, 52 & 65°C	(Barraza *et al.*, 1979)
	Heptane	Azeotropic	Isothermal	65, 80, 95°C	(Geiseler & Köhler, 1968)
		Azeotropic	Isothermal	26, 80, 94.4°C	(Barraza *et al.*, 1979)
		Azeotropic	Isothermal	80°C	(Gmehling *et al.*, 1993)
		Azeotropic	Isothermal	40.05°C	(Fuchs *et al.*, 1984)
2-Hexanone	Nonane	Azeotropic	Isobaric	200, 400, 600, 760mm Hg	(Gmehling & Onken, 2004)
4-Heptanone	Hexane	Zeotropic	Isothermal	65°C	(Maripuri & Ratcliff, 1972)

Apart from the pentanone case, there have been no documented cases of phase equilibrium measurement of multiple structural isomers of the same ketone paired with a normal alkane. While the two structural isomers with n-heptane could be used as the basis of the modelling study proposed here, it was deemed necessary to consider the case of three or more structural isomers to derive a trend, should one exist, in the ability of each polar model to predict phase equilibria as the carbonyl group shifts centrally. It is further apparent from the table that azeotropic behaviour is evident in systems where the ketone was paired with a normal alkane having a slightly larger carbon backbone and hence a similar boiling point, as suggested in the previous section. Having addressed the questions of existing data and the conditions of interest, it is necessary to generate experimental VLE data within this work, the means by which are discussed in the following section.

3.3. Phase Equilibria Measurement

Raal & Mühlbauer (1998) group the measurement of phase equilibria measurement into five principle categories, namely:

- Semimicro techniques
- Measurement of infinitely dilute activity coefficients
- Dew/bubble point methods
- Dynamic or recirculating methods
- Static methods

Semimicro techniques are employed when purification of a component is particularly difficult or when sufficiently pure chemicals are too expensive in the volumes necessary for phase equilibria using the dynamic or static methods. The infinite dilution activity coefficient provides a measure of the non-ideality of a system in the very dilute region, which is, from an industrial and economical perspective, the most expensive and most difficult part of a separation process. While this method does provide the most accurate representation of the dilute concentration regions, it does not, by its very nature, account for phase equilibria across the full composition spectrum. Dew/bubble point methods manipulate the volume of a mixture to produce a change in system pressure and thus induce the dew and bubble points for a given feed composition respectively. This method however, is resource intensive by its very nature and, at low pressure where the density of the phases differ considerably, has been largely overshadowed by the more successful dynamic and static methods. For a more in depth discussion of these less conventional techniques, the reader is directed to the work of Raal & Mühlbauer (1998).

Traditional means of measuring phase equilibria over a full binary composition spectrum are the dynamic and static methods, for the measurement of isobaric and isothermal phase equilibria, respectively. In general, industrial distillation processes are conducted at constant pressure (Smith *et al.,* 2005) and thus, isobaric VLE data are of practical interest. For this reason and due to the availability of a dynamic still, the measurement of isobaric phase equilibria are the focus of this work. In the sections that follow, the development of the dynamic method of phase equilibria measurement will be examined more rigorously. A similarly rigorous discussion of the development of static VLE apparatus is presented in the work of Raal & Mühlbauer (1998).

3.3.1. Othmer Dynamic Still

The Othmer still represented the most successful of the early dynamic VLE stills. The principle behind the dynamic stills based on this design is the recirculation of the condensed vapour phase produced from boiling a liquid charge. The vapour phase sample is taken from a condensate receiver situated before the boiling chamber, while the liquid phase is sampled directly from the boiling chamber, as represented by Figure 3.2.

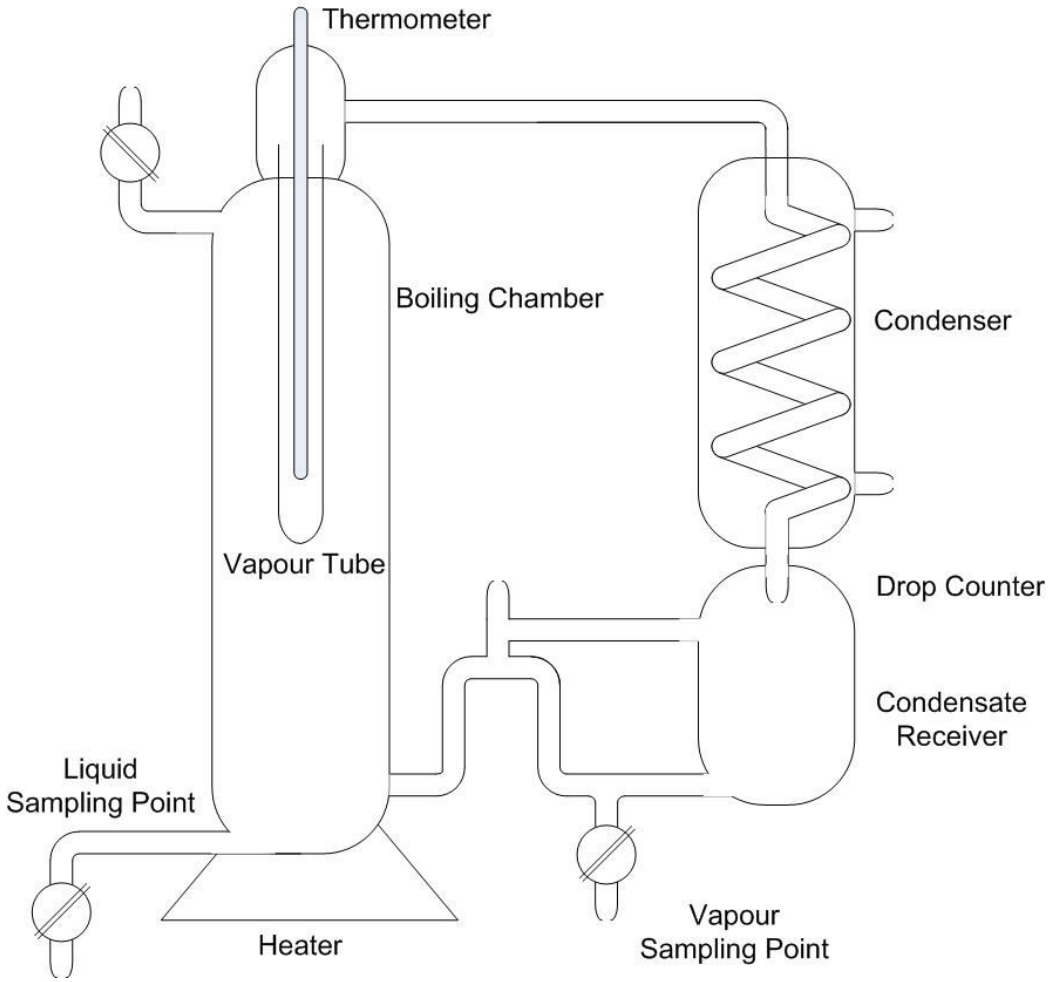

Figure 3.2: Dynamic VLE still based on Othmer principle. Figure redrawn and adapted from Raal & Mühlbauer (1998)

The structure of the Othmer still raises numerous concerns surrounding the reliability and accuracy of generated data (Raal & Mühlbauer, 1998).

- For a start, the vapour condensate receiver was found to be too large and raised the question of whether the vapour sample taken here was in fact in equilibrium with the liquid charge in the boiling flask.
- A major fault with the large boiling chamber is the likelihood of partial condensation of the vapour phase on the chamber walls. Any such condensate formation will inherently alter the equilibrium of the system and thus the measured equilibrium composition. Compensation for this in the form of a vacuum jacket is possible, although over compensating may lead to the wall being superheated; any splashing of liquid droplets on the walls could result in flashing of the liquid phase and produce the opposite problem.
- Accurate temperature measurement necessitates contact between the temperature probe and both equilibrium phases; in the Othmer still, only vapour phase temperature measurement is accounted for.

- The lack of stirring in the boiling chamber raises concerns of possible temperature profiles in the liquid charge. Combined with the overly large condensate receiver, this could result in flashing of a volatile rich vapour return upon contact with the liquid in the boiling chamber.

The aforementioned design flaws in the Othmer still have resulted in use of this design being discontinued for the generation of accurate phase equilibrium measurements. The circulation of only the vapour phase is simply inadequate for the generation of accurate phase equilibrium data. The circulation of both phases however, is a much more suitable alternative and was the principle behind the design of the Gillespie still.

3.3.2. Gillespie Dynamic Still

The circulation of both phases was originally pioneered by Lee (1931) through the use of a Cottrell tube. This device, developed by Frederick Cottrell (1919) is a simple tube responsible for drawing a column of liquid with slugs of vapour into contact with the thermometer to give an accurate reading of the equilibrium temperature. The movement of the vapour with entrained liquid provides time for mass transfer between the phases and equilibrium concentrations to be achieved at the temperature recorded by the thermometer over which the phases pass. Gillespie (1946) built on the design of Lee by separating the entrained liquid from the gas, as depicted in Figure 3.3.

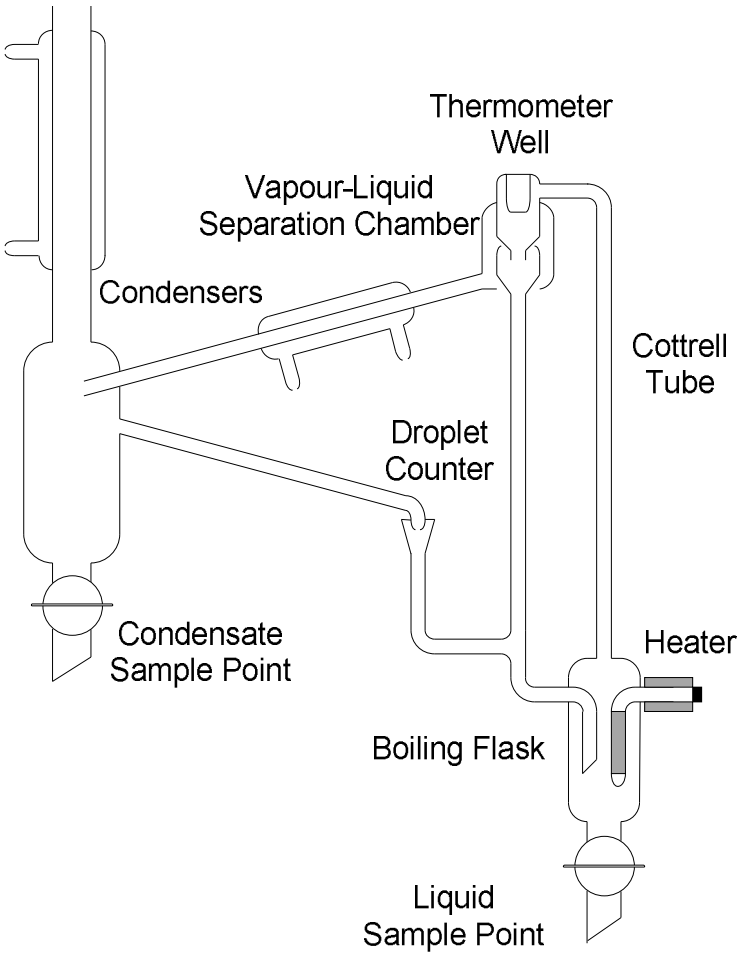

Figure 3.3: Original dynamic Gillespie VLE still. Figure redrawn and adapted from Raal & Mühlbauer (1998)

Here, the boiling mixture is pumped by the Cottrell tube and sprayed over the thermometer in the vapour-liquid separation chamber. The liquid returns to the boiling chamber while the vapour is condensed and passed through a condensate receiver before being returned to the boiling chamber. The original design, as presented in Figure 3.3. still exhibited certain design flaws (Raal & Mühlbauer, 1998):

- The liquid sample drawn from the boiling chamber is not the same as the liquid in equilibrium with the vapour sampled from the condensate trap.
- Partial condensation of the equilibrium vapour phase needed to be prevented through insulation of the separation chamber.
- The sampling procedure associated with the still disturbs its steady state operation and thus affects the measured equilibrium.

Subsequent modification of the Gillespie dynamic VLE still was performed by multiple authors in subsequent publications where the abovementioned shortcomings were addressed. This included the provision of a liquid sampling port following the vapour-liquid separation chamber; a smaller condensate receiver, with an equivalent liquid receiver, to allow for uninterrupted operation during sampling; insulation of necessary components of the still and mechanical stirring in the boiling chamber to ensure uniform liquid charge temperature. The reader is referred to the works of Malanowski (1982) and Raal & Mühlbauer (1998) for more information on the development of these changes.

Raal & Mühlbauer raise concern over the ability of a normal Cottrell tube to provide the necessary contact time and interfacial area required to achieve equilibrium. To this end authors have incorporated various means of increasing the interfacial area and contact time that the equilibrium phases have before being passed over the temperature measurement unit and ultimately split and returned. One such work was that by Yerazunis *et al.* (1964) who considered a packed vapour-liquid separation chamber, a design more recently modified and employed by the research group of Raal (Raal & Mühlbauer, 1998), who noted that employing a spirally curved Cottrell tube could achieve the same end.

While a packed chamber or a spiral Cottrell tube represent the most efficient means of low pressure vapour liquid equilibria measurement, it is the Gillespie principle that forms the foundation of the best available means of generating accurate isobaric phase equilibrium data. A Gillespie dynamic VLE still is employed for the generation of isobaric VLE data in this work, and is presented in Chapter 4.

3.4. Experimental Rationale

For isobaric experiments, the choice of system operating pressure is a balance between ensuring the presence of azeotropic behaviour and keeping the system temperatures low enough to minimise temperature gradients and thus heat losses from the apparatus. For azeotropic behaviour to be in evidence, the ketone isomers would need to be paired with n-alkanes exhibiting a similar boiling point. To this end, n-octane, n-nonane and n-decane were selected and an operating pressure of 40kPa chosen. With boiling points of 119°C, 115°C and 113°C for 2-, 3- & 4-heptanone and 95°C, 119°C and 141°C for n-octane,

n-nonane and n-decane respectively at this chosen pressure, these conditions were deemed ideally suited to the intentions of the experimental study and selected for this work.

3.5. Thermodynamic Consistency

Before the phase equilibria of any binary system can be considered accurate and later modelled, the reliability of the data needs to be tested for their conformance to our understanding of the physical phenomena responsible for the generation of that data. Thermodynamic consistency tests are a means by which the validity of experimental phase equilibria data are tested for their conformance to thermodynamic principles, in particular, the Gibbs-Duhem equation (Sandler, 2006):

$$0 = -\left(\frac{\partial \overline{\theta}}{\partial T}\right)_{P,N_i} dT - \left(\frac{\partial \overline{\theta}}{\partial P}\right)_{T,N_i} dP + \sum x_i d\overline{\theta_i} \tag{3.1}$$

The Gibbs-Duhem equation is a thermodynamic consistency relation which states that the partial properties of species making up a solution are not independent of each other (Smith *et al.,* 2005). Data that obey the Gibbs-Duhem equation are considered thermodynamically consistent, with no significant experimental error inherent and thus suitable for modelling purposes. Applying this relation to the excess Gibbs energy, and employing the appropriate thermodynamic relations yields (Sandler, 2006):

$$0 = \frac{\underline{H}^{ex}}{RT^2} dT - \frac{\underline{V}^{ex}}{RT} dP + \sum x_i d \ln \gamma_i \tag{3.2}$$

where $\underline{H}^{ex}$ and $\underline{V}^{ex}$ are the heat and volume of mixing respectively. For the special case of isothermal and isobaric conditions in a binary mixture, Equation 3.2 reduces to:

$$0 = x_1 \frac{d \ln \gamma_1}{dx_1} + x_2 \frac{d \ln \gamma_2}{x_1} \tag{3.3}$$

Values of the activity coefficient, and hence $ln\gamma_i$, can be determined from experimental data. Because this determination is independent of the Gibbs-Duhem equation, and the Gibbs-Duhem equation needs to be satisfied for data to be considered thermodynamically consistent, the relation presented in Equation 3.3 serves as a basis from which thermodynamic consistency tests can be derived. One such test is that of McDermott and Ellis (1965) and is presented in the following section.

3.5.1. McDermott-Ellis Consistency Test

The McDermott-Ellis consistency test is derived through integration of Equation 3.3 over all considered data points using the trapezoidal rule for integration, the result of which is (McDermott & Ellis, 1965):

$$0 = \sum_{i=1}^{N} (x_{ic} + x_{id})(\ln \gamma_{id} - \ln \gamma_{ic}) \tag{3.4}$$

Here, the summation is over all components for consecutive pairs of data points, *c* and *d*. While strict adherence to Equation 3.4 will confirm thermodynamic consistency of the data, this restriction is rather too limiting for experimental data where inherent procedural error is present. McDermott and Ellis however, chose to use the test on a point-to-point basis, considering each pair of consecutive data separately to identify inconsistent data as they appear (Sandler, 2006).

The criteria for judging between consistent and inconsistent data, according to the authors, is dependent upon the accuracy with which the vapour and liquid fractions are reported, giving the example of a maximum deviation in Equation 3.4 of 0.01 for accuracies in composition of ±0.001 (McDermott & Ellis, 1965). This criteria was later refined by Wisniak and Tamir (1977), who argued that the maximum deviation should not be considered a constant, but rather a function of the accuracies of the considered parameters, according to:

$$\begin{aligned} 0 = \sum_{i=1}^{N}(x_{ic}+x_{id})\left(\frac{1}{x_{ic}}+\frac{1}{x_{id}}+\frac{1}{y_{ic}}+\frac{1}{y_{id}}\right)\Delta x \\ + 2\sum_{i=1}^{N}|\ln\gamma_{id}-\ln\gamma_{ic}|\Delta x + \sum_{i=1}^{N}(x_{ic}+x_{id})\frac{\Delta P}{P} \\ + \sum_{i=1}^{N}(x_{ic}+x_{id})\beta_i\left(\frac{1}{|T_c+\delta_i|^2}+\frac{1}{|T_d+\delta_i|^2}\right)\Delta T \end{aligned} \tag{3.5}$$

where the ∠ terms are the accuracies of the measured mole fractions, pressure and temperature; and β_i and δ_i are the B_i and C_i constants of the component in question respectively.

The McDermott-Ellis consistency test presented here is a member of one of two broad classes of consistency tests, namely a point-to-point consistency test. The other broad class is the area test which aims to minimise the total deviation of all points from the Gibbs-Duhem equation, as per Equation 3.4. A thermodynamic consistency test that incorporates such a test is highlighted in the following section.

3.5.2. L/W Consistency Test

The starting point for the development of an area test is reconsideration of the Gibbs-Duhem equation in Equation 3.2. Integration of this equation over the entire composition range in a binary system yields:

$$\int_0^1 \ln\frac{\gamma_2}{\gamma_1}dx_1 = -\int_{T(x_1=0)}^{T(x_1=1)}\frac{\bar{H}^{ex}}{RT^2}dT + \int_{P(x_1=0)}^{P(x_1=1)}\frac{\bar{V}^{ex}}{RT}dP \tag{3.6}$$

Again, considering the isothermal and isobaric case, the integral reduces to:

$$\int_0^1 \ln\frac{\gamma_2}{\gamma_1}dx_1 = 0 \tag{3.7}$$

This equation is the basis for the area test for thermodynamic consistency; a plot of $ln(\gamma_2/\gamma_1)$ vs. x_1 yields a curve which crosses the x-axis somewhere along the composition spectrum. Theoretically, if the areas above and below the axis are equal, the data is considered thermodynamically consistent (Wisniak, 1994).

In true vapour-liquid equilibria experiments however this form of the equation is inapplicable as only one of temperature and pressure are held constant (the isothermal and isobaric cases respectively). In the isothermal case, the excess volume function may safely be assumed constant and thus Equation 3.7 holds and is a valid test for thermodynamic consistency (Wisniak, 1994). In the isobaric case however, the heat of mixing can almost never be neglected and thus needs to be accounted for. This is a significant hurdle as heat of mixing data is rarely available for the whole composition spectrum for a mixture, limiting the applicability of area tests to test for thermodynamic consistency in isothermal VLE experiments.

Wisniak took a different approach in the consideration of isobaric thermodynamic consistency testing by considering the relationship between the excess Gibbs free energy of a mixture and its boiling point at equilibrium rather than the Gibbs-Duhem equation (Wisniak, 1993). This is an important point to note as, because the model is not a direct derivative of the Gibbs-Duhem equation, data tested using the resulting model cannot be considered thermodynamically consistent on the basis of the results of this test alone. The relevant $\underline{G}^{ex}$-T relationship is presented in Equation 3.8:

$$\underline{G}^{ex} = RT \sum_i x_i \ln \gamma_i \tag{3.8}$$

Wisniak then applied the following assumptions to the formulation (Wisniak, 1993):

- All nonidealities of the fluid are concentrated in the liquid phase
- Heats of vaporisation of each component are either considered constant or an average value for the range of boiling points used
- Liquid molar volume is negligible compared with that of the vapour

The first assumption allows one to define the activity coefficient according to Equation 3.9, with the second and third allowing for the applicability of the Clausius-Clapeyron equation to estimate the ratio of the pure component vapour pressures to the total pressure according to Equation 3.10:

$$\gamma_i = \frac{y_i P}{x_i P_i^{vap}} \tag{3.9}$$

$$\ln \frac{P}{P_i^{vap}} = \frac{\Delta H_i^{vap}\left(T_i^{vap} - T\right)}{RT_i^{vap}T} = \frac{\Delta S_i^{vap}\left(T_i^{vap} - T\right)}{RT} \tag{3.10}$$

Here, the enthalpy and entropy terms are those of vaporisation, with P^{vap} and T^{vap} the vapour pressure and boiling point of the pure component. These equations may be incorporated into the expression in for the molar excess Gibbs free energy in Equation 3.8 to yield:

$$\underline{G}^{ex} = \sum_i x_i \Delta S_i^{vap} \left(T_i^{vap} - T\right) + RT \sum_i x_i \ln\left(\frac{y_i}{x_i}\right) \tag{3.11}$$

Wisniak defined the following two parameters:

$$\Delta S = \sum_i x_i \Delta S_i^{vap} \tag{3.12}$$

$$w = \sum_i x_i \ln\left(\frac{y_i}{x_i}\right) \tag{3.13}$$

to derive an expression for the bubble point of the mixture derived from Equation 3.11 (Wisniak, 1993):

$$T^{bub} = \sum_i \frac{T_i^{vap} x_i \Delta S_i^{vap}}{\Delta S} - \frac{\underline{G}^{ex}}{\Delta S} + \frac{RTw}{\Delta S} \tag{3.14}$$

It is this expression that is used by Wisniak to produce his thermodynamic consistency test. Rearranging and applying this relation to each equilibrium pair of vapour-liquid equilibrium data, *k*, yields (Wisniak, 1993):

$$L_k = \sum_k \frac{T_i^{vap} x_i \Delta S_i^{vap}}{\Delta S} - T^{bub} = \frac{\underline{G}^{ex}}{\Delta S} - \frac{RTw}{\Delta S} = W_k \tag{3.15}$$

Integration of each side of the equation over the whole composition range results in values of *L* and *W*, for which the test is named:

$$L = \int_0^1 L_k dx_1 = \int_0^1 W_k dx_1 = W \tag{3.16}$$

Thus equality of *L* and *W*, having been derived from an equilibrium expression, serves as a test for equilibrium and thus thermodynamic consistency of experimental data. As with the Gibbs-Duhem equation, the constraint of equality between *L* and *W* is rather too limiting for real experimental data considering procedural error; however which of the two contains the error cannot be determined, and so a deviation is defined (Wisniak, 1993):

$$D = 100 \frac{|L - W|}{L + W} \tag{3.17}$$

Wisniak proposes a maximum value for *D* of *3* to *5* to indicate thermodynamic consistency, with the lower limit based on the limits for the Herrington area test and the higher suggested to incorporate the uncertainty introduced when heats of vaporisation are unknown and must be estimated (Wisniak, 1993).

It was stated previously that the L/W test incorporates aspects of both an area test and point-to-point test. The former is due to the criteria placed on the value of *D* for the experimental data across the

whole composition range, while the latter arises due to the need for Equation 3.15 to be satisfied at every experimental point. This is a particularly useful aspect of the L/W consistency test as inconsistent data may be discarded as they arise. Finally, it is again emphasised that, because the L/W test was not derived from the Gibbs-Duhem equation, data proven consistent using this test may not necessarily adhere to the Gibbs-Duhem equation. Thus the L/W test should be used in conjunction with such tests as the McDermott-Ellis test considered in the previous section.

3.5.3. Summary of Thermodynamic Consistency

Thermodynamic consistency testing provides a means of testing the degree of experimental error in phase equilibria data and its adherence to the theoretical understanding of equilibrium conditions. Consistency of VLE data is an integral part of presenting phase equilibria data as it is the only means by which we can show the experimental data to be truly representative of the system dynamics.

It is important to note, however, that while experimental data have to be shown to be thermodynamically consistent, this condition is necessary but not sufficient to prove data is accurate. For this reason, where possible, data should be compared to existing measurements under similar conditions to improve confidence in the data. It is this last point that gives rise to the need for equipment verification, whereby the still being used is shown to produce accurate data by reproducing reliable data available in the literature.

Chapter 4 Materials & Methods

With the premise for the work presented in this thesis covered in the previous Chapters, focus now shifts to the means by which the work was done and the results obtained. In the sections that follow, the materials and apparatus used and the methods employed to meet the experimental objectives of the work are presented.

4.1. Materials

Table 4.1 lists the chemicals that were utilised in this study, with their assay and supplier listed.

Table 4.1: List of chemicals used in the experimental work and their suppliers

Component	Assay	Supplier
Ethanol	≥99.8%	Sigma Aldrich
1-Butanol	99.9%	Sigma Aldrich
2-Ethyl-1-hexanol	≥99.6%	Sigma Aldrich
n-Heptane	≥99%	Sigma Aldrich
n-Octane	≥99%	Merck
n-Nonane	≥99 %	Merck
n-Decane	≥99%	Sigma Aldrich
2-Butanone	≥99%	Sigma Aldrich
2-Heptanone	99%	Sigma Aldrich
3-Heptanone	98%	Sigma Aldrich
4-Heptanone	98%	Sigma Aldrich

Technical grade nitrogen (Afrox) was used for overpressure control in the phase equilibrim still, with ultra high purity helium and technical grade air (both Afrox) used for gas chromatography.

4.2. Apparatus

An all-glass dynamic recirculating still has been used to measure VLE data and is presented graphically in Figure 4.1. It is a commercial still (VLE 100 D) manufactured by Pilodist of Germany and a brief review of its operation is presented below.

4.2.1. Unit Description

With reference to Figure 4.1, whose full legend is provided in Appendix A, an electrical immersion heater (10) installed concentrically into the flow heater (1.3) supplies the heat necessary to partially evaporate the liquid mixture. Before entering a separation chamber, the vapour-liquid mixture passes through a spirally curled Cottrell tube (1.2) which allows for concentrated phase change. The separation chamber is constructed in a manner such that the entrainment of liquid drops in the vapour phase, or partial condensation of the vapour phase is prevented. The two-phase mixture is subsequently passed over the thermometer (7) for measurement of the equilibrium temperature. At this point, the phases are split, condensed and returned to the mixing chamber (1.1) where the mixture is mechanically stirred using a magnetic stirrer before being returned to the immersion heater and the circulation

procedure repeated. The still was modified to house an ultrasonic homogeniser (17) adjacent to the feed heater (1.3) to aid in the measurement of vapour-liquid-liquid equilibrium data. While the homogeniser is not used in this work, it is necessary to keep it fitted to the still to keep the unit sealed.

Equilibrium is achieved rather quickly (approximately 1 hour) due to continuous circulation of both vapour and liquid phases, according to the Gillespie principle, as well as the intense mechanical stirring of the relatively small liquid inventory. The unit is installed in an extraction cabinet for safety reasons, considering the flammable nature of the components being used. The maximum operating temperature of the still is 250°C, with the equilibrium temperatures measured using a Pt-100 probe connected to a digital Hart Scientific thermometer with an accuracy of 0.03°C at 0°C according to the original certificate of calibration.

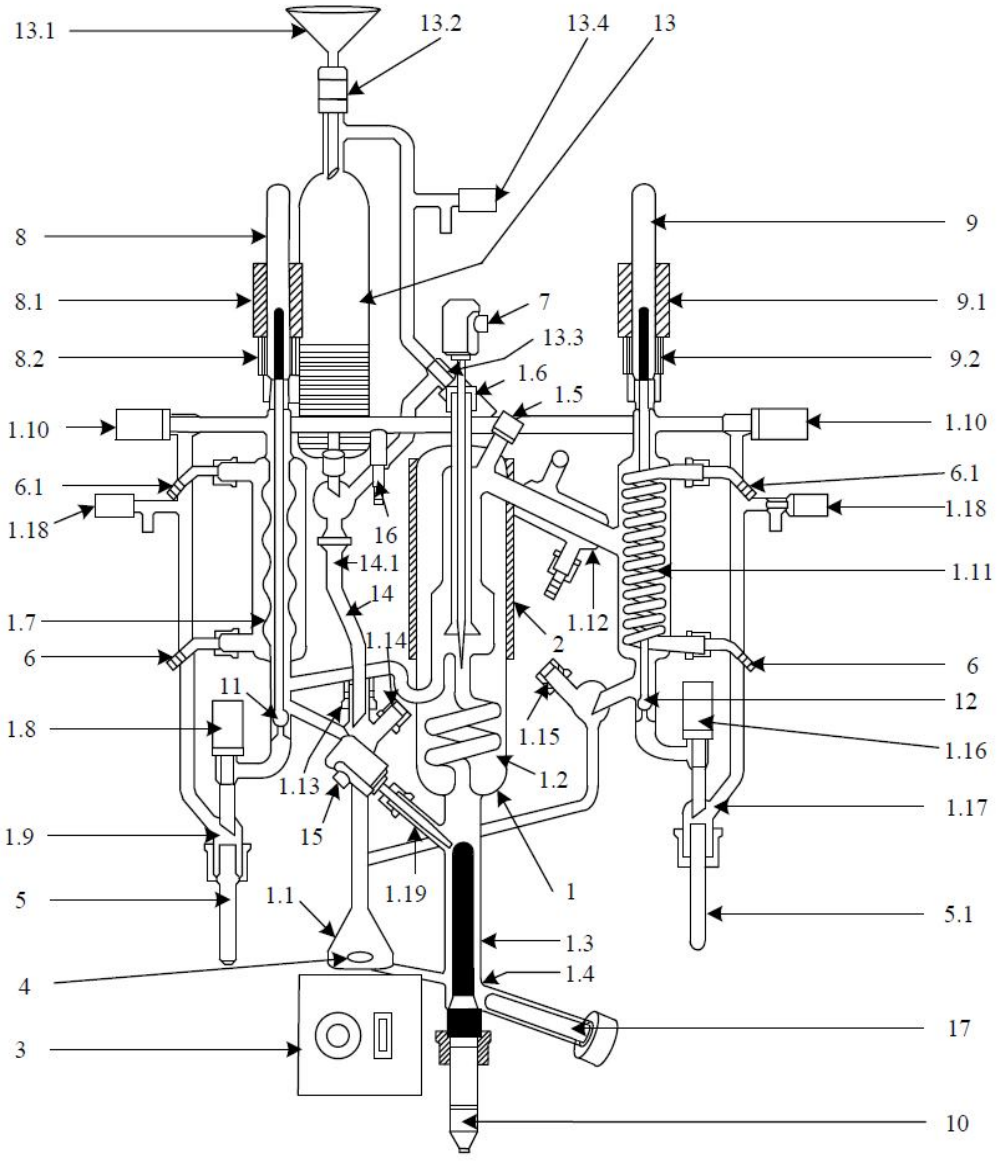

Figure 4.1: Schematic representation of the Pilodist dynamic recirculating still used for VLE measurements. Figure reprinted with permission (Pienaar, 2011)

4.2.2. System Modification

Originally, the system comprised two separate pressure transmitters; an overpressure transmitter (1bar abs ≤ P ≤ 4bar abs) at a quoted accuracy of 0.35% of full scale output (max 14mbar error) and an absolute pressure (0bar abs < P ≤ 1bar abs) for vacuum operation at a quoted accuracy of 0.1% of full scale output (max 1 mbar error). The overpressure transmitter was deemed not accurate enough considering the nature of the work to be performed on the still and so it was deemed necessary to replace it. In addition, while the accuracy of the vacuum transmitter was appropriate, the upper limit of its operable region meant that the accuracy was called into question during system verification, where runs were performed at 94 kPa or 94% of the maximum operating pressure. The solution was to replace the two separate pressure transmitters with a single unit having an acceptable accuracy over the extended pressure range. The installed Wika UT-10 unit has a maximum operating pressure of 1.6bar abs with a quoted accuracy of 0.1% of full scale output (max 1.6mbar error) according to the certificate of calibration. The temperature probes were also recalibrated at this time, with the vapour temperature probe found to have drifted since the previous calibration. All certificates of calibration can be found in Appendix B.

Changing the two pressure transmitters for a single unit necessitated changes to the hydraulic setup, details of which can be found in Appendix A, but also raised a problem regarding operation and control of the still. Under the original setup, pressure was measured and controlled using the Pilodist M101 pressure control system; specifically, the vacuum pump was operated by the system software which received a signal from the pressure transmitter and turned the pump on or off accordingly. Thus, simply removing the original transmitters was not an option; instead, the new transmitter needed to be installed parallel to the existing transmitters, the former giving the pressure measurement and the latter only present to ensure pump operation. Further, pressure control is achieved manually under the new setup, with a pressure set point chosen lower than the intended pressure and the amount of vacuum drawn throttled manually, as detailed below.

4.3. Experimental Procedure

In this section, a brief description of the experimental procedure is presented, with a more thorough and in-depth procedure presented in Appendix A. All numerical references in the procedure detailed below refer to Figure 4.1.

4.3.1. Preliminaries

Prior to operation of the still under either vacuum or overpressure conditions, it should be ensured that the still is dry to prevent contamination. If necessary, compressed air may be passed through the still to ensure this is the case. Under vacuum conditions, maintenance of the vacuum pump should be ensured while for overpressure, the nitrogen canister should be opened. Finally, the tap should be opened to ensure cooling water is passed through the cooling coils and condensers (1.11 & 1.12). The still can now be turned on and the controlling software opened.

4.3.2. Still Preparation

The intended operation of the still (vacuum vs overpressure) should be selected both on the hydraulic box of the still and within the software. With respect to the still itself, the homogeniser should be fitted and secured, with the discharge valve (1.4) closed prior to introduction of the feed mixture. Approximately 110mL can be charged to the feed burette, although this amount is variable according to the volatility of the mixture and the intended operation of the still. The feed volume should be sufficient to completely submerge the immersion heater (10) once introduced to the mixing chamber (1.1). The magnetic stirrer (3) should then be turned on to ensure constant mixing of the feed.

With respect to the software, set points for the operating pressure, heater power and mantle temperatures need to be set. These are once again dependent on the feed composition (and volatility) as well as the intended operating conditions. The heater power setting is input as a percentage and controls the heat supplied to the feed, which subsequently controls the temperature to which the feed is heated. If the power is set too low, the feed will not vaporise while if set too high, there will be no liquid return. Thus a balance needs to be found during operation to ensure a consistent return of both phases to be sampled. For the purposes of this study, the following approximate settings were employed:

- ~30% for n-Heptane/Butanone and Ethanol/1-Butanol at 1atm
- ~40% for heptanone mixtures with n-Octane at 400mbar
- ~50% for heptanone mixtures with n-Nonane at 400mbar
- ~60% for heptanone mixtures with n-Decane at 400mbar

For systems where the vapour temperature exceeds 100°C, use is made of the mantle heater to prevent partial condensation of the vapour phase on the mantle walls. Typically, the mantle temperature need only be set ~15°C lower than the vapour temperature to compensate for the simple on-off control of the heater.

The pressure set point is set to the pressure at which the work will be performed. With the systems modifications made however, pressure measurement and control is independent of the VLE software. For overpressure conditions, pressure control is achieved by balancing the amount of nitrogen entering the system through the overpressure regulator on the hydraulic box with that leaving through the aeration valves (1.18). For vacuum conditions, manual pressure regulation is achieved by setting the pressure set point approximately 50 mbar lower than the intended value to ensure constant operation of the vacuum pump, while the intended value can be achieved by regulating the amount of vacuum drawn on the system using the vacuum regulator valve on the hydraulic box. The maximum deviations in pressure associated with this manual control were ±2mbar, although this is considered a conservative estimate of the maximum fluctuations. The significance of these pressure fluctuations will be discussed further in Section 4.4.

4.3.3. Experimental Runs

The apparatus can be started through the software package. Under the appropriate power settings, liquid return should begin within 5 minutes of operation while vapour return should be evident within 20 minutes (depending on the boiling temperature and the ambient temperature of the feed). The concave nature of the sample wells (11 & 12) necessitates periodic flushing to prevent sample contamination. Flushing should be done approximately every 20 minutes, including immediately prior to sampling by:

- First, opening the solenoid valves (9) on both the vapour and liquid arms of the still using the remote control found on the floor of the extraction cabinet. The valves need only be opened briefly to wash away any liquid present around the well opening.
- The flushed liquid should be drained into the respective glass receiver vials (5 & 5.1) through the respective stop valves (1.8 & 1.16).
- Both under vacuum and at overpressure, the glass receiver vials need to be isolated before being removed from the still. Once the liquid has been collected within the glass receiver vials, the isolation valves (1.10) need to be shut before the aeration valves (1.18) are opened. This will break vacuum or release overpressure (as appropriate) within the sampling arms of the still, allowing the vials to be removed and the waste to be discarded. Upon replacing the vials, the aeration valves can be closed and the isolation valves opened to bring the arms back to system pressure.

Equilibrium is achieved within the still after approximately 60 minutes and is indicated by a steady vapour temperature recorded by the software. A steady return of both phases is necessary for accurate sampling, with a vapour return of no less than 30 drops per minute required for a large enough sample for GC analysis. Before taking vapour and liquid samples, the wells need to be flushed per the description given above. Samples are taken according to the same procedure detailed for flushing above, with the obvious exception that the collected samples are stored for analytical sample preparation rather than discarded. The vapour temperature should be monitored while the solenoid valves are opened to ensure its stays constant during sampling, as this temperature is the boiling temperature for the samples taken.

Once the sample has been taken, the particular experimental run has concluded and still operation can be stopped through the software package. Between experimental runs on a given day, the still needs to be brought back to ambient pressure before additional feed can be introduced. For overpressure operation, this is a simple matter of steadily closing the overpressure throttling valve on the hydraulic box, while for vacuum operation, the aeration valves (1.18) can be slowly opened to return the system to ambient pressure. The amount of additional feed required between runs is only that volume which will ensure complete submergence of the immersion heater (10) (generally ~10mL). With fresh feed added, it is possible to begin the next run according to the same method described here.

4.3.4. Draining and Washing

At the end of a day of experiments, the feed may be left in the still overnight if the intention is to carry on experimenting with a feed of a similar composition the following day. If, however, it is desired to begin experiments anew from the opposite end of the composition spectrum, it is necessary to drain and wash the still at the end of a day's runs. The purpose of washing the still is simply to remove any non-volatile liquids that would otherwise remain in the still overnight and result in contamination of the feed mixture in the next experimental run.

To this end, the mixture, mantle and immersion heater should be allowed to cool to ambient temperature before being drained through the discharge valve (1.4). Wash acetone (~110mL) can then be charged to the still and run for a period of 30 minutes at ambient pressure, with the appropriate pressure operation selected within the software. The solenoid valves should be opened during this period to ensure the sample wells are also washed with the resulting collected acetone discarded as per the flushing procedure. Afterwards, the acetone should similarly be allowed to cool before being drained, all aeration valves opened and the still left to dry overnight.

4.3.5. Analysis

Sample concentrations were quantified through gas chromatography using a Varian CP-3380 GC with a flame ionisation detector. A ZB Wax capillary column with dimensions 30m x 0.32mm x 1μm operated at a temperature of 250°C was used to quantify component concentrations in the experimental vapour and liquid phases. To this end, use was made of an internal standard, i.e. 2-butanone for n-octane containing systems and n-heptane for n-nonane and n-decane systems. Gas chromatography samples were prepared as follows:

- Sample vials were loaded with ~1.5mL of solvent, i.e. 2-ethyl-1-hexanol.
- Approximately 30mg of internal standard was added to the solvent, measured accurately to 10^{-5} g.
- Approximately the same mass of vapour/liquid sample was added to the solvent.

Each experimental run produced one vapour and one liquid sample from which to produce analytical samples. Two such analytical samples were prepared per phase with the average of the two samples reported as the experimental result for that phase.

Quantification was achieved by making use of a calibration curve based on responses for each system relative to its respective internal standard response at separate points along the compositional spectrum. Given that each mass of component will produce a distinct peak area and that the ratio of peak areas is proportional to the ratio of component masses, a calibration curve of the following form can be generated:

$$\frac{Area_{std}}{Area_{comp}} = m\frac{mass_{std}}{mass_{comp}} \tag{4.1}$$

Using samples of known mass, the response factor, *m*, can be determined for each component in each system and the above equation used to quantify the unknown masses of these components in the experimental vapour and liquid samples. Three samples of known mass for each binary system, lying at different points along the composition range, were run through the GC five times each to generate average points to which a straight line of the above form could be fit. Details of the response factor determination can be found in Appendix C, while an analysis of the compositional error is presented below.

4.4. Compositional Error Analysis

The major contributors to the quoted compositional error are those errors arising from the experimental conditions and those associated with the analysis procedure.

4.4.1. Experimental Effects

The inputs to the system during the experimental runs invariably have an impact on the experimental outputs. As an output, the equilibrium compositions are thus subject to errors associated with inputs to the VLE system and those associated with the compositional analysis. Operation of the still, as described above, is dependent on two user controlled factors, specifically the heater power and the isobaric pressure of the system. As the heater power is not variable during the running of the still, its impact on compositional error can be considered negligible. The effect of pressure fluctuations cannot be treated in the same way and have to be accounted for.

As previously stated, the maximum pressure deviations in the still were estimated to be ±2mbar. As will be presented later, but produced in Figure 4.2 for the purposes of the analysis here, the sPC-SAFT$_{JC}$ model produces an excellent prediction of the n-nonane/2-heptanone VLE data. This system exhibits large deviations from ideality as well as the smallest temperature range and will thus demonstrate the greatest pressure effects on the equilibrium compositions of all the considered systems. If we consider the model predictions of sPC-SAFT$_{JC}$ for the cases of maximum pressure deviation, the plots in Figure 4.2 result. Thus, the compositional deviations associated with the worst-case pressure fluctuations can be determined by considering the composition at a given temperature for each prediction (here, 0.013 mole fraction). This indicates that the pressure fluctuations may significantly influence the compositional accuracy, producing errors that are traditionally of the same order of magnitude associated with purely analytical error.

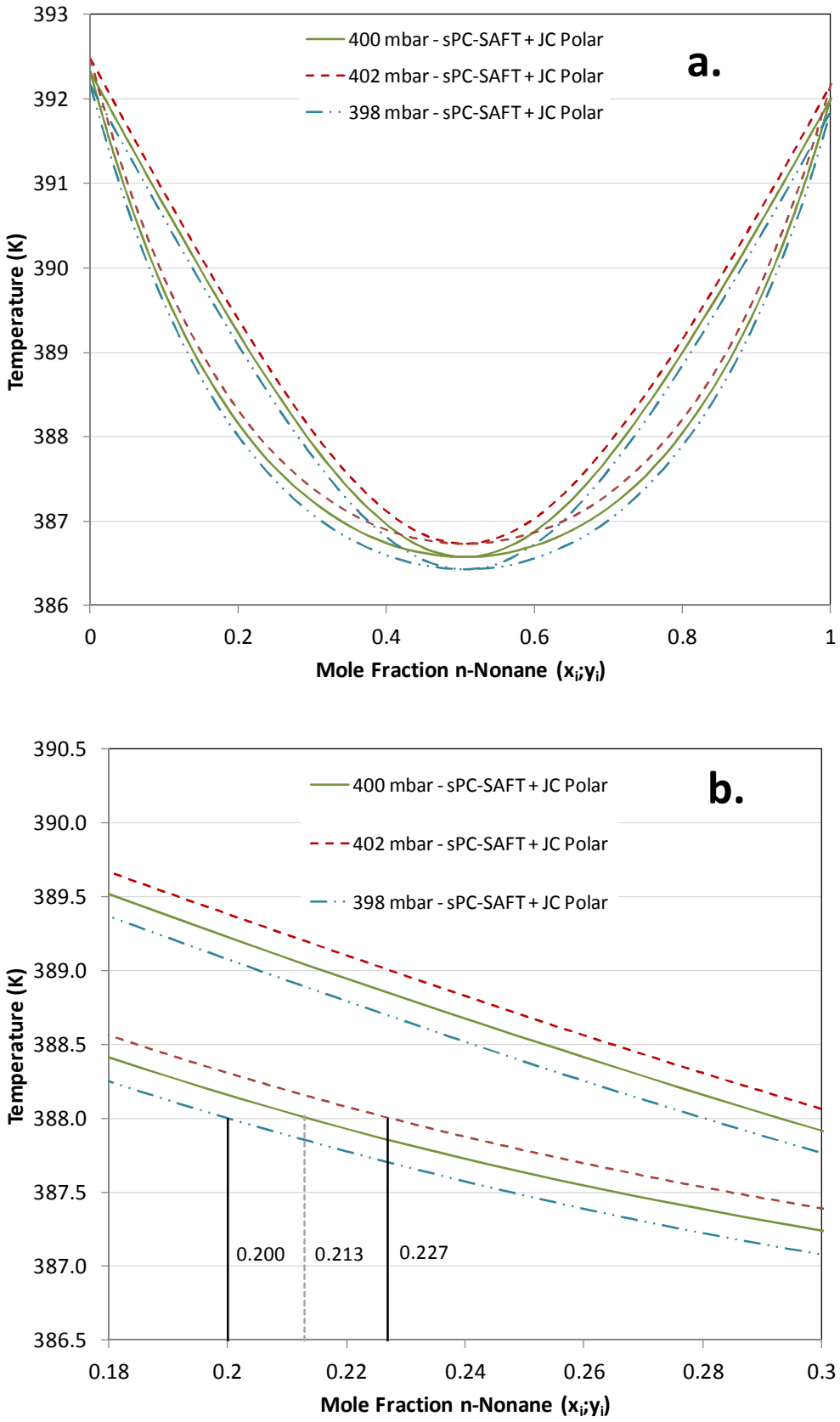

Figure 4.2: (a.) Effects of worst case pressure deviations on associated equilibrium composition measurements. (b.) Representative section of worst case deviations highlighting effects of pressure deviations on reported composition

However, as also previously mentioned, the ±2mbar case is a conservative estimate for the pressure fluctuations as, in general, control was maintained well within this value. To get an idea of the expected effect of pressure fluctuation on the equilibrium composition, we can consider the experimental output, specifically the vapour temperature. If we assume variations in the temperature are a direct result of the pressure fluctuations, we can get a better idea of the instantaneous pressure fluctuations and thus, in the manner demonstrated in Figure 4.2, an idea of the expected compositional error associated. This assumption is justified as thermal equilibrium is slower than mechanical equilibrium, with chemical equilibrium slower still and thus the compositional fluctuations will be slower than the pressure fluctuations and average out in a smaller range.

In general, fluctuations in temperature of 0.02°C were apparent just prior to sampling. If Figure 4.2b is reconsidered, the phase envelopes passing through the same sample composition at 0.02°C higher and lower may be plotted (diamonds of Figure 4.3), the corresponding pressure of these phase envelopes giving the true pressure fluctuations during sampling procedure. In this case, as apparent from Figure 4.3, the instantaneous pressure fluctuations are much smaller than the aforementioned 2mbar, with deviations of 0.2mbar seen to be the case. The associated compositional error can be achieved in the same manner is illustrated in Figure 4.2; for a given temperature (388 K), the predicted composition of the higher and lower pressure envelopes (circles in Figure 4.3) can be determined, with the associated deviation calculable from the model for the experimental data, here 0.002 mole fraction.

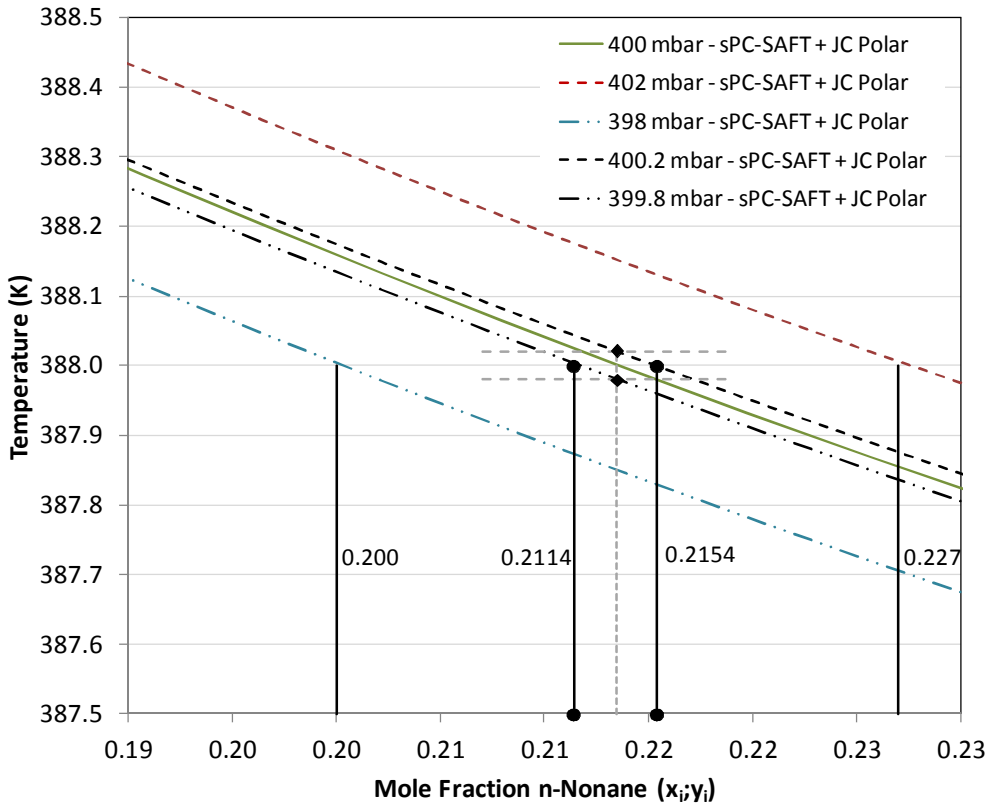

Figure 4.3: Effects of expected pressure deviations on associated equilibrium composition measurements. Phase envelopes indicated are those for the liquid phase, although an equivalent analysis could have been made in the vapour phase.

The analysis presented here was for the liquid phase in the low n-nonane concentration side of the azeotrope. Analysis of the vapour phase at the same sample temperature would have yielded an error of the same order of magnitude. It is true that worse deviations than those reported here could have been obtained closer to the azeotrope, but better ones were also possible if the sample point was taken closer to the pure component regions. Furthermore, incorporating a more ideal system would have negated the large errors associated with analysing the azeotropic region in the manner presented here completely. The selection of the region to analyse was thus made on the basis of an average applicable to the whole concentration range.

4.4.2. Analysis Effects

The preparation and running of analytical samples introduces a further source of possible compositional error. The determination of calibration curves, as presented in Appendix C, is of vital importance for any degree of confidence in reported concentrations from gas chromatography. However, these calibration curves can drift over time, due to wear and tear in the column and the running of different systems through the same column to name but two factors associated with this work. Thus it is also important to test the reproducibility of GC data once the analytical samples of a particular system have been analysed to quantify any drift in the GC predictions over time.

To this end, after each binary system's experimental samples had been run, three samples of known mass at different points along the composition spectrum were prepared and run through the GC using the same calibration curves generated for that system. In this manner, deviations in the predictions for each system could be determined and the maximum deviation based on the analysis procedure across all nine binary systems could be quantified. The full results of this error analysis are provided in Appendix C, resulting in a maximum analytical error of ±0.02 mole fraction.

4.4.3. Summary

While the errors associated with experimental effects and deviations in sample analysis are different by an order of magnitude, the former cannot be neglected in light of the latter. The compositional errors are additive; any compositional error introduced by pressure fluctuations during the still operation need to be added to those associated with the analysis of the samples. Thus, the total compositional error reported for this work is ±0.022 mole fraction. While this mole fraction is, in general, an order of magnitude higher than that which is typically reported for VLE measurements in the literature, it is believed to encompass the combined effects of all physical fluctuations and deviations on the experimental compositions.

Chapter 5 Experimental Results

With the means and methods detailed in the previous chapter, attention shifts now to the results of the experimental study. In this chapter, the VLE data for each of the nine systems detailed in Table 1.1 are presented and the observable phase behaviour analysed. Before new vapour-liquid equilibrium data could be generated however, system verification was necessary to provide a degree of confidence in the data generated by this study.

5.1. Verification

The choice of system for equipment verification was originally a system comprising molecules which would exhibit similar interactions to those expected in this study at a pressure not too dissimilar. For this reason, the n-heptane/2-butanone system at a pressure of 94kPa (Wisniak *et al.,* 1998) was originally chosen as reference. However, reproducing the reported data proved troublesome, with reproducibility of the x-y data possible but deviations in the T-xy data in evidence, as can be seen in Figures 5.1 & 5.2. In particular, it is evident that the generated data differs appreciably temperature-wise in the high 2-butanone concentration region, with no such deviations apparent in the x-y plot. It was this deviation from reference data that lead to the system modifications and recalibrations highlighted in the previous chapter. It was found that there existed a constant drift (~0.1°C) in the temperature readings since the probes had previously been calibrated.

The temperature drift found through recalibration was not significant enough to account for the discrepancies apparent in the T-xy data in Figure 5.1. With this result in mind, the reference work for verification was re-assessed. Wisniak *et al.* (1998) were the only authors to have previously measured phase equilibria for this system, under these conditions. While their data for the system was compared to isobaric measurements for the same system at a different pressure (101.3kPa, measured by Steinhauser & White (1949)), no explicit verification of their equipment was presented in the work. This is not to say that Wisniak's results are erroneous, but rather that the absence of such verification must raise some doubts over the accuracy of the temperature measurement in the same manner that doubts were raised over the temperature accuracy in this work.

With the system subsequently modified (as highlighted in Chapter 4), it was decided to verify the equipment against a system with two independent sets of agreeing data to be as confident as possible in the reliability of generated data. For this reason, the isobaric equilibrium for the ethanol/1-butanol system at an absolute pressure of 1.013bar was selected for system verification, the results of which are presented in Figures 5.3 & 5.4, where a high degree of agreement is evident between experimental and reference data. While there may appear to be some systematic deviation in the experimental data from the reference data in the high ethanol concentration space, if the compositional error associated with this work (±0.022 mole fraction) is taken into consideration, this small deviation is accounted for.

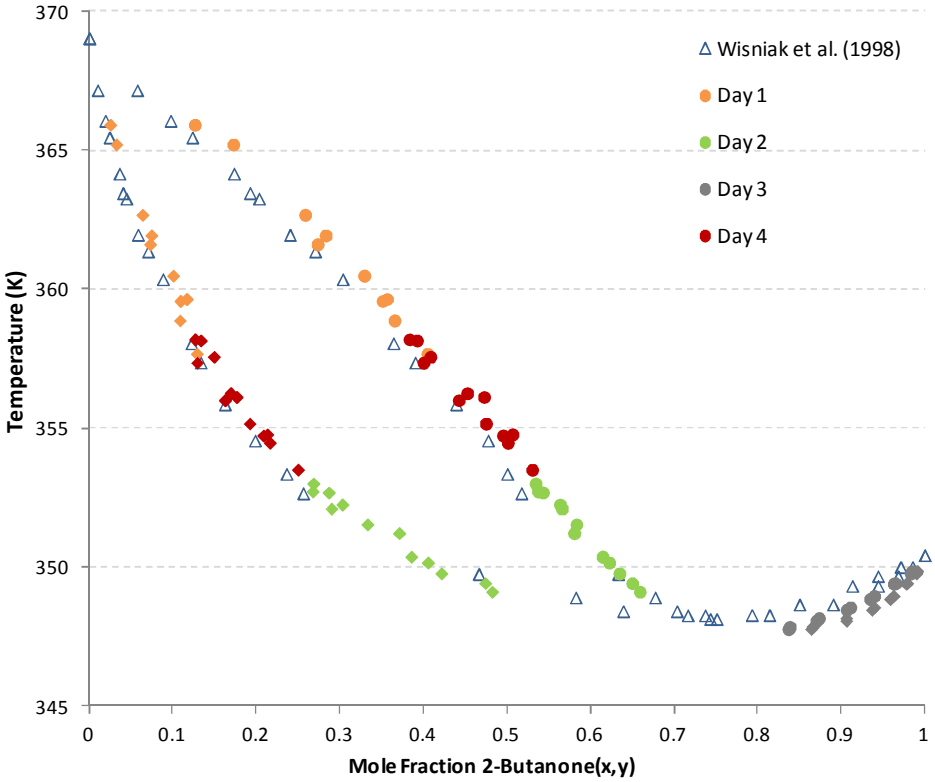

Figure 5.1: T-xy representation of experimental and reference VLE data for the verification system n-heptane/2-butanone at 94kPa

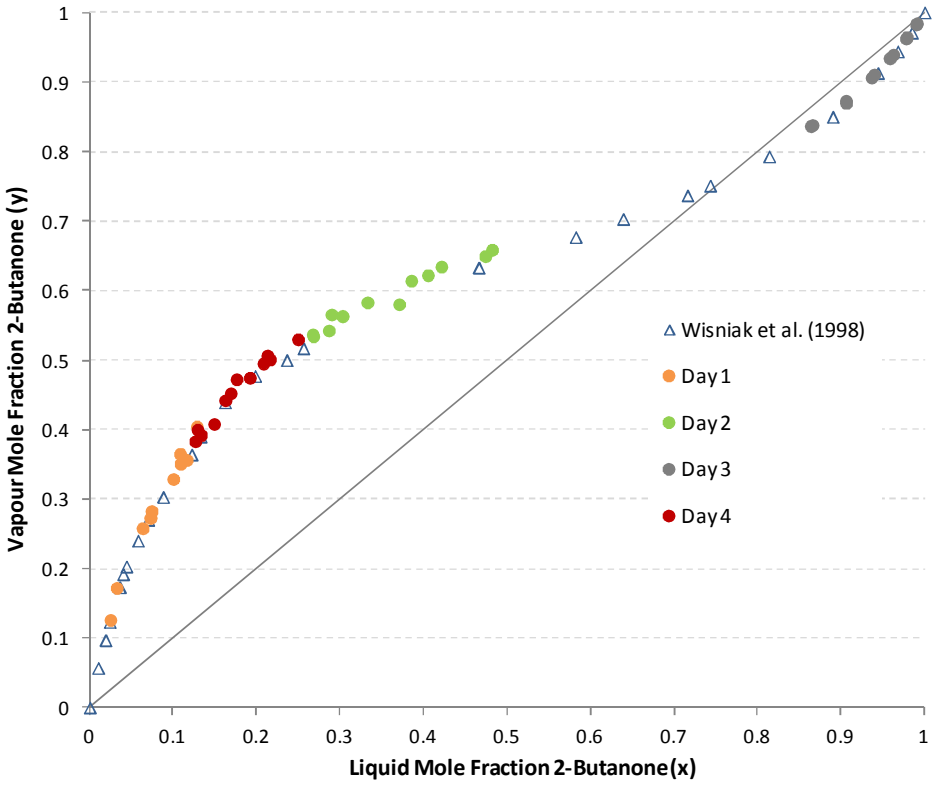

Figure 5.2: x-y representation of experimental and reference VLE data for the verification system n-heptane/2-butanone at 94kPa

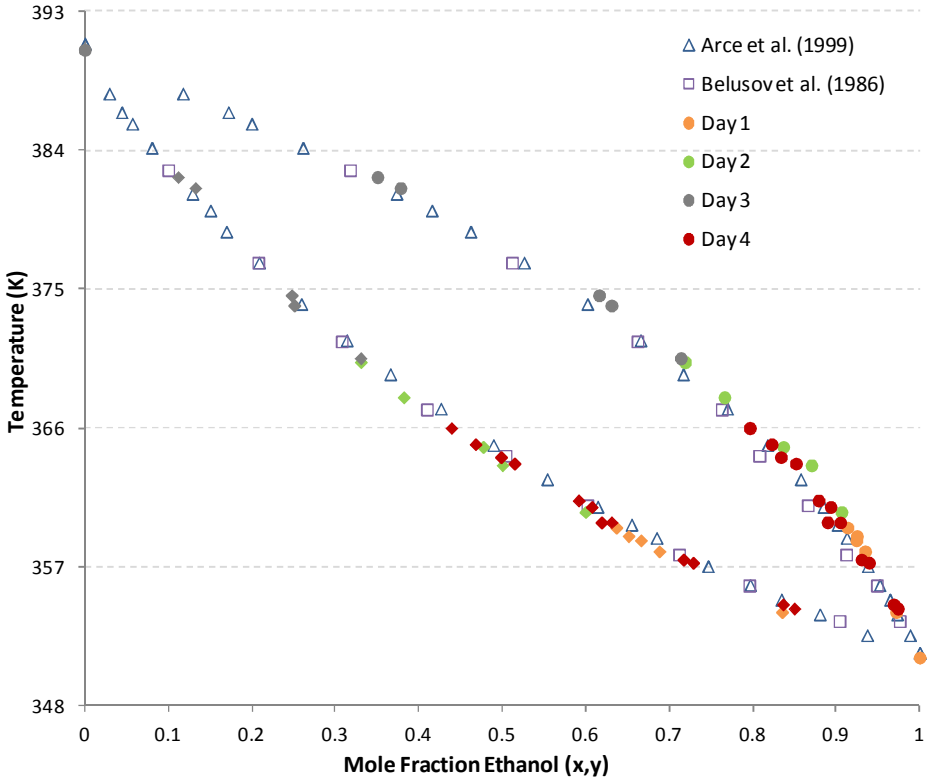

Figure 5.3: T-xy representation of experimental and reference VLE data for the verification system ethanol/1-butanol at 1.013bar

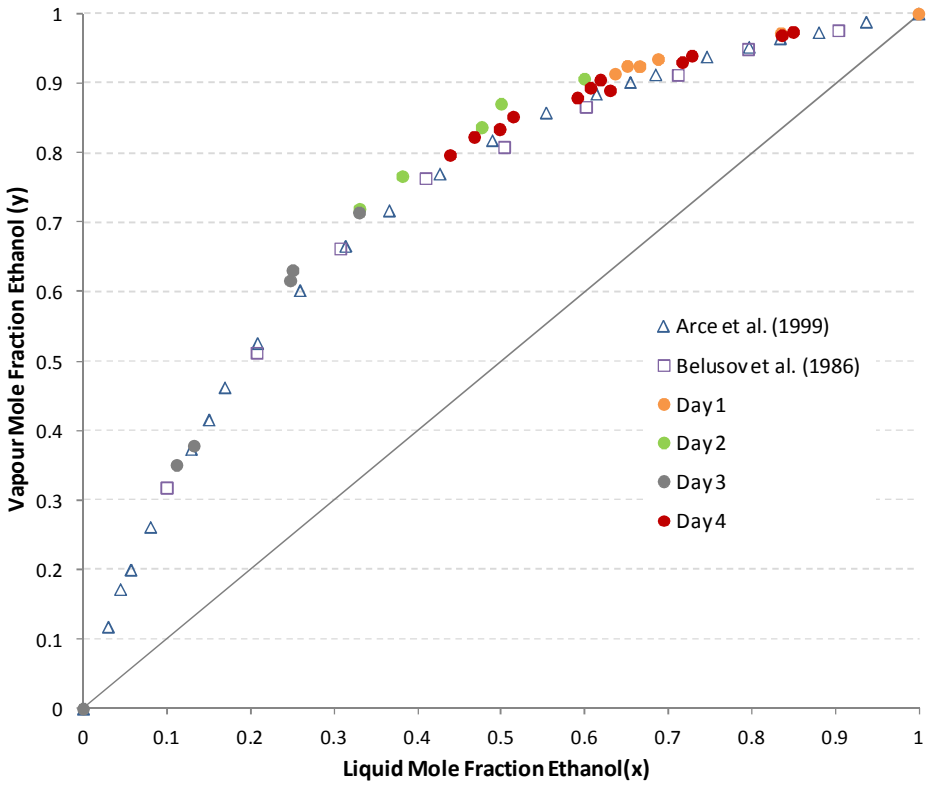

Figure 5.4 x-y representation of experimental and reference VLE data for the verification system ethanol/1-butanol at 1.013bar

The measured data were tested for thermodynamic consistency, passing both the L/W consistency test (all D ≤ 3.380) and the McDermott-Ellis consistency test, details of which are presented in Appendix E. With the system verified, it was possible to move on to the generation of new VLE data pertinent to this study.

5.2. n-Octane Systems

The VLE data generated for each of the heptanone isomers with n-octane is presented in Figure 5.5, with the experimental data provided in Appendix D.

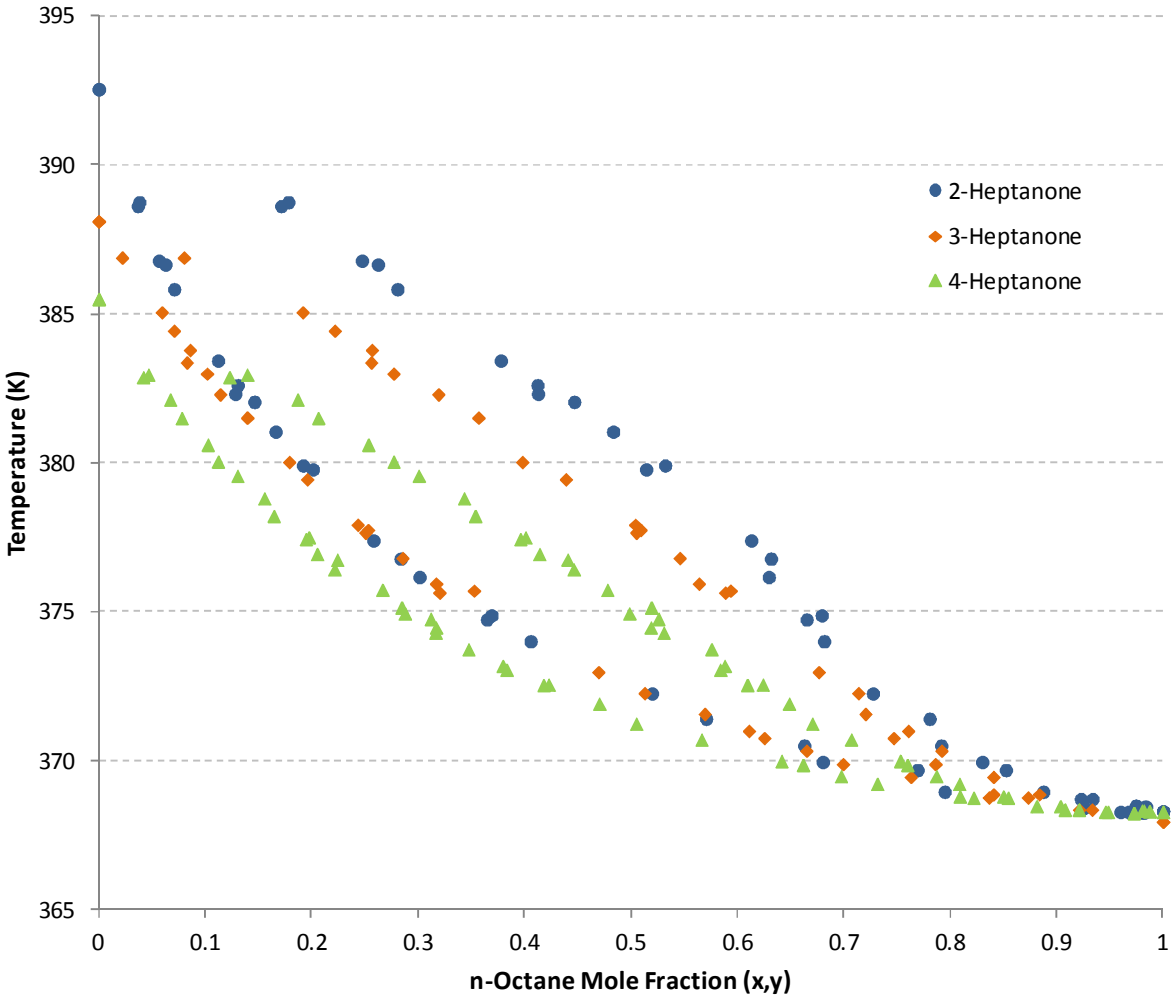

Figure 5.5: Combined VLE data for all n-octane/x-heptanone systems at 40kPa

When analysing the combined VLE results for n-octane with each heptanone structural isomer in Figure 5.5, it is evident that each system exhibits similarly non-ideal behaviour in the high n-octane region. Indeed, each system appears to exhibit a minimum boiling azeotrope at ca. 98 mole% n-octane and temperatures just lower than the n-octane boiling point (ca. 95.1°C). By definition, at the azeotropic point the equilibrium vapour and liquid compositions are equal; thus the existence of an azeotrope can be confirmed graphically by locating the x-intercept in a plot of *(y-x) vs. x* representation of experimental data. In this fashion, the curves for the 2- & 4-heptanone cases with n-octane clearly cross the x-axis in Figure

5.6. Although no data points were found below the x-axis for 3-heptanone, the trend of the other two structural isomers suggests the existence of an azeotrope of a similar composition.

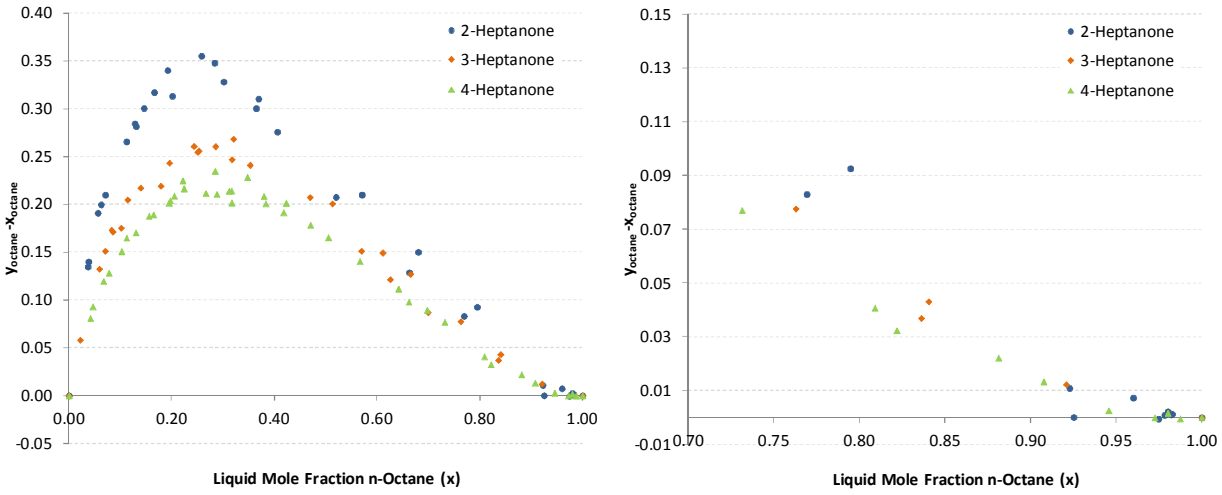

Figure 5.6: Plot of (y-x) vs. x yielding azeotropic composition in VLE of n-octane with each heptanone isomer

Of more importance to this study however, is the effect of the shifting functional group between heptanone's structural isomers. Each system displays similar behaviour in the high n-octane region, while changes in behaviour are apparent as the concentration of the relevant heptanone increases. This would be expected as, at high n-octane concentrations, the polar interactions between *x*-heptanone molecules are diluted as the local concentration of like-molecules decreases. The decrease in polar forces as the carbonyl group shifts more centrally manifests itself in the decrease in respective boiling points, but the nature of the equilibria are the same as indicated by the constant shape of the phase envelopes.

The generated vapour liquid equilibrium data for each of the three systems containing n-octane and one of the structural isomers of heptanone are presented in Figures 5.7 to 5.12. Repeatability of the experimental data is exhibited by the overlapping of data in the same compositional region on separate days of experiments. Thermodynamic consistency tests in the form of the L/W consistency test and the McDermott-Ellis consistency test were performed on all data. The maximum value of D for the L/W consistency test was 3.012, less than the recommended maximum of 5, although most points were well under the lower threshold value of 3. With regard to the point-to-point consistency test, all values of D were lower than their respective D_{max} values, exhibiting thermodynamic consistency according to the McDermott-Ellis consistency test.

5.2.1. n-Octane/2-Heptanone

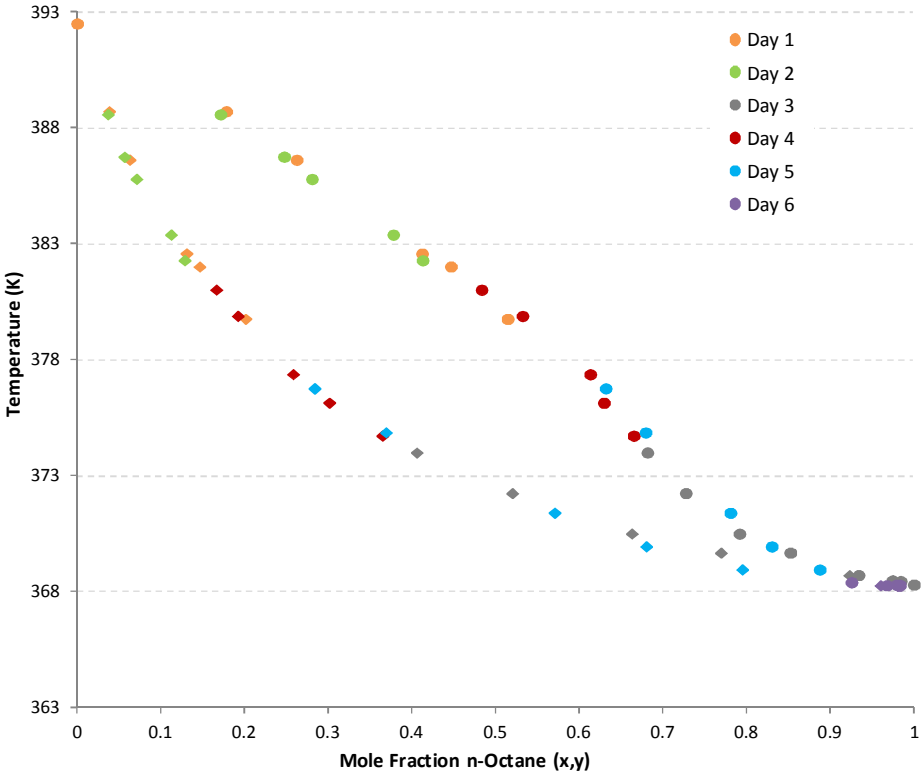

Figure 5.7: T-xy representation of experimental VLE data for n-octane /2-heptanone system at 40kPa

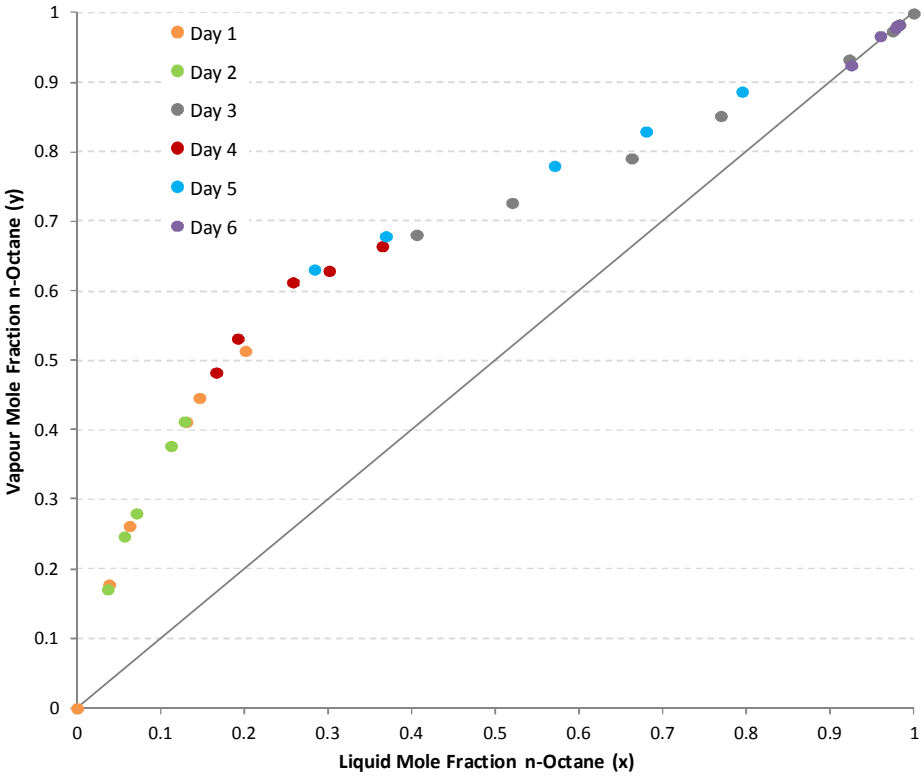

Figure 5.8: x-y representation of experimental VLE data for n-octane/2-heptanone system at 40kPa

5.2.2. n-Octane/3-Heptanone

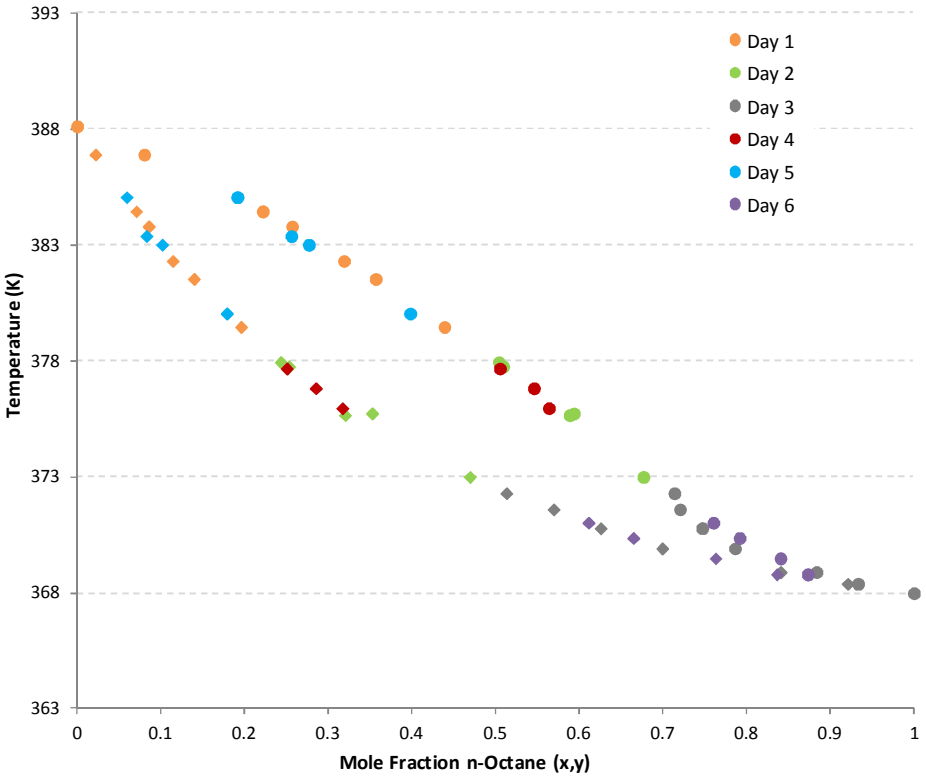

Figure 5.9: T-xy representation of experimental VLE data for n-octane/3-heptanone system at 40kPa

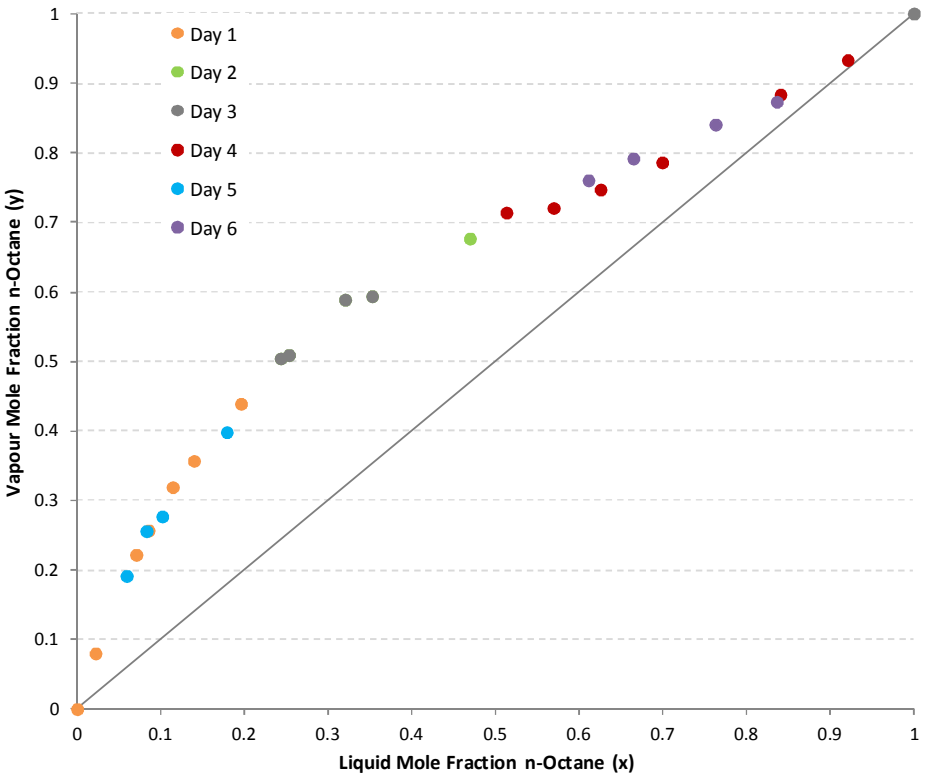

Figure 5.10: x-y representation of experimental VLE data for n-octane/3-heptanone system at 40kPa

5.2.3. n-Octane/4-Heptanone

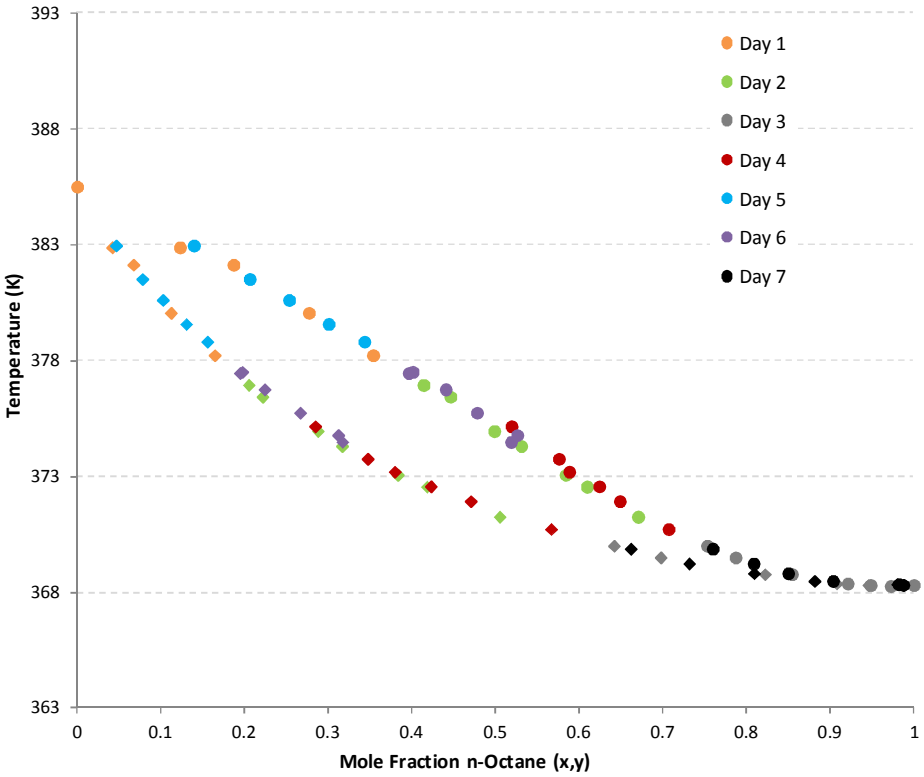

Figure 5.11: T-xy representation of experimental VLE data for n-octane/4-heptanone system at 40kPa

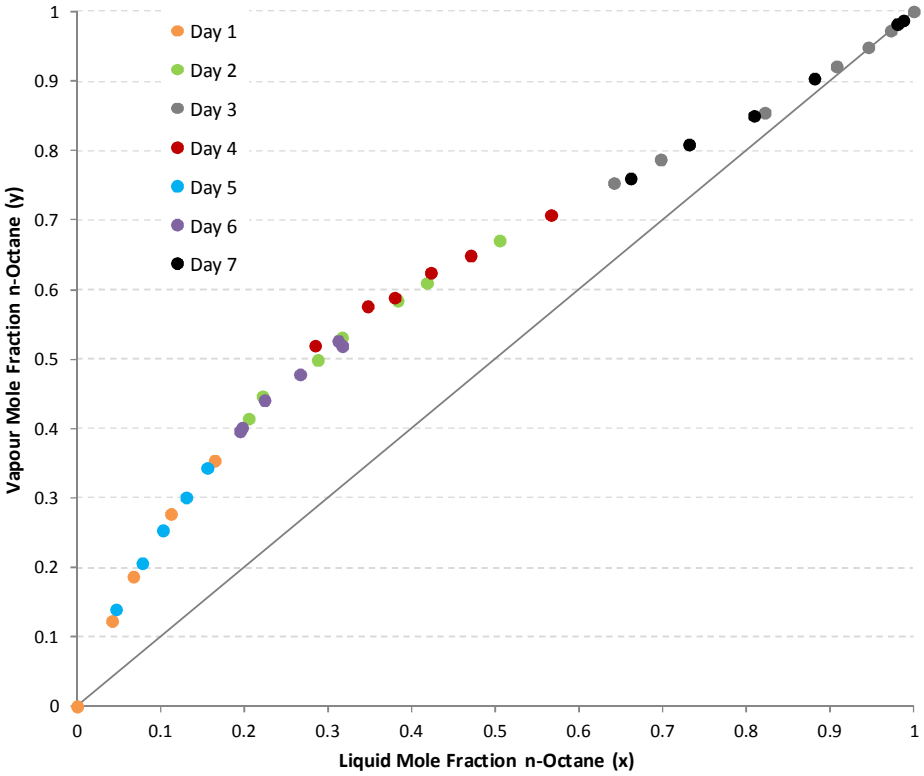

Figure 5.12: x-y representation of experimental VLE data for n-octane/4-heptanone system at 40kPa

5.3. n-Nonane Systems

The combined results for the n-nonane/*x*-heptanone systems are presented in Figure 5.13, with the relevant experimental data provided in Appendix D

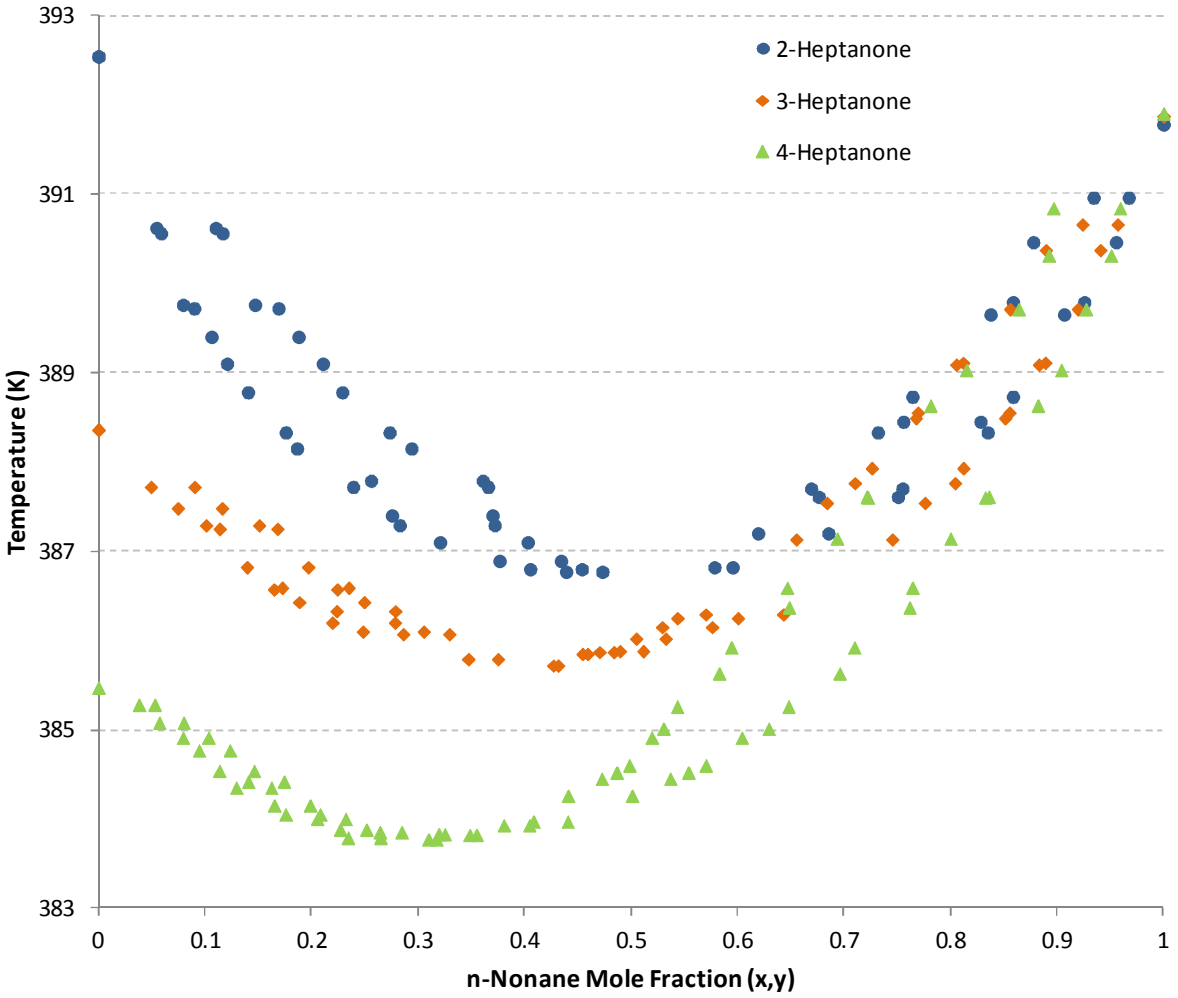

Figure 5.13: Combined VLE data for all n-nonane/x-heptanone systems at 40kPa

Despite the very small temperature range evident in Figure 5.13 for the n-nonane/*x*-heptanone systems, it is evident that there exists a minimum boiling azeotrope for each system at 40kPa. In the case of 2-heptanone, the azeotrope occurs at ca.53 mole% n-nonane and 113.5°C; at ca.44 mole% n-nonane and 112.5°C for the 3-heptanone case and in the n-nonane/4-heptanone system, the azeotrope exists at ca.34 mole% n-nonane and 110.6°C. The azeotropic compositions are determinable in the fashion described in Section 5.2 using Figure 5.14, while the azeotropic temperatures are the minima witnessed experimentally as per Figure 5.13.

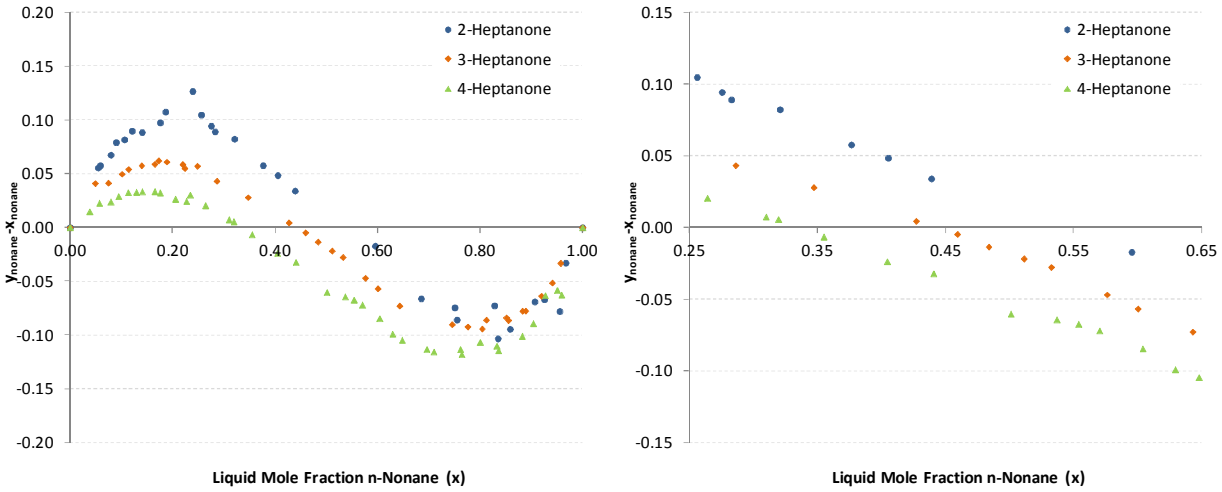

Figure 5.14: Plot of (y-x) vs. x yielding azeotropic composition in VLE of n-nonane with each heptanone isomer

As is the case with the n-octane systems, near-identical behaviour of the systems in the high alkane concentration region is apparent in all cases. The differing strength of the polar forces is again shown by the differing boiling points of the three isomers, but the shapes of the phase envelopes support this observation here more so than in the case of the n-octane systems. In the case of 2-heptanone, the most polar of the three structural isomers with the carbonyl group next to the terminal methyl group, the azeotrope with n-nonane is some 5°C lower than the pure ketone boiling point and this temperature difference decreases as the carbonyl group shifts centrally (3°C and 1.5°C for 3- and 4- heptanone respectively). Thus, the experimental data support the expectation that the polar interactions are diminished as the effects of structural hindrance increase when the polar carbonyl group moves from a terminal carbon to the middle of the chain.

Each system's data are represented independently in Figures 5.15 to 5.20, with repeatability of the data in evidence from agreement of data taken on different days. Thermodynamic consistency testing showed a maximum D value of 1.090 for the L/W consistency test, well below the recommended maximum of 5. All D values were found to be lower than their respective D_{max} values according to the McDermott-Ellis consistency test, with details of thermodynamic consistency testing detailed in Appendix E.

5.3.1. n-Nonane/2-Heptanone

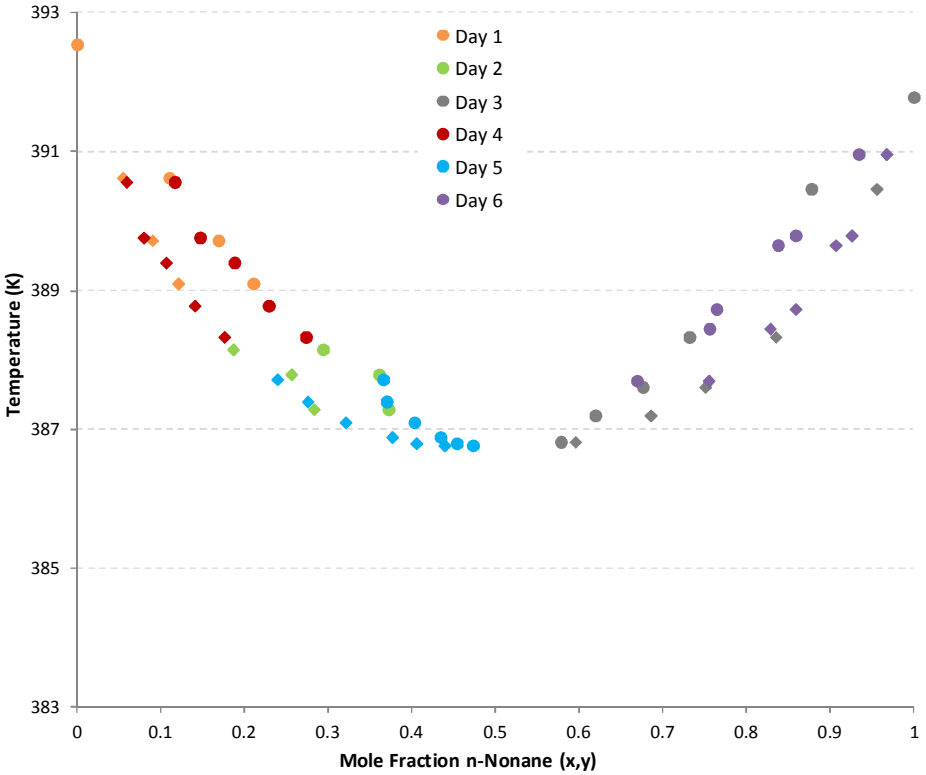

Figure 5.15: T-xy representation of experimental VLE data for n-nonane/2-heptanone system at 40kPa

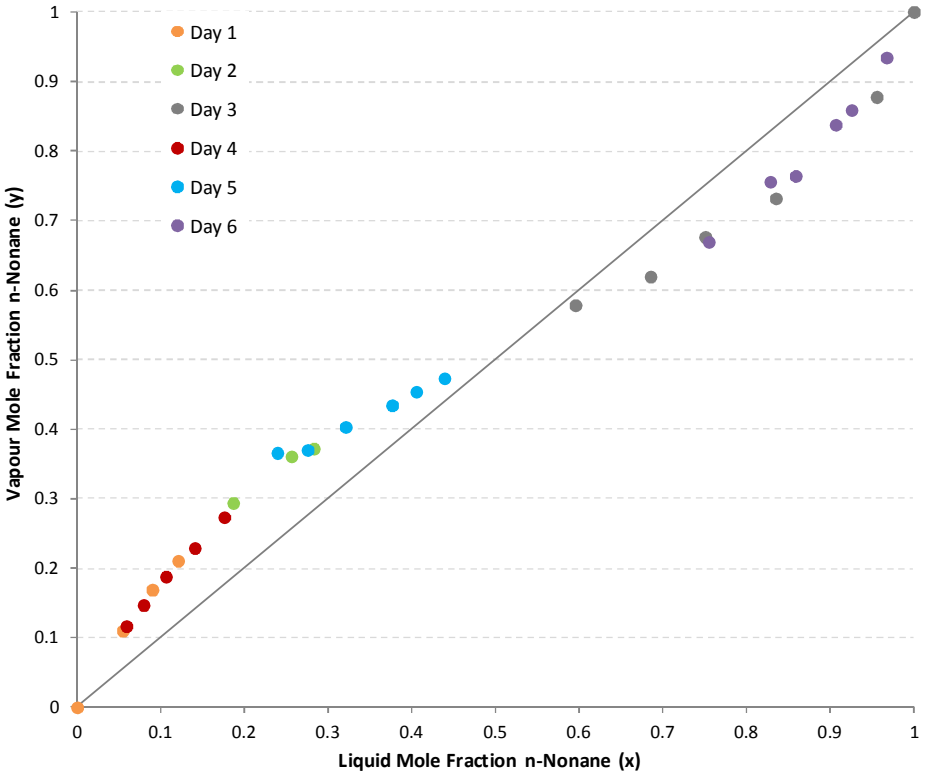

Figure 5.16: x-y representation of experimental VLE data for n-nonane/2-heptanone system at 40kPa

5.3.2. n-Nonane/3-Heptanone

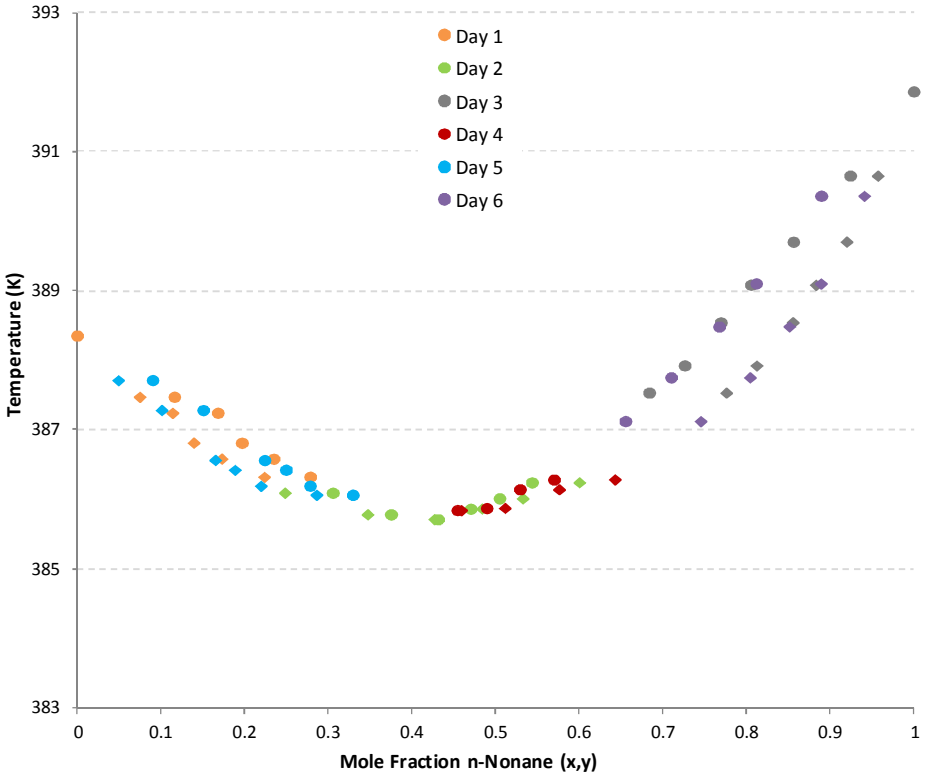

Figure 5.17: T-xy representation of experimental VLE data for n-nonane/3-heptanone system at 40kPa

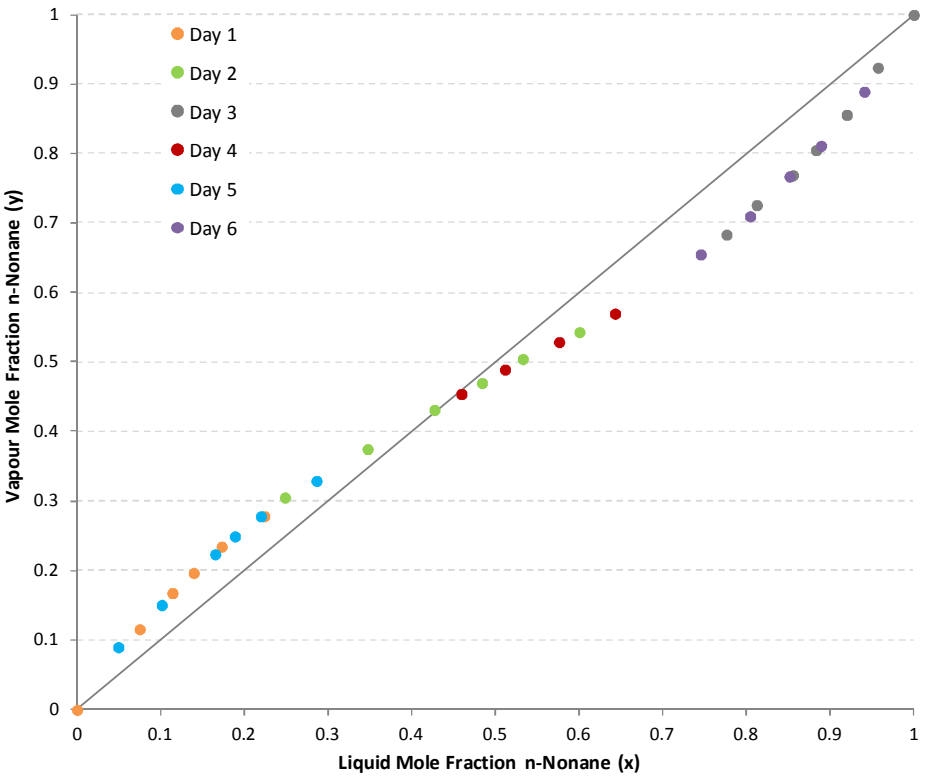

Figure 5.18: x-y representation of experimental VLE data for n-nonane/3-heptanone system at 40kPa

5.3.3. n-Nonane/4-Heptanone

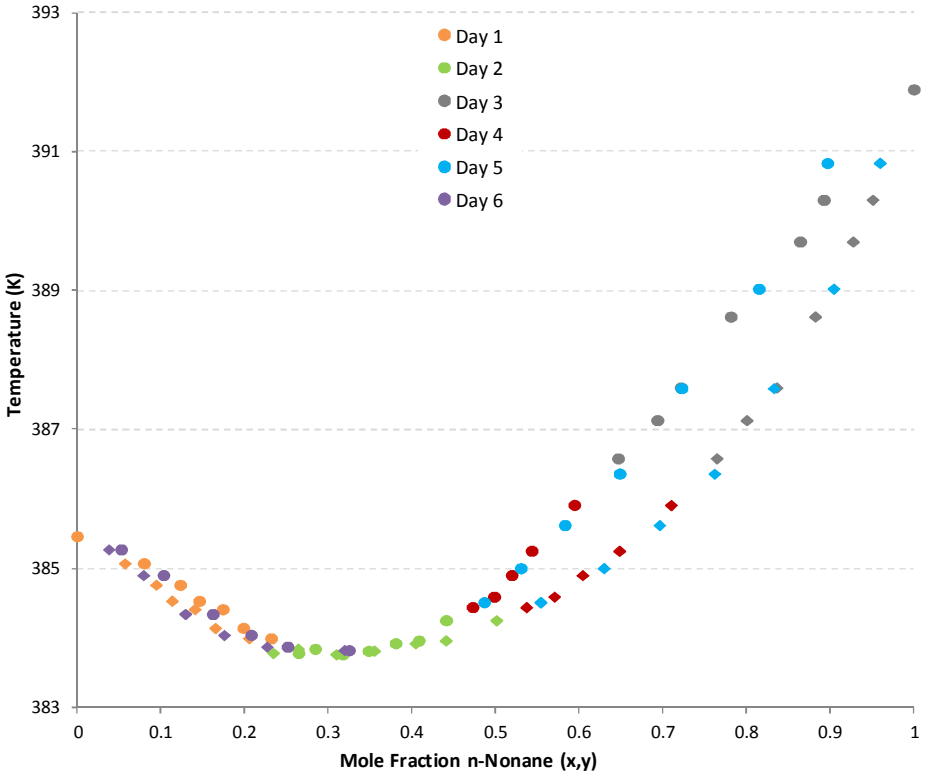

Figure 5.19: T-xy representation of experimental VLE data for n-nonane/4-heptanone system at 40kPa

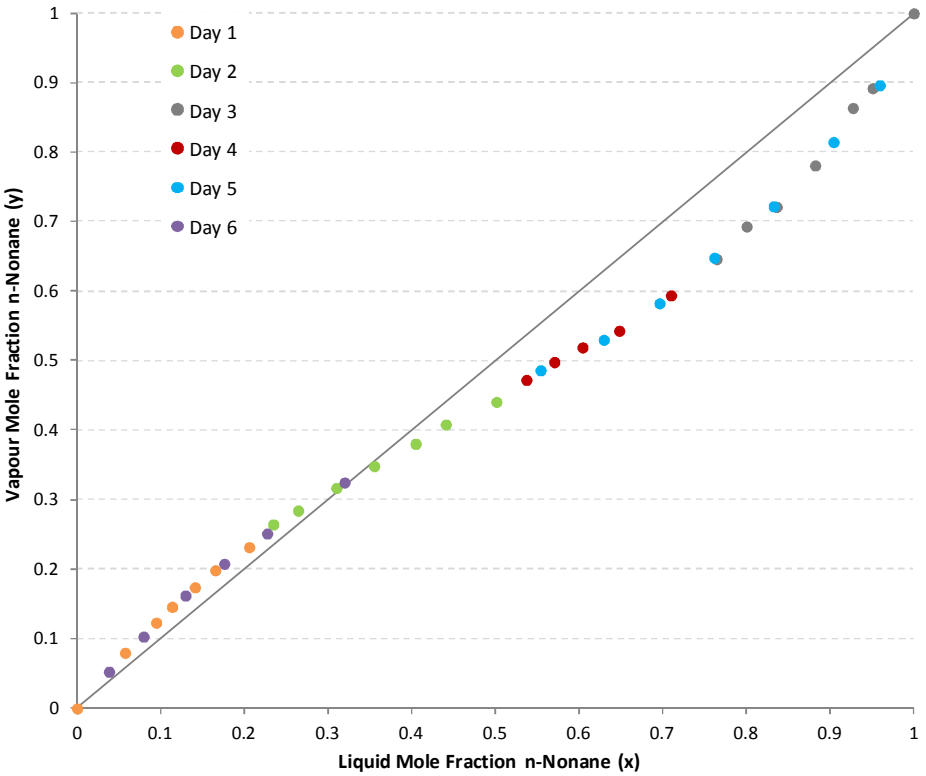

Figure 5.20: x-y representation of experimental VLE data for n-nonane/4-heptanone system at 40kPa

5.4. n-Decane Systems

The experimental VLE data for n-decane with each of the heptanone structural isomers are presented in Figure 5.21. The experimental data can be found in Appendix D.

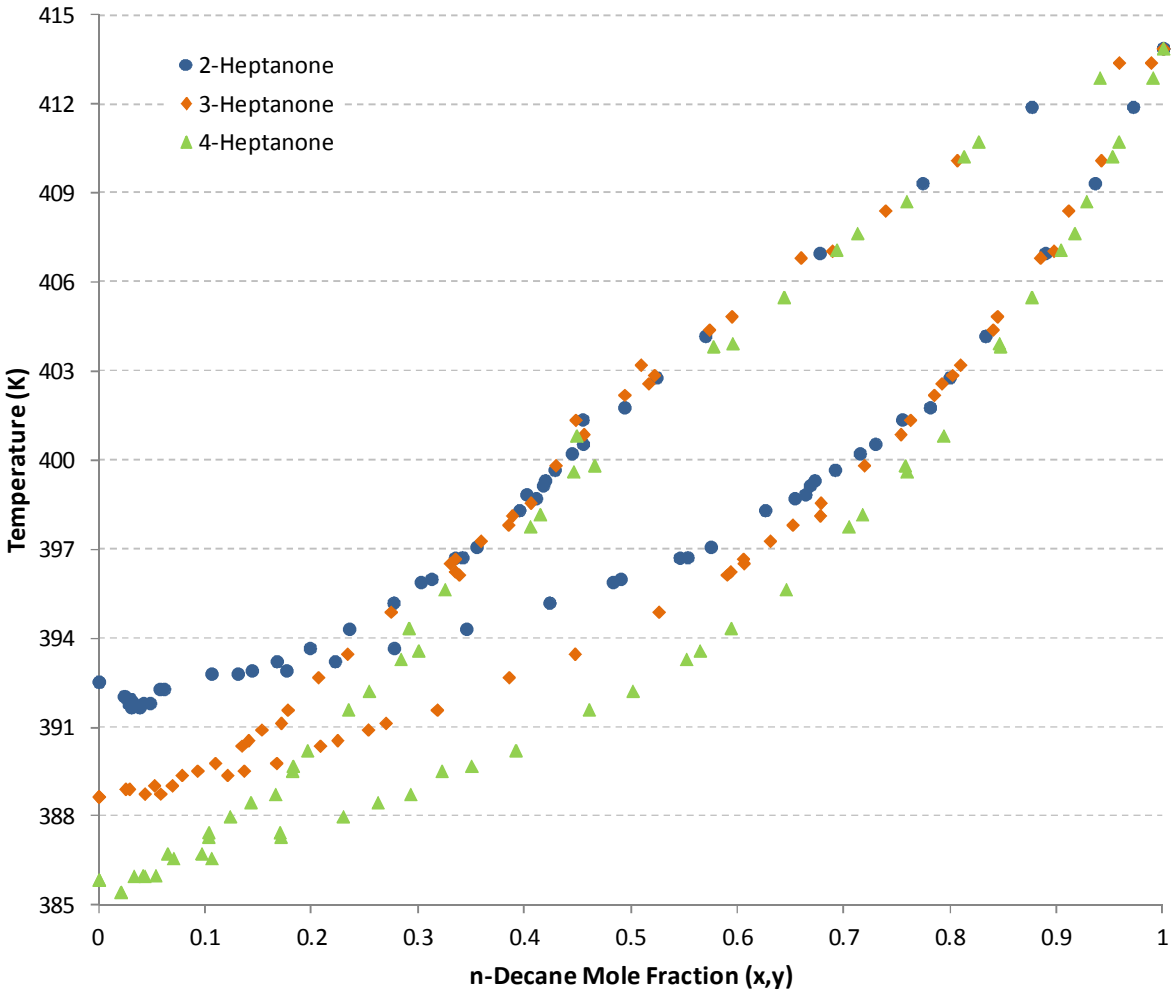

Figure 5.21: Combined VLE data for all n-decane/x-heptanone systems at 40kPa

The decane/*x*-heptanone systems exhibit much the same behaviour as the n-octane and n-nonane cases before, with qualitative similarities between the different isomers' phase behaviour apparent in the shape of the phase envelopes. The similar phase behaviour of each heptanone isomer with n-decane, in the high alkane concentration region, is more pronounced in this case than previously; with practically identical phase behaviour evident up to overall mixture concentrations of 40 mole% *n*-heptanone. This is to be expected however as the additional methyl group in the non-polar alkane molecule only serves to further dampen polar effects by increasing the separation of carbonyl groups in the high n-decane composition range.

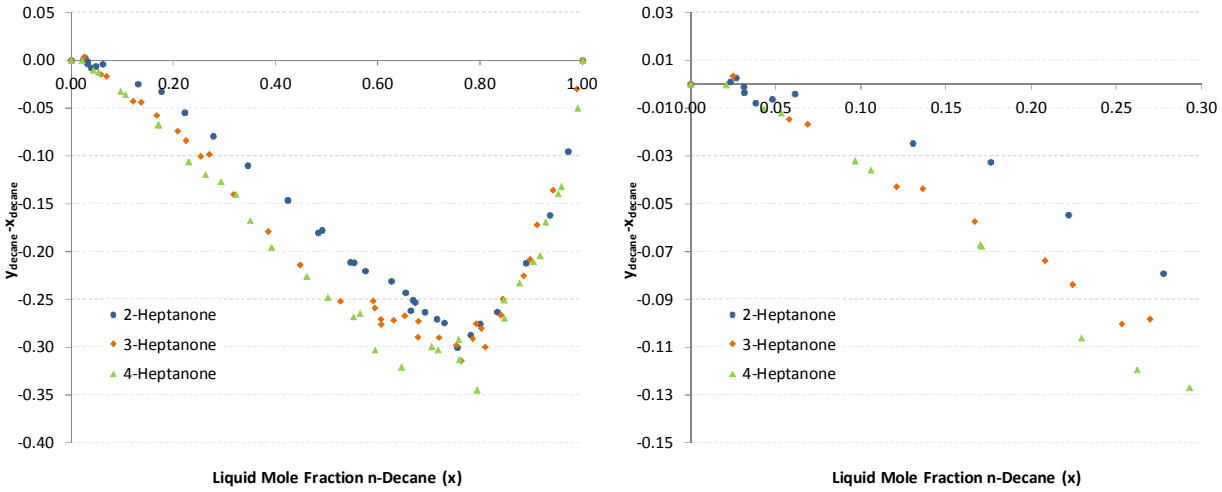

Figure 5.22: Plot of (y-x) vs. x yielding azeotropic composition in VLE of n-decane with each heptanone isomer

Temperature minima only slightly lower than the boiling points of the respective *x*-heptanone in each system were observed experimentally, suggesting the existence of azeotropes in the low (<5 mole%) n-decane region. These azeotropic temperatures are apparent from Figure 5.21 at 118.5°C for 2-heptanone, 115.4°C for 3-heptanone and 112.3°C for the 4-heptanone isomer. From Figure 5.22, it is apparent that azeotropes for all three heptanone isomers exist in the region of 2-3 mole% n-decane, with data points for all three systems clearly visible above the x-axis. Confirmation of these azeotropes are difficult analytically from a gas chromatography stand point due to the large difference in peak sizes generated by the very small concentration of decane and the large peaks of the respective ketones. The fair degree of scatter in the n-decane/2-heptanone system around the suspected azeotrope is testament to this.

The individual systems are depicted in Figures 5.23 to 5.28, where, once again, repeatability of the data between runs is in evidence. All n-decane/*x*-heptanone data were found to be thermodynamically consistent. A maximum D value of 1.641, well within the prescribed maximum, was found for the L/W consistency test, with all pairs of data points shown to be consistent by the McDermott-Ellis consistency test.

5.4.1. n-Decane/2-Heptanone

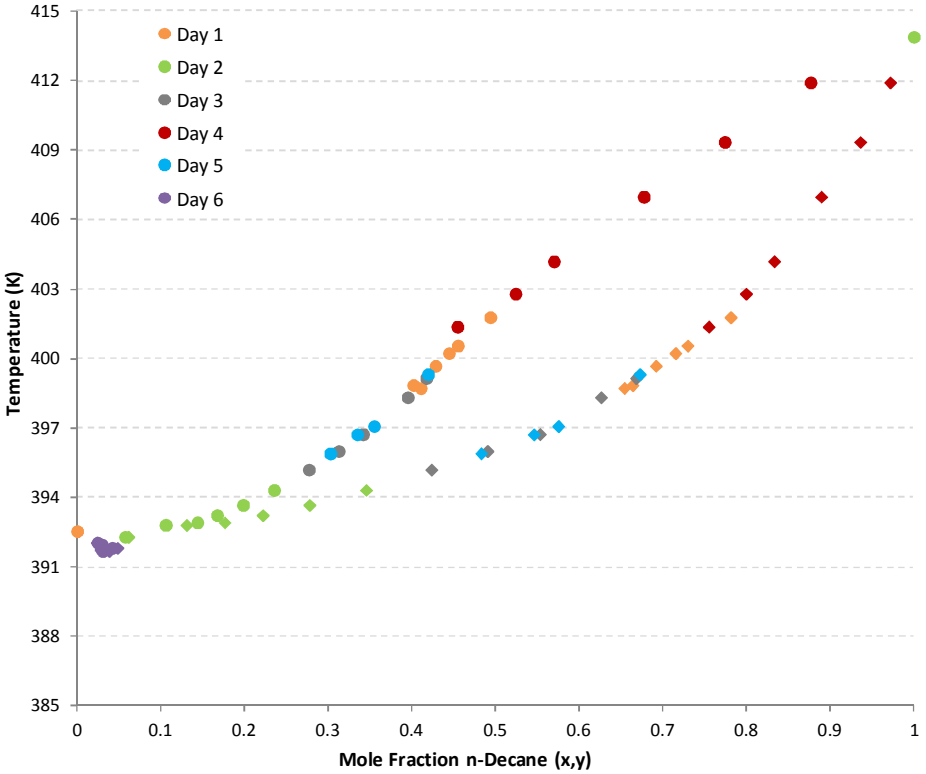

Figure 5.23: T-xy representation of experimental VLE data for n-decane/2-heptanone system at 40kPa

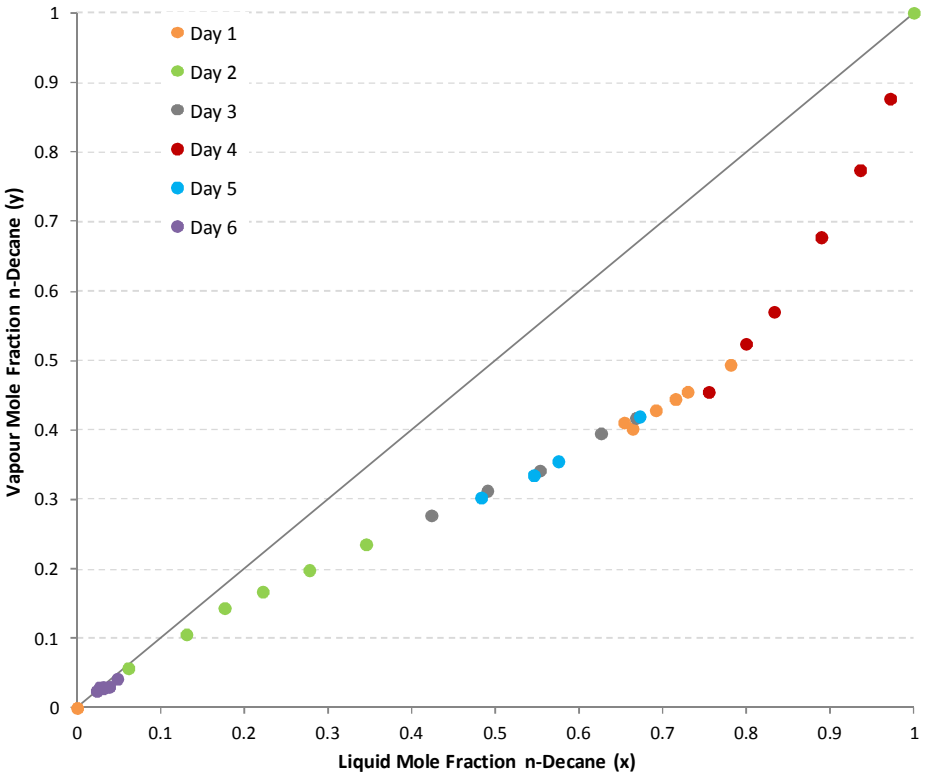

Figure 5.24: x-y representation of experimental VLE data for n-decane/2-heptanone system at 40kPa

5.4.2. n-Decane/3-Heptanone

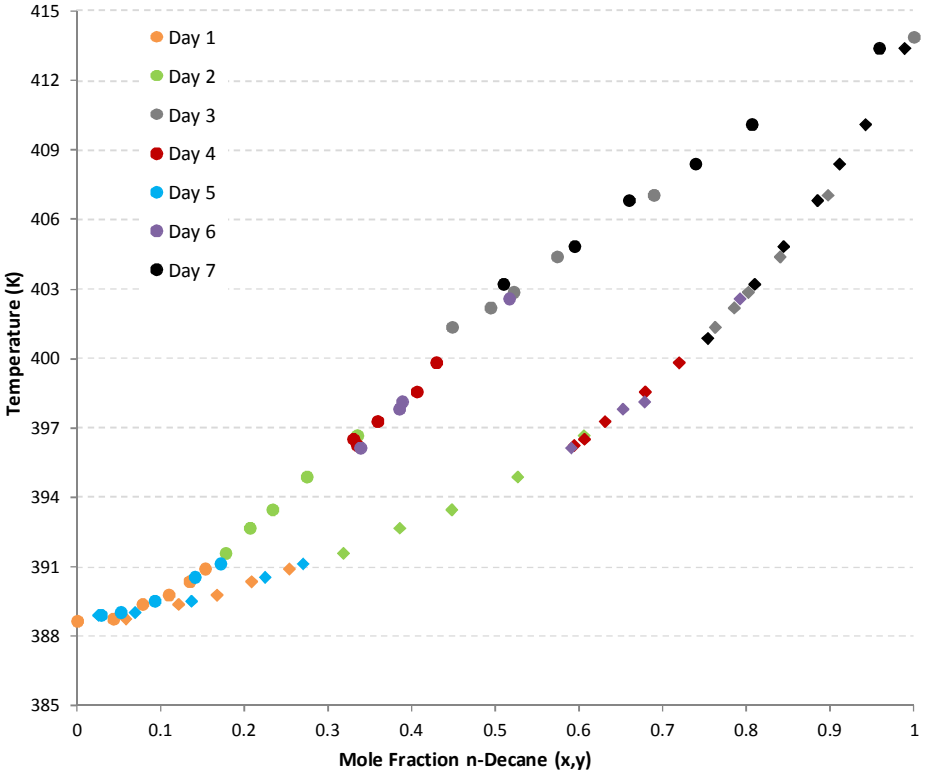

Figure 5.25: T-xy representation of experimental VLE data for n-decane/3-heptanone system at 40kPa

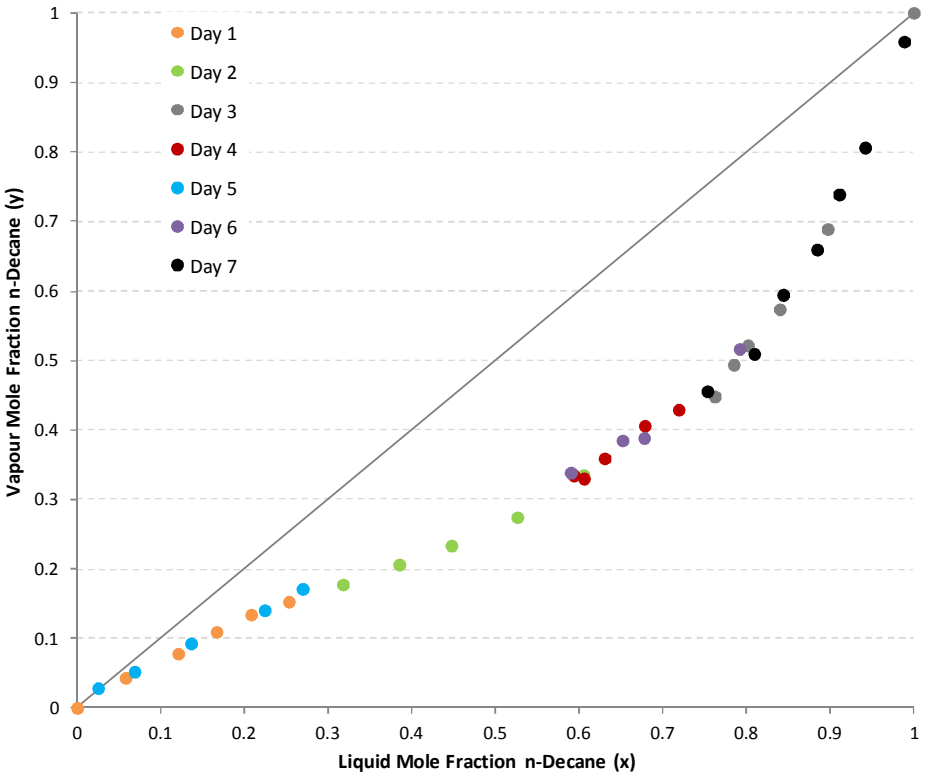

Figure 5.26: x-y representation of experimental VLE data for n-decane/2-heptanone system at 40kPa

5.4.3. n-Decane/4-Heptanone

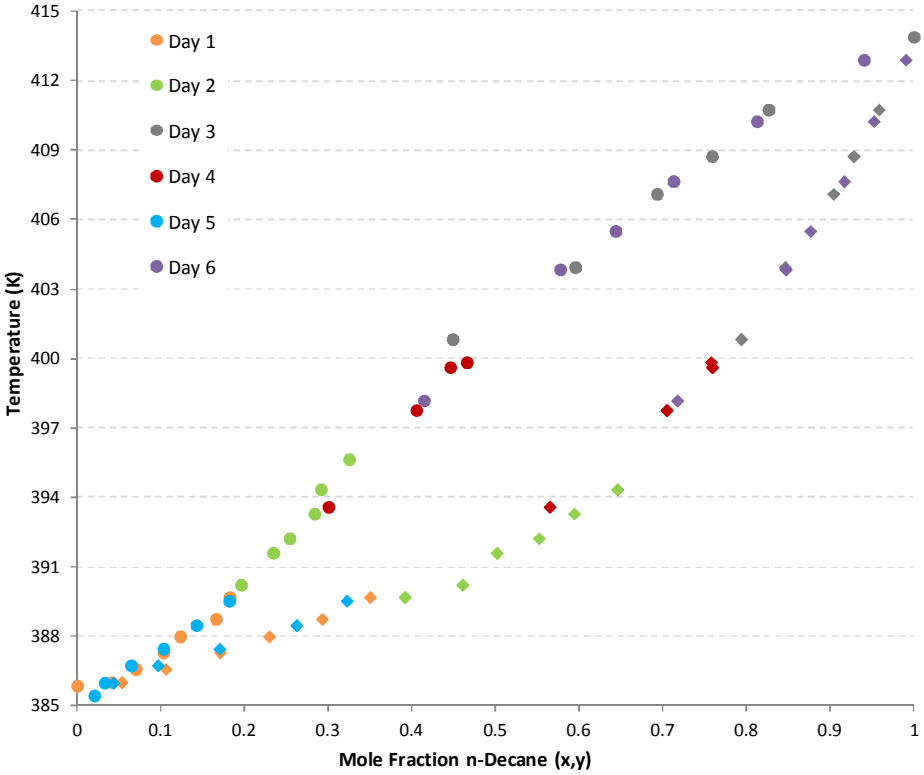

Figure 5.27: T-xy representation of experimental VLE data for n-decane/4-heptanone system at 40kPa

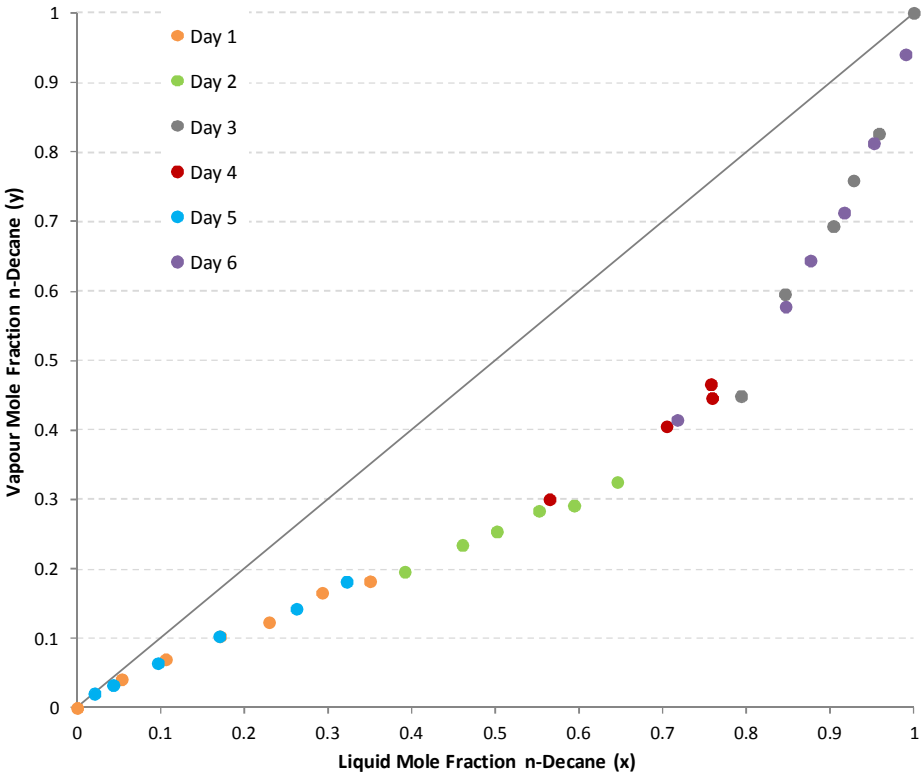

Figure 5.28: x-y representation of experimental VLE data for n-decane/4-heptanone system at 40kPa

5.5. Experimental Summary

In this chapter, isobaric VLE data were generated for the nine binary ketone/n-alkane systems of interest to this work. Experimentally, it appears that each of these systems exhibits a minimum boiling azeotrope at 40kPa, the compositions and temperatures of which are summarised in Table 5.1. While the azeotropes in the n-nonane systems are clearly visible in the middle of the composition spectrum, the azeotropes found in the n-octane and n-decane systems are found at opposite extremes of the composition ranges. From a thermodynamic modelling perspective, accurate prediction of the highly non-ideal behaviour and the azeotropic point in the n-nonane systems will be a priority, while for the n-octane and n-decane systems, prediction the azeotrope at these extreme regions of the composition space will provide a stringent test of the model.

Table 5.1: Summary of experimentally measured azeotropic temperatures and compositions. Systems displaying a "~" indicate instances where the azeotrope was not witnessed experimentally but its existence was approximated from trends seen in systems comprising the other isomers.

	Azeotropic Temperature °C	Azeotropic Composition mole% n-alkane
n-Octane/2-Heptanone	95.1	98%
n-Octane/3-Heptanone	~95.1	~98%
n-Octane/4-Heptanone	95.1	98%
n-Nonane/2-Heptanone	113.5	53%
n-Nonane/3-Heptanone	112.5	44%
n-Nonane/4-Heptanone	110.6	34%
n-Decane/2-Heptanone	118.5	3%
n-Decane/3-Heptanone	~115.4	~2%
n-Decane/4-Heptanone	112.3	2%

The focus of the modelling work presented in Chapter 6 which follows will not simply be correct prediction of the azeotropic point however. The primary aim of the work is to assess the effect of the shifting functional group between structural isomers on their binary phase behaviour, and the ability of the considered polar sPC-SAFT models to accurately predict the observed phenomena. These experimental trends are readily apparent from Figures 5.5, 5.13 & 5.21 and will provide an excellent reference with which the performance of the thermodynamic models can be compared.

Chapter 6 Thermodynamic Modelling Results

The focus of the modelling procedure is to determine the ability of the polar sPC-SAFT models to successfully predict (and in lieu of appropriate prediction, to correlate) the binary phase behaviour witnessed experimentally in the nine binary ketone/alkane systems presented in Chapter 5. This section thus assesses the modelling capacity of both sPC-SAFT$_{JC}$ and sPC-SAFT$_{GV}$, with the non-polar sPC-SAFT variant included as reference.

6.1. Regression Method

The first step in modelling the measured equilibria data is to determine pure component parameters for all components in question. Traditionally, model parameters are regressed against pure component properties including saturated vapour pressure (P^{sat}), liquid density (ρ^{liq}) and, less frequently, heat of vaporisation (ΔH^{vap}). Within the polar PC-SAFT framework however, regressing parameters against only pure component data has proved problematic.

6.1.1. Regression Obstacles

In the case of the Jog & Chapman polar contribution, Sauer & Chapman (2003) have noted that fitting the four pure component parameters solely against pure component data results in a broad minimum for the objective function. The result is multiple parameter sets that are able to accurately represent the pure component data, only one of which is applicable when applied to mixture data however. In their original polar contribution work, Gross & Vrabec (2006) noted that, when fitted solely to pure component data, the best fit for the JC polar model is often that which omits the polar contribution; that is, fitting parameters to pure component data alone tends to drive x_p to zero. This suggests that, in some cases, the model struggles to distinguish the effects of polar interactions from dispersive forces. To overcome this problem, one of two routes is typically taken:

i. VLE data is included in the regression procedure
ii. Correlations are used for homologous series to set the value of the polar parameter

The inclusion of VLE data in the regression procedure has been typified for PC-SAFT$_{JC}$ by Dominik *et al.* (2005), who stressed that the second component considered in the binary mixture data should be well documented parametrically and contain no functionality. Inclusion of binary mixture data was later extended to sPC-SAFT$_{JC}$ and sPC-SAFT$_{GV}$ by de Villiers *et al.* (2011) where, as in the case of Dominik *et al.* (2005), n-alkanes were the second component of choice when selecting binary data for parameter regression.

Gross & Vrabec (2006) originally kept their polar parameter (n_p) equal to unity for molecules containing a single polar group and thus claimed their model's advantage over the PC-SAFT$_{JC}$. They

argued that, by having a non-adjustable polar parameter, their model could produce an optimum set of pure component parameters capable of correlating binary mixture data to the same degree as PC-SAFT$_{JC}$ without the need for binary mixture data in the regression. However, Vega *et al.* (2002) showed that the axial alignment of the dipole moment in Gross & Vrabec's reference fluid results in a more dampened effect on the component physical properties than is the case with the perpendicularly aligned dipole in Jog & Chapman's model. Furthermore, in a recent study of the applicability of polar PC-SAFT models to water/alcohol/alkane systems, Al-Saifi *et al.,* (2008) found that, in general, the performance of PC-SAFT$_{JC}$ was better than that of PC-SAFT$_{GV}$. Al-Saifi *et al.* attributed this to the fact that the magnitude of the polar interactions is larger for PC-SAFT$_{JC}$ than for PC-SAFT$_{GV}$. Thus, de Villiers *et al.* (2011) argued that this parameter should be adjustable and included in the regression procedure, to compensate for the expected underestimation of polar effects in the GV-term.

The use of correlations to set the value of the polar parameter was demonstrated by Sauer & Chapman (2003) as well as Dominik *et al.* (2005). To address the problem of a broad minimum in the objective function under the JC polar framework that resulted in a zero polar contribution, these authors showed that there exists a relationship between the fraction of polar segments (x_p) and the segment number (m) between sequential members of a homologous series. That is, for molecules of increasing chain length, containing the same functionality, the product of x_p and m stays approximately constant. If the polar parameter could be set constant, the three remaining non-polar parameters could be readily determined through regression, bypassing the broad minimum seen when regressing all four parameters.

Sauer & Chapman (2003) made use of this observation in a parametric study of ketones in the PC-SAFT and Chen-Kreglewski SAFT (CK-SAFT) frameworks, where a correlation for the segment number as a function of molecular weight and a constant value of 0.5 for the x_pm product were used. Dominik *et al.* (2005) expanded upon this idea by first determining the x_pm product for one member of a homologous series, where all parameters were determined through traditional regression, and keeping this value constant for the determination of x_p for the other members of the series. de Villiers *et al.* (2011) made the observation independent of regressed components by deriving an empirical correlation for the relationship between x_p and molecular weight with functional group specific constants employed. The idea was extended to the Gross & Vrabec polar framework, with a similar correlation developed, both of which are presented below along with the relevant ketone specific constants in Table 6.1:

$$x_p = \frac{K}{(A \cdot M_W + B) \cdot \mu^2} \tag{6.1}$$

$$n_p = \frac{K \cdot (A \cdot M_W + B)}{\mu^2} \tag{6.2}$$

Table 6.1: Constants for correlations for polar (ketone) parameters. Reproduced from de Villiers et al. (2011).

Correlation	K	A	B
x_p	4.9316	0.02871	0.47537
n_p	4.4208	0.02258	1.3821

6.1.2. Regression Algorithm

The *TRSolutions* software package, as developed by de Villiers in the Separations Technology research group at Stellenbosch University, was used to regress pure component parameters and model the experimentally observed phase equilibria. While various different objective functions can be found in the open literature, the most common is limited to fitting saturated vapour pressure and liquid density data according to:

$$OF = \sum_{i=1}^{NP}\left[\left(\frac{P_i^{sat,calc} - P_i^{sat,exp}}{P_i^{sat,exp}}\right)^2 + \left(\frac{\rho_i^{sat,calc} - \rho_i^{sat,exp}}{\rho_i^{sat,exp}}\right)^2\right] \quad (6.3)$$

In such a regression function, equal weighting is given to the fitting of each pure component property.

It has been shown that limiting the objective function to the minimisation of errors in only first order compositional and volume derivatives tends to limit the application of the determined parameters (de Villiers, 2011). In particular, temperature derivative properties including heat of vaporisation and heat capacity are, in general, poorly predicted by such parameters. While considering P_i^{sat} and ρ_i^{sat} over a reduced temperature range brings in a degree of temperature dependence, the resultant parameters are generally still only appropriate for the prediction of saturated vapour pressure and saturated liquid density. Extension to multicomponent phase equilibria follows naturally because of its primary dependence of the aforementioned pure component properties.

In order to account appropriately for thermodynamic properties other than saturated vapour pressure and liquid density, properties such as speed of sound (Lafitte *et al.,* 2006), critical properties and heat of vaporisation (Lafitte *et al.,* 2007) have previously been included in the objective function. While the inclusion of such data will, in theory, result in the generation of more rounded parameter sets, it is important that the inclusion of any such data in the regression function doesn't result in a significant decrease of performance in the equation of state's prediction of multicomponent phase equilibria. For this reason, regression weights are often given to each property included in the regression.

While the focus of this study is indeed multicomponent phase equilibria, the more holistic approach of incorporating a first order temperature derivative property, in the form of heat of vaporisation data, to the objective function is adopted here. Appropriate regression weights are given to each property to emphasise a high predictive capacity for the VLE data while still allowing for good predictions of all pure component properties considered.

The regression procedure within the *TRSolutions* software package makes use of the Levenberg-Marquart algorithm with a least squares objective function, as detailed in Equation (6.4): Pure component data used were from DIPPR correlations in the temperature range $0.5<T_r<0.9$.

$$OF = \sum_{i=1}^{NP}\left[\alpha\left(\frac{P_i^{sat,calc}-P_i^{sat,exp}}{P_i^{sat,exp}}\right)^2+\beta\left(\frac{\rho_i^{sat,calc}-\rho_i^{sat,exp}}{\rho_i^{sat,exp}}\right)^2 + \gamma\left(\frac{\Delta H_i^{vap,calc}-\Delta H_i^{vap,exp}}{\Delta H_i^{vap,xp}}\right)^2\right] \tag{6.4}$$

In Equation 6.4, α, β and γ are regression weights. When binary VLE data are incorporated, the objective function becomes:

$$OF = \sum_{i=1}^{NP}\left[\alpha\left(\frac{P_i^{sat,calc}-P_i^{sat,exp}}{P_i^{sat,exp}}\right)^2+\beta\left(\frac{\rho_i^{sat,calc}-\rho_i^{sat,exp}}{\rho_i^{sat,exp}}\right)^2 + \gamma\left(\frac{\Delta H_i^{vap,calc}-\Delta H_i^{vap,exp}}{\Delta H_i^{vap,exp}}\right)^2 + \varepsilon\left(X_i^{VLE,error}\right)^2\right] \tag{6.5}$$

where the incorporated VLE error accounts for errors in both the experimental vapour phase mole fraction and the experimental saturation temperature.

6.1.3. Regression Alternatives

Pure component parameters were generated for sPC-SAFT, sPC-SAFT$_{JC}$ and sPC-SAFT$_{GV}$. In order to ensure the optimal parameter set is obtained for each component, and to assess the impact of considering different regression alternatives, five different regression procedures were considered:

i. Traditional pure component parameter regression
   - Only pure component data (P_i^{sat}, ρ_i^{sat} and ΔH^{vap}) were considered in the parameter regression procedure.

ii. Correlations for the polar parameter
   - The correlations detailed in Equations 6.1 and 6.2 above were used to set the value of the polar parameter (x_p and n_p).

iii. Inclusion of n-octane + *x*-heptanone VLE data
   - The experimental phase equilibria data for each heptanone isomer with n-octane was included in the regression of the respective heptanone's parameters.

iv. Inclusion of n-nonane + *x*-heptanone VLE data

- The experimental phase equilibria data for each heptanone isomer with n-nonane was included in the regression of the respective heptanone's parameters.

v. Inclusion of n-decane + *x*-heptanone VLE data

- The experimental phase equilibria data for each heptanone isomer with n-decane was included in the regression of the respective heptanone's parameters.

The latter four regression alternatives are only applicable for polar molecules. Thus, for the n-alkane molecules considered, the regression procedure will thus yield only one set of component parameters for each of the three equations of state. The three structural isomers of heptanone will each have one set of parameters for sPC-SAFT and five sets for each of the polar variants.

For regressions using only pure component data or those using only the correlation for setting the polar parameter, regression weightings of 4, 2 & 1 were used for P_i^{sat}, ρ_i^{sat} and ΔH^{vap} respectively. When VLE data were considered in the regression procedure, the weightings were initially 10, 8, 4 & 1 for P_i^{sat}, ρ_i^{sat}, ΔH^{vap} and the included VLE data respectively so as to emphasise the importance of pure component data being well predicted by the parameters. These regression weights were those used in previous successful regression runs within the Separations Technology research group (de Villers, 2011) and served as the basis this work. The incorporation of VLE data only serves to tweak predictions to produce a better fit of experimental VLE data.

6.2. Regressed Parameters

Table 6.2 provides the regressed parameters for each component for each regression alternative considered, with relevant deviations from the pure component properties listed. All regressed parameters produce good correlations of the respective pure component data, with saturated vapour pressure correlated to within 3%, liquid density within 2% and heat of vaporisation within 2.5%. Parameters for the polar molecules regressed according to the first and second regression procedures (that is, considering only pure component data in the regression procedure) produce the best fits of the three pure component properties. This is to be expected however, as this is the same data against which the EOS's are regressed. It is worth noting that the inclusion of the VLE data in the regression does not significantly affect the correlation of pure component properties. It should be noted that the parameters for each isomer determined by the second regression procedure, or setting the polar parameter value according to Equations 6.1 and 6.2, are necessarily in exact agreement with those of de Villiers *et al.* (2011) and serves as verification of the regression procedure.

It is also apparent from Table 6.2 that it was not possible to regress 4-heptanone parameters for sPC-SAFT$_{JC}$ using only pure component data in the regression, without fixing the value of the fraction of polar segments according to Equation 6.1. Regardless of initial guess or boundary conditions, the value of

x_p was constantly forced to zero, or the lower boundary value if such was set, if all four pure component parameters were included in the regression. It is apparent that the broad minimum for the objective function, noted by previous authors and detailed in Section 6.1.1, exists in this case. It is interesting that this was true only for 4-heptanone, as it was possible to regress all four pure component parameters for the more polar cases of 2-heptanone and 3-heptanone. Considering the values of n_p regressed for the heptanone isomers, it is apparent that the values are significantly greater than unity, justifying the decision not to fix its value during the regression procedure.

The regressed parameters were then applied to the experimental VLE data to assess the ability of the polar sPC-SAFT equations of state to model the phase equilibria observed, the results of which are presented in the following section.

Table 6.2: Regressed model parameters for each component using the relevant regression schemes

	Molec. Weight	σ	m	ε/k	n_p/x_p	μ	ΔP^{sat}	$\Delta \rho^{sat}$	ΔH^{vap}
	g/mol	Å		K		D	%	%	%
n-Octane									
sPC-SAFT									
sPC-SAFT$_{GV}$	114.23	3.8213	3.8468	241.87	-	-	0.14	0.60	1.09
sPC-SAFT$_{JC}$									
n-Nonane									
sPC-SAFT									
sPC-SAFT$_{GV}$	128.2	3.8282	4.2533	243.05	-	-	0.19	0.53	0.84
sPC-SAFT$_{JC}$									
n-Decane									
sPC-SAFT									
sPC-SAFT$_{GV}$	142.29	3.8506	4.6153	245.37	-	-	0.26	0.56	1.26
sPC-SAFT$_{JC}$									
2-Heptanone									
sPC-SAFT	114.18	3.6390	3.9799	257.28	-	-	0.68	1.05	1.59
sPC-SAFT$_{GV}$									
Pure Comp Data		3.6761	3.8550	248.99	2.5062	2.61	0.71	0.60	1.37
n_p Correlation		3.6764	3.8533	248.48	2.5689	2.61	0.72	0.57	1.35
n-Octane VLE	114.18	3.6511	3.8853	241.09	3.1581	2.61	2.93	0.54	0.99
n-Nonane VLE		3.6596	3.8753	242.66	3.0447	2.61	2.53	0.32	1.04
n-Decane VLE		3.6653	3.8715	243.45	2.9732	2.61	2.76	0.30	1.03
sPC-SAFT$_{JC}$									
Pure Comp Data		3.7761	3.6238	260.26	0.1700	2.61	0.28	1.19	1.64
x_p Correlation		3.8097	3.5428	260.50	0.2016	2.61	0.23	1.23	1.68
n-Octane VLE	114.18	3.8314	3.4982	256.36	0.2488	2.61	1.85	1.16	1.84
n-Nonane VLE		3.8287	3.5062	256.74	0.2436	2.61	1.50	1.18	1.86
n-Decane VLE		3.8103	3.5637	254.77	0.2352	2.61	2.01	1.28	1.90
3-Heptanone									
sPC-SAFT	114.18	3.5516	4.1822	248.96	-	-	1.35	0.25	2.07
sPC-SAFT$_{GV}$									
Pure Comp Data		3.5798	4.0848	245.50	1.5172	2.81	1.28	0.13	1.94
n_p Correlation		3.5879	4.0497	240.27	2.2160	2.81	1.35	0.25	1.80
n-Octane VLE	114.18	3.5761	4.0710	238.59	2.2595	2.81	2.75	0.43	1.56
n-Nonane VLE		3.5750	4.0723	238.44	2.2721	2.81	2.69	0.46	1.56
n-Decane VLE		3.5538	4.1542	237.03	2.1621	2.81	3.86	0.53	1.34
sPC-SAFT$_{JC}$									
Pure Comp Data		3.9138	3.2658	246.14	0.3385	2.81	0.43	0.57	2.26
x_p Correlation		3.7355	3.6810	251.35	0.1739	2.81	0.72	0.45	2.01
n-Octane VLE	114.18	3.7247	3.7110	250.78	0.1658	2.81	1.75	0.48	1.84
n-Nonane VLE		3.7369	3.6791	251.18	0.1733	2.81	1.45	0.48	1.88
n-Decane VLE		3.7036	3.7914	247.60	0.1617	2.81	2.64	1.20	1.66
4-Heptanone									
sPC-SAFT	114.18	3.6731	3.8533	256.82	-	-	0.16	1.07	0.86
sPC-SAFT$_{GV}$									
Pure Comp Data		3.7089	3.7215	240.08	3.5687	2.68	0.11	0.25	0.33
n_p Correlation		3.7115	3.7269	247.25	2.4365	2.68	0.08	0.56	0.54
n-Octane VLE	114.18	3.7098	3.7247	247.00	2.4332	2.68	1.45	0.52	0.42
n-Nonane VLE		3.7036	3.7412	246.39	2.4451	2.68	1.30	0.50	0.42
n-Decane VLE		3.6757	3.8454	242.68	2.4791	2.68	1.84	0.91	0.51
sPC-SAFT$_{JC}$									
Pure Comp Data		-	-	-	-	-	-	-	-
x_p Correlation		3.8338	3.4555	260.36	0.1830	2.68	0.67	1.23	1.09
n-Octane VLE	114.18	3.8305	3.4742	257.38	0.1981	2.68	1.21	1.21	1.26
n-Nonane VLE		3.8303	3.4770	256.76	0.2023	2.68	1.23	1.22	1.38
n-Decane VLE		3.8292	3.4783	256.29	0.2050	2.68	1.42	1.19	1.41

6.3. VLE Prediction Results

Tables 6.3 and 6.4 summarise the results of the pure predictions and correlations of each model, for each regression alternative, to each system respectively. Both the sPC-SAFT$_{GV}$ and sPC-SAFT$_{JC}$ variants produce good pure predictions of the experimental VLE data in all but a few instances. Due to the inability to regress 4-heptanone parameters for sPC-SAFT$_{JC}$ using only pure component data, highlighted previously, no VLE predictions are possible for this regression alternative.

In cases where poor predictions are in evidence, excellent correlations are possible using small binary interaction parameters, as typified in Figures 6.1 & 6.2 for the n-decane/3-heptanone system using pure component parameters for sPC-SAFT$_{JC}$. Even the non-polar sPC-SAFT variant can be made to fit the data using an appropriate binary interaction parameter and it is the incorporation of this correction to the dispersive term that produces the better correlative fit in Figure 6.2 as compared to the predictive fit in Figure 6.1. Pure prediction and correlation results like those presented for the n-decane/3-heptanone system below are provided for all nine binary systems using all five regression procedures in Appendix F.

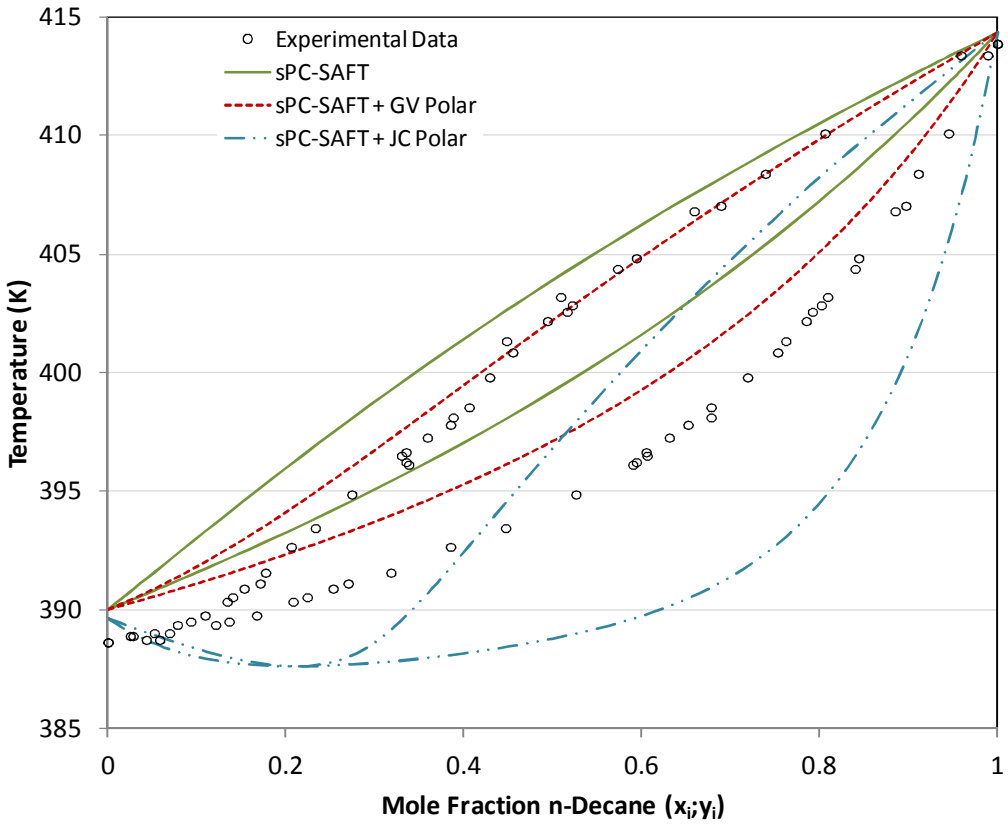

Figure 6.1:Pure predictions for isobaric VLE in n-decane/3-heptanone system at 40kPa. Only pure component data included in parameter regression

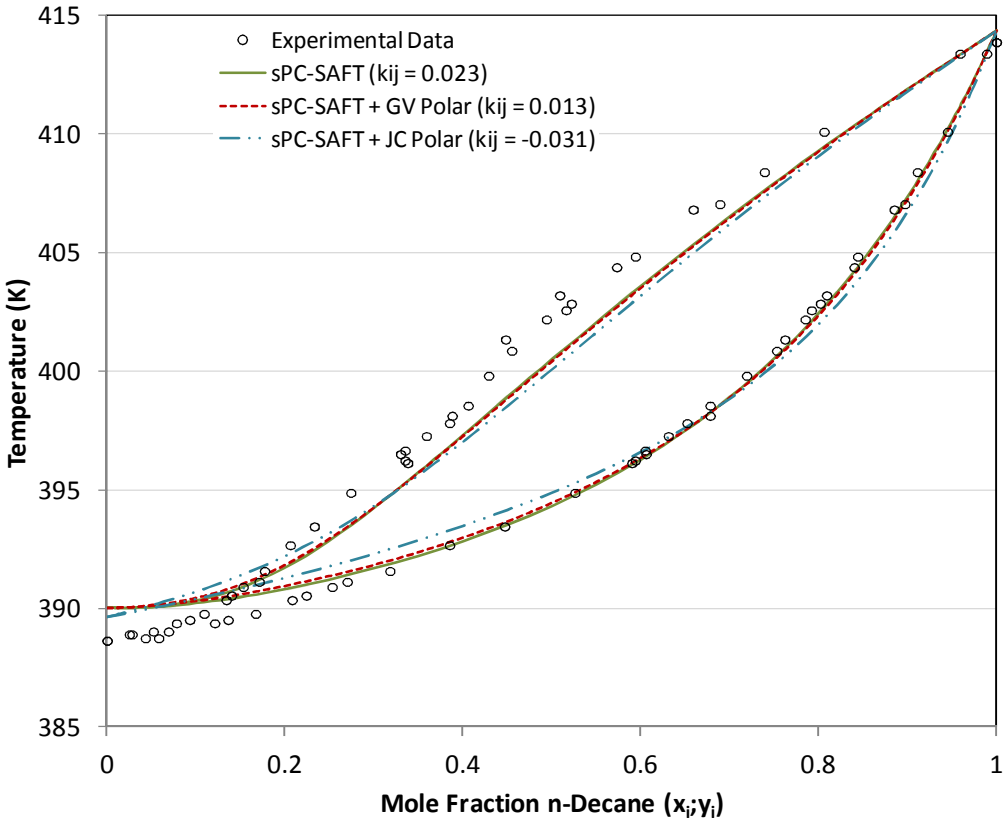

Figure 6.2: Correlations for isobaric VLE in n-decane/3-heptanone system at 40kPa. Only pure component data included in parameter regression

In general, the inclusion of VLE data in the regression procedure increases the accuracy of the model predictions of the VLE. This is true not only when the parameters for the system included in the regression are applied, but also when parameters generated using one of the other two binary systems are used. Indeed, in terms of the deviations as defined, the sPC-SAFT$_{GV}$ predictions for the n-octane/4-heptanone system are best when the parameters using n-decane/4-heptanone VLE in the regression are applied, to name but one such instance.

The thermodynamic modelling results of each alkane with the three heptanone isomers are more thoroughly investigated in the following sections. The discussion of the results is presented first, followed by the figures for the combined predictions for each regression procedure in each model.

Table 6.3: Pure prediction results for thermodynamic modelling of experimental VLE data

Regression Data	sPC-SAFT		sPC-SAFT$_{GV}$		sPC-SAFT$_{JC}$	
	Δy (x10^2)	ΔT (K)	Δy (x10^2)	ΔT (K)	Δy (x10^2)	ΔT (K)
n-Octane/2-Heptanone						
Pure Component Data			4.760	1.493	5.444	1.828
n_p/x_p Correlation			4.631	1.400	4.757	1.280
n-Octane VLE	7.849	3.674	3.710	0.299	3.656	0.212
n-Nonane VLE			3.922	0.382	3.745	0.250
n-Decane VLE			4.141	0.460	3.880	0.283
n-Nonane/2-Heptanone						
Pure Component Data			2.864	1.346	3.719	1.692
n_p/x_p Correlation			2.703	1.254	2.891	1.159
n-Octane VLE	6.421	3.488	1.158	0.322	1.361	0.207
n-Nonane VLE			1.479	0.237	1.509	0.155
n-Decane VLE			1.732	0.233	1.649	0.143
n-Decane/2-Heptanone						
Pure Component Data			3.280	1.493	3.732	1.971
n_p/x_p Correlation			3.181	1.383	3.069	1.353
n-Octane VLE	6.049	4.071	1.883	0.555	1.855	0.360
n-Nonane VLE			2.101	0.275	2.002	0.235
n-Decane VLE			2.189	0.180	2.002	0.221
n-Octane/3-Heptanone						
Pure Component Data			3.602	1.981	6.457	5.157
n_p/x_p Correlation			1.877	0.642	1.626	0.335
n-Octane VLE	5.549	3.459	2.114	0.248	2.139	0.265
n-Nonane VLE			2.068	0.258	1.915	0.313
n-Decane VLE			2.363	0.227	2.094	0.254
n-Nonane/3-Heptanone						
Pure Component Data			2.598	1.828	6.444	4.411
np/xp Correlation			0.947	0.634	0.501	0.253
n-Octane VLE	4.384	3.111	0.690	0.154	0.821	0.173
n-Nonane VLE			0.647	0.163	0.590	0.154
n-Decane VLE			1.001	0.140	0.831	0.130
n-Decane/3-Heptanone						
Pure Component Data			4.732	2.131	5.208	5.146
n_p/x_p Correlation			3.458	0.707	3.110	0.397
n-Octane VLE	6.572	3.676	2.871	0.364	2.982	0.260
n-Nonane VLE			2.855	0.378	2.888	0.275
n-Decane VLE			2.864	0.244	2.824	0.194
n-Octane/4-Heptanone						
Pure Component Data			1.167	1.198	-	-
n_p/x_p Correlation			1.639	0.251	2.292	0.541
n-Octane VLE	5.243	3.018	1.889	0.130	1.957	0.112
n-Nonane VLE			1.824	0.139	1.791	0.137
n-Decane VLE			1.843	0.129	1.735	0.217
n-Nonane/4-Heptanone						
Pure Component Data			1.448	1.110	-	-
n_p/x_p Correlation			1.014	0.275	1.465	0.584
n-Octane VLE	4.406	2.891	0.899	0.090	0.897	0.111
n-Nonane VLE			0.885	0.096	0.744	0.082
n-Decane VLE			0.858	0.102	0.644	0.145
n-Decane/4-Heptanone						
Pure Component Data			2.067	1.230	-	-
n_p/x_p Correlation			2.583	0.440	2.980	0.800
n-Octane VLE	5.699	3.192	2.365	0.245	2.448	0.259
n-Nonane VLE			2.365	0.260	2.372	0.190
n-Decane VLE			2.283	0.242	2.269	0.156

Table 6.4: Correlation results for thermodynamic modelling of experimental VLE data

Regression Data	sPC-SAFT		sPC-SAFT$_{GV}$		sPC-SAFT$_{JC}$	
	Δy (x10^2)	ΔT (K)	Δy (x10^2)	ΔT (K)	Δy (x10^2)	ΔT (K)
n-Octane/2-Heptanone						
Pure Component Data			3.152	0.307	3.385	0.230
n_p/x_p Correlation			3.145	0.315	3.398	0.235
n-Octane VLE	3.260	0.246	3.812	0.314	3.790	0.225
n-Nonane VLE			3.922	0.382	3.745	0.250
n-Decane VLE			3.830	0.282	3.758	0.221
n-Nonane/2-Heptanone						
Pure Component Data			0.914	0.294	1.229	0.196
n_p/x_p Correlation			0.899	0.304	1.230	0.199
n-Octane VLE	1.224	0.207	1.550	0.244	1.647	0.143
n-Nonane VLE			1.487	0.237	1.542	0.153
n-Decane VLE			1.586	0.210	1.632	0.141
n-Decane/2-Heptanone						
Pure Component Data			2.196	0.381	2.022	0.327
n_p/x_p Correlation			2.210	0.386	2.043	0.312
n-Octane VLE	2.003	0.374	2.196	0.212	1.977	0.228
n-Nonane VLE			2.171	0.222	1.996	0.238
n-Decane VLE			2.138	0.207	1.967	0.232
n-Octane/3-Heptanone						
Pure Component Data			1.518	0.357	1.735	0.532
n_p/x_p Correlation			1.416	0.375	1.687	0.326
n-Octane VLE	1.594	0.389	2.175	0.244	2.224	0.270
n-Nonane VLE			2.153	0.247	2.142	0.273
n-Decane VLE			2.320	0.202	2.281	0.242
n-Nonane/3-Heptanone						
Pure Component Data			0.426	0.241	0.818	0.471
np/xp Correlation			0.460	0.346	0.369	0.220
n-Octane VLE	0.541	0.233	0.651	0.158	0.699	0.146
n-Nonane VLE			0.635	0.165	0.630	0.154
n-Decane VLE			0.872	0.097	0.856	0.130
n-Decane/3-Heptanone						
Pure Component Data			2.947	0.454	3.164	0.675
n_p/x_p Correlation			3.048	0.592	2.948	0.408
n-Octane VLE	2.894	0.41	2.877	0.363	2.831	0.262
n-Nonane VLE			2.883	0.372	2.856	0.288
n-Decane VLE			2.791	0.252	2.781	0.209
n-Octane/4-Heptanone						
Pure Component Data			1.306	0.348	-	-
n_p/x_p Correlation			1.511	0.190	1.875	0.146
n-Octane VLE	1.793	0.191	1.941	0.134	2.020	0.130
n-Nonane VLE			1.871	0.142	1.928	0.130
n-Decane VLE			1.907	0.132	1.966	0.127
n-Nonane/4-Heptanone						
Pure Component Data			1.078	0.382	-	-
n_p/x_p Correlation			0.766	0.195	0.691	0.084
n-Octane VLE	0.719	0.113	0.881	0.093	0.795	0.093
n-Nonane VLE			0.860	0.100	0.745	0.081
n-Decane VLE			0.890	0.094	0.774	0.084
n-Decane/4-Heptanone						
Pure Component Data			2.396	0.610	-	-
n_p/x_p Correlation			2.302	0.359	2.236	0.170
n-Octane VLE	2.201	0.193	2.256	0.240	2.211	0.165
n-Nonane VLE			2.259	0.253	2.223	0.163
n-Decane VLE			2.246	0.242	2.217	0.162

6.3.1. n-Octane Systems

In the case of the 2-heptanone equilibria, it is apparent that the predictions using both pure component data and those where the polar parameter is fixed, provide a good fit of the vapour phase but the liquid phase is over predicted. Incorporation of VLE data produces an improved liquid phase prediction, at the expense of accuracy for the vapour phase prediction. If binary interaction parameters are fit in the former cases, as shown in Figures 6.3 & 6.4, the same trend is evident; liquid phase prediction is corrected at the expense of accuracy in the vapour phase, particularly in the equal concentration region.

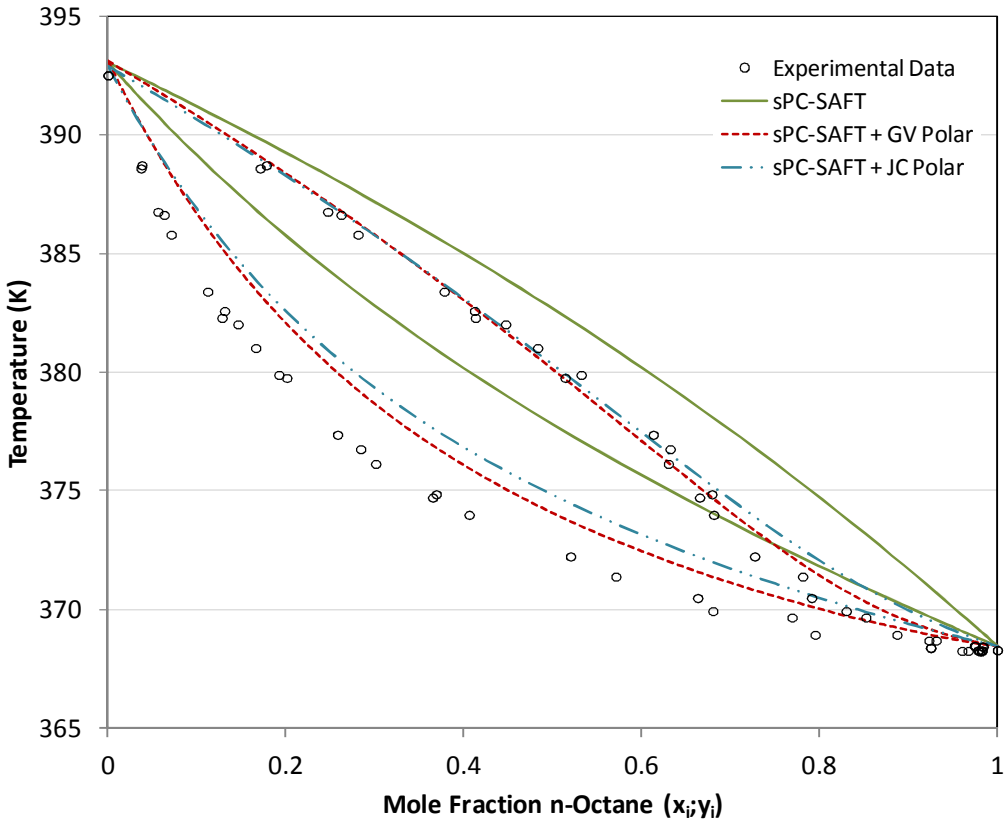

Figure 6.3: Pure predictions for isobaric VLE in n-octane/2-heptanone system at 40kPa. Correlation for polar parameter (x_p/n_p) used with pure component data in parameter regression.

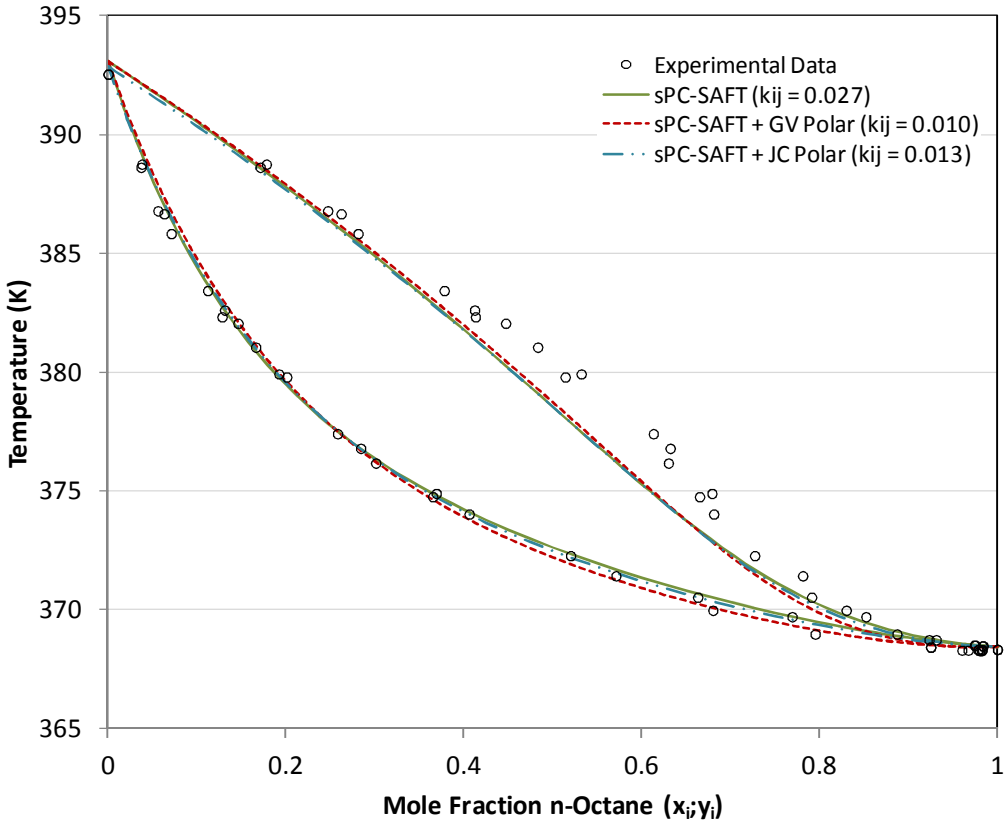

Figure 6.4: Correlations for isobaric VLE in n-octane/2-heptanone system at 40kPa. Correlation for polar parameter (x_p/n_p) used with pure component data in parameter regression.

In the case of the 3-heptanone equilibria, "standard" sPC-SAFT$_{JC}$ produces a particularly poor prediction, without even a qualitative agreement in evidence. The equivalent sPC-SAFT$_{GV}$ prediction is somewhat better, but still only provides some qualitative agreement. In both cases, better agreement with the experimental data can be achieved by fitting small binary interaction parameters akin to that seen in Figures 6.1 and 6.2. Much better predictions of the experimental data are in evidence when the polar parameter is fixed according to Equations 6.1 and 6.2 as well as with the incorporation of VLE data in the regression procedure. This is emphasised by the large difference in the value of the polar parameter between the standard regression (n_p = 1.5172 & x_p = 0.3385) and the parameters of the other four, agreeing predictions (n_p = ±2.2 & x_p = ±0.17). The liquid phase is well predicted by both models using the latter parameter sets, although, particularly in the sPC-SAFT$_{JC}$ case, deviations in the vapour phase are still apparent in the equal-concentration range.

Considering 4-heptanone, the standard regression parameter set produces a qualitatively poor prediction of the experimental data for the sPC-SAFT$_{GV}$ model, with the azeotrope predicted at a much lower n-octane concentration. Good agreement with experimental data is evident for the other four parameter sets, particularly for the GV-model. For sPC-SAFT$_{JC}$, the lack of regressed parameters means no prediction is possible using the standard regression procedure. When the polar parameter is set however, good qualitative agreement with experimental data is apparent, although as before, the liquid phase is over predicted. Including a binary interaction parameter rectifies the liquid phase discrepancy but once again the vapour phase prediction is compromised.

Table 6.5 details the predictions of the azeotropic points by both models for each regression procedure for all three n-octane systems. The correct prediction of the azeotropic point in such a high concentration region provides a stern test of any thermodynamic model and both models exhibit somewhat mixed results. When VLE data is incorporated in the regression, the azeotrope is well correlated by both models. Neither model consistently predicts the azeotropic point when VLE data is absent from the regression procedure, although correlations of sPC-SAFT$_{GV}$ more frequently predict the azeotrope than those of sPC-SAFT$_{JC}$. The effect of adding a binary interaction parameter to correlate the data is thus made clear from Table 6.5; while the trend is not necessarily influenced by its introduction, a binary interaction parameter allows the models to predict the azeotropic point in some cases where the pure prediction could not.

Table 6.5: Comparison between experimentally determined azeotropic points and the pure predictions and correlations of each model in the n-octane/x-heptanone systems

	Experimental Results		**Regression Procedure**		**Pure Predictions**		**Correlations**	
	Temp (°C)	**Comp. (mole% n-octane)**			**Temp (°C)**	**Comp. (mole% n-octane)**	**Temp (°C)**	**Comp. (mole% n-octane)**
n-octane/ 2-heptanone	95.1	98%	sPC-SAFT$_{GV}$	Pure Component Data	NP	NP	95.3	98%
				n_p Correlation	NP	NP	95.3	97%
				n-Octane VLE	95.2	95%	95.2	96%
				n-Nonane VLE	95.2	97%	95.2	96%
				n-Decane VLE	95.3	99%	95.3	99%
			sPC-SAFT$_{JC}$	Pure Component Data	NP	NP	NP	NP
				x_p Correlation	NP	NP	NP	NP
				n-Octane VLE	95.3	99%	95.3	99%
				n-Nonane VLE	NP	NP	NP	NP
				n-Decane VLE	NP	NP	NP	NP
n-octane/ 3-heptanone	~95.1	~98%	sPC-SAFT$_{GV}$	Pure Component Data	NP	NP	NP	NP
				n_p Correlation	NP	NP	95.3	99%
				n-Octane VLE	NP	NP	NP	NP
				n-Nonane VLE	95.3	99%	NP	NP
				n-Decane VLE	NP	NP	NP	NP
			sPC-SAFT$_{JC}$	Pure Component Data	92.37	75%	95.2	95%
				x_p Correlation	NP	NP	NP	NP
				n-Octane VLE	NP	NP	NP	NP
				n-Nonane VLE	NP	NP	NP	NP
				n-Decane VLE	NP	NP	NP	NP
n-octane/ 4-heptanone	95.1	98%	sPC-SAFT$_{GV}$	Pure Component Data	94.4	84%	95.0	90%
				n_p Correlation	95.2	95%	95.2	93%
				n-Octane VLE	95.2	95%	95.2	95%
				n-Nonane VLE	95.2	93%	95.2	95%
				n-Decane VLE	95.2	93%	95.2	95%
			sPC-SAFT$_{JC}$	Pure Component Data	-	-	-	-
				x_p Correlation	NP	NP	NP	NP
				n-Octane VLE	95.3	98%	95.3	99%
				n-Nonane VLE	95.3	97%	95.3	98%
				n-Decane VLE	95.3	95%	95.3	98%

"NP" – Azeotrope Not Predicted – indicates the inability of the relevant prediction/correlation to predict the presence of the azeotrope.

The sPC-SAFT$_{GV}$ and sPC-SAFT$_{JC}$ predictions for the n-octane/*x*-heptanone systems are presented in Figures 6.5 to 6.10.

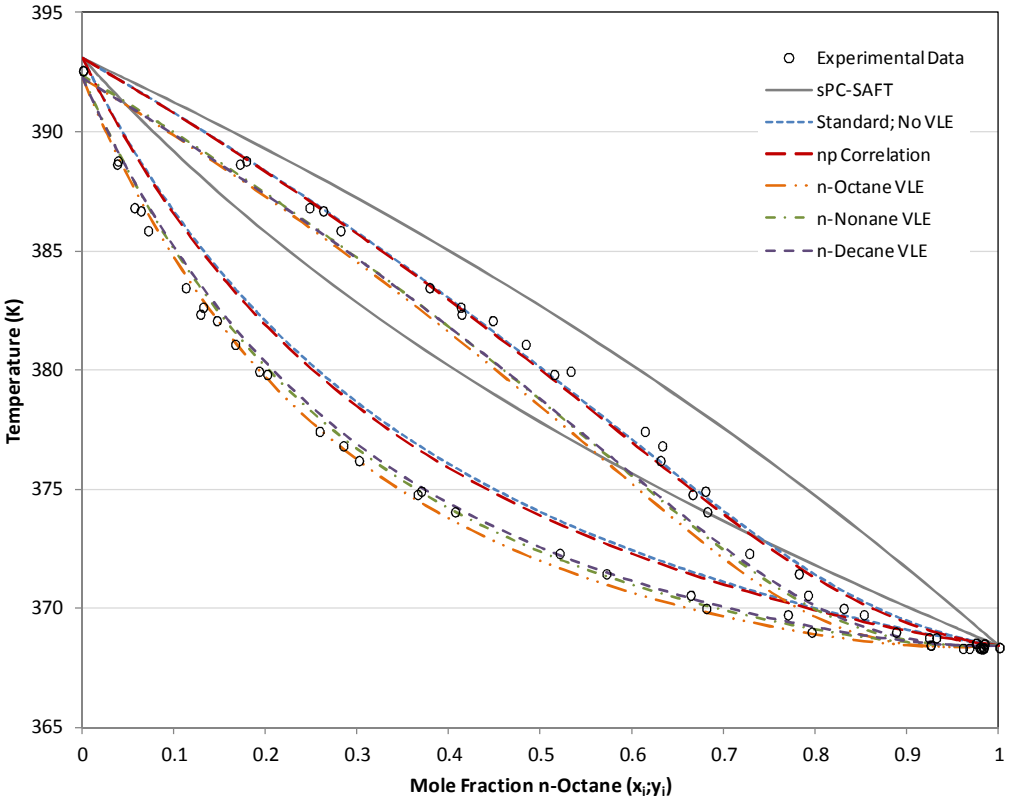

Figure 6.5: Pure predictions for all variants of parameter regression for sPC-SAFT$_{GV}$ in n-octane/2-heptanone system at 40kPa

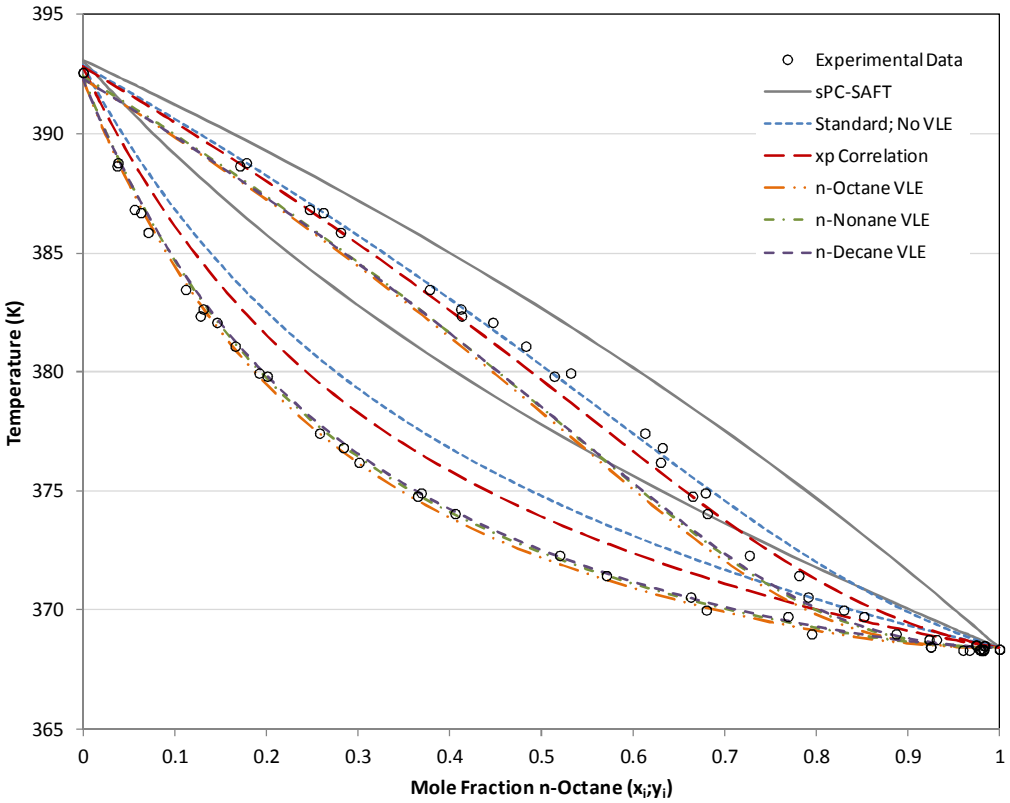

Figure 6.6: Pure predictions for all variants of parameter regression for sPC-SAFT$_{JC}$ in n-octane/2-heptanone system at 40kPa

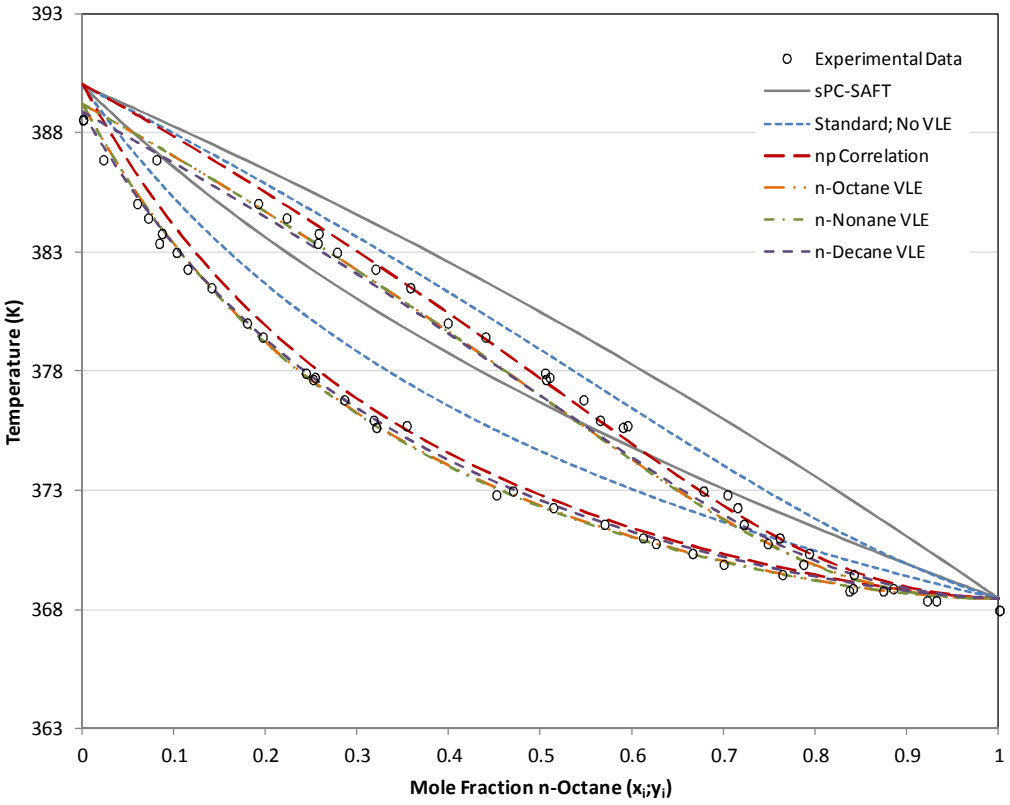

Figure 6.7: Pure predictions for all variants of parameter regression for sPC-SAFT$_{GV}$ in n-octane/3-heptanone system at 40kPa

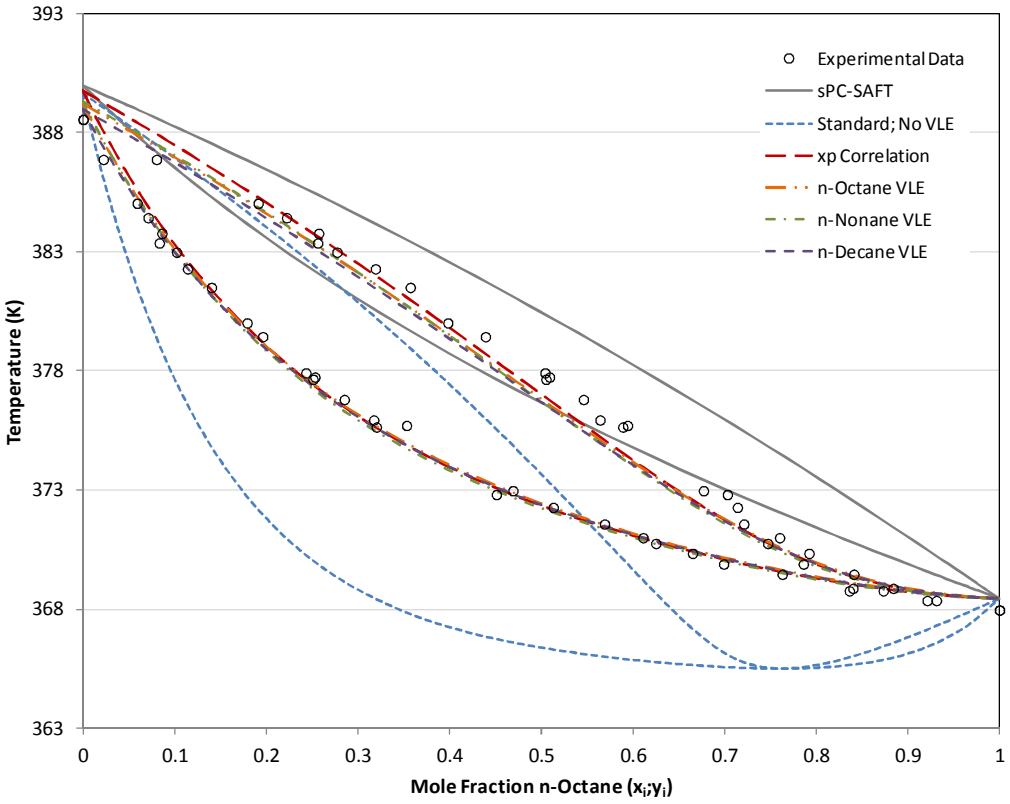

Figure 6.8: Pure predictions for all variants of parameter regression for sPC-SAFT$_{JC}$ in n-octane/3-heptanone system at 40kPa

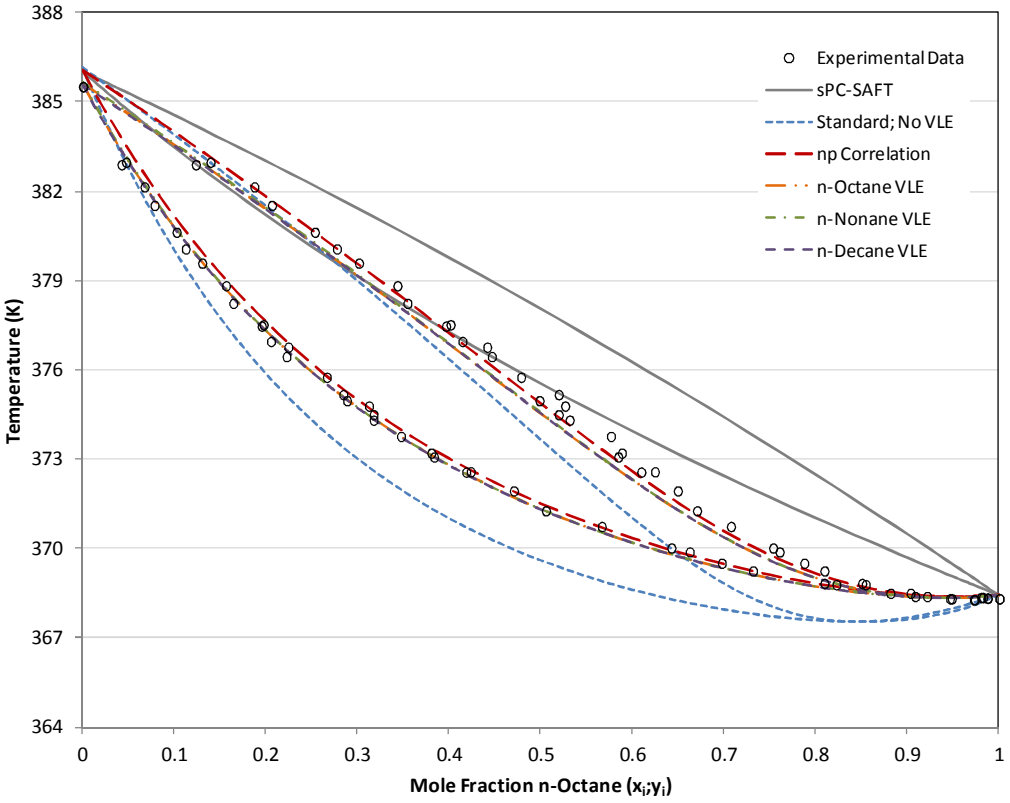

Figure 6.9: Pure predictions for all variants of parameter regression for sPC-SAFT$_{GV}$ in n-octane/4-heptanone system at 40kPa

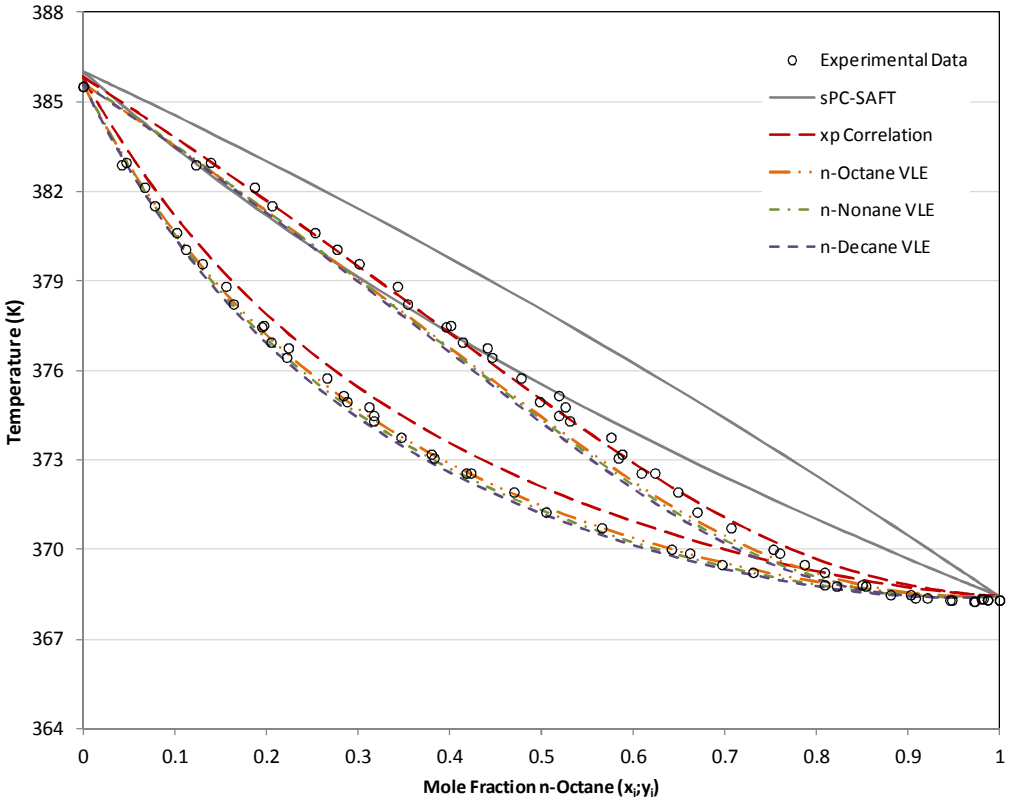

Figure 6.10: Pure predictions for all variants of parameter regression for sPC-SAFT$_{JC}$ in n-octane/4-heptanone system at 40kPa

6.3.2. n-Nonane Systems

The n-nonane systems provide a more stringent test of the ability of the parameter sets, given the very small temperature range in evidence in all three systems as well as the obvious azeotrope in each case. In the case of 2-heptanone, predictions made with parameters which lacked VLE data in the regression procedure produce good qualitative agreement with the experimental data, but the azeotropic temperature is over predicted by some 2°C, indicating that the polar interactions are under predicted. Incorporation of VLE data improves the prediction in both models, although incorporating the n-octane data produces a worse prediction of the azeotrope temperature than either the n-nonane or n-decane cases.

For the 3-heptanone case, the standard sPC-SAFT$_{JC}$ prediction is so poor its full inclusion would overly distort the axes of the combined plots, akin to that given for the n-octane/2-heptanone predictions in Figures 6.5 & 6.6), with the degree of non-ideality severely over predicted by this parameter set. As can be seen in Figures 6.11 & 6.12 however, even this deviation can be rectified, with the model brought into better qualitative agreement with experimental data by applying a small binary interaction parameter.

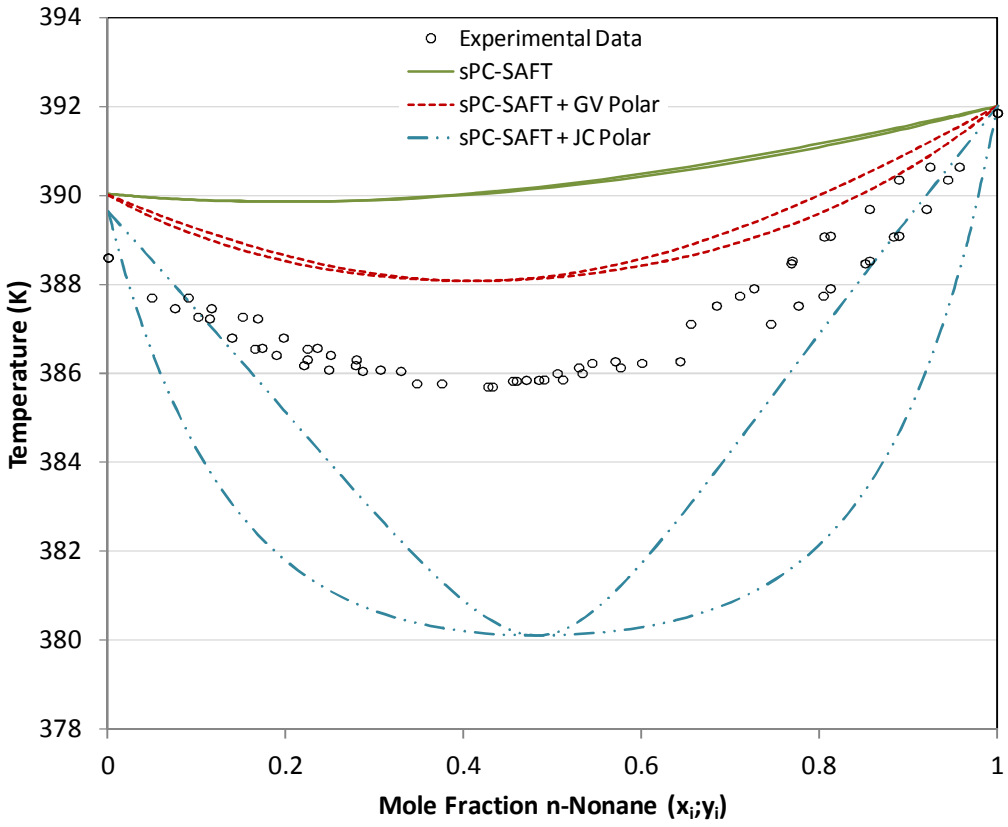

Figure 6.11: Pure predictions for isobaric VLE in n-nonane/3-heptanone system at 40kPa. Only pure component data included in parameter regression.

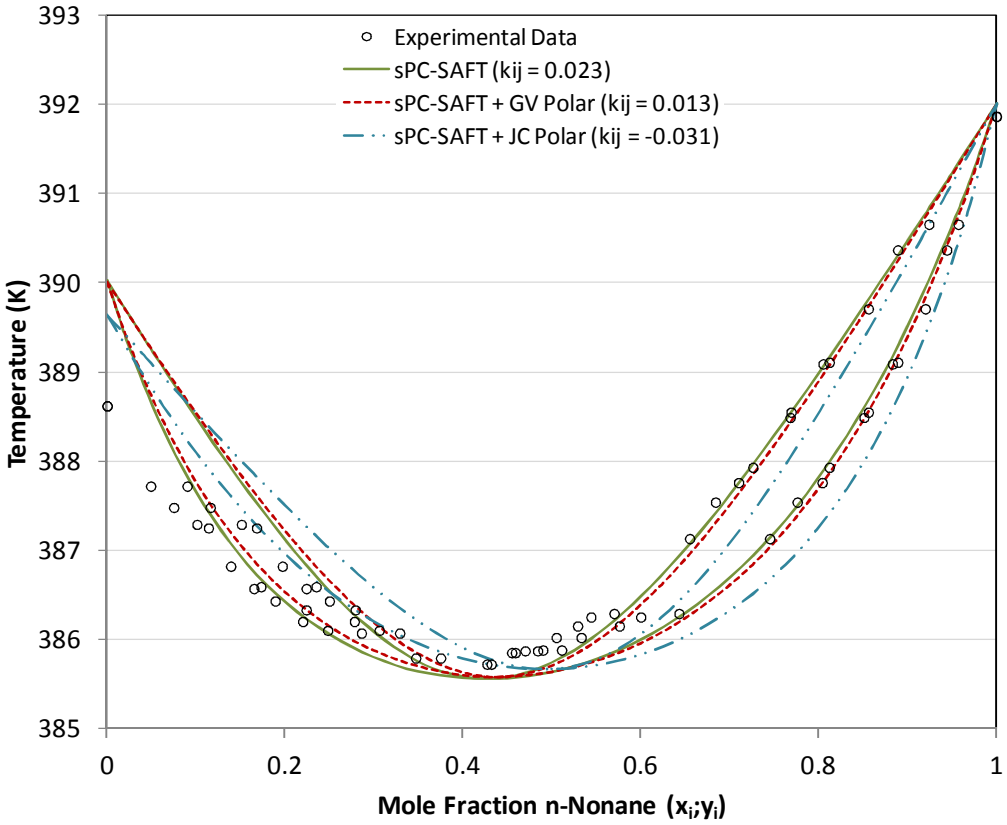

Figure 6.12: Correlations for isobaric VLE in n-nonane/3-heptanone system at 40kPa. Only pure component data included in parameter regression.

As with the 2-heptanone system, setting the value of the polar parameter in the regression is not sufficient to produce a perfect fit of the data for sPC-SAFT$_{GV}$, but an acceptable prediction is evident when setting x_p by Equation 6.1. Deviations in the latter are only evident in the low n-nonane composition space and are influenced by under-prediction of the pure heptanone boiling point.

The standard sPC-SAFT$_{GV}$ prediction for the 4-heptanone system is poor, over predicting the deviations from ideality resulting in the azeotropic temperature being approximately 2 °C lower than that observed experimentally. The prediction of sPC-SAFT$_{GV}$ with n_p set by Equation 6.2 is in excellent agreement with the experimental data, with deviations only arising as a result of the slightly over estimated pure heptanone boiling temperature. The experimental data is well predicted by all three parameter sets where VLE data was included in the regression. Overall, both polar variants of sPC-SAFT produce excellent predictions of the phase behaviour in particularly tricky systems, where the temperature range in question is as small as 6°C.

Of great practical and industrial concern is the ability of the thermodynamic model to predict the azeotropic point with accuracy. Unlike the n-octane systems before and the n-decane systems which follow, presence of the azeotropic point in the middle of the compositions range allows for the ability of each model to predict the reported azeotropic point to be assessed with a degree of confidence. In a manner similar to that used to find the experimental azeotropic composition, the model prediction for the

azeotropic composition can be determined by finding the x-intercept of model prediction curve in a plot of (y-x) vs. x as illustrated for the n-nonane/2-heptanone case in Figure 6.13 for sPC-SAFT$_{GV}$.

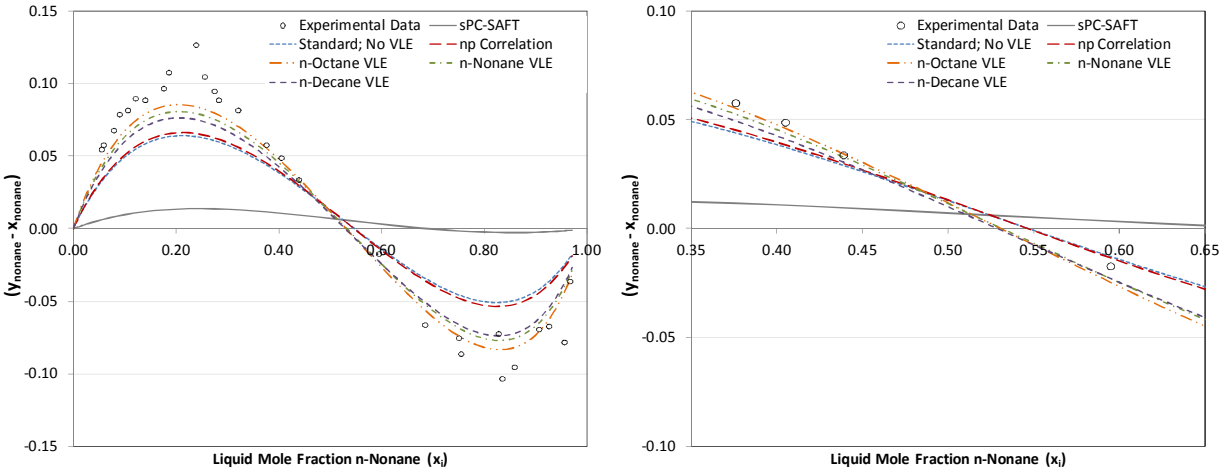

Figure 6.13: Plot of (y-x) vs. x yielding azeotropic composition predicted by sPC-SAFT$_{GV}$ in n-nonane/2-heptanone system for each regression procedure.

The predicted azeotropic compositions and temperatures by each model, in terms of both pure predictions and correlations, for each of the n-nonane/*x*-heptanone systems are summarised in Table 6.6, with the predictions for the n-nonane/*x*-heptanone systems for both polar models given in Figures 6.14 to 6.19.

Table 6.6: Comparison between experimentally determined azeotropic points and the pure predictions and correlations of each model in the n-nonane/x-heptanone systems

	Experimental Results		Regression Procedure		Pure Predictions		Correlations	
	Temp (°C)	Comp. (mole% n-nonane)			Temp (°C)	Comp. (mole% n-nonane)	Temp (°C)	Comp. (mole% n-nonane)
n-nonane/ 2-heptanone	113.5	53%	sPC-SAFT$_{GV}$	Pure Component Data	115.1	55%	113.3	55%
				n_p Correlation	115.0	55%	113.3	53%
				n-Octane VLE	113.0	53%	113.4	54%
				n-Nonane VLE	113.4	53%	113.4	53%
				n-Decane VLE	113.4	53%	113.4	53%
			sPC-SAFT$_{JC}$	Pure Component Data	115.8	51%	113.4	53%
				x_p Correlation	115.0	51%	113.5	51%
				n-Octane VLE	113.2	52%	113.5	51%
				n-Nonane VLE	113.4	51%	113.4	51%
				n-Decane VLE	113.4	51%	113.4	51%
n-nonane/ 3-heptanone	112.5	44%	sPC-SAFT$_{GV}$	Pure Component Data	115.0	41%	112.5	44%
				n_p Correlation	113.3	46%	112.5	46%
				n-Octane VLE	112.5	44%	112.5	44%
				n-Nonane VLE	112.5	44%	112.5	44%
				n-Decane VLE	112.7	43%	112.5	43%
			sPC-SAFT$_{JC}$	Pure Component Data	107.0	48%	112.6	49%
				x_p Correlation	112.7	44%	112.5	44%
				n-Octane VLE	112.7	42%	112..5	42%
				n-Nonane VLE	112.5	43%	112.5	43%
				n-Decane VLE	112.5	42%	112.5	42%
n-nonane/ 4-heptanone	110.6	34%	sPC-SAFT$_{GV}$	Pure Component Data	109.5	41%	110.9	39%
				n_p Correlation	111.1	35%	110.8	35%
				n-Octane VLE	110.8	33%	110.7	33%
				n-Nonane VLE	110.7	33%	110.7	33%
				n-Decane VLE	110.7	33%	110.7	33%
			sPC-SAFT$_{JC}$	Pure Component Data	-	-	-	-
				x_p Correlation	111.4	29%	110.6	32%
				n-Octane VLE	110.7	31%	110.6	32%
				n-Nonane VLE	110.6	32%	110.6	32%
				n-Decane VLE	110.5	32%	110.6	32%

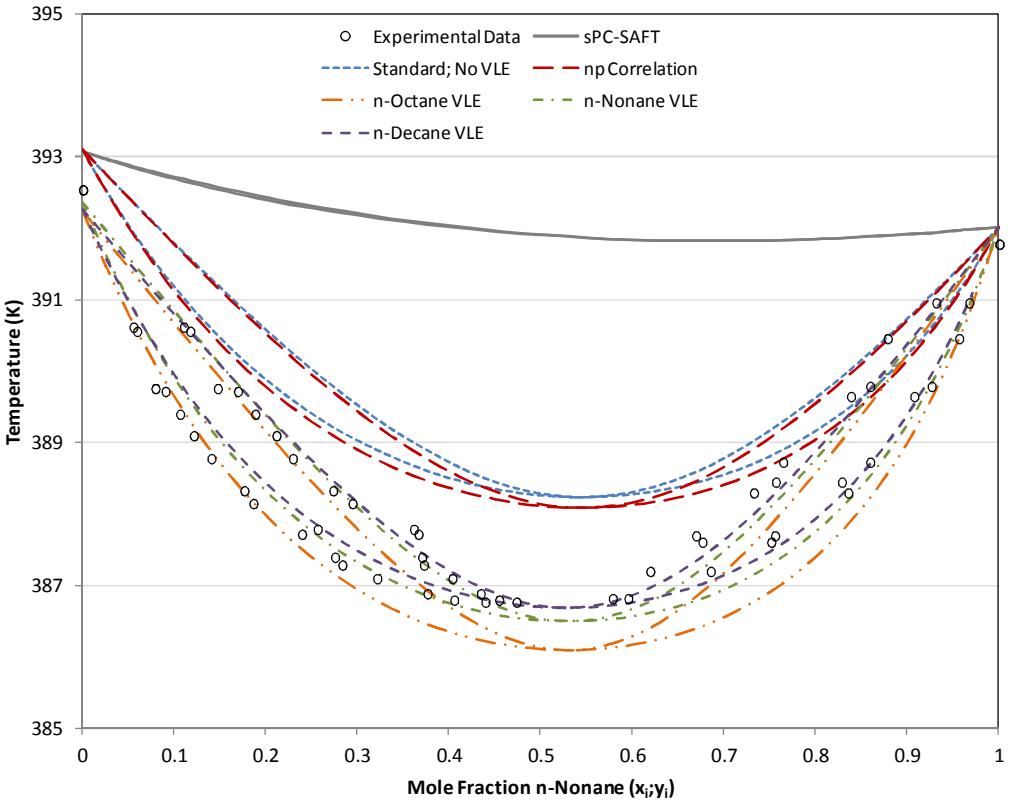

Figure 6.14: Pure predictions for all variants of parameter regression for sPC-SAFT$_{GV}$ in n-nonane/2-heptanone system at 40kPa

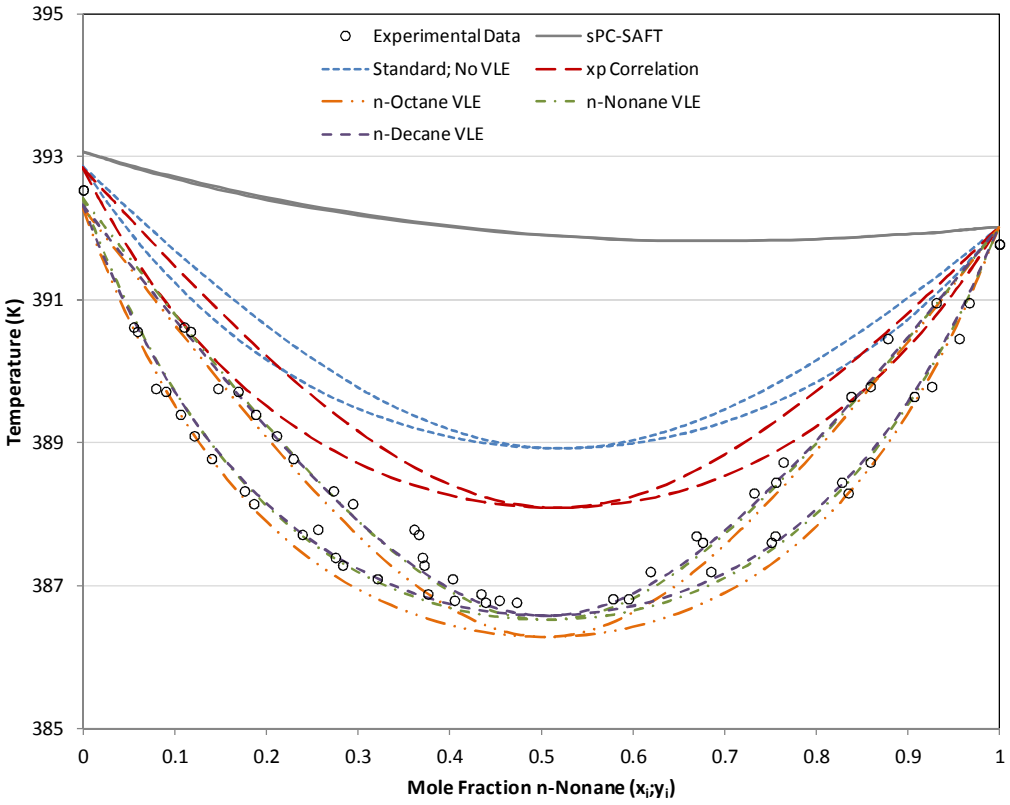

Figure 6.15: Pure predictions for all variants of parameter regression for sPC-SAFT$_{JC}$ in n-nonane/2-heptanone system at 40kPa

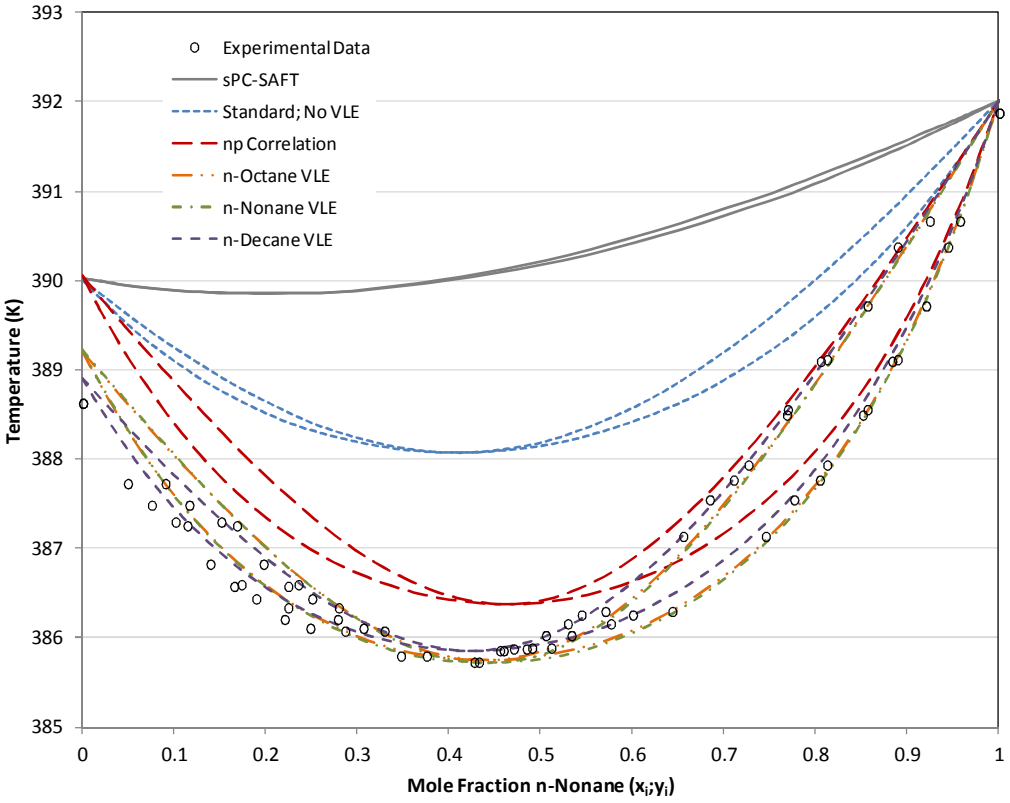

Figure 6.16: Pure predictions for all variants of parameter regression for sPC-SAFT$_{GV}$ in n-nonane/3-heptanone system at 40kPa

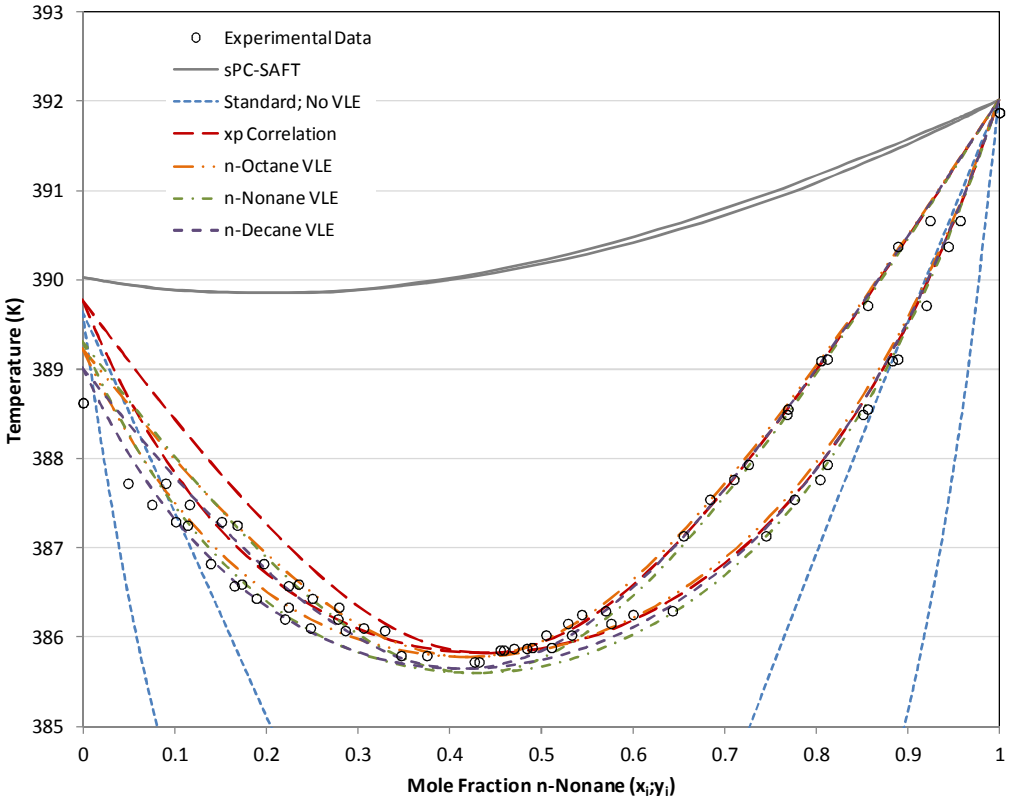

Figure 6.17: Pure predictions for all variants of parameter regression for sPC-SAFT$_{JC}$ in n-nonane/3-heptanone system at 40kPa

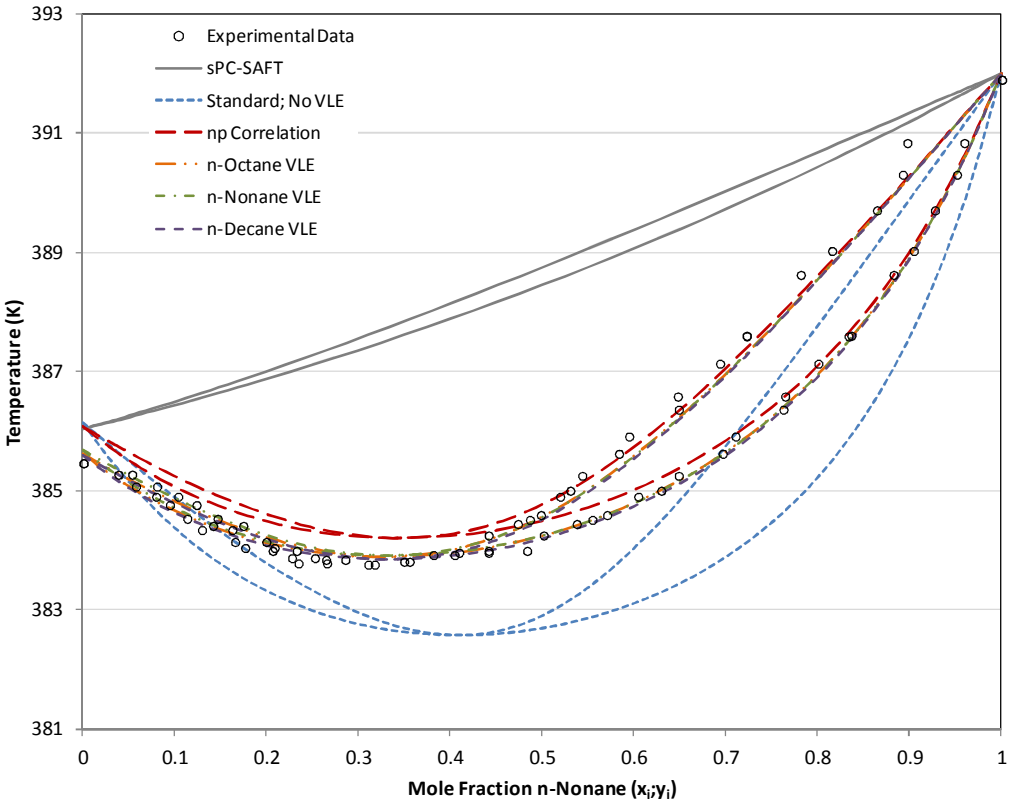

Figure 6.18: Pure predictions for all variants of parameter regression for sPC-SAFT$_{GV}$ in n-nonane/4-heptanone system at 40kPa

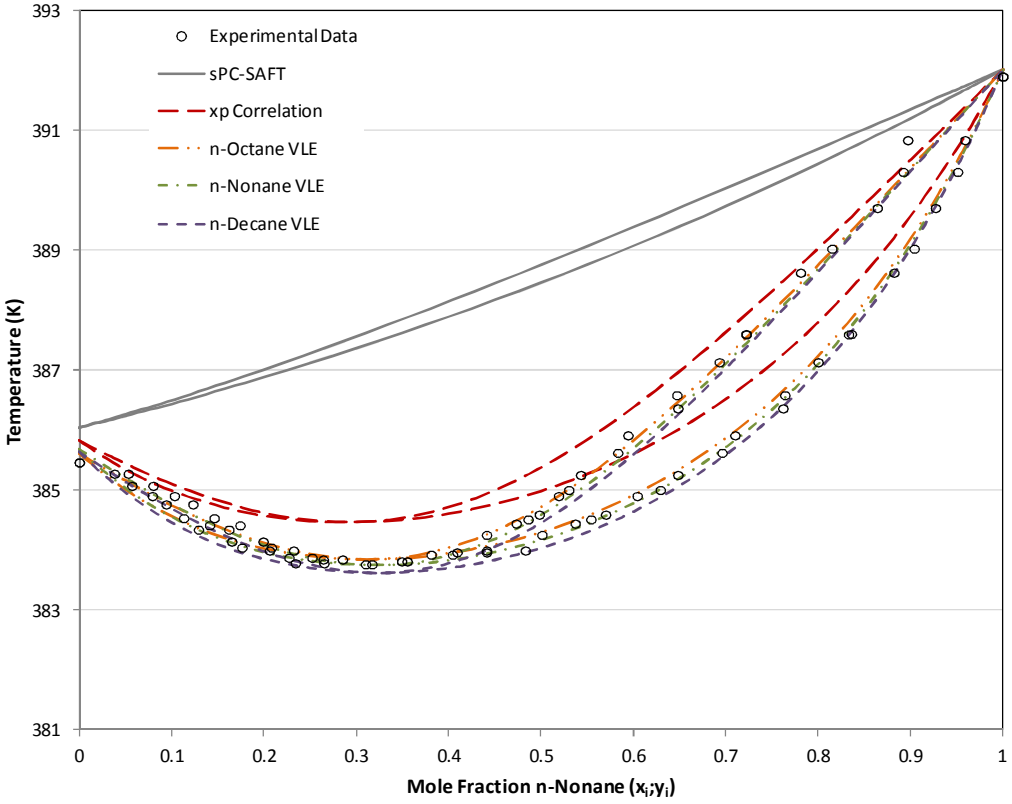

Figure 6.19: Pure predictions for all variants of parameter regression for sPC-SAFT$_{JC}$ in n-nonane/4-heptanone system at 40kPa

6.3.3. n-Decane Systems

The n-decane systems with 2-, 3- & 4-heptanone exhibit similar trends to those seen in the n-octane and n-nonane systems examined above. With respect to 2-heptanone with n-decane, the two sets of parameters without VLE incorporated into the regression procedure produce fair predictions of the vapour phase in the mid to high n-decane composition space, but the prediction worsens approaching the pure heptanone vapour pressure. The parameters for the standard regression procedure in sPC-SAFT$_{JC}$ produce a particularly poor prediction, but in all four cases, the liquid phase is poorly correlated. Binary interaction parameters (see Figures 6.20 and 6.21) rectify the liquid phase discrepancy but, as seen for the n-octane systems previously, accuracy in the vapour phase prediction suffers as a result.

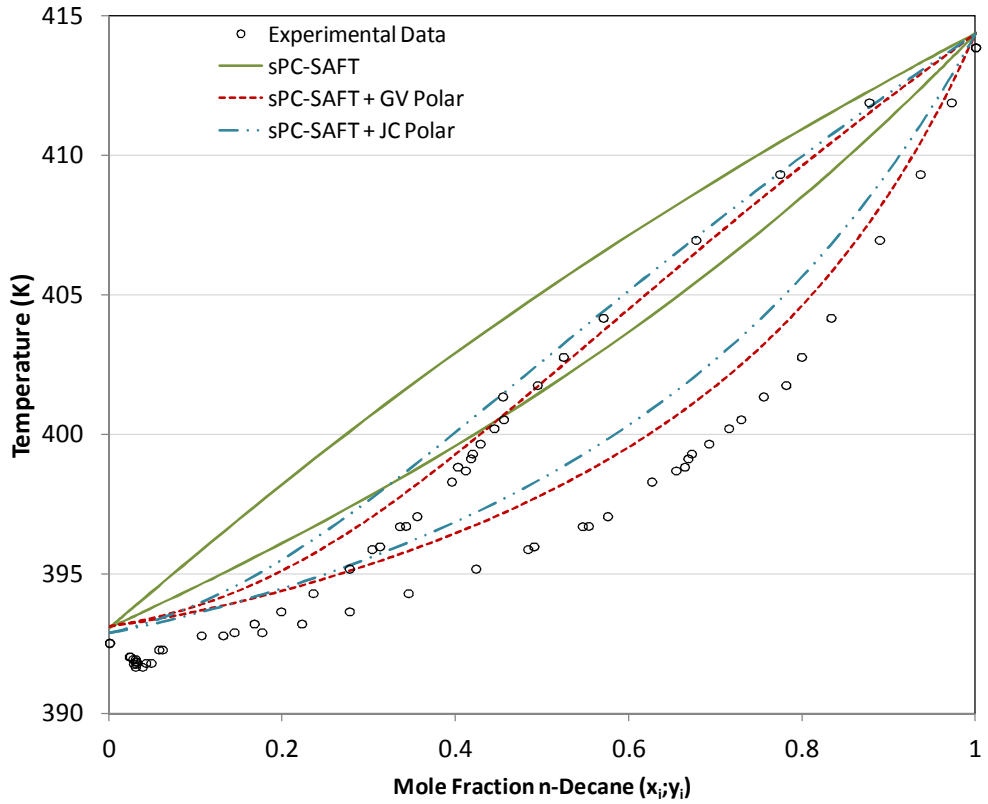

Figure 6.20: Pure predictions for isobaric VLE in n-decane/2-heptanone system at 40kPa. Only pure component data included in parameter regression

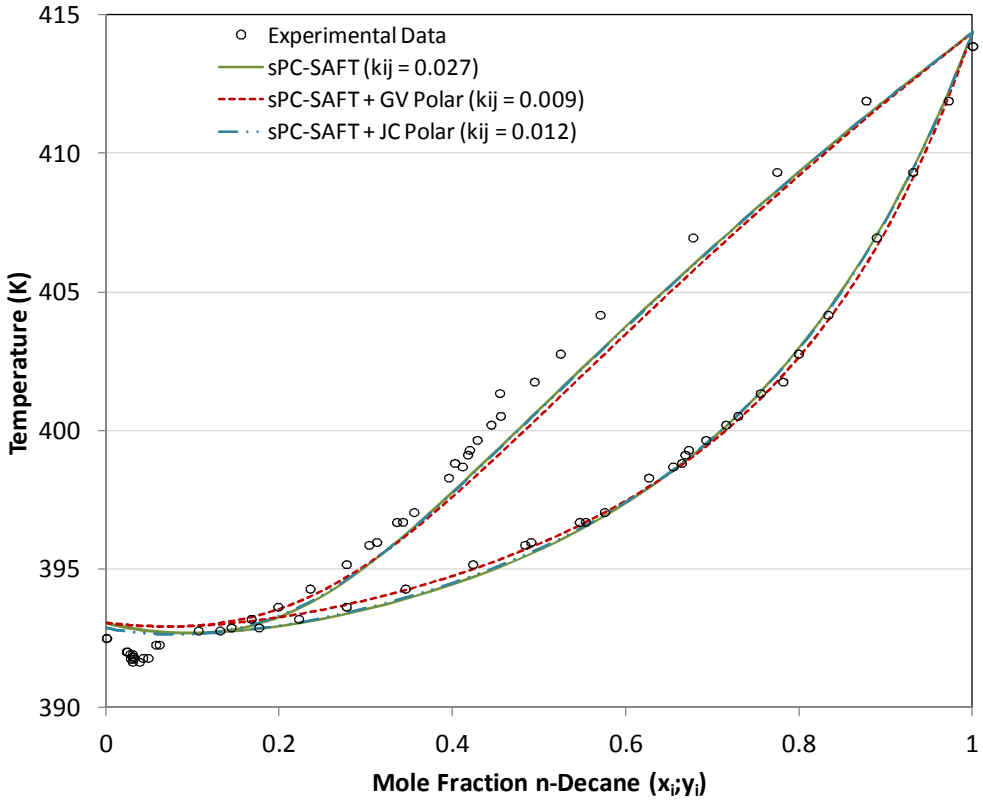

Figure 6.21: Correlations for isobaric VLE in n-decane/2-heptanone system at 40kPa. Only pure component data included in parameter regression

Incorporating VLE data into the regression procedure results in a prediction which correlates the liquid phase with a high degree of accuracy, but the dew point curve is under predicted in both models. The fact that the same trend was apparent with the n-octane systems suggests this may be an inherent flaw shared by both of the polar sPC-SAFT models.

The standard regression parameters for sPC-SAFT$_{JC}$ produce a poor prediction of the n-decane – 3-heptanone VLE and the equivalent sPC-SAFT$_{GV}$ parameters exhibit only qualitative agreement with the data in the high n-decane region. For both models, incorporating VLE data does not offer significant improvement over the predictions of the parameter set where the n_p and x_p are set in the regression procedure. All such predictions are in very good agreement with experimental liquid phase data, but again the vapour phase is under predicted. The large difference in quality of prediction between the standard regression procedure and the latter four is highlighted by the large difference in the values of the parameters generated (see Table 6.2.)

Considering the n-decane/4-heptanone system predictions, apart from the standard regression parameters for sPC-SAFT$_{GV}$, excellent correlation of the experimental results is apparent in both models for all four regression procedures. In particular, the sPC-SAFT$_{GV}$ predictions excel where there is no apparent difference between the parameter set where n_p is held constant and the three parameter sets where VLE was included. This point is re-enforced by the similarity of the generated parameters for each of the four regression procedures in Table 6.2.

As with the n-octane and n-nonane systems previously, the ability of each model to accurately predict the azeotropic point in each n-decane/*x*-heptanone system is of interest. An unfortunate result regarding n-decane systems is the apparent inability of the models to correlate the azeotropic points. Indeed, only the n-decane/2-heptanone azeotrope is predicted by the models and even this is only achievable through incorporation of VLE data in the regression procedure, as indicated in Figure 6.22 for sPC-SAFT$_{GV}$. The fact that only the azeotrope of the most polar isomer can be predicted lends support to the observation that the model predictions worsen as the functional group shifts centrally and thus the polar interactions are diminished.

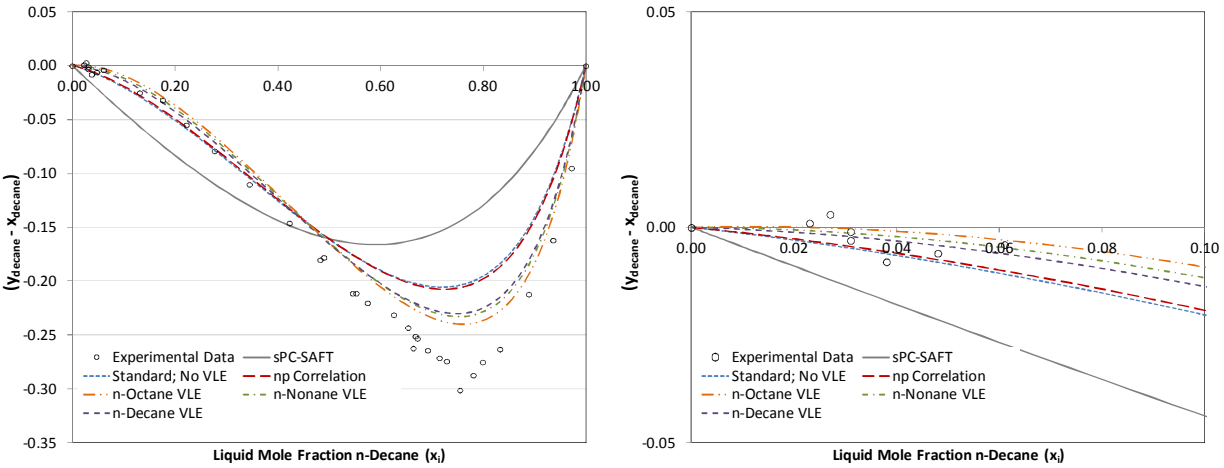

Figure 6.22: Plot of (y-x) vs. x yielding azeotropic composition predicted by sPC-SAFT$_{GV}$ in n-decane/2-heptanone system for each regression procedure. The azeotropic point can only be predicted by incorporating VLE data in the regression procedure.

Polar sPC-SAFT predictions for the three experimental systems containing n-decane are presented in Figures 6.23 to 6.28.

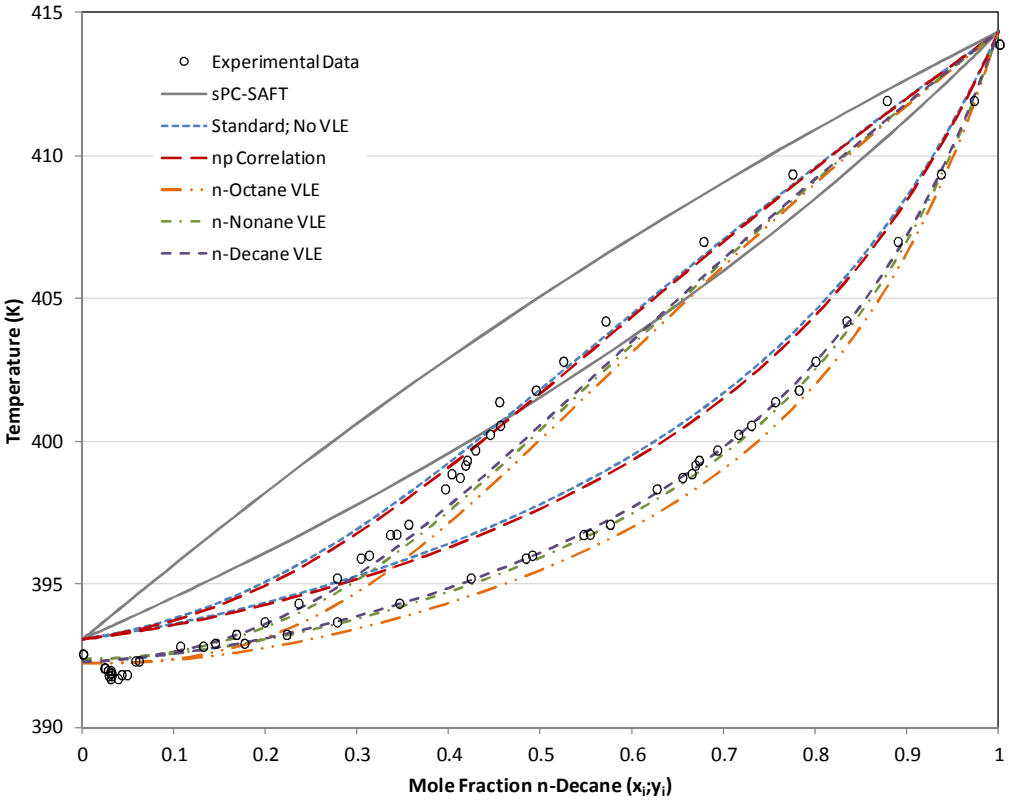

Figure 6.23: Pure predictions for all variants of parameter regression for sPC-SAFT$_{GV}$ in n-decane/2-heptanone system at 40kPa

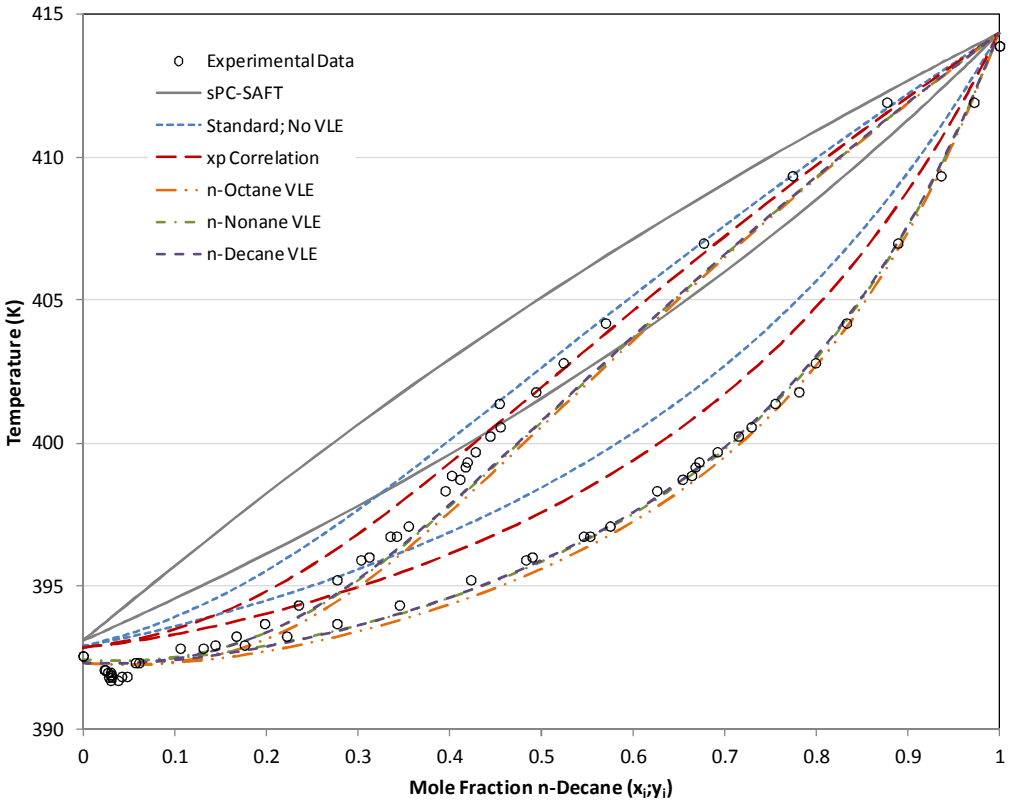

Figure 6.24: Pure predictions for all variants of parameter regression for sPC-SAFT$_{JC}$ in n-decane/2-heptanone system at 40kPa

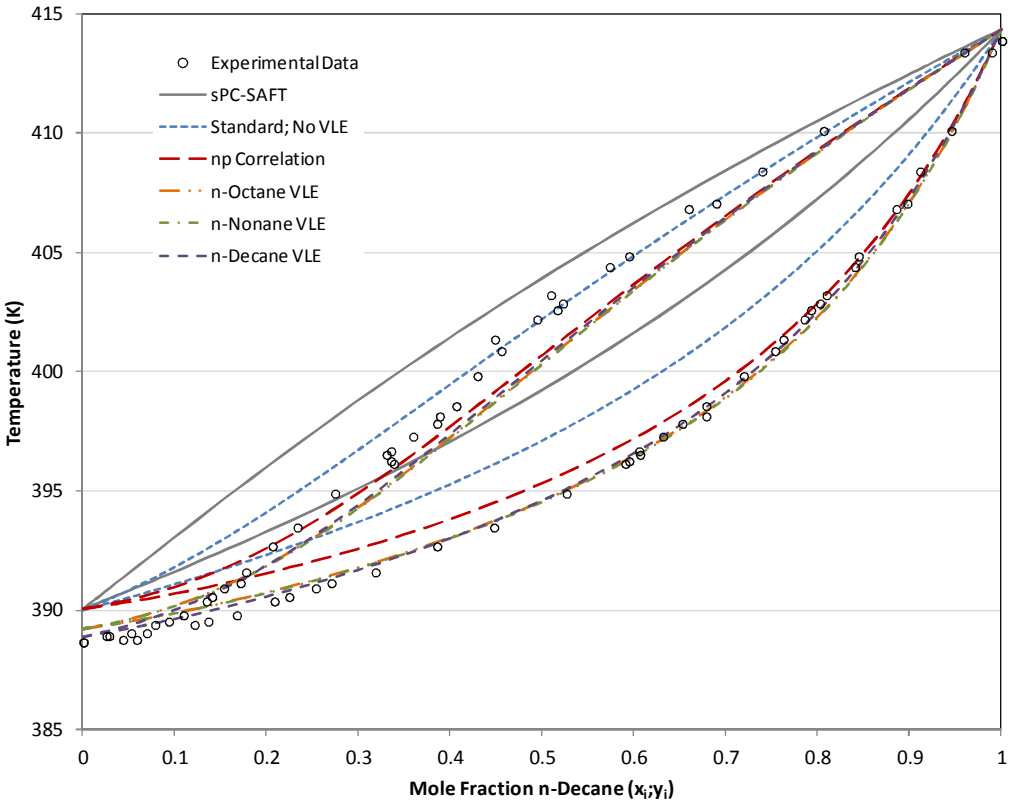

Figure 6.25: Pure predictions for all variants of parameter regression for sPC-SAFT$_{GV}$ in n-decane/3-heptanone system at 40kPa

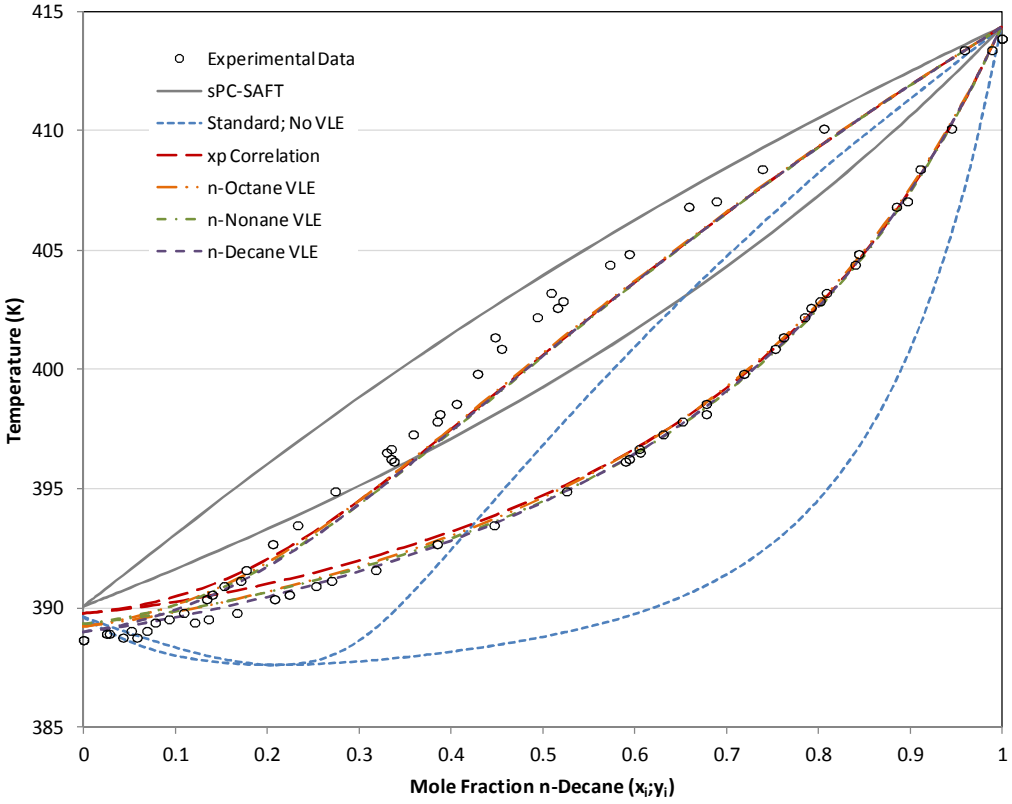

Figure 6.26: Pure predictions for all variants of parameter regression for sPC-SAFT$_{JC}$ in n-decane/3-heptanone system at 40kPa

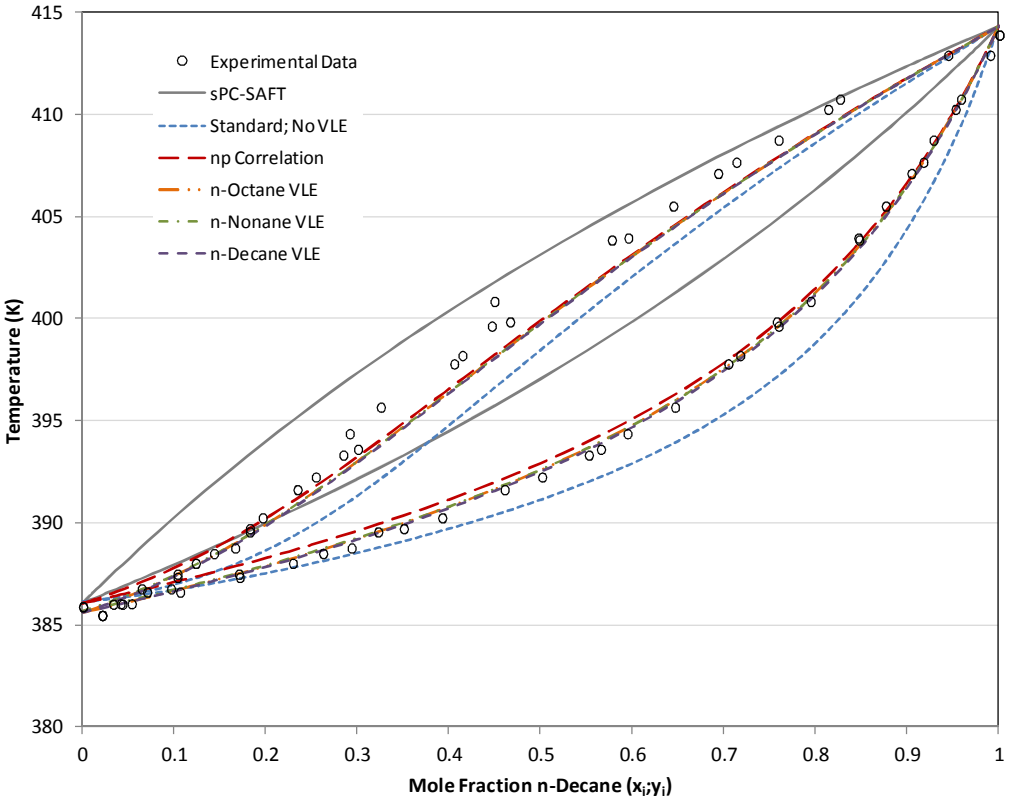

Figure 6.27: Pure predictions for all variants of parameter regression for sPC-SAFT$_{GV}$ in n-decane/4-heptanone system at 40kPa

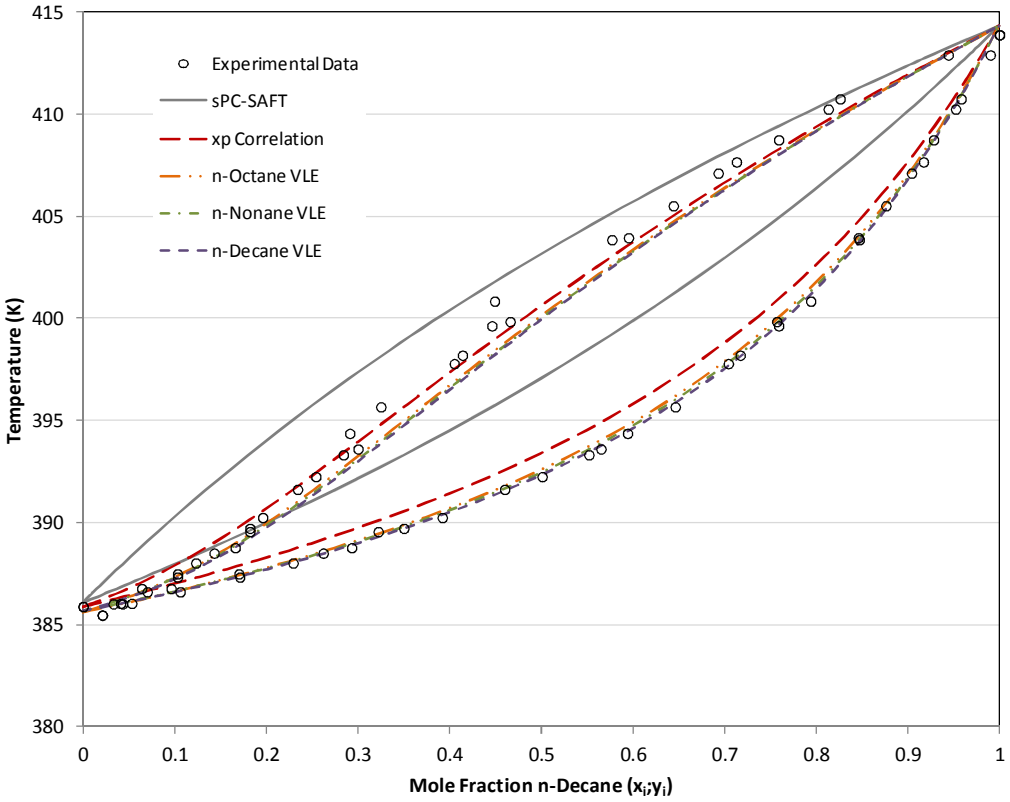

Figure 6.28: Pure predictions for all variants of parameter regression for sPC-SAFT$_{JC}$ in n-decane/4-heptanone system at 40kPa

6.3.4. Independent System: n-Hexane – 4-Heptanone

In the previous sections, the heptanone parameter sets generated by the five different regression procedures outlined in Section 6.1.3. have only been applied to VLE data measured in this work. However, a truly rigorous test of the generated parameters would be their application to independently measured VLE data. As highlighted in Chapter 3, the only reported case of measured VLE data containing a heptanone structural isomer and an n-alkane is the n-hexane/4-heptanone system at 338.15K, measured by Maripuri & Ratcliff (1972). In this section, the parameters generated for 4-heptanone are used for the prediction of this isothermal equilibrium.

Tables 6.7 and 6.8 present the deviations of the pure predictions and correlations from the data respectively. The respective model predictions are presented in Figures 6.29 and 6.30.

Table 6.7: Pure prediction results for thermodynamic modelling of n-hexane – 4-heptanone VLE data at 338.15 K

Regression Data	sPC-SAFT		sPC-SAFT$_{GV}$		sPC-SAFT$_{JC}$	
	Δy (x10²)	ΔP (%)	Δy (x10²)	ΔP (%)	Δy (x10²)	ΔP (%)
Pure Component Data			0.615	10.750	-	-
np/xp Correlation			0.269	4.400	0.300	4.002
n-Octane VLE	0.970	9.362	0.277	4.517	0.370	5.144
n-Nonane VLE			0.263	4.608	0.408	5.492
n-Decane VLE			0.265	4.527	0.430	5.851

Table 6.8: Pure prediction results for thermodynamic modelling of n-hexane – 4-heptanone VLE data at 338.15 K

Regression Data	sPC-SAFT		sPC-SAFT$_{GV}$		sPC-SAFT$_{JC}$	
	Δy (x10²)	ΔP (%)	Δy (x10²)	ΔP (%)	Δy (x10²)	ΔP (%)
Pure Component Data			0.275	2.659	-	-
np/xp Correlation			0.285	2.573	0.334	2.625
n-Octane VLE	0.389	2.863	0.334	2.552	0.328	2.569
n-Nonane VLE			0.321	2.559	0.312	2.551
n-Decane VLE			0.304	2.567	0.312	2.555

The non-polar sPC-SAFT variant correlates the liquid phase equilibria well enough, but the inability to account for polar interaction is highlighted by the poor prediction of the vapour phase. Apart from the predictions of the standard regression parameter set for sPC-SAFT$_{GV}$, all parameter sets for the polar models produce equally good predictions of the limited experimental data points. However, given that a prediction was not even possible for the traditional sPC-SAFT$_{JC}$ parameter set, the performance of the corresponding sPC-SAFT$_{GV}$ parameters is good. In particular, it becomes apparent that the choice of VLE data incorporated into the parameter regression does not affect the quality of the prediction in this system.

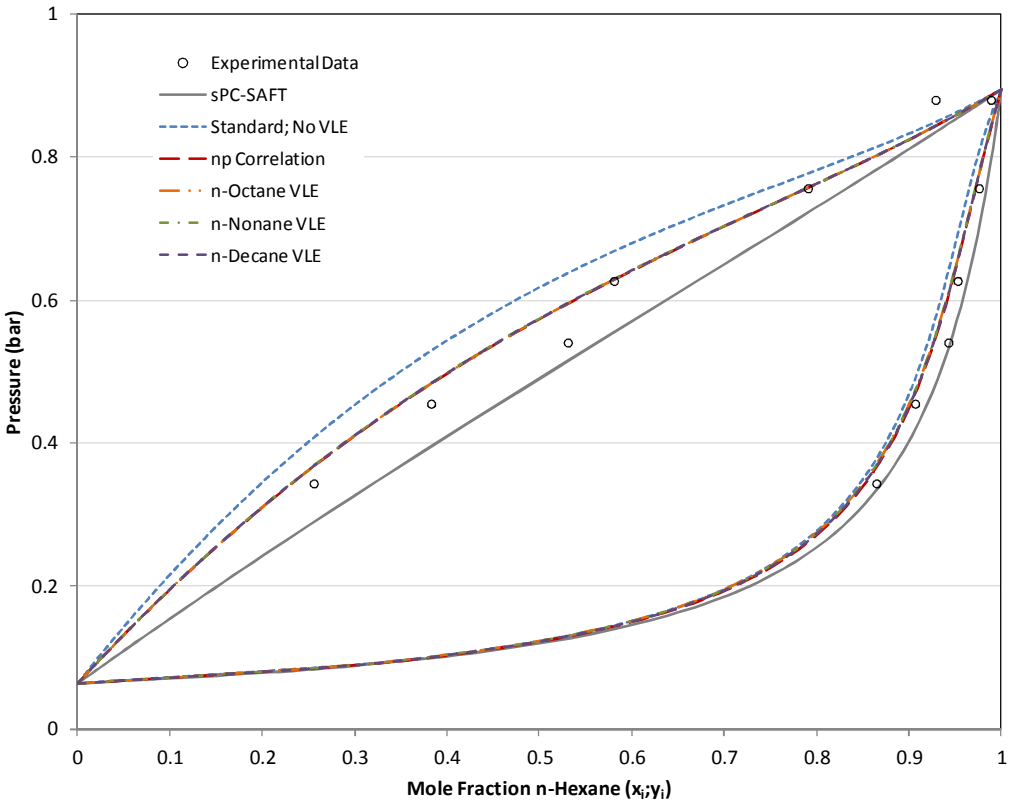

Figure 6.29: Pure predictions for all variants of parameter regression for sPC-SAFT$_{GV}$ in n-hexane/4-heptanone system at 338.15K

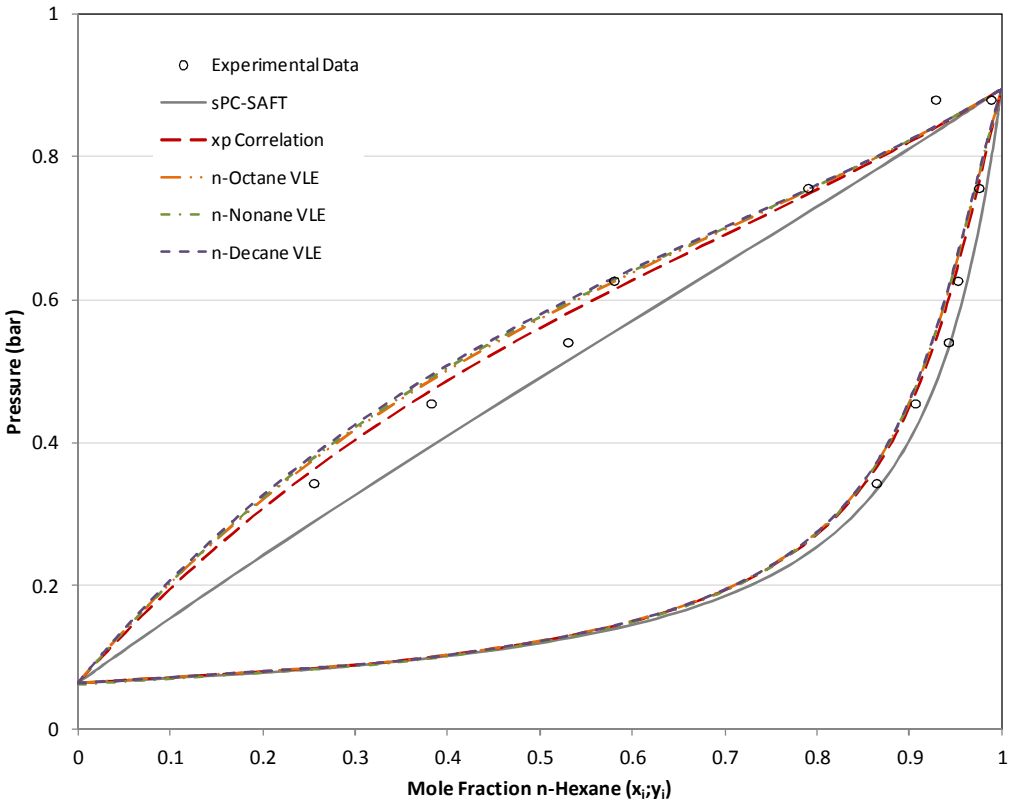

Figure 6.30: Pure predictions for all variants of parameter regression for sPC-SAFT$_{JC}$ in n-hexane/4-heptanone system at 338.15K

6.3.5. Prediction Results Highlights

The performance of both sPC-SAFT$_{GV}$ and sPC-SAFT$_{JC}$ in predicting the phase equilibria investigated in this work is largely excellent, with a high degree of accuracy apparent form pure prediction results. The incorporation of small binary interaction parameters makes up for any and all deficiencies in the pure predictions. Some of the major points raised in the modelling results are discussed below.

Shortcomings of the Standard Regression Procedure

The performance of the parameters determined by the traditional regression procedure of fitting parameters to pure component data is significant; the phase equilibrium predictions of each isomer with a particular normal alkane worsened as the polar carbonyl group shifted centrally for both models. The worsened predictions were more significant in the case of sPC-SAFT$_{JC}$, as highlighted by the case of n-nonane with each structural isomer in Figure 6.31. With all three n-alkanes considered, the most polar of the isomers (2-heptanone) was qualitatively represented, the 3-heptanone VLE was qualitatively poor and no parameters could even be regressed for the least polar of the three isomers.

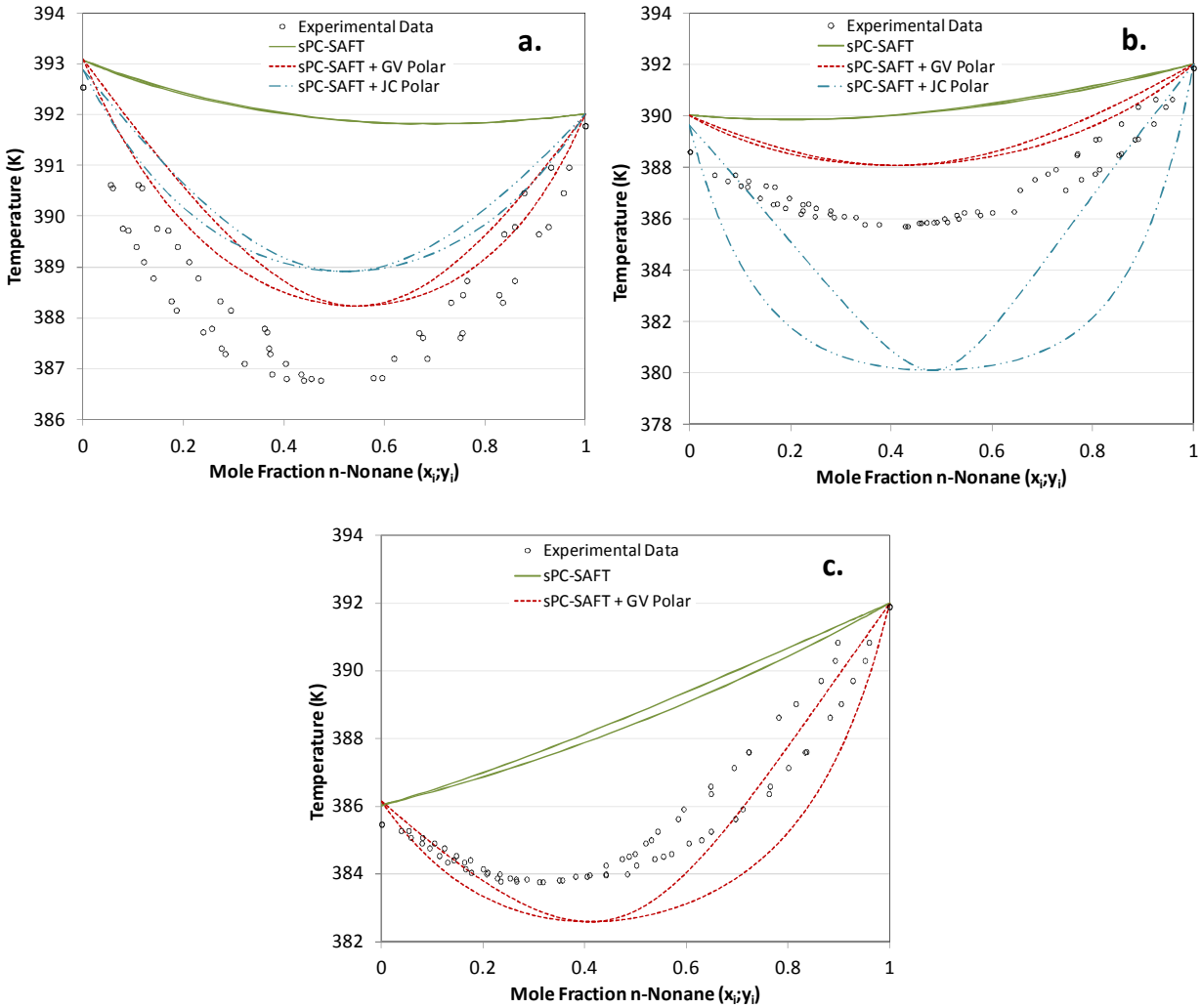

Figure 6.31: Pure predictions for isobaric VLE in (a.) n-nonane/2-heptanone, (b.) n-nonane/3-heptanone & (c.) n-nonane/4- heptanone systems at 40kPa. Only pure component data included in parameter regression. The worsening predictions of the sPC-SAFT$_{JC}$ parameter sets are highlighted in this progression.

This phenomenon can be best described with reference to the difficulty with which parameters are regressed for the sPC-SAFT$_{JC}$ model, as highlighted in Section 6.1.1. In the case of the most polar isomer, it appears a distinction can still be made between the polar and dispersive contributions of the model, but this distinction becomes less obvious, and thus the predictions less accurate, as the polar interactions are dampened with the carbonyl group shifting centrally. The inability to regress parameters for 4-heptanone using only pure component data suggests that this distinction has disappeared, with the aforementioned broad minimum in the objective function resulting in an optimum parameter set with no polar contribution.

The standard regression procedure of the sPC-SAFT$_{GV}$ model does not appear to suffer from the same limitations as its sPC-SAFT$_{JC}$ counterpart. This is readily seen not only in the graphical model predictions, but also in the value of the parameters themselves; the sPC-SAFT$_{JC}$ parameters cannot even be brought into accordance with the other four, more accurate sets in Table 6.2 when the values of the latter parameters are used as initial guesses for the former. It is interesting that four pure component parameters can be regressed with only pure component data under the sPC-SAFT$_{GV}$ framework, but not so for sPC-SAFT$_{JC}$. It would seem that the broad minimum in the objective function for the latter does not exist in the case of the former, and that the third order perturbation theory on which the Gross & Vrabec's polar term is based provides a more robust foundation than the first order perturbation theory of Jog & Chapman's term. Confirmation of this however would require a more in-depth investigation of the polar terms themselves and is beyond the scope of this work.

Systematic Model Deviations

The predictions of the n-octane and n-decane VLE data highlight the systematic deviation of the model in predicting both phases accurately, depending on the nature of the regression procedure. When VLE data are absent, the models predict the vapour phase accurately, but deviations are apparent in the predicted bubble curve, notably in the equal concentration region. The opposite is true when the VLE data are incorporated; the liquid phase is well presented but the vapour phase prediction is compromised. Consultation of the relevant *x*-y plot, as for the prediction of sPC-SAFT$_{GV}$ for the n-octane/2-heptanone system in Figure 6.32, reveals that the predictions based on the parameter sets which included VLE in the regression procedure more accurately predict the experimental behaviour. Thus, the case where the liquid phase is more accurately predicted is the more accurate model fit. This explains the reason behind accuracy in the vapour phase being lost in favour of accuracy in the liquid phase when binary interaction parameters are fit to data for the two cases of parameter sets regressed without VLE data (see e.g. Figures 6.3 & 6.4).

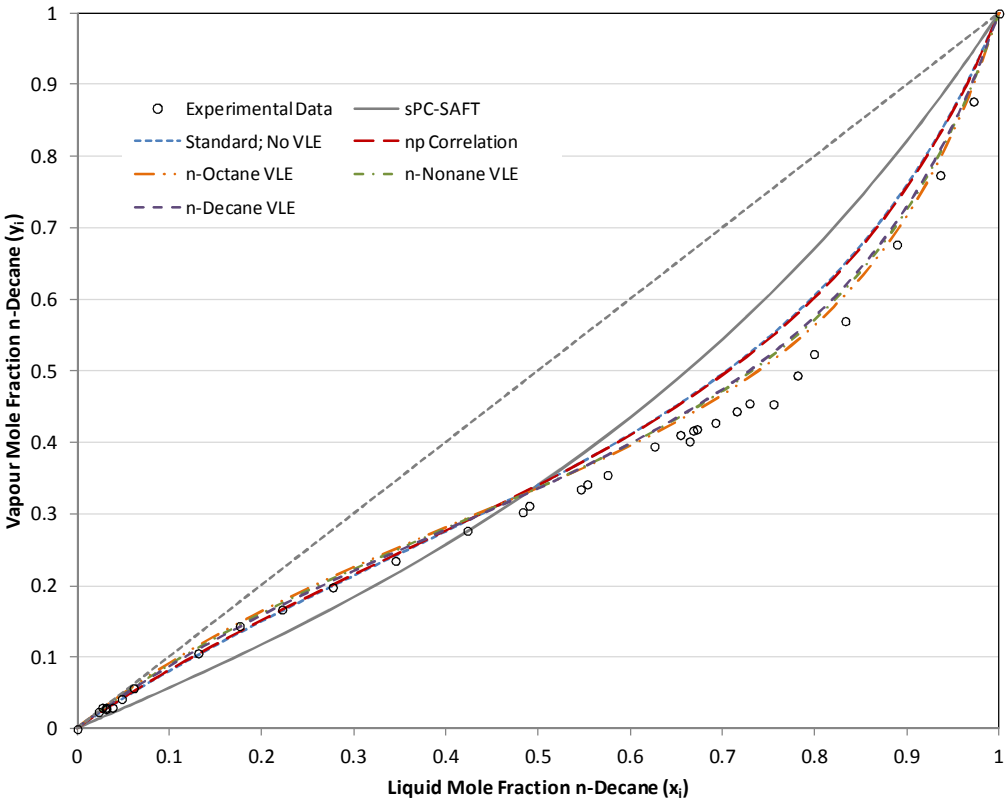

Figure 6.32: x-y plot for n-decane/2-heptanone system with associated sPC-SAFT$_{GV}$ predictions. The more accurate prediction evident for the three cases of parameter sets including VLE data in the regression show that the T-xy plots favouring liquid phase prediction over vapour phase prediction are more accurate. This is a representative plot and applies to all cases where this systematic deviation is in evidence.

The consistency of this deviation, for all six systems and all four regression procedures in both models (48 cases), suggests this is an inherent fundamental flaw shared by both models. It should be noted that these deviations are comparatively small however and do not detract considerably from the overall performance of the models. The absence of this deviation in the n-nonane systems could be as a result of the azeotropic composition lying in the middle of the composition spectrum, and thus the region of largest deviation, at the considered pressure. Given that the deviations are apparent for both n-octane and n-decane, its stands to reason that this deviation could manifest itself in the n-nonane systems at pressures where the azeotrope is not in this equal concentration range. A possible source of this error is the assumption of a temperature and phase independent dipole moment in both models, although a more thorough investigation would be necessary to confirm or deny this possibility.

Effect of Setting Polar Parameters

In general, sPC-SAFT$_{GV}$ marginally outperforms sPC-SAFT$_{JC}$ in all predictions. This is particularly true when considering the least polar isomer in all four n-alkane instances considered, both when the polar parameter is set and when VLE data are included in parameter regression. Indeed, the performance of sPC-SAFT$_{GV}$ when using the n_p correlation of Equation 6.2 suggests VLE data incorporation is not necessary for a good fit of the experimental data. Particularly in the case of the less polar structural isomers, setting the value of the polar parameter rectifies the shortcomings of the

sPC-SAFT$_{JC}$ standard regression procedure parameters in all cases, as highlighted in the n-decane/3-heptanone case in Figure 6.33.

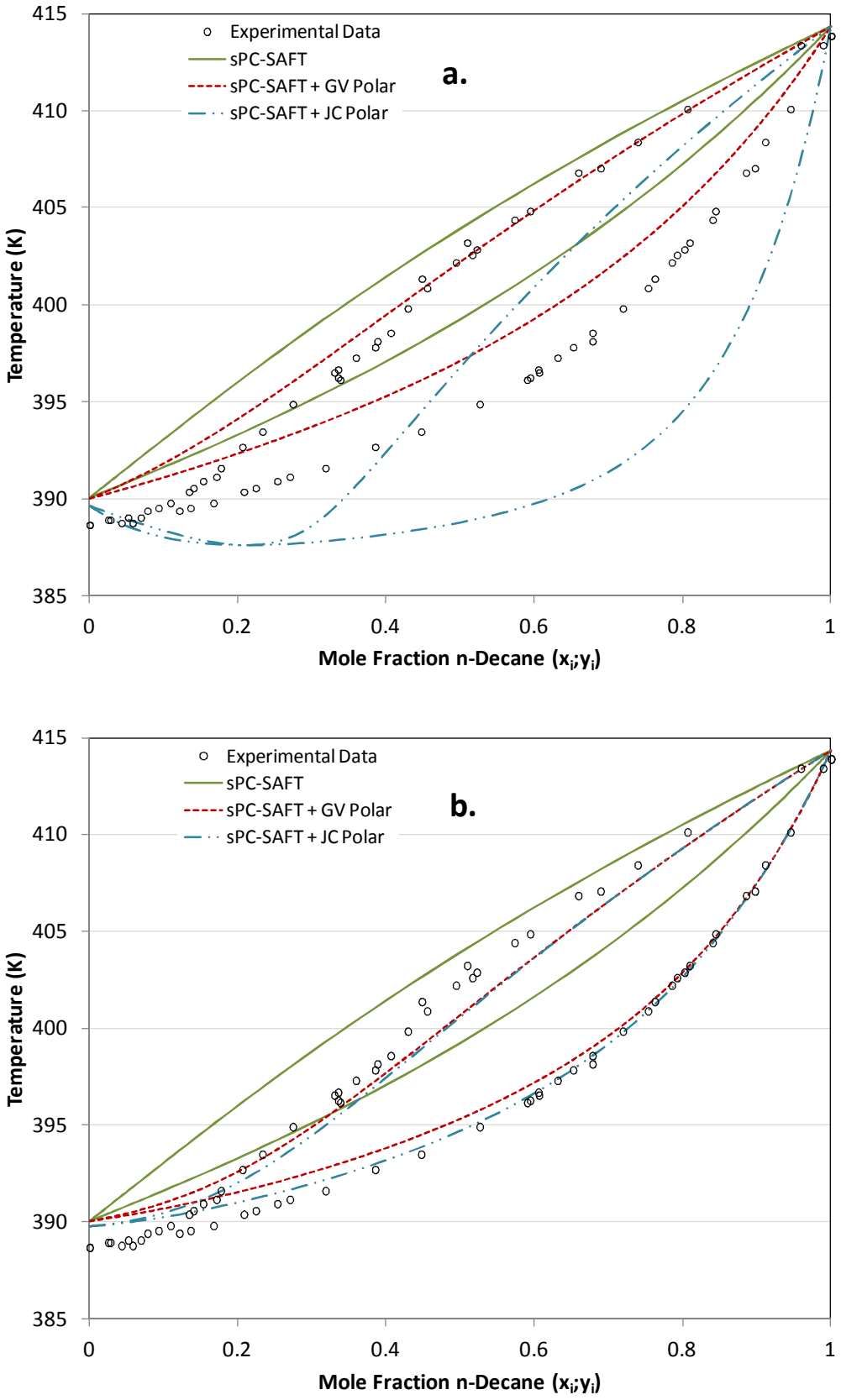

Figure 6.33: Pure predictions for isobaric VLE in n-decane/3- heptanone system at 40kPa. The ability to rectify shortcomings of standard regression procedure (a.) by setting the polar parameter (b.)is highlighted.

While there appears to be some bias on the part of both polar models to better predict the VLE of the more polar structural isomer when all four parameters are regressed, by setting the value of the polar parameter according to the x_p/n_p correlations of Equations 6.1 & 6.2, this bias is removed. Equally good predictions of VLE data are made for each structural isomer, paired with each of the n-alkanes considered. Setting the value of the polar parameter thus seems to be the easiest means of producing parameter sets for polar compounds, regardless of structure, as alternate VLE data for the component in question are not always available and correlations of the form of Equations 6.1 and 6.2 have been determined for most polar functional groups (de Villiers *et al.,* 2011).

Deviations in 3-Heptanone Predictions

With respect to the equilibria of the 3-heptanone containing systems, it is apparent from Figure 6.34 that the models consistently over predict the boiling point of the ketone as compared to the experimental data, when VLE data are not included in the parameter regression. Indeed, in the case of n-nonane/3-heptanone, this over prediction distorts an otherwise excellent prediction for the constant x_p/n_p cases by shifting the heptanone-rich side of the azeotrope roughly 1°C higher.

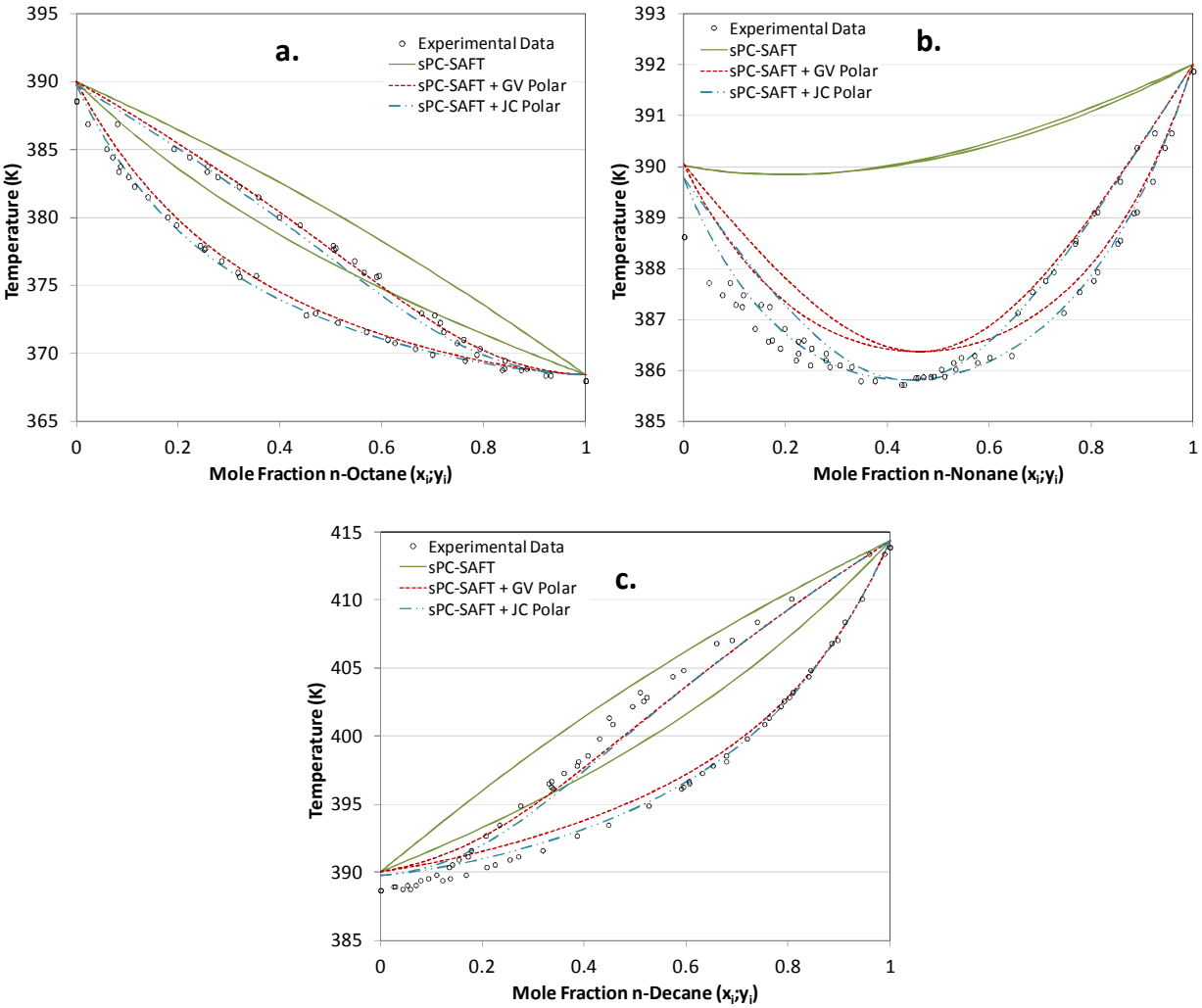

Figure 6.34: Pure predictions for isobaric VLE in (a.) n-octane/3-heptanone, (b.) n-nonane/2-heptanone & (c.) n-decane /3-heptanone systems at 40kPa. Correlation for polar parameter (x_p/n_p) used with pure component data in parameter regression. In each case, deviation in the prediction of 3-heptanone's boiling point distorts accuracy of model prediction.

The reason for this deviation is the nature of the regression procedure; in the absence of VLE data, parameters are fit to pure component data in the form of DIPPR correlations and the deviation is thus a discrepancy between the experimental data and the DIPPR correlation. This does not imply that the author believes the correlation is wrong *per se*, but a clarification is necessary. The DIPPR database employs correlations of pure component data fit to multiple data sets. The resulting correlation is the best fit for all data sets considered and thus has an inherent accuracy itself. Plotting the DIPPR correlation against its reference data in the pressure region of interest, as per Figure 6.35, it becomes apparent that deviations of some 1.8°C exist between the correlation and its own reference data. This deviation may be in the opposite direction to that exhibited by the experimental datum point, but the experimental data agree well with the measurements of the only other 3-heptanone vapour pressure study found in the literature (Wu & Sandler, 1988).

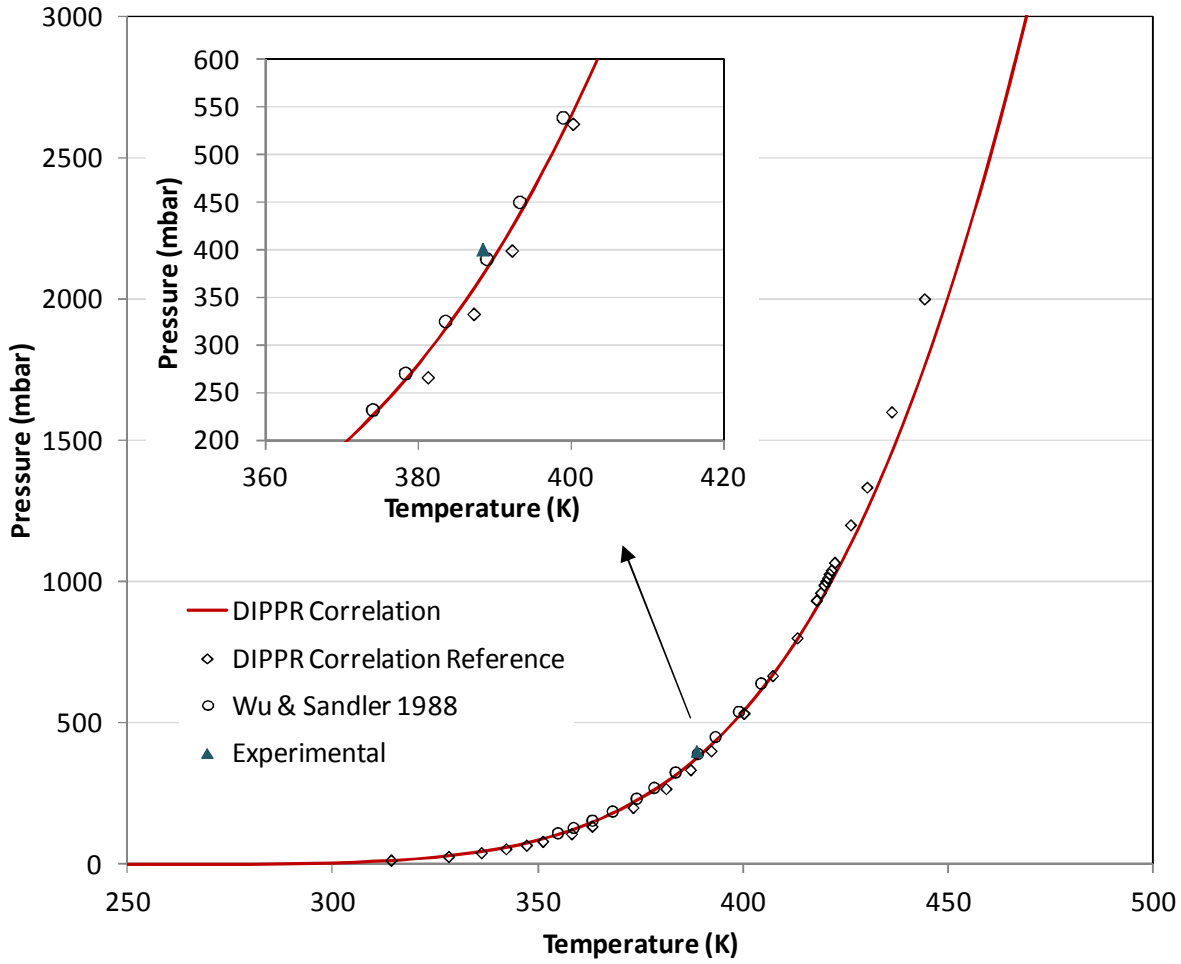

Figure 6.35: Illustration of the deviations inherent in the DIPPR correlation from its own reference data. This serves as justification of the deviation in 3-heptanone boiling point between experimental data and the models based on this DIPPR correlation.

Thus, given the magnitude of the deviation between the correlation and its own reference data, as well as the agreement of the experimental data with that of an independent third party source, it is concluded that, while the error indicated by Figure 6.31 may appear significant, even distorting the model predictions as a result, the deviation in boiling point is acceptable. Furthermore, it can be seen that the

inclusion of VLE data in the regression procedure remedies this discrepancy and allows for a better fit of the data. This observation thus serves as a recommendation for the inclusion of VLE data when possible.

Effect of Including Binary VLE Data

The choice of binary VLE data for inclusion in parameter regression appears arbitrary, with all three cases considered for each system producing equally good predictions of the experimental data. This lends itself to the conclusion that the parameter sets generated through incorporation of VLE data are unique and represent the true minimum of the objective function. If we are very critical of this process, it could be said that VLE of a longer chained alkane than the system of interest should be used for the best prediction of a system of interest. To clarify, considering the n-nonane systems of Figures 6.14 and 6.15, the predictions of the parameter sets using n-octane VLE produce worse deviations than when the longer n-nonane or n-decane are used, although this difference is only very slight. The performance of all parameter sets where VLE was included in the regression is excellent, with this fact emphasised by the identical parameter sets and predictions for the independently measured n-hexane/4-heptanone system.

Chapter 7 Conclusions & Recommendations

7.1. Conclusions

The aims of this work were to determine the effect of a shifting carbonyl group in a non-branched mid length ketone on the associated phase behaviour of the respective isomers with a non-polar second component, and the ability of the sPC-SAFT model, with the Jog & Chapman and Gross & Vrabec polar terms, to accurately predict the observed phenomena. To this end, experimental vapour liquid equilibrium data had to be generated for the nine binary systems comprising one of the three structural isomers of heptanone and an alkane of similar length from n-octane, n-nonane and n-decane. Model parameters in the polar sPC-SAFT framework were generated for each component and the fit of each model to the experimental phase equilibrium data was assessed. Thus, with reference to the objectives outlined in Section 1.3:

Objective (i.) VLE data generation

Isobaric experimental data were generated on a modified Gillespie dynamic still at a pressure of 40kPa. The quoted accuracies of the pressure and temperature were 0.1% of full scale output (1.6mbar) and 0.03°C at 0°C respectively. Compositional measurements, where errors comprised a sum of pressure effects and analytical errors, were found to be accurate within ±0.022 mole fraction. The experimental apparatus was verified through the reproduction of two sets of agreeing ethanol/1-butanol data at 1.013bar measured by independent parties. All generated experimental data were found to be thermodynamically consistent according to both the L/W and McDermott-Ellis consistency tests.

For a given heptanone isomer, similar qualitative trends in phase equilibrium behaviour were apparent with each of the considered n-alkane molecules. In the high n-alkane concentration region, near identical phase envelopes were apparent for each heptanone isomer, highlighting the diminishing effects of polar interaction as the distance between polar ketone molecules increases. As the concentration of the heptanone increased however, the increasing polar interactions manifested themselves in different boiling points and shifted, but qualitatively similar, dew and bubble curves. Minimum boiling azeotropes were apparent in all nine systems:

- ca. 98 mole% n-octane in all three n-octane/*x*-heptanone systems
- 53 mole%, 44 mole% and 34 mole% n-nonane in the 2-heptanone, 3-heptanone and 4-heptanone cases respectively
- ca 3 mole% n-decane in all three n-decane /*x*-heptanone systems

With the experimental data measured, focus could be shifted to the modelling aims of the project.

Objective (ii.) Parameter generation

Pure component parameter sets were regressed for the heptanone isomers for both sPC-SAFT$_{JC}$ and sPC-SAFT$_{GV}$ using five different regression procedures. The first was traditional fitting of the segment diameter (σ), segment number (m) and segment energy (ε/k) and the appropriate polar parameter (x_p/n_p) to correlations of the pure component vapour pressure, saturated liquid density and the heat of vaporisation. The inclusion of the measured binary VLE data with each alkane in addition to pure component properties, and the setting of the polar parameter according to the correlations of de Villiers *et al.* (2011) made up the other four regression procedures. These were only necessary in the case of 4-heptanone using sPC-SAFT$_{JC}$ due to the presence of a broad minimum in the objective function, resulting in the inability to produce a parameter set with a non-zero polar parameter. However all five parameter sets were employed for each ketone isomer to provide a meaningful comparison of the performance of each parameter set.

The parameters were found to reproduce pure component properties with a high degree of accuracy in all cases, with only a small loss of accuracy apparent when VLE data was included in the regression procedure. Similar parameter values were generated by each of the latter four regression procedures, but the parameters regressed under the traditional regression procedure, particularly the polar parameter, were markedly different. This was further emphasised by the performance of each parameter set in predicting the experimentally measured equilibrium data.

Objectives (iii.) & (iv.)Thermodynamic modelling of experimental data & model assessment

The modelling of the experimental data using traditionally regressed parameters raised concern over the ability of the models to account for the changing interactions associated with functional group shift. The predictions of both sPC-SAFT$_{GV}$ and sPC-SAFT$_{JC}$ deteriorated as the carbonyl group shifted centrally, with the effect more pronounced in the case of the Jog & Chapman polar term. The phase behaviour of 2-heptanone with each alkane was predicted with a fair degree of accuracy, poor qualitative agreement with the 3-heptanone systems was apparent and no predictions were even possible for the 4-heptanone systems. The magnitude of the n_p values generated and the success with which they predicted the experimental phase behaviour served as justification for not setting their value equal to unity in the regression procedure, and supports the same conclusion originally drawn by authors in this research group.

The discrepancy in performance between the models may be a result of the nature of the polar term, where a discernable difference between dispersion and polar effect cannot be made. Further reason may be the fact that first order perturbation theory is used in Jog & Chapman's polar term, while third order perturbation theory is used by Gross and Vrabec. This theory is supported by the fact that all four parameters can be regressed for all three polar molecules using sPC-SAFT$_{GV}$ without the broad minimum in the objective function widely reported for sPC-SAFT$_{JC}$. A more detailed study than that presented in this work would be necessary to confirm this hypothesis however.

Objective (v.) Effect of different regression procedures

The performance of the parameter sets where the polar term is set and the three cases where VLE data are included in the regression procedure are excellent, with pure predictions exhibiting good agreement with experimental data in all nine cases. Indeed it is only in the n-nonane systems, where strong non-ideality exists in a small temperature range, that the parameter sets with VLE data included outperform their polar correlation counterparts. The parameter sets where VLE data were included do not only provide good predictions of the binary system included in the regression procedure, but for all the systems investigated. This is supported by the equally good performance of all three parameter sets where VLE was included in predicting the phase equilibrium in the independently measured n-hexane/4-heptanone system.

Summary

Thus, there are obvious shortcomings in the ability of the polar sPC-SAFT models to predict the phase equilibria of all structural isomers of a polar molecule with the same accuracy using traditional parameter regression procedures. The problems identified here require further attention if the development of a truly fundamental thermodynamic model capable of predicting phase equilibria in all polar system is to be achieved. However, this problem appears to be remedied through the use of correlations to set the polar parameter, allowing for the easier regression of only the three non-polar component parameters, or the inclusion of a binary VLE data set. The resulting predictions are of a very high standard and could be used seamlessly for the prediction of phase equilibrium of different structural isomers of polar molecules.

7.2. Recommendations

The following recommendations are made in light of the results of this work:

- The possibility of online GC analysis should be considered to minimise compositional error associated with experimental measurements. Not only will this allow for faster sample quantification, but the exclusive use of the GC for VLE sample analysis will minimise chances of drifting calibration curves and reduce associated error.
- A study of similar nature could be conducted in longer length ketones, as well as other polar groups (aldehydes, esters, ethers). In this manner, the ability of the polar sPC-SAFT models to correlate varying degrees of polar interaction could be assessed and the findings presented in this work could be confirmed.
- A study into the effect of a non-constant dipole moment in the polar terms could be undertaken. A point raised by numerous authors, the use of a constant gas phase dipole moment in the polar contributions to the SAFT models has been highlighted as a major flaw, and remedying this point could result in a more comprehensive model being developed, possibly even overcoming the major drawbacks highlighted in this work.

References

Acre, A., Rodil, E., & Soto, A. (1999) Extractive distillation of 2-methoxy-2-methylpropane + ethanol using 1-butanol as entrainer: Equilibria and simulation. *The CanadianJournal of Chemical Engineering, 77(6),* 1135-1140.

Alder, B. J., Young, D. A., & Mark, M. A. (1972). Studies in molecular dynamics. X. corrections to the augmented van der waals theory for the square well fluid. *Journal of Chemical Physics, 56*(6), 3013-3029.

Al-Saifi, N. M., Hamad, E. Z., & Englezos, P. (2008). Prediction of vapor-liquid equilibrium in water-alcohol-hydrocarbon systems with the dipolar perturbed-chain SAFT equation of state. *Fluid Phase Equilibria, 271*(1-2), 82-93.

Barker, J. A., & Henderson, D. (1967). Perturbation theory and equation of state for fluids. II. A successful theory of liquids. *Journal of Chemical Physics, 47*(11), 4714-4721.

Barker, J. A., & Henderson, D. (1967). Perturbation theory and equation of state for fluids: The square-well potential. *Journal of Chemical Physics, 47*(8), 2856-2861.

Barraza, R., Díaz, S., Edwards, J., & Tapia, P. (1979). Thermodynamics of the systems n-hexane/3-pentanone, n-hexane/acetone and n-heptane/3-pentanone mixtures. *Zeitschrift Für Physikalische Chemie, 117*(117), 43-54.

Belusov, V. P., Gkhoneimi, Kh. F., & Shulgin, I. L. (1986). *VINITI Database RAS* (Code: 6296-86)

Boublik, T. (1992). Perturbation theory of polar nonspherical molecule fluids. *Molecular Physics, 76*, 327-336.

Carnahan, N. F., & Starling, K. E. (1969). Equation of state for nonattracting rigid spheres. *Journal of Chemical Physics, 51*(2), 635-636.

Chapman, W. G., Gubbins, K. E., Jackson, G., & Radosz, M. (1989). SAFT: Equation-of-state solution model for associating fluids. *Fluid Phase Equilibria, 52*(C), 31-38.

Chapman, W. G., Gubbins, K. E., Jackson, G., & Radosz, M. (1990). New reference equation of state for associating liquids. *Industrial and Engineering Chemistry Research, 29*(8), 1709-1721.

Chen, S. S., & Kreglewski, A. (1977). Applications of the augmented van der waals theory of fluids. I. pure fluids. *Berichte Der Bunsengesellschaft Für Physikalische Chemie, 81*(10), 1048-1052.

Cotterman, R. L., Schwarz, B. J., & Prausnitz, J. M. (1986). Molecular thermodynamics for fluids at low and high densities. part I: Pure fluids containing small or large molecules. *AIChE Journal, 32*(11), 1787-1798.

Cottrell, F. G. (1919). On the determination of boiling points of solutions. *Journal of the American Chemical Society, 41*(5), 721-729.

de Villiers, A. J. (2011). Evaluation and improvement of the sPC-SAFT equation of state for complex mixtures. (Doctor of Philosophy (Chemical Engineering), Stellenbosch University).

de Villiers, A. J., Schwarz, C. E., & Burger, A. J. (2011). Improving vapour-liquid-equilibria predictions for mixtures with non-associating polar components using sPC-SAFT extended with two dipolar terms. *Fluid Phase Equilibria, 305*(2), 174-184.

de Villiers, A. J., Schwarz, C. E., & Burger, A. J. (2011). New association scheme for 1-alcohols in alcohol/water mixtures with sPC-SAFT: The 2C association scheme. *Industrial and Engineering Chemistry Research, 50*(14), 8711-8725.

DIPPR 801 Database. *Design institute for physical properties* Sponsored by AIChE.

Dominik, A., Chapman, W. G., Kleiner, M., & Sadowski, G. (2005). Modeling of polar systems with the perturbed-chain SAFT equation of state. investigation of the performance of two polar terms. *Industrial and Engineering Chemistry Research, 44*(17), 6928-6938.

Economou, I. G. (2002). Statistical associating fluid theory: A successful model for the calculation of thermodynamic and phase equilibrium properties of complex fluid mixtures. *Industrial and Engineering Chemistry Research, 41*(5), 953-962.

Economou, I. G., & Donohue, M. D. (1991). Chemical, quasi-chemical and perturbation theories for associating fluids. *AIChE Journal, 37*(12), 1875-1894.

Fuchs, R., Krenzer, L., & Gaube, J. (1984). Excess properties of binary mixtures composed of a polar component and an alkane. *Berichte Der Bunsengesellschaft Für Physikalische Chemie, 88*, 642-649.

Geiseler, G., & Köhler, H. (1968). Thermodynamisches verhalten der mischsysteme methyläthylketoxim/n-heptan, diäthylketon/n-heptan und methyläthylketoxim/diäthylketon. *Berichte Der Bunsengesellschaft Für Physikalische Chemie, 72*(6), 697-706.

Gmehling, J., & Onken, U. (2003). *Vapour-liquid equilibrium collection. ketones (supplement 2).* Frankfurt: DECHEMA.

Gmehling, J., Onken, U., & Rarey, J. R. (1993). *Vapour-liquid equilibrium collection. ketones (supplement 1).* Frankfurt: DECHEMA.

Grenner, A., Kontogeorgis, G. M., von Solms, N., & Michelsen, M. L. (2007). Modeling phase equilibria of alkanols with the simplified PC-SAFT equation of state and generalized pure compound parameters. *Fluid Phase Equilibria, 258*(1), 83-94.

Gross, J. (2005). An equation-of-state contribution for polar components: Quadrupolar molecules. *AIChE Journal, 51*(9), 2556-2568.

Gross, J., & Sadowski, G. (2000). Application of perturbation theory to a hard-chain reference fluid: An equation of state for square-well chains. *Fluid Phase Equilibria, 168*(2), 183-199.

Gross, J., & Sadowski, G. (2001). Perturbed-chain SAFT: An equation of state based on a perturbation theory for chain molecules. *Industrial and Engineering Chemistry Research, 40*(4), 1244-1260.

Gross, J., & Sadowski, G. (2002). Application of the perturbed-chain SAFT equation of state to associating systems. *Industrial and Engineering Chemistry Research, 41*(22), 5510-5515.

Gross, J., & Vrabec, J. (2006). An equation-of-state contribution for polar components: Dipolar molecules. *AIChE Journal, 52*(3), 1194-1204.

Gubbins, K. E., & Twu, C. H. (1978). Thermodynamics of polyatomic fluid mixtures - I. theory. *Chemical Engineering Science, 33*(7), 863-878.

Hanson, D. O., & van Winkle, M. (1967). Alteration of the relative volatility of n-hexane -1-hexene by oxygenated and chlorinated solvents. *Journal of Chemical and Engineering Data, 12*(3), 319-325.

Huang, S. H., & Radosz, M. (1990). Equation of state for small, large, polydisperse, and associating molecules. *Industrial and Engineering Chemistry Research, 29*(11), 2284-2294.

Huang, S. H., & Radosz, M. (1991). Equation of state for small, large, polydisperse, and associating molecules: Extension to fluid mixtures. *Industrial and Engineering Chemistry Research, 30*(8), 1994-2005.

Jog, P. K., & Chapman, W. G. (1999). Application of Wertheim's thermodynamic perturbation theory to dipolar hard sphere chains. *Molecular Physics, 97*(3), 307-319.

Jog, P. K., Sauer, S. G., Blaesing, J., & Chapman, W. G. (2001). Application of dipolar chain theory to the phase behavior of polar fluids and mixtures. *Industrial and Engineering Chemistry Research, 40*(21), 4641-4648.

Johnson, J. K., Müller, E. A., & Gubbins, K. E. (1994). Equation of state for Lennard-Jones chains. *Journal of Physical Chemistry C, 98*(25), 6413-6419.

Kehiaian, H. V., Porcedda, S., Marongiu, B., Lepori, L., & Matteoli, E. (1991). Thermodynamics of binary mixtures containing linear or cyclic alkanones + n-alkanes or + cycloalkanes. *Fluid Phase Equilibria, 63*(3), 231-257.

Kleiner, M., & Gross, J. (2006). An equation of state contribution for polar components: Polarizable dipoles. *AIChE Journal, 52*(5), 1951-1961.

Kleiner, M., & Sadowski, G. (2007). Modeling of polar systems using PCP-SAFT: An approach to account for induced-association interactions. *Journal of Physical Chemistry C, 111*(43), 15544-15553.

Kraska, T., & Gubbins, K. E. (1996). Phase equilibria calculations with a modified SAFT equation of state. 1. pure alkanes, alkanols, and water. *Industrial and Engineering Chemistry Research, 35*(12), 4727-4737.

Kraska, T., & Gubbins, K. E. (1996). Phase equilibria calculations with a modified SAFT equation of state. 2. binary mixtures of n-alkanes, 1-alkanols, and water. *Industrial and Engineering Chemistry Research, 35*(12), 4738-4746.

Lafitte, T., Bessieres, D., Piñeiro, M. M., & Daridon, J. -. (2006). Simultaneous estimation of phase behavior and second-derivative properties using the statistical associating fluid theory with variable range approach. *Journal of Chemical Physics, 124*(2)

Lafitte, T., Piñeiro, M. M., Daridon, J. -., & Bessières, D. (2007). A comprehensive description of chemical association effects on second derivative properties of alcohols through a SAFT-VR approach. *Journal of Physical Chemistry B, 111*(13), 3447-3461.

Lee, S. C. (1930). Partial pressure isotherms II. *The Journal of Physical Chemistry, 35*(12), 3558-3582.

Lísal, M., Aim, K., Mecke, M., & Fischer, J. (2004). Revised equation of state for two-center Lennard-Jones fluids. *International Journal of Thermophysics, 25*(1), 159-173.

Liu, H., & Hu, Y. (1996). Molecular thermodynamic theory for polymer systems part II. equation of state for chain fluids. *Fluid Phase Equilibria, 122*(1-2), 75-97.

Malesiński, W. (1965). Azeotropy and other theoretical problems of vapour-liquid equilibrium (1st ed.). Poland: Interscience Publishers.

Mansoori, G. A., Carnahan, N. F., Starling, K. E., & Leland, T. W. J. (1971). Equilibrium thermodynamic properties of the mixture of hard spheres. *Journal of Chemical Physics, 54*(4), 1523-1525.

Maripuri, V. C., & Ratcliff, G. A. (1972). Isothermal vapour-liquid equilibria in binary mixtures of ketones and alkanes. *Journal of Applied Chemistry and Biotechnology, 22*(8), 899-903.

McDermott, C., & Ellis, S. R. M. (1965). A multicomponent consistency test. *Chemical Engineering Science, 20*(4), 293-296.

Michelsen, M. L., & Mollerup, J. M. (2007). In Stenby E. H. (Ed.), *Thermodynamic models: Fundamentals & computational aspects* (Second ed.). Denmark: Tie-Line Publications.

Müller, E. A., & Gubbins, K. E. (2001). Molecular-based equations of state for associating fluids: A review of SAFT and related approaches. *Industrial and Engineering Chemistry Research, 40*(10), 2193-2211.

NguyenHuynh, D., Passarello, J. -., de Hemptinne, J. -., & Tobaly, P. (2011). Extension of polar GC-SAFT to systems containing some oxygenated compounds: Application to ethers, aldehydes and ketones. *Fluid Phase Equilibria, 307*(2), 142-159.

Peng, D. -Y & Robinson, D. B. (1976). A new two-constant equation of state. *Industrial and Engineering Chemistry Fundamentals, 15*(1), 59-64.

Pienaar, C. (2011). Evaluation of entrainers for the dehydration of C2 and C3 alcohols via azeotropic distillation. (Master of Science in Engineering, Stellenbosch University.

Pierotti, G. J., Deal, C. H., & Derr, E. L. (1959). Activity coefficients and molecular structure. *Industrial and Engineering Chemistry, 51*(1), 95-102.

Raal, J. D., & Mühlbauer, A. L. (1998). *Phase equilibria: Measurement and computation*. Washington: Taylor & Francis.

Reed, T. M., & Gubbins, K. E. (1973). *Applied statistical mechanics*. New York: McGraw-Hill.

Rushbrooke, G. S., Stell, G., & Høye, J. S. (1973). Theory of polar liquids I. dipolar hard spheres. *Molecular Physics, 26*(5), 1199-1215.

Saager, B., & Fischer, J. (1992). Construction and application of physically based equations of state. part II. the dipolar and quadrupolar contributions to the helmholtz energy. *Fluid Phase Equilibria, 72*, 67-88.

Sandler, S. I. (2006). *Chemical, biochemical, and engineering thermodynamics* John Wiley & Sons, Inc.

Sauer, S. G., & Chapman, W. G. (2003). A parametric study of dipolar chain theory with applications to ketone mixtures. *Industrial and Engineering Chemistry Research, 42*(22), 5687-5696.

Scheller, W. A., & Rao, S. V. N. (1973). Isothermal vapor-liquid equilibrium data for system heptane-2-pentanone at 90deg C. *Journal of Chemical and Engineering Data, 18*(2), 223.

Smith, J. M., Van Ness, H. C., & Abbott, M. M. (2005). In Jeans S., White K. L. (Eds.), *Introduction to chemical engineering thermodynamics* (7th ed.). New York: McGraw-Hill. Soave, G. (1972). Equilibrium constants from a modified redlich-kwong equation of state. *Chemical Engineering Science, 27*(6), 1197-1203.

Steinhauser, H. H., & White, R. R. (1949). Vapor-liquid equilibria data for ternary mixtures: Methyl ethyl ketone-n-heptane-toluene system. *Industrial and Engineering Chemistry, 41*(12), 2912-2920.

Takeo, M., Nishi, K., Nitta, T., & Katayama, T. (1979). Isothermal vapor—liquid equilibria for two binary mixtures of heptane with 2-butanone and 4-4-methyl-2-pentanone measured by a dynamic still with a pressure regulation. *Fluid Phase Equilibria, 3*(2–3), 123-131.

Tan, S. P., Adidharma, H., & Radosz, M. (2008). Recent advances and applications of statistical associating fluid theory. *Industrial and Engineering Chemistry Research, 47*(21), 8063-8082.

Tumakaka, F., Gross, J., & Sadowski, G. (2005). Thermodynamic modeling of complex systems using PC-SAFT. *Fluid Phase Equilibria, 228–229*(0), 89-98.

Tumakaka, F., & Sadowski, G. (2004). Application of the perturbed-chain SAFT equation of state to polar systems. *Fluid Phase Equilibria, 217*(2), 233-239.

Twu, C. H., & Gubbins, K. E. (1978). Thermodynamics of polyatomic fluid mixtures - II. polar, quadrupolar and octopolar molecules. *Chemical Engineering Science, 33*(7), 879-887.

van der Waals, J. D. Over de continuïteit van den gas- en vloeistoftoestand. (PhD, University of Leiden).

Vega, C., McBride, C., & Menduiña, C. (2002). The second virial coefficient of the dipolar two center Lennard-Jones model. *Physical Chemistry Chemical Physics, 4*(13), 3000-3007.

Von Solms, N., Kouskoumvekaki, I. A., Michelsen, M. L., & Kontogeorgis, G. M. (2006). Capabilities, limitations and challenges of a simplified PC-SAFT equation of state. *Fluid Phase Equilibria, 241*(1-2), 344-353.

Von Solms, N., Michelsen, M. L., & Kontogeorgis, G. M. (2003). Computational and physical performance of a modified PC-SAFT equation of state for highly asymmetric and associating mixtures. *Industrial and Engineering Chemistry Research, 42*(5), 1098-1105.

Von Solms, N., Michelsen, M. L., & Kontogeorgis, G. M. (2004). Applying association theories to polar fluids. *Industrial and Engineering Chemistry Research, 43*(7), 1803-1806.

Wei, Y. S., & Sadus, R. J. (2000). Equations of state for the calculation of fluid-phase equilibria. *AIChE Journal, 46*(1), 169-196.

Wertheim, M. S. (1984). Fluids with highly directional attractive forces. I. statistical thermodynamics. *Journal of Statistical Physics, 35*(1-2), 19-34.

Wertheim, M. S. (1984). Fluids with highly directional attractive forces. II. thermodynamic perturbation theory and integral equations. *Journal of Statistical Physics, 35*(1-2), 35-47.

Wertheim, M. S. (1986). Fluids of dimerizing hard spheres, and fluid mixtures of hard spheres and dispheres. *Journal of Chemical Physics, 85*(5), 2929-2936.

Wertheim, M. S. (1986). Fluids with highly directional attractive forces. III. multiple attraction sites. *Journal of Statistical Physics, 42*(3-4), 459-476.

Wertheim, M. S. (1986). Fluids with highly directional attractive forces. IV. equilibrium polymerization. *Journal of Statistical Physics, 42*(3-4), 477-492.

Wisniak, J., Fishman, E., & Shaulitch, R. (1998). Isobaric vapor-liquid equilibria in the systems 2-butanone + heptane and 2-butanone + oxolane. *Journal of Chemical and Engineering Data, 43*(4), 537-540.

Wisniak, J. (1993). A new test for the thermodynamic consistency of vapor-liquid equilibrium. *Industrial and Engineering Chemistry Research, 32*(7), 1531-1533.

Wisniak, J. (1994). The herington test for thermodynamic consistency. *Industrial and Engineering Chemistry Research, 33*(1), 177-180.

Wisniak, J., & Tamir, A. (1977). Vapor-liquid equilibria in the ternary systems water-formic acid-acetic acid and water-acetic acid-propionic acid. *Journal of Chemical and Engineering Data, 22*(3), 253-260.

Wolbach, J. P., & Sandler, S. I. (1998). Using molecular orbital calculations to describe the phase behaviour of cross-associating mixtures. *Industrial and Engineering Chemistry Research, 37*(8), 2917-2928.

Wu, H. S., & Sandler, S. I. (1988). Vapor-liquid equilibria for binary mixtures of butyl ether with 2-furaldehyde and with 2-, 3-, and 4-heptanone. *Journal of Chemical and Engineering Data, 33*(3), 316-321.

Xu, K., Li, Y. -., & Liu, W. -. (1998). Application of perturbation theory to chain and polar fluids. pure alkanes, alkanols and water. *Fluid Phase Equilibria, 142*(1-2), 55-66.

Yerazunis, S., Plowright, J. D., & Smola, F. M. (1964). Vapor-liquid equilibrium determination by a new apparatus. *American Institute of Chemical Engineers Journal, 10*(5), 660-665.

Appendix A Detailed Methodology

A.1. Detailed Operating Procedure

In this section, a detailed step-by-step methodology for still operation is given. The still diagram presented in the Materials & Methods chapter is reprinted here for ease of reference.

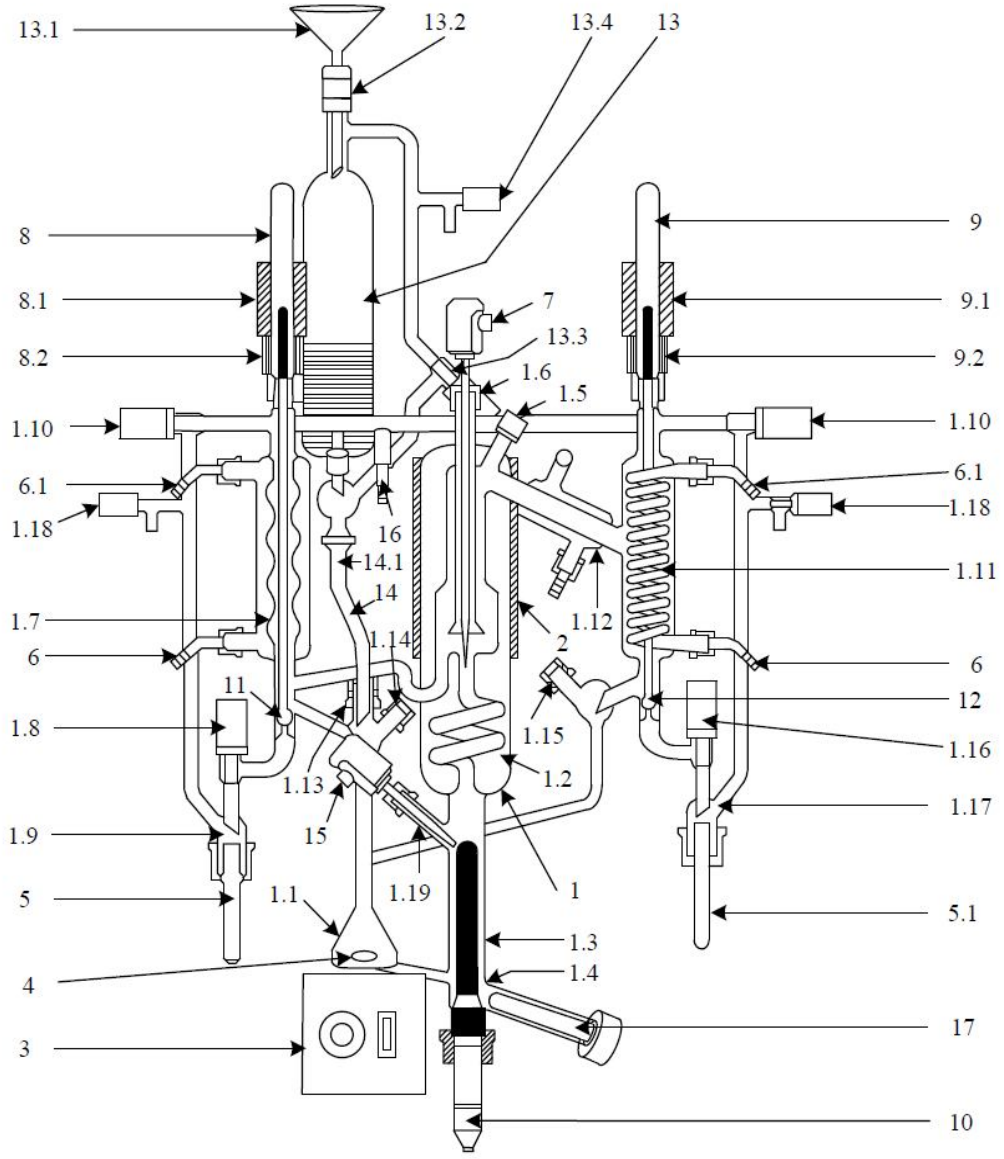

Figure A. 1: Schematic representation of the Pilodist dynamic recirculating still used for VLE measurements. Figure reprinted with permission (Pienaar, 2011)

Table A. 1: Legend for experimental apparatus of Figure A.1

No.	Description	No.	Description	No.	Description
1.	Glass body of phase equilibrium apparatus	1.16	Vapour phase stop valve	9.1	Vapour phase solenoid coils
1.1	Mixing chamber	1.17	Vapour phase sampling nozzle	9.2	Spacer
1.2	Cottrell pump with silvered vacuum jacket	1.18	Aeration valves	10.	Immersion heater rod
1.3	Flow heater	1.19	Temperature probe nozzle	11.	Liquid phase valve rod
1.4	Discharge valve	2.	Heating jacket	12.	Vapour phase valve rod
1.5	Sampling nozzle (vapour phase)	3.	Magnetic stirrer	13.	Feed burette
1.6	Temperature probe nozzle	4.	Stirring magnet	13.1	Funnel
1.7	Liquid phase cooler	5.	Liquid phase glass receiver tube	13.2	Feed burette filler nozzle
1.8	Liquid phase stop valve	5.1	Vapour phase glass receiver tube	13.3	Feed burette stop valve
1.9	Sampling nozzle (liquid phase)	6.	Hose connection olive – inlet	13.4	Feed burette aeration valve
1.10	Stop valve	6.1	Hose connection olive – outlet	14.	Inlet line
1.11	Condenser	7.	Temperature sensor	15.	Temperature sensor
1.12	Condenser	8.	Valve caps	16.	Glass connecting olive for vacuum or overpressure
1.13	Liquid phase filler nozzle	8.1	Liquid phase solenoid coils	17.	Ultrasonic homogeniser probe
1.14	Liquid phase sampling nozzle	8.2	Spacer		
1.15	Vapour phase sampling nozzle	9.	Valve caps		

A.1.1. Preliminaries

The following should be ensured prior to operation of the apparatus on each day of experimentation:

i. The oil level in the pump should be midrange in the oil sight glass and have the appropriate clarity. For a low level, the oil needs to be topped up while a murky or bubbly appearance in the sight may necessitate replacement as per the pump's user manual.
ii. The still needs to be dry before introducing the new feed material to ensure contamination is avoided. Washing with acetone, as discussed below, should prevent contamination but, if

necessary, compressed air should be passed through the apparatus for an appropriate period of time to make sure the wash acetone has completely evaporated.

iii. The flow of cooling water through condensers (1.11 & 1.12) and the liquid cooler (1.7) should be checked.

For overpressure operation only:

iv. The overpressure throttle valve on the hydraulic box should be closed fully. The nitrogen canister can then be opened, with only a small flow necessary through the regulator.

The still can now be turned on using the green power switch, the computer powered up and the software opened.

i. The intended operation of the still (vacuum vs. overpressure) should be selected by switching the three-way valve on the hydraulic box to the desired operation, with the same functionality selected in the software. For operation at atmospheric conditions, either "Pressure" or "Vacuum" may be selected on the three-way valve, but "ATM" needs to be selected in the software.

ii. Before introducing the feed mixture, the ultrasonic homogeniser needs to be fitted and secured with the discharge valve (1.4) and the feed burette tap closed. The liquid and vapour stop valves (1.8, & 1.16) as well as the aeration valves (1.18) should also be closed before the run commences.

iii. The feed burette can now be charged with the feed. For a given binary pair (component A – component B), it is advisable to begin experiments with one of the pure components. The pure component vapour pressure is not only a logical starting point on one extreme of the composition range, but also gives an initial degree of confidence in the measured mixture data. A volume of approximately 110ml should be introduced although this amount is variable according to the volatility of the mixture and type of operation. For a more volatile feed and under vacuum operation, a slightly larger volume (±120ml) is required to compensate for feed losses over the course of operation, while less (±100ml) would be necessary for heavier feed mixtures.

iv. The tap on the feed burette can now be opened and the feed introduced to the mixing chamber. It should be ensured that the immersion heater (10) is completely submerged. With this, the feed burette tap can be closed and the magnetic stirrer switched on.

v. It should now be ensured that the glass receiver vials (5 & 5.1) and sampling nozzle caps (1.14 &1.15) are securely fitted with all aeration valves (1.18 & 13.4) and the feed burette stop valve (13.3) closed. The stop valves (1.10) should be open to ensure the entire apparatus maintains equal pressure during operation.

vi. It is now necessary to input appropriate power settings and temperature and pressure set points.

- The heater power setting is dependent on both the volatility of the components in the feed liquid as well as the system pressure. It is important to choose a power setting high enough to vaporise the inventory but not so much as to only produce a vapour return. As an example, a power setting of 18% is sufficient to produce both a liquid and vapour return for pure acetone (T_b=56°C) at atmospheric pressure, but a setting of 65% is necessary to produce the same results for n-decane (T_b=142°C) at 40kPa. Thus for the purposes of this work, power settings were selected as follows:
    - ~30% for n-Heptane/Butanone and Ethanol/1-Butanol at 1atm
    - ~40% for heptanone mixtures with n-Octane at 400mbar
    - ~50% for heptanone mixtures with n-Nonane at 400mbar
    - ~60% for heptanone mixtures with n-Decane at 400mbar
- Pressure set points (SP):
    - Under vacuum operation, the apparatus is operated and pressure regulated by the Pilodist M101 control system. However, after the system modification discussed above, the pressure registered by the controller's transmitter exhibits a constant deviation from the true pressure shown by the Wika UT-10 unit. Furthermore, control is sluggish and exhibits large fluctuations (generally 5-10mbar above and below the set point), with a greater degree of control possible by manually fine tuning the pressure using the vacuum throttle valve on the hydraulic box. To achieve this manual control however, the controller has to be bypassed by choosing a set point pressure lower (~50mbar) than the intended operating pressure so that the vacuum pump will be constantly running. By throttling the amount of vacuum pulled from the system, the pressure can be maintained within ±0.5mbar of the intended operating pressure.
    - For overpressure operation, the apparatus has no automatic control, and so no set point input is necessary. Manual regulation of the system pressure is achieved by balancing the supply of nitrogen through the manual throttling valve with that allowed to escape through the stop valves. In this manner, a fairly constant pressure (±1mbar fluctuations) can be maintained subject to constant atmospheric pressure and uninterrupted nitrogen supply.
- The mantle heater need only be used for vapour temperatures in excess of 100°C so as to prevent partial condensation of the vapour phase on the mantle walls. When so used, the heater's set point should be set at least 15°C lower than the vapour temperature. The controller on the mantle heater is simple on/off control, with no apparent buffer zone resulting in the mantle temperature increasing further after the set point is reached. The mantle temperature will thus exceed the vapour temperature without the aforementioned 15°C buffer.

A.1.2. Experimental Runs

The apparatus may now be turned on using the "Start" button on the user interface of the software.

- Under vacuum operation, the pump will begin drawing vacuum and system pressure should be allowed to stabilise before fine tuning the pressure to the desired operating pressure using the vacuum throttling valve.

During operation, the sample wells need to be periodically flushed to prevent contamination of the final vapour and liquid samples. When the liquid and vapour are drawn from the respective sample wells, a fine liquid film remains on the stop valves (1.8 & 1.16). Flushing the wells approximately every 20 minutes ensures a representative sample is drawn at the end of the run. To flush the sample wells:

- The liquid and vapour solenoid valves should be opened with the Pilodist remote controller on the floor of the extraction cabinet.
- The collected liquid should be drained into the respective glass receiver vials by opening the respective stop valves after which the valves should be closed again.

vii. Phase equilibrium is attained after approximately 60 minutes and is indicated by a steady vapour temperature, with only small fluctuations in the second decimal point apparent. Furthermore, the condensate return on the liquid side should be steady and a droplet return rate of approximately 30 drops per minute should be apparent on the vapour side. To take the vapour and liquid samples:

- The sample wells should be flushed once more (as described above)
- For vacuum operation, the glass receiver vials need to be isolated. With the sample well stop valves (1.8 & 1.16) closed, the stop valves on the body of the still (1.10) can be closed to isolate the glass receiver tubes. If the stop valves are not closed, vacuum will be broken in the whole apparatus and the run will have to be restarted. Vacuum can then be broken by opening the aeration valves(1.18).
- The waste from flushing the sample wells can be removed by unfastening the glass receiver vials.
- The tubes must be washed with acetone and dried before being replaced, with any liquid film on the sampling nozzles (1.15 & 1.17) wiped away
- At this point, the solenoid valves (11 & 12) can be opened in the same manner as when flushing, to take what will constitute the vapour and liquid sample for the run. The solenoid valves should be opened for about 5 seconds to draw a large enough volume of each phase. The vapour temperature should be monitored in this time to ensure no significant temperature drift occurs during the sampling procedure. The indicated vapour temperature is the boiling point for that vapour-liquid pair.

- With the receiver tubes refastened, the aeration valves (1.18) can be closed and the stop valves (1.10) reopened to bring the receiver tubes to operating pressure
- When the pressure has stabilised, the sample wells can be drained by opening the stop valves (1.8 & 1.16) and removing the equilibrium samples in the same manner as described above*

Once the sample has been taken, the run can be ended by selecting "Stop" on the user interface, the magnetic stirrer stopped and the apparatus can be brought back to ambient pressure:

- For vacuum operation, slowly opening the aeration.
- For overpressure operation, closing the overpressure throttling valve.

If the still is initially charged with component A, small amounts of component B can be added to move along the composition spectrum with successive runs. The volume added between runs (roughly 10ml) should just be enough to top the feed up to the initial volume. In the case of non-volatile components, it may be necessary to drain some of the liquid mixture through the discharge valve (1.4). This would be to allow a large enough quantity of the second component to be added to produce an appreciable shift along the composition axis with the next run.

- Under vacuum operation, it is possible to do this immediately as, after bringing the apparatus back up to ambient pressure, the liquid mixture is no longer boiling.
- Under overpressure conditions however, the liquid mixture should be allowed to cool below its boiling point at ambient pressure before draining.

Once the still has been drained and topped up as necessary, the next experimental run can be executed according to the procedure detailed in steps v. through ix. above. In general, a single day of experimental runs will not result in data covering half the composition range. As such, the liquid in the still at the end of the day may be left over night, with runs resuming the following day.

A.1.3. Draining & Washing

When changing the initial feed from one pure component to the other within a binary pair, or when changing from one binary system to another, it is necessary to drain and wash the apparatus. The cleaning procedure to be followed is thus as follows:

viii. The mixture, mantle and immersion heater should be allowed to cool.
ix. The mixture can then be drained through the discharge valve (1.4).
x. The ultrasonic homogeniser should be unfastened and removed to drain any remaining liquid in this port.
xi. The ultrasonic homogeniser can be reattached and the discharge valve closed
xii. The feed burette can be now be charged with 110ml of wash acetone and passed through the feed burette tap into the mixing chamber. The magnetic stirrer may now be turned on.

xiii. The power setting and mantle temperature should be appropriately changed (18% and room temperature respectively) before selecting "ATM" operation on the user interface and "Starting" the run.

xiv. The apparatus need only run for about 30min before a steady vapour and condensate return are evident. This will "wash" the internals of the apparatus, but the solenoid valves should be opened to wash the liquid and sample wells. The wells can be drained through the stop valves as before, thus flushing the liquid film around these taps. This step can be repeated to ensure thorough flushing.

xv. The apparatus can now be stopped, allowed to cool and drained as before.

At the end of each day of experiments:

xvi. The apparatus can be turned off via the green power switch, the software closed and the computer powered down.

xvii. The nitrogen cylinder should be closed.

xviii. The cooling water tap should be closed

xix. After washing, all valves on the apparatus should be left open to allow the still to dry overnight.

A.2. System Hydraulic Modifications

The modifications to the dynamic still necessitated reworking the hydraulic setup to accommodate the new overall pressure transmitter. While the new pressure transmitter would be used for pressure readings during still operation, the fact that still operation depended upon receiving signals from the original pressure transmitters necessitated leaving these in and simply adding the new transmitter. These modifications are summarised in the following figures.

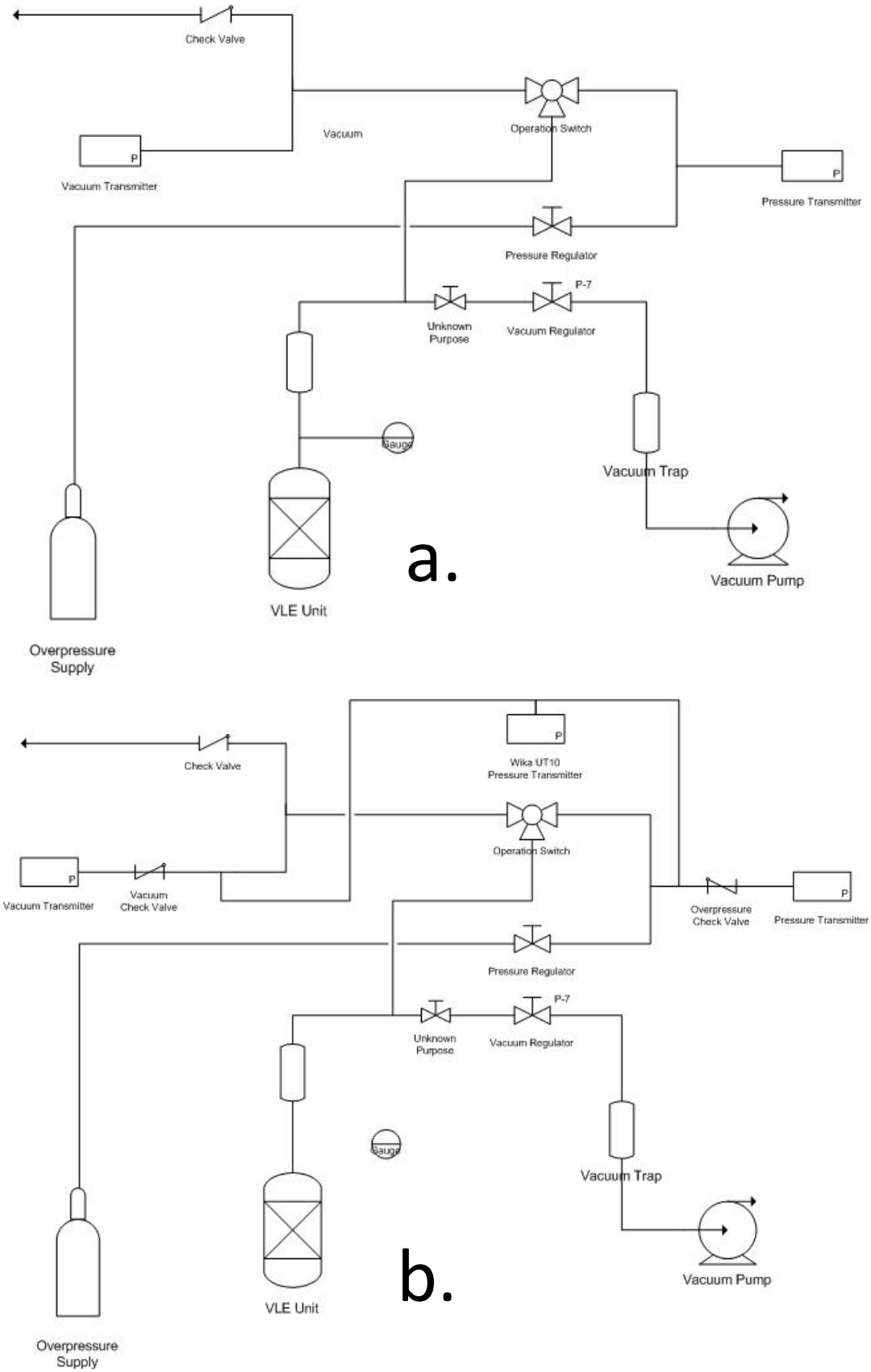

Figure A. 2: Hydraulic setup in dynamic VLE still (a.) before system modification and (b.) after the new pressure transmitter installed

Appendix B Certificates of Calibration

ALEXANDER WIEGAND SE & Co. KG

WIKA

zertifiziert nach DIN ISO 9001
certified by DIN ISO 9001
DQS Reg. Nr. 1830-01

UniTrans

Messwertprotokoll für Drucktransmitter

Test certificate for Pressure Transmitter

Gerätedaten: Instrument Data:

Kopf-Nr. Head No.	Messbereichsanfang Start of Range	Messbereichsende End of Range	Druckeinheit Unit of Pressure	Genauigkeit [%] Accuracy [%]
SZ65	0	1,6	bar / abs.	0,1

Ausgang bei 20°C: Output at 20°C:

Nullpunkt Zero		Endwert Full Scale	
3,99	mA	20,00	mA

Kennlinienwerte: Characteristics:

Referenzdruck Ref Pressure		Linearitätsabweichung [%] Deviation of linearity [%]	
[%]	[bar]	bei / at 10°C	bei / at 40°C
0	0,000	0,000	0,000
10	0,160	0,020	0,001
20	0,320	0,021	0,002
30	0,480	0,021	0,013
40	0,640	0,024	0,005
50	0,800	0,016	-0,005
60	0,960	0,014	0,014
70	1,120	0,003	0,009
80	1,280	0,028	0,010
90	1,440	0,022	0,009
100	1,600	0,000	0,000

Linearitätsabweichung [%]:

Deviation of linearity [%]:

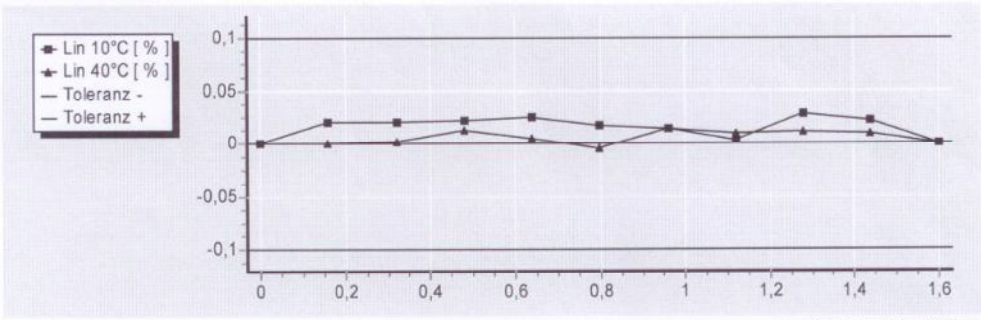

Referenzdruck [bar]
Ref ressure [bar]

Datum: 10.09.2012 Date:

geprüft von : 012 testet by:

Die Produktionsabteilung für Druckmessgeräte wird unterstützt und überwacht von dem WIKA DKD-Kalibrationslabor für Druck DKD-K-03701

The pressure department is supported and monitored by the WIKA pressure DKD-Calibration-Laboratory-DKD-K-03701

Druck + Temperatur

WIKA Alexander Wiegand SE & Co. KG
Alexander-Wiegand-Straße 30
63911 Klingenberg
Germany

Tel. +49 9372 132-0
Fax +49 9372 132-406
E-Mail info@wika.de
www.wika.de

TC Ltd, Units 1-6, Brimington Rd North, Chesterfield, S41 9BE, United Kingdom
Email: callab@tc.co.uk - Web: www.tc.co.uk
Tel: 01895 252222 - Fax: 01895 273540

KALIBRIERSCHEIN

Datum der Messung:	23 Dezember 2010
Auftraggeber:	Pilodist GmbH
Anschrift Auftraggeber:	Auf Der KaiserFuhr 43 53127 Bonn
Bestell-Nr. Auftraggeber:	Fax Vom 14.12.2010
Auftrag-Nr. TC GmbH:	AU23339
Auftragsdatum:	14 Dezember 2010
Kalibriergegenstand:	Pt100 6.0mm x 200mm
Serien Nr.	AU23339/1B
Typenbezeichnung:	16-1-6.0-4-200-CE1A-R100-1/10-2Mtrs RT47/NO BRAID/SMALL Platin-Widerstandsthermometer
Umgebungstemperatur:	20°C +/- 2°C

Seite 1 von 1
Zugelassener Unterzeichner:
L R Walker
K M Donaldson
KDonaldson

Kalibrierschein-Nr:
10034-1B

Kalibrierverfahren: Das Thermometer wurde durch Vergleich mit zwei Referenz-Widerstandsthermometern kalibriert. Die Kalibrierung erfolgte in einem gerührtem Wasserbad der Firma Grant und einem Hart Trockenblock-Kalibrator. Alle Messungen können auf nationale Normale zurückgeführt werden. Die Widerstände wurden mit Präzisions-Digitalmultimetern gemessen. Alle Messungen wurden unter kontrollierten Umgebungsbedingungen unter Verwendung von Geräten mit bekannten und zurückverfolgbaren Werten durchgeführt. Die Temperaturmessungen lassen sich auf die Internationale Temperaturskala ITS-90 zurückführen. Die Umrechnung der Widerstandswerte des Thermometers erfolgte gemäß IEC60751:2008.

Referenz-Temperatur (°C)	Widerstand Prüfling (Ω)	Temperatur kalkuliert gem. IEC (°C)	Fehler (°C)
49.88	119.369	49.93	0.05
199.83	175.832	199.93	0.10

Die Eintauchtiefe des geprüften Thermometers betrug 150mm

Kalibriert von: T Heath

Datum der Kalibrierung: 23 Dezember 2010

Die angegebenen signifikanten Stellen erleichtern dem Anwender des Kalibrierscheins die Interpolation, sie entsprechen nicht der tatsächlichen Messunsicherheit. Die Angaben zur Messgröße erfolgen ohne Berücksichtigung der Messunsicherheit.

Bemerkung: Es liegt in der Verantwortung des Anwenders die Langzeitdrift sowie die Messunsicherheit unter den Bedingungen der Nutzung zu bestimmen.

Issue 02/01

Unique Metrology
Eskom Research & Innovation Centre
Lower Germiston Road • Rosherville
P O Box 145296 • Bracken Gardens • 1452
Tel: 011 626 3808 • Cell: 083 254 3635 • Fax: 086 610 4196
Web: www.unimet.co.za

sanas Calibration Laboratory
306 205

SANAS ACCREDITED CALIBRATION LABORATORY No 306

TEMPERATURE METROLOGY

CERTIFICATE OF CALIBRATION

Date of issue : 26/11/2012

Certificate No : 1211T4452-1

Technical Signatory

M Mathieson.

The results of all measurements are traceable to the national measuring standards.

The values in this certificate are correct at the time of calibration. Subsequently the accuracy will depend on such factors as the care executed in handling and use of the device, and the frequency of use. Recalibration should be performed after the period so chosen to ensure that the instrument's accuracy remains within the desired limits.

This certificate is issued in accordance with the conditions of the accreditation granted by the South African National Accreditation System (SANAS). It is a correct record of the measurements made. This certificate may not be reproduced other than in full except with prior written approval of the issuing laboratory. Legal liability shall be limited to the cost of recalibration and or certification, but the applicant indemnifies Unique Metrology (Pty) Ltd against any consequential or other loss.

The South African National Accreditation System (SANAS) is a member of the International Laboratory Accreditation Cooperation (ILAC) Mutual Recognition Arrangement (MRA). This arrangement allows for the mutual recognition of technical test and calibration data by the member accreditation bodies worldwide. For more information on the Arrangement please contact www.ilac.org.

Unique Metrology
Eskom Research & Innovation Centre
Lower Germiston Road • Rosherville
P O Box 145296 • Bracken Gardens • 1452
Tel: 011 626 3808 • Cell: 083 254 3635 • Fax: 086 610 4196
Web: www.unimet.co.za

sanas Calibration Laboratory 306 205

CERTIFICATE OF CALIBRATION

Certificate Number	: 1211T4452-1		
Calibration of a	: PT100 Resistance Thermometer		
Manufacturer & Type	: Wika 4 wire		
Serial Number	: TE-7855		
Calibrated for	: University of Stellenbosch, Process Engineering, Stellenbosch.		
Procedure Number	: 53-166-03		
Date of Calibration	: 23/11/2012		
Date of Issue	: 26/11/2012		
Laboratory Environment	: 21.4°C.		
Reference Standards	: 306-S-21	Fluke 9144 Block Calibrator	S/N B26027
	306-S-07	Hewlett Packard Multimeter	S/N 1206L5
	306-S-05	Time Electronics Current Sourse	S/N 3146A70688

Reference Temperature °C	Indicated Reading Ohms	Equivalent Temperature °C	Correction °C
40	115.565	40.1	-0.1
80	130.950	80.2	-0.1
140	153.622	140.1	-0.1
200	175.952	200.3	-0.3

The uncertainty of measurement is ± 0.3°C
The reported uncertainty is based on a standard uncertainty multiplied by a coverage factor of k=2, which unless specifically stated otherwise, provides a confidence level of 95%, in accordance with the Guide to the Uncertainty in Measurement, first edition, 1993.

Comments: The correction should be added to the indicated temperature to obtain the actual temperature.
The PT100 was submerged to a constant depth of 150mm in the block calibrator during the calibration.

Calibrated by : AJ Mathieson

Technical Signatory

Appendix C GC Calibration Curves & Error Analysis Results

C.1. GC Calibration Curves

n-Octane/2-Heptanone

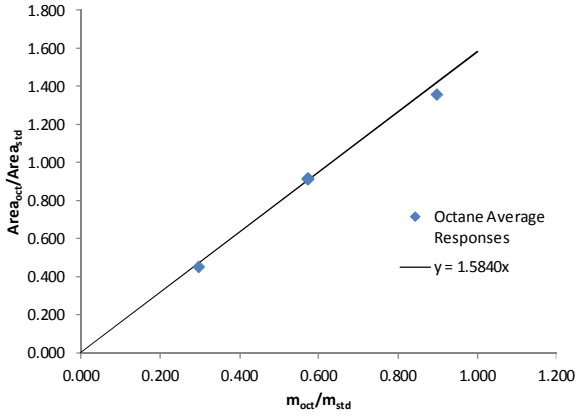

Figure C. 1: n-Octane calibration curve for GC analysis in n-octane/2-heptanone system

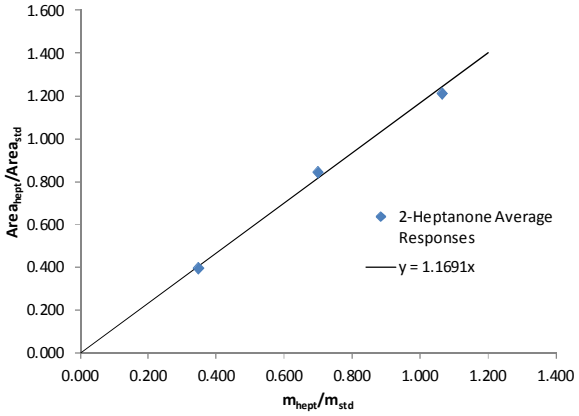

Figure C. 2: 2-Heptanone calibration curve for GC analysis in n-octane/2-heptanone system

Table C. 1: Data used in calibration curve generation for n-octane – 2-heptanone system

Resp 1	*Mass (g)*	*RESP1A*		*RESP1B*		*RESP1C*		*RESP1D*		*RESP1E*	
		Area	*Response Factor*	*Area*	*Response Factor*	*Area*	*Response Factor*	*Area*	*Response Factor*	*Area*	*Response Factor*
n-Octane	0.0072	407052	1.5219	490355	1.5260	415973	1.5283	410999	1.5233	415192	1.5384
2-Heptanone	0.0258	1088868	1.1361	1324015	1.1498	1104343	1.1323	1103961	1.1419	1112562	1.1504
2-Butanone (IS)	0.0243	902702	1.0000	1084531	1.0000	918592	1.0000	910606	1.0000	910855	1.0000

Resp 2	*Mass (g)*	*RESP2A*		*RESP2B*		*RESP2C*		*RESP2D*		*RESP2E*	
		Area	*Response Factor*	*Area*	*Response Factor*	*Area*	*Response Factor*	*Area*	*Response Factor*	*Area*	*Response Factor*
n-Octane	0.0143	830801	1.6061	974401	1.5911	818299	1.5991	817894	1.6034	815381	1.6009
2-Heptanone	0.0174	764733	1.2150	905978	1.2158	753796	1.2106	752254	1.2120	750935	1.2117
2-Butanone (IS)	0.0250	904334	1.0000	1070671	1.0000	894644	1.0000	891776	1.0000	890458	1.0000

Resp 3	*Mass (g)*	*RESP3A*		*RESP3B*		*RESP3C*		*RESP3D*		*RESP3E*	
		Area	*Response Factor*	*Area*	*Response Factor*	*Area*	*Response Factor*	*Area*	*Response Factor*	*Area*	*Response Factor*
n-Octane	0.0227	1281771	1.5380	1405461	1.4458	1264411	1.5268	1276008	1.5338	1279152	1.5379
2-Heptanone	0.0087	369582	1.1571	422344	1.1336	366830	1.1558	369161	1.1578	368847	1.1571
2-Butanone (IS)	0.0253	928864	1.0000	1083428	1.0000	922982	1.0000	927223	1.0000	927026	1.0000

n-Nonane/2-Heptanone

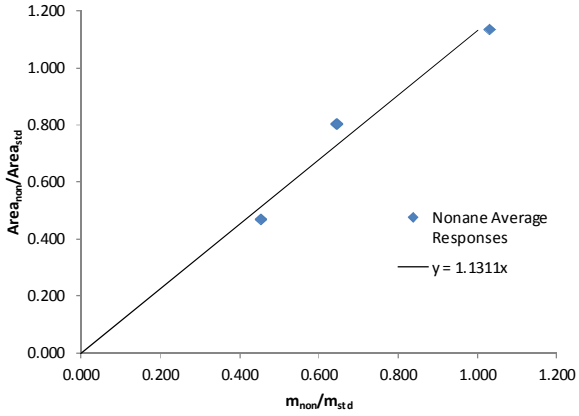

Figure C. 3: n-Nonane calibration curve for GC analysis in n-nonane/2-heptanone system

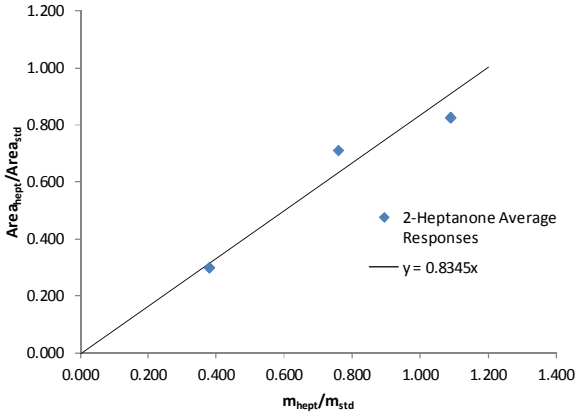

Figure C. 4: 2-Heptanone calibration curve for GC analysis in n-nonane/2-heptanone system

Table C. 2: Data used in calibration curve generation for n-nonane – 2-heptanone system

Resp 1	*Mass (g)*	*RESP1A*		*RESP1B*		*RESP1C*		*RESP1D*		*RESP1E*	
		Area	*Response Factor*	*Area*	*Response Factor*	*Area*	*Response Factor*	*Area*	*Response Factor*	*Area*	*Response Factor*
n-Nonane	0.0279	1504185	1.0986	1645324	1.0939	1515615	1.1198	1647737	1.1016	1630598	1.1094
2-Heptanone	0.0102	398855	0.7968	436171	0.7932	401991	0.8124	434214	0.7940	432130	0.8042
n-Heptane (IS)	0.0271	1329934	1.0000	1460991	1.0000	1314633	1.0000	1452909	1.0000	1427701	1.0000

Resp 2	*Mass (g)*	*RESP2A*		*RESP2B*		*RESP2C*		*RESP2D*		*RESP2E*	
		Area	*Response Factor*	*Area*	*Response Factor*	*Area*	*Response Factor*	*Area*	*Response Factor*	*Area*	*Response Factor*
n-Nonane	0.0230	1399699	1.2757	1348094	1.2250	1371239	1.2506	1219323	1.2489	1199463	1.2498
2-Heptanone	0.0270	1226088	0.9519	1199418	0.9284	1201202	0.9332	1085936	0.9475	1068838	0.9487
n-Heptane (IS)	0.0357	1703083	1.0000	1708180	1.0000	1701927	1.0000	1515390	1.0000	1489709	1.0000

Resp 3	*Mass (g)*	*RESP3A*		*RESP3B*		*RESP3C*		*RESP3D*		*RESP3E*	
		Area	*Response Factor*	*Area*	*Response Factor*	*Area*	*Response Factor*	*Area*	*Response Factor*	*Area*	*Response Factor*
n-Nonane	0.012	583411	1.0412	582018	1.0451	532970	1.0332	581939	1.0358	580330	1.0386
2-Heptanone	0.0288	1025074	0.7623	1021985	0.7646	941362	0.7604	1022604	0.7584	1020406	0.7609
n-Heptane (IS)	0.0265	1237374	1.0000	1229871	1.0000	1139147	1.0000	1240726	1.0000	1233880	1.0000

n-Decane/2-Heptanone

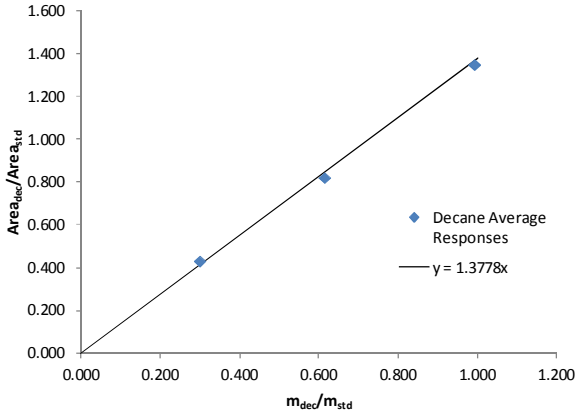

Figure C. 5: n-Decane calibration curve for GC analysis in n-decane/2-heptanone system

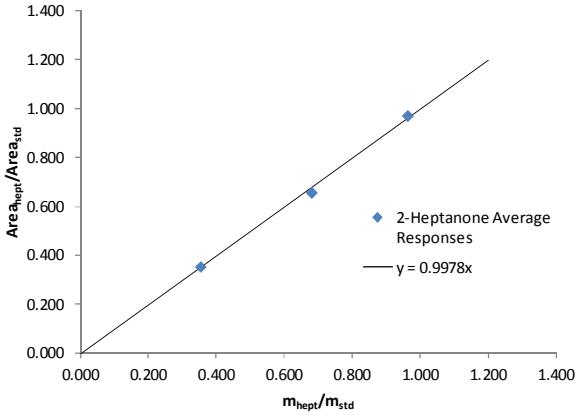

Figure C. 6: 2-Heptanone calibration curve for GC analysis in n-decane/2-heptanone system

Table C. 3: Data used in calibration curve generation for n-decane – 2-heptanone system

Resp 1	*Mass (g)*	*RESP1A*		*RESP1B*		*RESP1C*		*RESP1D*		*RESP1E*	
		Area	*Response Factor*	*Area*	*Response Factor*	*Area*	*Response Factor*	*Area*	*Response Factor*	*Area*	*Response Factor*
n-Decane	0.0243	2311446	1.3485	2281434	1.3559	2262524	1.3523	2243244	1.3545	2262854	1.3917
2-Heptanone	0.0086	610251	1.0059	601634	1.0104	593779	1.0028	587100	1.0017	591652	1.0281
n-Heptane (IS)	0.0245	1728231	1.0000	1696394	1.0000	1686810	1.0000	1669724	1.0000	1639396	1.0000

Resp 2	*Mass (g)*	*RESP2A*		*RESP2B*		*RESP2C*		*RESP2D*		*RESP2E*	
		Area	*Response Factor*	*Area*	*Response Factor*	*Area*	*Response Factor*	*Area*	*Response Factor*	*Area*	*Response Factor*
n-Decane	0.0164	1357676	1.3413	1372896	1.3538	1349272	1.3422	1339322	1.3223	1484434	1.3208
2-Heptanone	0.0181	1091898	0.9774	1103712	0.9861	1082268	0.9755	1081982	0.9679	1175252	0.9475
n-Heptane (IS)	0.0267	1647896	1.0000	1651014	1.0000	1636608	1.0000	1648980	1.0000	1829681	1.0000

Resp 3	*Mass (g)*	*RESP3A*		*RESP3B*		*RESP3C*		*RESP3D*		*RESP3E*	
		Area	*Response Factor*	*Area*	*Response Factor*	*Area*	*Response Factor*	*Area*	*Response Factor*	*Area*	*Response Factor*
n-Decane	0.0083	711345	1.4306	800593	1.4439	710291	1.4224	724786	1.4593	704750	1.4272
2-Heptanone	0.0266	1613845	1.0127	1787352	1.0058	1608779	1.0053	1641396	1.0312	1596643	1.0089
n-Heptane (IS)	0.0277	1659506	1.0000	1850463	1.0000	1666534	1.0000	1657579	1.0000	1647943	1.0000

n-Octane/3-Heptanone

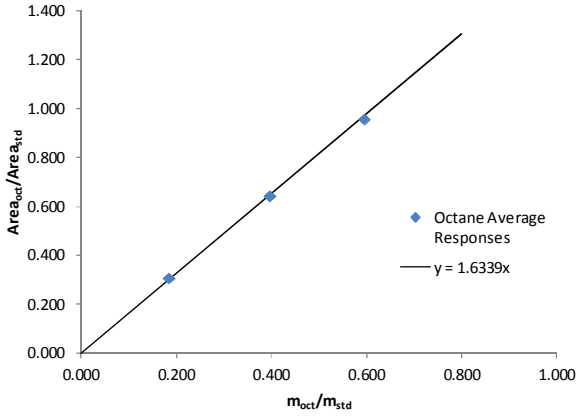

Figure C. 7: n-Octane calibration curve for GC analysis in n-octane/3-heptanone system

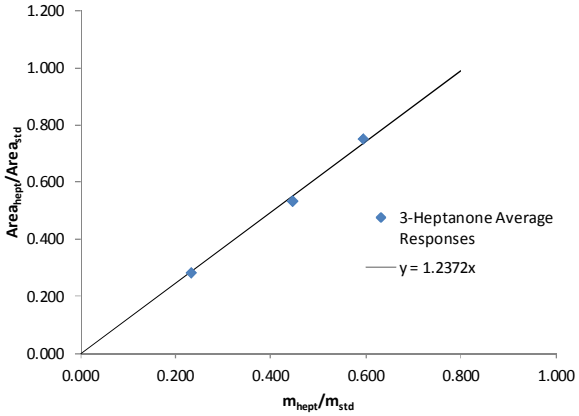

Figure C. 8: 3-Heptanone calibration curve for GC analysis in n-octane/3-heptanone system

Table C. 4: Data used in calibration curve generation for n-octane – 3-heptanone system

Resp 1	*Mass (g)*	*RESP1A*		*RESP1B*		*RESP1C*		*RESP1D*		*RESP1E*	
		Area	*Response Factor*	*Area*	*Response Factor*	*Area*	*Response Factor*	*Area*	*Response Factor*	*Area*	*Response Factor*
n-Octane	0.0083	547684	1.6715	549368	1.6719	512160	1.6813	550732	1.6686	546862	1.6590
3-Heptanone	0.0267	1344017	1.2751	1343801	1.2713	1259110	1.2849	1346023	1.2678	1340394	1.2640
Butanone (IS)	0.0451	1780443	1.0000	1785459	1.0000	1655254	1.0000	1793387	1.0000	1791171	1.0000

Resp 2	*Mass (g)*	*RESP2A*		*RESP2B*		*RESP2C*		*RESP2D*		*RESP2E*	
		Area	*Response Factor*	*Area*	*Response Factor*	*Area*	*Response Factor*	*Area*	*Response Factor*	*Area*	*Response Factor*
n-Octane	0.0161	1042379	1.6241	1049413	1.6260	1044128	1.6178	1135774	1.6322	1125993	1.6124
3-Heptanone	0.0180	866872	1.2081	872734	1.2095	865646	1.1997	947529	1.2179	936216	1.1991
Butanone (IS)	0.0406	1618455	1.0000	1627503	1.0000	1627481	1.0000	1754788	1.0000	1761045	1.0000

Resp 3	*Mass (g)*	*RESP3A*		*RESP3B*		*RESP3C*		*RESP3D*		*RESP3E*	
		Area	*Response Factor*	*Area*	*Response Factor*	*Area*	*Response Factor*	*Area*	*Response Factor*	*Area*	*Response Factor*
n-Octane	0.0235	1558893	1.6049	1552476	1.5931	1547204	1.5983	1545310	1.5942	1693999	1.6530
3-Heptanone	0.0091	462065	1.2284	463406	1.2280	459103	1.2248	460497	1.2268	497172	1.2528
Butanone (IS)	0.0395	1632707	1.0000	1638032	1.0000	1627096	1.0000	1629296	1.0000	1722519	1.0000

n-Nonane/3-Heptanone

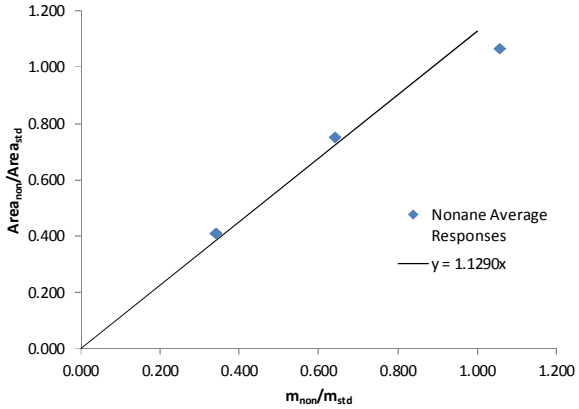

Figure C. 9: n-Nonane calibration curve for GC analysis in n-nonane/3-heptanone system

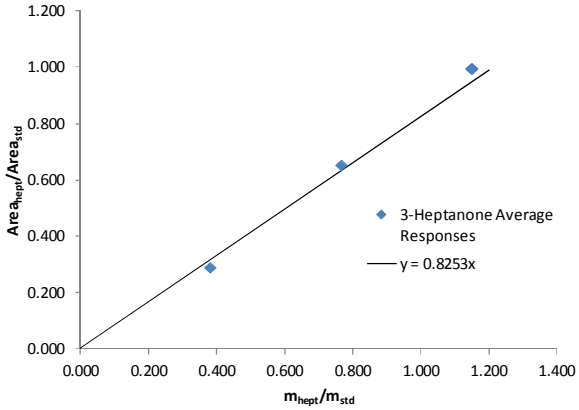

Figure C. 10: 3-Heptanone calibration curve for GC analysis in n-nonane/3-heptanone system

Table C. 5: Data used in calibration curve generation for n-nonane – 3-heptanone system

Resp 1	*Mass (g)*	*RESP1A*		*RESP1B*		*RESP1C*		*RESP1D*		*RESP1E*	
		Area	*Response Factor*	*Area*	*Response Factor*	*Area*	*Response Factor*	*Area*	*Response Factor*	*Area*	*Response Factor*
n-Nonane	0.0084	619779	1.1519	626531	1.2169	681891	1.2232	619914	1.2220	680829	1.2096
3-Heptanone	0.0283	1511611	0.8339	1515834	0.8739	1649738	0.8784	1502039	0.8789	1634838	0.8621
n-Heptane (IS)	0.0246	1575711	1.0000	1507748	1.0000	1632542	1.0000	1485643	1.0000	1648362	1.0000

Resp 2	*Mass (g)*	*RESP2A*		*RESP2B*		*RESP2C*		*RESP2D*		*RESP2E*	
		Area	*Response Factor*	*Area*	*Response Factor*	*Area*	*Response Factor*	*Area*	*Response Factor*	*Area*	*Response Factor*
n-Nonane	0.0154	1125675	1.1813	1118503	1.1904	1090565	1.1880	1080198	1.1643	1051763	1.1405
3-Heptanone	0.0184	1004323	0.8821	892760	0.7952	953875	0.8697	959446	0.8655	931112	0.8450
n-Heptane (IS)	0.0240	1485094	1.0000	1464309	1.0000	1430646	1.0000	1445913	1.0000	1437204	1.0000

Resp 3	*Mass (g)*	*RESP3A*		*RESP3B*		*RESP3C*		*RESP3D*		*RESP3E*	
		Area	*Response Factor*	*Area*	*Response Factor*	*Area*	*Response Factor*	*Area*	*Response Factor*	*Area*	*Response Factor*
n-Nonane	0.0258	1275536	1.0105	1283110	1.0353	1230959	1.0180	1184609	0.9896	1158724	0.9937
3-Heptanone	0.0093	349357	0.7678	345739	0.7739	331863	0.7614	322993	0.7485	312146	0.7426
n-Heptane (IS)	0.0244	1193801	1.0000	1172080	1.0000	1143578	1.0000	1132114	1.0000	1102784	1.0000

n-Decane/3-Heptanone

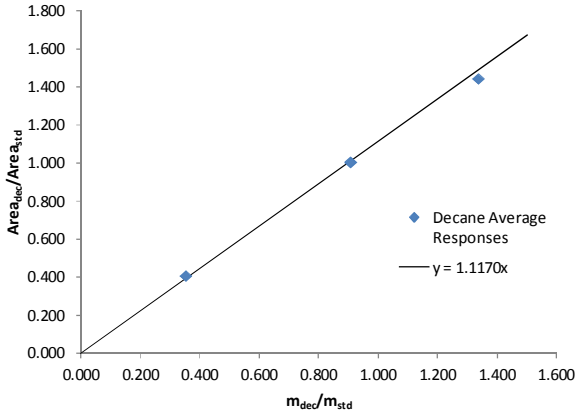

Figure C. 11: n-Decane calibration curve for GC analysis in n-decane/3-heptanone system

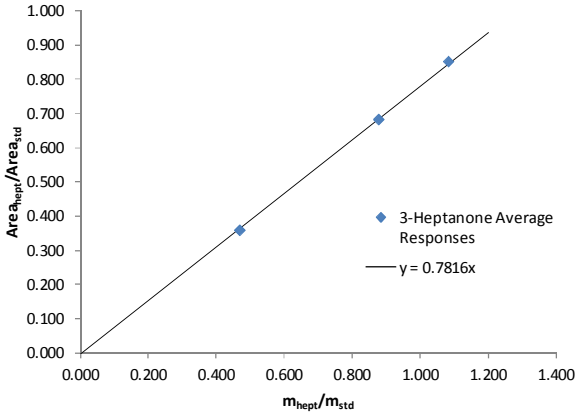

Figure C. 12: 3-Heptanone calibration curve for GC analysis in n-decane/3-heptanone system

Table C. 6: Data used in calibration curve generation for n-decane – 3-heptanone system

Resp 1	*Mass (g)*	*RESP1A*		*RESP1B*		*RESP1C*		*RESP1D*		*RESP1E*	
		Area	*Response Factor*	*Area*	*Response Factor*	*Area*	*Response Factor*	*Area*	*Response Factor*	*Area*	*Response Factor*
n-Decane	0.0070	493557	1.1550	497523	1.1574	491325	1.1623	489668	1.1537	498606	1.1674
3-Heptanone	0.0215	1033031	0.7870	1041117	0.7885	1027843	0.7916	1025405	0.7866	1044111	0.7959
Heptane (IS)	0.0199	1214861	1.0000	1222041	1.0000	1201754	1.0000	1206648	1.0000	1214200	1.0000

Resp 2	*Mass (g)*	*RESP2A*		*RESP2B*		*RESP2C*		*RESP2D*		*RESP2E*	
		Area	*Response Factor*	*Area*	*Response Factor*	*Area*	*Response Factor*	*Area*	*Response Factor*	*Area*	*Response Factor*
n-Decane	0.0145	903100	1.1135	900470	1.1060	897771	1.1072	905231	1.1093	934064	1.1130
3-Heptanone	0.0140	613972	0.7840	614335	0.7815	613554	0.7837	615211	0.7808	630822	0.7785
Heptane (IS)	0.0160	894946	1.0000	898357	1.0000	894740	1.0000	900475	1.0000	926068	1.0000

Resp 3	*Mass (g)*	*RESP3A*		*RESP3B*		*RESP3C*		*RESP3D*		*RESP3E*	
		Area	*Response Factor*	*Area*	*Response Factor*	*Area*	*Response Factor*	*Area*	*Response Factor*	*Area*	*Response Factor*
n-Decane	0.0215	1321898	1.0774	1325282	1.0836	1330319	1.0833	1340721	1.0832	1319028	1.0826
3-Heptanone	0.0075	330485	0.7722	331082	0.7760	331488	0.7738	332465	0.7700	329151	0.7744
Heptane (IS)	0.0161	918762	1.0000	915852	1.0000	919573	1.0000	926906	1.0000	912409	1.0000

n-Octane/4-Heptanone

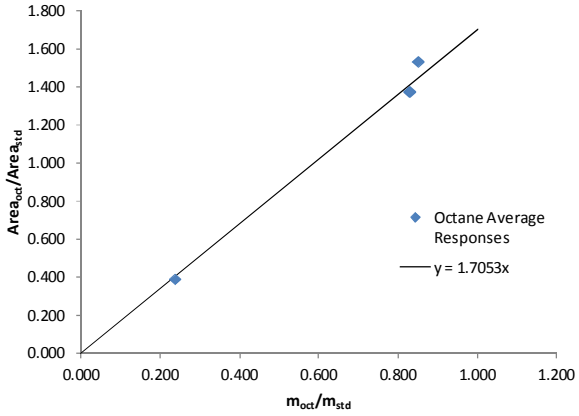

Figure C. 13: n-Octane calibration curve for GC analysis in n-octane/4-heptanone system

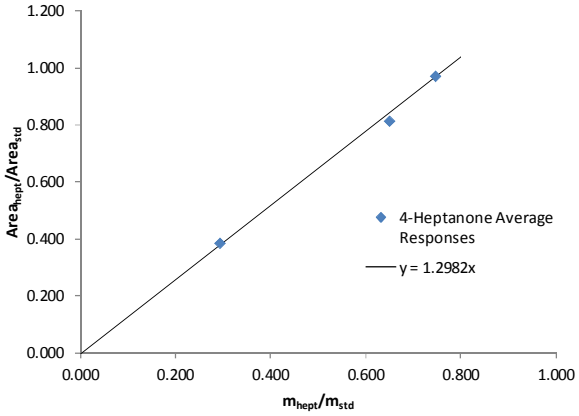

Figure C. 14: 4-Heptanone calibration curve for GC analysis in n-octane/4-heptanone system

Table C. 7: Data used in calibration curve generation for n-octane – 4-heptanone system

Resp 1	*Mass (g)*	*RESP1A*		*RESP1B*		*RESP1C*		*RESP1D*		*RESP1E*	
		Area	*Response Factor*	*Area*	*Response Factor*	*Area*	*Response Factor*	*Area*	*Response Factor*	*Area*	*Response Factor*
n-Octane	0.0063	398399	1.6563	409492	1.6524	408240	1.6462	411615	1.6465	413795	1.6437
4-Heptanone	0.0198	993835	1.3146	1017927	1.3069	1012375	1.2989	1029561	1.3104	1031048	1.3031
Butanone (IS)	0.0266	1015614	1.0000	1046350	1.0000	1047070	1.0000	1055499	1.0000	1062929	1.0000

Resp 2	*Mass (g)*	*RESP2A*		*RESP2B*		*RESP2C*		*RESP2D*		*RESP2E*	
		Area	*Response Factor*	*Area*	*Response Factor*	*Area*	*Response Factor*	*Area*	*Response Factor*	*Area*	*Response Factor*
n-Octane	0.0174	1136214	1.7068	1086961	1.6411	1072123	1.6493	1099967	1.6775	1034039	1.6323
4-Heptanone	0.0136	655048	1.2590	649111	1.2538	643752	1.2671	644461	1.2575	621577	1.2553
Butanone (IS)	0.0210	803406	1.0000	799389	1.0000	784521	1.0000	791381	1.0000	764559	1.0000

Resp 3	*Mass (g)*	*RESP3A*		*RESP3B*		*RESP3C*		*RESP3D*		*RESP3E*	
		Area	*Response Factor*	*Area*	*Response Factor*	*Area*	*Response Factor*	*Area*	*Response Factor*	*Area*	*Response Factor*
n-Octane	0.0181	1237032	1.8232	1214697	1.8038	1234459	1.7970	1233350	1.8025	1254619	1.8011
4-Heptanone	0.0062	311399	1.3399	305767	1.3256	311216	1.3226	309514	1.3206	319166	1.3376
Butanone (IS)	0.0213	798436	1.0000	792447	1.0000	808414	1.0000	805210	1.0000	819725	1.0000

n-Nonane/4-Heptanone

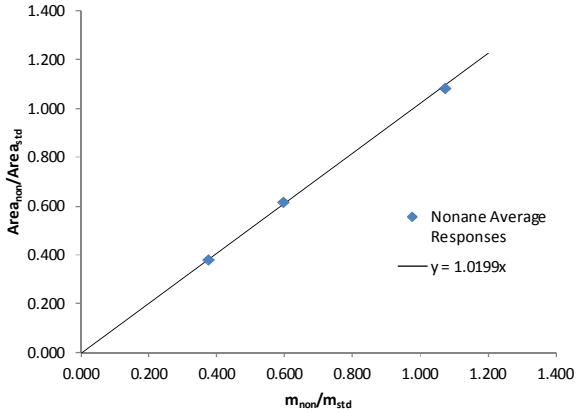

Figure C. 15: n-Nonane calibration curve for GC analysis in n-nonane/4-heptanone system

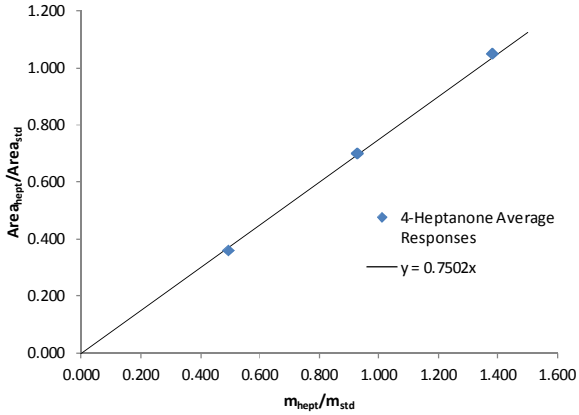

Figure C. 16: 4-Heptanone calibration curve for GC analysis in n-nonane/4-heptanone system

Table C. 8: Data used in calibration curve generation for n-nonane – 4-heptanone system

Resp 1	*Mass (g)*	*RESP1A*		*RESP1B*		*RESP1C*		*RESP1D*		*RESP1E*	
		Area	*Response Factor*	*Area*	*Response Factor*	*Area*	*Response Factor*	*Area*	*Response Factor*	*Area*	*Response Factor*
n-Nonane	0.0176	1150744	1.0084	1186487	1.0147	1178119	1.0061	1195020	1.0142	1187960	1.0070
4-Heptanone	0.0081	383622	0.7304	394516	0.7331	394149	0.7314	397131	0.7324	398400	0.7338
Heptane (IS)	0.0164	1063352	1.0000	1089524	1.0000	1091096	1.0000	1097899	1.0000	1099298	1.0000

Resp 2	*Mass (g)*	*RESP2A*		*RESP2B*		*RESP2C*		*RESP2D*		*RESP2E*	
		Area	*Response Factor*	*Area*	*Response Factor*	*Area*	*Response Factor*	*Area*	*Response Factor*	*Area*	*Response Factor*
n-Nonane	0.0099	670818	1.0373	677835	1.0414	674006	1.0374	671989	1.0303	661693	1.0300
4-Heptanone	0.0154	760787	0.7563	763257	0.7538	769772	0.7616	768016	0.7570	756466	0.7570
Heptane (IS)	0.0166	1084314	1.0000	1091390	1.0000	1089422	1.0000	1093631	1.0000	1077182	1.0000

Resp 3	*Mass (g)*	*RESP3A*		*RESP3B*		*RESP3C*		*RESP3D*		*RESP3E*	
		Area	*Response Factor*	*Area*	*Response Factor*	*Area*	*Response Factor*	*Area*	*Response Factor*	*Area*	*Response Factor*
n-Nonane	0.0062	434093	1.0348	428567	1.0163	439709	1.0099	434640	1.0061	431037	1.0043
4-Heptanone	0.0228	1189558	0.7711	1190137	0.7675	1210421	0.7560	1199367	0.7549	1195104	0.7572
Heptane (IS)	0.0165	1116368	1.0000	1122202	1.0000	1158718	1.0000	1149702	1.0000	1142248	1.0000

n-Decane/4-Heptanone

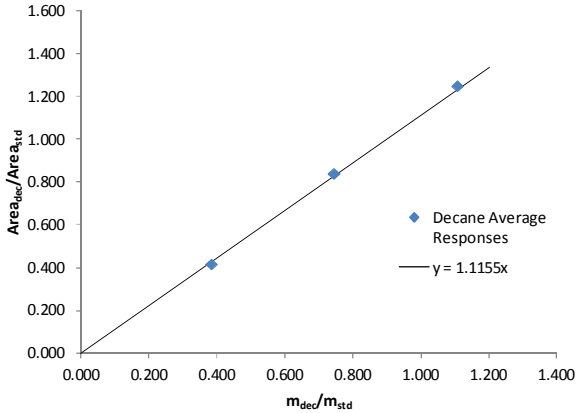

Figure C. 17: n-Decane calibration curve for GC analysis in n-decane/4-heptanone system

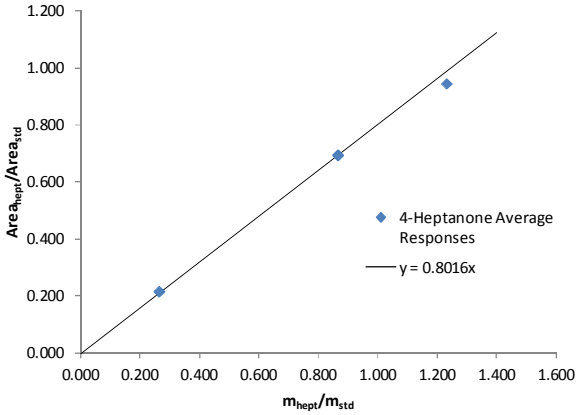

Figure C. 18: 4-Heptanone calibration curve for GC analysis in n-decane/4-heptanone system

Table C. 9: Data used in calibration curve generation for n-decane – 4-heptanone system

Resp 1	*Mass (g)*	*RESP1A*		*RESP1B*		*RESP1C*		*RESP1D*		*RESP1E*	
		Area	*Response Factor*	*Area*	*Response Factor*	*Area*	*Response Factor*	*Area*	*Response Factor*	*Area*	*Response Factor*
n-Decane	0.0186	1237030	1.1066	1226632	1.0972	1404717	1.1444	1298368	1.1417	1340648	1.1517
4-Heptanone	0.0044	221088	0.8360	215687	0.8156	240451	0.8281	223893	0.8323	229679	0.8341
Heptane (IS)	0.0168	1009702	1.0000	1009734	1.0000	1108724	1.0000	1027151	1.0000	1051432	1.0000

Resp 2	*Mass (g)*	*RESP2A*		*RESP2B*		*RESP2C*		*RESP2D*		*RESP2E*	
		Area	*Response Factor*	*Area*	*Response Factor*	*Area*	*Response Factor*	*Area*	*Response Factor*	*Area*	*Response Factor*
n-Decane	0.0125	747984	1.1664	719606	1.1292	694361	1.1300	704989	1.1249	694550	1.0980
4-Heptanone	0.0145	599798	0.8063	599156	0.8105	579302	0.8127	586008	0.8061	581712	0.7928
Heptane (IS)	0.0168	861848	1.0000	856477	1.0000	825884	1.0000	842317	1.0000	850124	1.0000

Resp 3	*Mass (g)*	*RESP3A*		*RESP3B*		*RESP3C*		*RESP3D*		*RESP3E*	
		Area	*Response Factor*	*Area*	*Response Factor*	*Area*	*Response Factor*	*Area*	*Response Factor*	*Area*	*Response Factor*
n-Decane	0.0067	421878	1.0922	438721	1.1088	423102	1.0755	416272	1.0800	413747	1.0857
4-Heptanone	0.0215	939626	0.7581	994568	0.7833	967779	0.7666	952284	0.7699	944531	0.7724
Heptane (IS)	0.0175	1008911	1.0000	1033508	1.0000	1027530	1.0000	1006709	1.0000	995357	1.0000

C.2. Error Analysis

n-Octane/2-Heptanone

Table C. 10: Repeatability results for GC error analysis in n-Octane/2-Heptanone system

Sample	n-Oct Mass	2-Hept Mass	Standard Mass	n-Oct Mole Frac	2-Hept Mole Frac	n-Oct Area	2-Hept Area	Standard Area	Predicted n-Oct Mass	Predicted 2-Hept Mass	Predicted n-Oct Mole Fract	Predicted 2-Hept Mole Frac	Absolute GC Error Mole Fracn	Absolute GC Error Mole Frac (WC1)*	Absolute GC Error Mole Frac (WC2)*	Ave Absolute GC Error Mole Frac
2KNOWA-1	0.0266	0.0092	0.0272	0.743	0.257	1396551	394829	854218	0.0287	0.0108	0.728	0.272	0.015	0.018	0.013	
2KNOWA-2	0.0266	0.0092	0.0272	0.743	0.257	1138096	315614	803634	0.0249	0.0091	0.731	0.269	0.012	0.014	0.009	0.014
2KNOWA-3	0.0266	0.0092	0.0272	0.743	0.257	1312027	367665	843315	0.0273	0.0101	0.729	0.271	0.014	0.016	0.011	
2KNOWB-1	0.0163	0.0194	0.0268	0.456	0.544	676323	650087	743894	0.0157	0.0200	0.440	0.560	0.017	0.019	0.014	
2KNOWB-2	0.0163	0.0194	0.0268	0.456	0.544	705588	668864	780481	0.0157	0.0196	0.443	0.557	0.013	0.016	0.010	0.016
2KNOWB-3	0.0163	0.0194	0.0268	0.456	0.544	664895	642589	734869	0.0157	0.0200	0.439	0.561	0.018	0.021	0.015	
2KNOWC-1	0.0081	0.0283	0.0294	0.222	0.778	539833	1418682	1120904	0.0091	0.0318	0.223	0.777	0.001	0.002	0.003	
2KNOWC-2	0.0081	0.0283	0.0294	0.222	0.778	507292	1394287	1081428	0.0089	0.0324	0.215	0.785	0.007	0.010	0.004	0.006
2KNOWC-3	0.0081	0.0283	0.0294	0.222	0.778	549617	1387458	1149976	0.0091	0.0303	0.230	0.770	0.008	0.005	0.010	

**WC1 and WC2 account for weighing error affecting the used reference composition. In the former case, the mass of the alkane is increased by 0.00001g (error of scale) with the heptanone decreased by the same amount, the opposite is true of WC2 and the difference between the prediction and these worst case reference compositions is that reported.*

n-Nonane/2-Heptanone

Table C. 11: Repeatability results for GC error analysis in n-nonane/2-heptanone system

Sample	n-Non Mass	2-Hept Mass	Standard Mass	n-Non Mole Frac	2-Hept Mole Frac	n-Non Area	2-Hept Area	Standard Area	Predicted n-Non Mass	Predicted 2-Hept Mass	Predicted n-Non Mole Fract	Predicted 2-Hept Mole Frac	Absolute GC Error Mole Fracn	Absolute GC Error Mole Frac (WC1)*	Absolute GC Error Mole Frac (WC2)*	Ave Absolute GC Error Mole Frac
3KNOWA-1	0.027	0.0106	0.0217	0.694	0.306	1636385	481837	1296084	0.0242	0.0097	0.691	0.309	0.004	0.006	0.001	0.004
3KNOWA-2	0.027	0.0106	0.0217	0.694	0.306	1751971	497035	1309121	0.0257	0.0099	0.698	0.302	0.004	0.002	0.007	
3KNOWA-3	0.027	0.0106	0.0217	0.694	0.306	1724381	489257	1257300	0.0263	0.0101	0.698	0.302	0.004	0.002	0.007	
3KNOWB-1	0.0182	0.0218	0.0229	0.426	0.574	1128301	1029610	1311407	0.0174	0.0215	0.419	0.581	0.008	0.010	0.005	0.009
3KNOWB-2	0.0182	0.0218	0.0229	0.426	0.574	1132664	1041799	1337449	0.0171	0.0214	0.417	0.583	0.010	0.012	0.007	
3KNOWB-3	0.0182	0.0218	0.0229	0.426	0.574	1091020	1000462	1273295	0.0173	0.0216	0.417	0.583	0.009	0.012	0.007	
3KNOWC-1	0.0093	0.0313	0.0227	0.209	0.791	640044	1558196	1278188	0.0100	0.0332	0.213	0.787	0.003	0.001	0.006	0.002
3KNOWC-2	0.0093	0.0313	0.0227	0.209	0.791	615883	1533952	1288137	0.0096	0.0324	0.209	0.791	0.001	0.003	0.002	
3KNOWC-3	0.0093	0.0313	0.0227	0.209	0.791	614760	1542350	1328116	0.0093	0.0316	0.208	0.792	0.002	0.004	0.001	

n-Decane/2-Heptanone

Table C. 12: Repeatability results for GC error analysis in n-decane/2-heptanone system

Sample	n-Dec Mass	2-Hept Mass	Standard Mass	n-Dec Mole Frac	2-Hept Mole Frac	n-Dec Area	2-Hept Area	Standard Area	Predicted n-Dec Mass	Predicted 2-Hept Mass	Predicted n-Dec Mole Fract	Predicted 2-Hept Mole Frac	Absolute GC Error Mole Fracn	Absolute GC Error Mole Frac (WC1)*	Absolute GC Error Mole Frac (WC2)*	Ave Absolute GC Error Mole Frac
4KNOWA-1	0.0257	0.0107	0.021	0.658	0.342	1777032	556701	1270024	0.0213	0.0092	0.650	0.350	0.009	0.012	0.006	0.005
4KNOWA-2	0.0257	0.0107	0.021	0.658	0.342	1821868	554209	1229723	0.0226	0.0095	0.656	0.344	0.002	0.005	0.001	
4KNOWA-3	0.0257	0.0107	0.021	0.658	0.342	1814019	550161	1254423	0.0220	0.0092	0.657	0.343	0.001	0.004	0.002	
4KNOWB-1	0.0243	0.0207	0.0215	0.485	0.515	1773562	1145005	1323329	0.0209	0.0186	0.474	0.526	0.011	0.014	0.009	0.012
4KNOWB-2	0.0243	0.0207	0.0215	0.485	0.515	1748114	1125862	1316293	0.0207	0.0184	0.474	0.526	0.011	0.013	0.009	
4KNOWB-3	0.0243	0.0207	0.0215	0.485	0.515	1710614	1113280	1338324	0.0199	0.0179	0.472	0.528	0.013	0.016	0.011	
4KNOWC-1	0.0086	0.0242	0.0217	0.222	0.778	613847	1242649	1296883	0.0075	0.0208	0.223	0.777	0.001	0.002	0.004	0.002
4KNOWC-2	0.0086	0.0242	0.0217	0.222	0.778	612856	1252793	1327521	0.0073	0.0205	0.221	0.779	0.001	0.003	0.002	
4KNOWC-3	0.0086	0.0242	0.0217	0.222	0.778	606187	1247052	1332798	0.0072	0.0203	0.220	0.780	0.002	0.004	0.001	

n-Octane/3-Heptanone

Table C. 13: Repeatability results for GC error analysis in n-octane/2-heptanone system

Sample	n-Oct Mass	3-Hept Mass	Standard Mass	n-Oct Mole Frac	3-Hept Mole Frac	n-Oct Area	3-Hept Area	Standard Area	Predicted n-Oct Mass	Predicted 3-Hept Mass	Predicted n-Oct Mole Fract	Predicted 3-Hept Mole Frac	Absolute GC Error Mole Fracn	Absolute GC Error Mole Frac (WC1)*	Absolute GC Error Mole Frac (WC2)*	Ave Absolute GC Error Mole Frac
5KNOWA-1	0.0236	0.0086	0.0277	0.733	0.267	1660445	503512	1221818	0.0230	0.0092	0.714	0.286	0.019	0.022	0.016	0.020
5KNOWA-2	0.0236	0.0086	0.0277	0.733	0.267	1635896	495753	1191370	0.0233	0.0093	0.714	0.286	0.019	0.022	0.016	
5KNOWA-3	0.0236	0.0086	0.0277	0.733	0.267	1638920	502973	1237442	0.0225	0.0091	0.712	0.288	0.021	0.024	0.018	
5KNOWB-1	0.0165	0.0195	0.0293	0.458	0.542	1108973	974634	1181649	0.0168	0.0195	0.463	0.537	0.004	0.002	0.007	0.003
5KNOWB-2	0.0165	0.0195	0.0293	0.458	0.542	1106862	991556	1188646	0.0167	0.0198	0.458	0.542	0.000	0.003	0.003	
5KNOWB-3	0.0165	0.0195	0.0293	0.458	0.542	1124992	1013260	1201288	0.0168	0.0200	0.457	0.543	0.002	0.004	0.001	
5KNOWC-1	0.0069	0.0294	0.0282	0.190	0.810	475099	1382872	1101955	0.0074	0.0286	0.206	0.794	0.016	0.014	0.019	0.014
5KNOWC-2	0.0069	0.0294	0.0282	0.190	0.810	475853	1416642	1109993	0.0074	0.0291	0.203	0.797	0.013	0.010	0.015	
5KNOWC-3	0.0069	0.0294	0.0282	0.190	0.810	481019	1428436	1116342	0.0074	0.0292	0.203	0.797	0.013	0.010	0.016	

n-Nonane/3-Heptanone

Table C. 14: Repeatability results for GC error analysis in n-nonane/3-heptanone system

Sample	n-Non Mass	3-Hept Mass	Standard Mass	n-Non Mole Frac	3-Hept Mole Frac	n-Non Area	3-Hept Area	Standard Area	Predicted n-Non Mass	Predicted 3-Hept Mass	Predicted n-Non Mole Fract	Predicted 3-Hept Mole Frac	Absolute GC Error Mole Fracn	Absolute GC Error Mole Frac (WC1)*	Absolute GC Error Mole Frac (WC2)*	Ave Absolute GC Error Mole Frac
6KNOWA-1	0.0274	0.0104	0.0251	0.701	0.299	2012474	536205	1383346	0.0323	0.0118	0.710	0.290	0.008	0.006	0.011	0.010
6KNOWA-2	0.0274	0.0104	0.0251	0.701	0.299	1875647	498390	1324406	0.0315	0.0114	0.710	0.290	0.009	0.006	0.012	
6KNOWA-3	0.0274	0.0104	0.0251	0.701	0.299	2149805	563944	1569089	0.0305	0.0109	0.713	0.287	0.012	0.009	0.014	
6KNOWB-1	0.0174	0.0206	0.0222	0.429	0.571	1495736	1213445	1479228	0.0199	0.0221	0.445	0.555	0.016	0.013	0.018	0.017
6KNOWB-2	0.0174	0.0206	0.0222	0.429	0.571	1487062	1219556	1454933	0.0201	0.0225	0.443	0.557	0.013	0.011	0.016	
6KNOWB-3	0.0174	0.0206	0.0222	0.429	0.571	1727490	1370351	1526126	0.0223	0.0242	0.451	0.549	0.021	0.019	0.024	
6KNOWC-1	0.0082	0.0302	0.0217	0.195	0.805	728075	1860361	1555105	0.0090	0.0315	0.203	0.797	0.008	0.006	0.011	0.006
6KNOWC-2	0.0082	0.0302	0.0217	0.195	0.805	720931	1903164	1550054	0.0089	0.0323	0.198	0.802	0.003	0.001	0.006	
6KNOWC-3	0.0082	0.0302	0.0217	0.195	0.805	759954	1962459	1552206	0.0094	0.0332	0.201	0.799	0.007	0.004	0.009	

n-Decane/3-Heptanone

Table C. 15: Repeatability results for GC error analysis in n-decane/3-heptanone system

Sample	n-Dec Mass	3-Hept Mass	Standard Mass	n-Dec Mole Frac	3-Hept Mole Frac	n-Dec Area	3-Hept Area	Standard Area	Predicted n-Dec Mass	Predicted 3-Hept Mass	Predicted n-Dec Mole Fract	Predicted 3-Hept Mole Frac	Absolute GC Error Mole Fracn	Absolute GC Error Mole Frac (WC1)*	Absolute GC Error Mole Frac (WC2)*	Ave Absolute GC Error Mole Frac
7KNOWA-1	0.0268	0.0112	0.0207	0.658	0.342	2113544	675643	1368285	0.0286	0.0131	0.637	0.363	0.020	0.023	0.017	0.014
7KNOWA-2	0.0268	0.0112	0.0207	0.658	0.342	2081491	640463	1359070	0.0284	0.0125	0.646	0.354	0.012	0.014	0.009	
7KNOWA-3	0.0268	0.0112	0.0207	0.658	0.342	2081203	638901	1350212	0.0286	0.0125	0.647	0.353	0.011	0.014	0.008	
7KNOWB-1	0.0153	0.0212	0.0213	0.367	0.633	1286517	1210780	1363467	0.0180	0.0242	0.374	0.626	0.007	0.004	0.010	0.004
7KNOWB-2	0.0153	0.0212	0.0213	0.367	0.633	1283394	1229163	1377136	0.0178	0.0243	0.370	0.630	0.003	0.000	0.005	
7KNOWB-3	0.0153	0.0212	0.0213	0.367	0.633	1266626	1218415	1389968	0.0174	0.0239	0.369	0.631	0.002	0.001	0.004	
7KNOWC-1	0.0132	0.0313	0.0212	0.253	0.747	1072816	1711467	1383334	0.0147	0.0336	0.260	0.740	0.008	0.005	0.010	0.008
7KNOWC-2	0.0132	0.0313	0.0212	0.253	0.747	1088626	1738896	1398085	0.0148	0.0337	0.260	0.740	0.007	0.005	0.009	
7KNOWC-3	0.0132	0.0313	0.0212	0.253	0.747	1090446	1731116	1382178	0.0150	0.0340	0.261	0.739	0.008	0.006	0.010	

n-Octane/4-Heptanone

Table C. 16: Repeatability results for GC error analysis in n-octane/4-heptanone system

Sample	n-Oct Mass	4-Hept Mass	Standard Mass	n-Oct Mole Frac	4-Hept Mole Frac	n-Oct Area	4-Hept Area	Standard Area	Predicted n-Oct Mass	Predicted 4-Hept Mass	Predicted n-Oct Mole Fract	Predicted 4-Hept Mole Frac	Absolute GC Error Mole Fracn	Absolute GC Error Mole Frac (WC1)*	Absolute GC Error Mole Frac (WC2)*	Ave Absolute GC Error Mole Frac
8KNOWA-1	0.0231	0.0082	0.0289	0.738	0.262	1450799	419525	1074301	0.0229	0.0087	0.725	0.275	0.013	0.017	0.010	0.013
8KNOWA-2	0.0231	0.0082	0.0289	0.738	0.262	1441890	413950	1054246	0.0232	0.0087	0.726	0.274	0.012	0.015	0.009	
8KNOWA-3	0.0231	0.0082	0.0289	0.738	0.262	1468293	427133	1074161	0.0232	0.0089	0.723	0.277	0.015	0.018	0.011	
8KNOWB-1	0.0154	0.0164	0.0289	0.484	0.516	1108538	903354	1167137	0.0161	0.0172	0.483	0.517	0.001	0.004	0.002	0.003
8KNOWB-2	0.0154	0.0164	0.0289	0.484	0.516	1113888	909590	1175654	0.0161	0.0172	0.482	0.518	0.002	0.005	0.001	
8KNOWB-3	0.0154	0.0164	0.0289	0.484	0.516	1101548	900753	1174423	0.0159	0.0171	0.482	0.518	0.002	0.005	0.001	
8KNOWC-1	0.0078	0.0213	0.0280	0.268	0.732	585598	1186021	1229298	0.0078	0.0208	0.273	0.727	0.005	0.002	0.009	0.004
8KNOWC-2	0.0078	0.0213	0.0280	0.268	0.732	576617	1183626	1240738	0.0076	0.0206	0.270	0.730	0.002	0.001	0.006	
8KNOWC-3	0.0078	0.0213	0.0280	0.268	0.732	576829	1183585	1215586	0.0078	0.0210	0.271	0.729	0.003	0.001	0.006	

n-Nonane/4-Heptanone

Table C. 17: Repeatability results for GC error analysis in n-nonane/4-heptanone system

Sample	n-Non Mass	4-Hept Mass	Standard Mass	n-Non Mole Frac	4-Hept Mole Frac	n-Non Area	4-Hept Area	Standard Area	Predicted n-Non Mass	Predicted 4-Hept Mass	Predicted n-Non Mole Fract	Predicted 4-Hept Mole Frac	Absolute GC Error Mole Fracn	Absolute GC Error Mole Frac (WC1)*	Absolute GC Error Mole Frac (WC2)*	Ave Absolute GC Error Mole Frac
9KNOWA-1	0.0273	0.0092	0.0217	0.725	0.275	2173391	548282	1378543	0.0303	0.0105	0.721	0.279	0.005	0.008	0.002	0.004
9KNOWA-2	0.0273	0.0092	0.0217	0.725	0.275	2309307	561122	1286398	0.0345	0.0115	0.728	0.272	0.003	0.000	0.006	
9KNOWA-3	0.0273	0.0092	0.0217	0.725	0.275	2333165	587249	1382575	0.0324	0.0112	0.721	0.279	0.004	0.007	0.001	
9KNOWB-1	0.0179	0.018	0.0219	0.470	0.530	1336900	1022544	1323487	0.0196	0.0205	0.460	0.540	0.010	0.013	0.007	0.014
9KNOWB-2	0.0179	0.018	0.0219	0.470	0.530	1202416	942861	1197759	0.0195	0.0209	0.454	0.546	0.016	0.019	0.013	
9KNOWB-3	0.0179	0.018	0.0219	0.470	0.530	1158668	912108	1177371	0.0191	0.0206	0.453	0.547	0.017	0.020	0.014	
9KNOWC-1	0.0084	0.0286	0.0239	0.207	0.793	456360	1162150	1097808	0.0088	0.0307	0.204	0.796	0.004	0.006	0.001	0.003
9KNOWC-2	0.0084	0.0286	0.0239	0.207	0.793	367907	932176	1004422	0.0078	0.0269	0.204	0.796	0.003	0.005	0.000	
9KNOWC-3	0.0084	0.0286	0.0239	0.207	0.793	471619	1189550	1075716	0.0093	0.0320	0.205	0.795	0.002	0.005	0.000	

n-Decane/4-Heptanone

Table C. 18: Repeatability results for GC error analysis in n-decane/4-heptanone system

Sample	n-Dec Mass	3-Hept Mass	Standard Mass	n-Dec Mole Frac	3-Hept Mole Frac	n-Dec Area	3-Hept Area	Standard Area	Predicted n-Dec Mass	Predicted 3-Hept Mass	Predicted n-Dec Mole Fract	Predicted 3-Hept Mole Frac	Absolute GC Error Mole Fracn	Absolute GC Error Mole Frac (WC1)*	Absolute GC Error Mole Frac (WC2)*	Ave Absolute GC Error Mole Frac
0KNOWA-1	0.0252	0.0096	0.0222	0.678	0.322	1748115	498222	1166774	0.0298	0.0121	0.663	0.337	0.015	0.018	0.012	0.010
0KNOWA-2	0.0252	0.0096	0.0222	0.678	0.322	1756059	479211	1209322	0.0289	0.0113	0.673	0.327	0.005	0.008	0.002	
0KNOWA-3	0.0252	0.0096	0.0222	0.678	0.322	1739908	484801	1113481	0.0311	0.0124	0.668	0.332	0.010	0.013	0.007	
0KNOWB-1	0.0175	0.0207	0.0219	0.404	0.596	1445001	1251846	1278676	0.0222	0.0274	0.393	0.607	0.011	0.013	0.008	0.010
0KNOWB-2	0.0175	0.0207	0.0219	0.404	0.596	1171168	1005500	1147950	0.0200	0.0245	0.395	0.605	0.009	0.011	0.006	
0KNOWB-3	0.0175	0.0207	0.0219	0.404	0.596	1431288	1240240	1264682	0.0222	0.0275	0.393	0.607	0.011	0.014	0.008	
0KNOWC-1	0.0163	0.0267	0.0206	0.329	0.671	1101076	1335391	1172228	0.0173	0.0300	0.316	0.684	0.012	0.015	0.010	0.009
0KNOWC-2	0.0163	0.0267	0.0206	0.329	0.671	756399	908852	941258	0.0148	0.0254	0.318	0.682	0.010	0.012	0.008	
0KNOWC-3	0.0163	0.0267	0.0206	0.329	0.671	1368674	1610573	1277922	0.0198	0.0332	0.323	0.677	0.006	0.008	0.004	

Appendix D Experimental Results

Verification: Ethanol/1-Butanol

Table D. 1: Vapour – liquid equilibrium experimental results for verification system: ethanol/1-butanol at 1.013bar

	T	T_{dev}	$X_{Ethanol}$	ΔX	$X_{Eth,\,avg}$	$Y_{Ethanol}$	ΔY	$Y_{Eth,\,avg}$	Y-X
Ethanol	351.14	0.02	1.0000	-	1.0000	1.0000	-	1.0000	0.0000
JC1011a	354.08	0.02	0.8343 0.8363	0.0021	0.8353	0.9724 0.9715	0.0009	0.9720	0.1382 0.1352
JC1013a	358.01	0.01	0.6919 0.6848	0.0071	0.6883	0.9352 0.9340	0.0012	0.9346	0.2433 0.2492
JC1013b	358.73	0.02	0.6629 0.6694	0.0065	0.6662	0.9233 0.9252	0.0019	0.9243	0.2604 0.2558
JC1014a	359.00	0.02	0.6492 0.6536	0.0045	0.6514	0.9244 0.9252	0.0008	0.9248	0.2752 0.2715
JC1014b	359.55	0.02	0.6393 0.6341	0.0053	0.6367	0.9122 0.9151	0.0029	0.9136	0.2729 0.2810
JC1021b	360.56	0.02	0.5995 0.6003	0.0008	0.5999	0.9042 0.9085	0.0043	0.9064	0.3047 0.3082
JC1022a	363.59	0.02	0.5011 0.4996	0.0015	0.5003	0.8697 0.8710	0.0013	0.8704	0.3686 0.3714
JC1022b	364.78	0.02	0.4799 0.4743	0.0056	0.4771	0.8393 0.8340	0.0053	0.8367	0.3595 0.3597
JC1024b	367.99	0.01	0.3825 0.3817	0.0007	0.3821	0.7678 0.7647	0.0031	0.7663	0.3853 0.3830
JC1025b	370.27	0.02	0.3310 0.3306	0.0004	0.3308	0.7134 0.7245	0.0111	0.7190	0.3824 0.3939
JC1031a	381.54	0.02	0.1388 0.1264	0.0124	0.1326	0.3779 0.3788	0.0009	0.3783	0.2391 0.2524
JC1031b	382.25	0.02	0.1118 0.1117	0.0001	0.1118	0.3497 0.3515	0.0018	0.3506	0.2379 0.2398
JC1032a	373.93	0.01	0.2501 0.2517	0.0016	0.2509	0.6260 0.6358	0.0098	0.6309	0.3759 0.3841
JC1032b	374.59	0.01	0.2475 0.2482	0.0007	0.2479	0.6215 0.6107	0.0108	0.6161	0.3740 0.3625
JC1033b	370.52	0.02	0.3311 0.3298	0.0013	0.3305	0.7151 0.7127	0.0024	0.7139	0.3840 0.3829
JC1041a	354.31	0.02	0.8504 0.8497	0.0008	0.8501	0.9735 0.9742	0.0007	0.9738	0.1230 0.1245
JC1041b	354.58	0.01	0.8370 0.8359	0.0010	0.8364	0.9692 0.9687	0.0005	0.9689	0.1323 0.1328
JC1042a	357.28	0.01	0.7277 0.7300	0.0023	0.7288	0.9396 0.9395	0.0000	0.9396	0.2119 0.2096

	T	T_{dev}	$X_{Ethanol}$	ΔX	$X_{Eth,\ avg}$	$Y_{Ethanol}$	ΔY	$Y_{Eth,\ avg}$	Y-X
JC1042b	357.48	0.01	0.7174 0.7169	0.0006	0.7172	0.9308 0.9299	0.0009	0.9303	0.2133 0.2130
JC1043a	359.89	0.01	0.6366 0.6017	0.0349	0.6192	0.9038 0.9059	0.0021	0.9048	0.2672 0.3042
JC1043b	359.90	0.01	0.6344 0.6272	0.0072	0.6308	0.8854 0.8939	0.0085	0.8896	0.2509 0.2667
JC1044a	360.89	0.02	0.6099 0.6048	0.0050	0.6073	0.8941 0.8928	0.0013	0.8934	0.2842 0.2880
JC1044b	361.31	0.02	0.5919 0.5915	0.0005	0.5917	0.8789 0.8792	0.0004	0.8791	0.2869 0.2878
JC1045a	363.70	0.01	0.5161 0.5133	0.0028	0.5147	0.8522 0.8514	0.0008	0.8518	0.3361 0.3381
JC1045b	364.11	0.02	0.5006 0.4965	0.0041	0.4986	0.8348 0.8329	0.0019	0.8339	0.3342 0.3364
JC1046a	364.95	0.02	0.4668 0.4695	0.0027	0.4682	0.8214 0.8241	0.0027	0.8227	0.3546 0.3545
JC1046b	366.00	0.02	0.4406 0.4380	0.0026	0.4393	0.7966 0.7965	0.0001	0.7965	0.3560 0.3585
1-Butanol	390.49	0.01	0.0000	-	0.0000	0.0000	-	0.0000	0.0000

n-Octane/2-Heptanone

Table D. 2: Vapour – liquid equilibrium experimental results for n-octane/2-heptanone at 40kPa

	T	T_{dev}	$X_{n\text{-}Octane}$	ΔX	$X_{Oct,\ avg}$	$Y_{n\text{-}Octane}$	ΔY	$Y_{Oct,\ avg}$	$Y\text{-}X$
n-Octane	368.32	0.02	1.0000	-	1.0000	1.0000	-	1.0000	0.0000
JC232	388.75	0.02	0.0381 0.0383	0.0003	0.0382	0.1770 0.1794	0.0024	0.1782	0.1389 0.1411
JC233	386.66	0.02	0.0625 0.0629	0.0004	0.0627	0.2615 0.2633	0.0017	0.2624	0.1991 0.2003
JC234	382.61	0.02	0.1311 0.1303	0.0008	0.1307	0.4128 0.4116	0.0013	0.4122	0.2818 0.2813
JC235	382.05	0.02	0.1428 0.1497	0.0069	0.1462	0.4461 0.4473	0.0012	0.4467	0.3033 0.2976
JC236	379.79	0.02	0.2015 0.2008	0.0006	0.2012	0.5140 0.5146	0.0006	0.5143	0.3126 0.3138
JC242	388.62	0.02	0.0370 0.0363	0.0008	0.0366	0.1722 0.1704	0.0018	0.1713	0.1352 0.1341
JC243	386.79	0.02	0.0553 0.0575	0.0021	0.0564	0.2472 0.2474	0.0001	0.2473	0.1919 0.1899
JC244	385.83	0.02	0.0699 0.0717	0.0018	0.0708	0.2805 0.2807	0.0003	0.2806	0.2106 0.2090
JC245	383.43	0.02	0.1100 0.1142	0.0041	0.1121	0.3769 0.3784	0.0014	0.3777	0.2669 0.2642
JC246	382.32	0.02	0.1267 0.1299	0.0032	0.1283	0.4200 0.4055	0.0145	0.4128	0.2933 0.2756
JC251	368.47	0.01	0.9829 0.9826	0.0004	0.9827	0.9837 0.9844	0.0007	0.9840	0.0007 0.0018
JC252	368.50	0.02	0.9744 0.9751	0.0007	0.9748	0.9736 0.9748	0.0011	0.9742	-0.0008 -0.0003
JC253	368.73	0.02	0.9227 0.9230	0.0003	0.9228	0.9349 0.9324	0.0025	0.9337	0.0123 0.0095
JC254	369.70	0.02	0.7674 0.7712	0.0038	0.7693	0.8526 0.8521	0.0005	0.8523	0.0852 0.0809
JC255	370.52	0.02	0.6640 0.6615	0.0025	0.6628	0.7887 0.7941	0.0055	0.7914	0.1246 0.1326
JC256	372.27	0.02	0.5184 0.5214	0.0030	0.5199	0.7313 0.7234	0.0079	0.7274	0.2130 0.2021
JC257	374.02	0.02	0.4043 0.4072	0.0029	0.4057	0.6807 0.6823	0.0015	0.6815	0.2764 0.2751
JC261	374.75	0.02	0.3629 0.3665	0.0036	0.3647	0.6633 0.6667	0.0034	0.6650	0.3004 0.3002
JC262	376.17	0.02	0.3027 0.2999	0.0028	0.3013	0.6399 0.6191	0.0208	0.6295	0.3372 0.3192
JC263	377.40	0.02	0.2582 0.2577	0.0004	0.2580	0.6102 0.6159	0.0056	0.6131	0.3521 0.3581

	T	T_{dev}	$X_{n\text{-}Octane}$	ΔX	$X_{Oct,\ avg}$	$Y_{n\text{-}Octane}$	ΔY	$Y_{Oct,\ avg}$	$Y\text{-}X$
JC265	379.92	0.02	0.1930 0.1909	0.0021	0.1920	0.5327 0.5315	0.0012	0.5321	0.3397 0.3406
JC266	381.05	0.02	0.1650 0.1674	0.0023	0.1662	0.4849 0.4817	0.0032	0.4833	0.3198 0.3143
JC271	368.97	0.02	0.7949 0.7948	0.0001	0.7948	0.8880 0.8868	0.0012	0.8874	0.0931 0.0921
JC272	369.97	0.02	0.6832 0.6771	0.0061	0.6801	0.8271 0.8331	0.0061	0.8301	0.1439 0.1560
JC273	371.42	0.02	0.5700 0.5712	0.0012	0.5706	0.7784 0.7827	0.0043	0.7806	0.2084 0.2115
JC275	374.89	0.02	0.3690 0.3690	0.0001	0.3690	0.6757 0.6829	0.0072	0.6793	0.3068 0.3139
JC276	376.79	0.02	0.2835 0.2837	0.0002	0.2836	0.6304 0.6327	0.0024	0.6315	0.3469 0.3490
JC281	368.31	0.02	0.9822 0.9820	0.0002	0.9821	0.9854 0.9809	0.0045	0.9832	0.0032 -0.0010
JC282	368.27	0.02	0.9806 0.9797	0.0009	0.9802	0.9823 0.9825	0.0002	0.9824	0.0017 0.0028
JC283	368.31	0.02	0.9786 0.9780	0.0006	0.9783	0.9796 0.9788	0.0008	0.9792	0.0010 0.0008
JC284	368.29	0.02	0.9594 0.9606	0.0012	0.9600	0.9650 0.9696	0.0046	0.9673	0.0056 0.0090
JC285	368.42	0.02	0.9253 0.9252	0.0001	0.9252	0.9238 0.9268	0.0030	0.9253	-0.0015 0.0017
2-Hept	392.54	0.01	0.0000	-	0.0000	0.0000	-	0.0000	0.0000

n-Nonane/2-Heptanone

Table D. 3: Vapour – liquid equilibrium experimental results for n-nonane/2-heptanone at 40kPa

	T	T_{dev}	$X_{n\text{-}Nonane}$	ΔX	$X_{Non,\ avg}$	$Y_{n\text{-}Nonane}$	ΔY	$Y_{Non,\ avg}$	$Y\text{-}X$
n-Nonane	391.78	0.02	1.0000	-	1.0000	1.0000	-	1.0000	0.0000
JC311	390.62	0.02	0.0542 0.0549	0.0007	0.0545	0.1101 0.1100	0.0001	0.1101	0.0559 0.0552
JC312	389.72	0.02	0.0897 0.0898	0.0002	0.0897	0.1695 0.1685	0.0010	0.1690	0.0798 0.0786
JC313	389.10	0.02	0.1213 0.1202	0.0011	0.1208	0.2116 0.2095	0.0021	0.2106	0.0903 0.0893
JC321	388.15	0.02	0.1867 0.1860	0.0008	0.1864	0.2940 0.2938	0.0002	0.2939	0.1072 0.1078
JC322	387.79	0.02	0.2557 0.2563	0.0006	0.2560	0.3603 0.3613	0.0010	0.3608	0.1046 0.1050
JC323	387.29	0.02	0.2828 0.2829	0.0001	0.2829	0.3723 0.3717	0.0007	0.3720	0.0895 0.0887
JC331	390.46	0.02	0.9554 0.9556	0.0001	0.9555	0.8764 0.8789	0.0026	0.8776	-0.0791 -0.0766
JC332	388.33	0.02	0.8354 0.8344	0.0010	0.8349	0.7323 0.7311	0.0012	0.7317	-0.1031 -0.1033
JC333	387.61	0.02	0.7491 0.7522	0.0030	0.7507	0.6786 0.6738	0.0047	0.6762	-0.0706 -0.0783
JC334	387.20	0.02	0.6866 0.6840	0.0027	0.6853	0.6144 0.6241	0.0097	0.6192	-0.0722 -0.0599
JC335	386.82	0.02	0.5958 0.5950	0.0008	0.5954	0.5786 0.5779	0.0007	0.5783	-0.0172 -0.0171
JC341	390.56	0.02	0.0577 0.0601	0.0024	0.0589	0.1175 0.1156	0.0020	0.1166	0.0599 0.0555
JC342	389.76	0.02	0.0798 0.0791	0.0007	0.0794	0.1466 0.1471	0.0005	0.1469	0.0669 0.0681
JC343	389.40	0.02	0.1063 0.1060	0.0004	0.1062	0.1882 0.1876	0.0006	0.1879	0.0818 0.0817
JC344	388.78	0.02	0.1411 0.1398	0.0013	0.1405	0.2294 0.2284	0.0010	0.2289	0.0883 0.0886
JC345	388.33	0.02	0.1759 0.1758	0.0001	0.1759	0.2737 0.2730	0.0007	0.2734	0.0978 0.0972
JC351	387.72	0.02	0.2395 0.2388	0.0008	0.2391	0.3676 0.3641	0.0035	0.3658	0.1281 0.1253
JC352	387.40	0.02	0.2756 0.2753	0.0002	0.2755	0.3682 0.3715	0.0032	0.3699	0.0927 0.0961
JC353	387.10	0.02	0.3193 0.3222	0.0029	0.3208	0.4020 0.4042	0.0022	0.4031	0.0827 0.0820
JC354	386.89	0.02	0.3761 0.3768	0.0007	0.3765	0.4341 0.4342	0.0001	0.4342	0.0580 0.0574

	T	T_{dev}	$X_{n\text{-}Nonane}$	ΔX	$X_{Non,\ avg}$	$Y_{n\text{-}Nonane}$	ΔY	$Y_{Non,\ avg}$	$Y\text{-}X$
JC355	386.80	0.02	0.4044 0.4061	0.0017	0.4053	0.4536 0.4540	0.0005	0.4538	0.0491 0.0479
JC356	386.77	0.02	0.4371 0.4409	0.0038	0.4390	0.4733 0.4728	0.0005	0.4730	0.0362 0.0319
JC361	390.96	0.02	0.9670 0.9675	0.0005	0.9672	0.9332 0.9353	0.0020	0.9343	-0.0337 -0.0322
JC362	389.79	0.02	0.9257 0.9254	0.0002	0.9256	0.8593 0.8581	0.0012	0.8587	-0.0664 -0.0673
JC363	389.65	0.02	0.9058 0.9073	0.0016	0.9066	0.8379 0.8373	0.0006	0.8376	-0.0678 -0.0700
JC364	388.73	0.02	0.8585 0.8587	0.0002	0.8586	0.7640 0.7643	0.0003	0.7642	-0.0945 -0.0944
JC365	388.45	0.02	0.8281 0.8283	0.0002	0.8282	0.7550 0.7563	0.0012	0.7556	-0.0731 -0.0721
JC366	387.70	0.02	0.7548 0.7550	0.0002	0.7549	0.6698 0.6683	0.0015	0.6691	-0.0850 -0.0866
2-Hept	392.54	0.01	0.0000	-	0.0000	0.0000	-	0.0000	0.0000

n-Decane/2-Heptanone

Table D. 4: Vapour – liquid equilibrium experimental results for n-decane/2-heptanone at 40kPa

	T	T_{dev}	$X_{n\text{-}Decane}$	ΔX	$X_{Dec,\ avg}$	$Y_{n\text{-}Decane}$	ΔY	$Y_{Dec,\ avg}$	$Y\text{-}X$
n-Decane	413.88	0.02	1.0000	-	1.0000	1.0000	-	1.0000	0.0000
JC421	401.78	0.02	0.7640 0.7979	0.0340	0.7809	0.4970 0.4905	0.0065	0.4937	-0.2670 -0.3075
JC422	400.55	0.02	0.7301 0.7289	0.0011	0.7295	0.4584 0.4514	0.0070	0.4549	-0.2716 -0.2775
JC423	400.23	0.02	0.7157 0.7143	0.0014	0.7150	0.4440 0.4447	0.0007	0.4443	-0.2717 -0.2696
JC424	399.68	0.02	0.6918 0.6915	0.0003	0.6917	0.4304 0.4262	0.0043	0.4283	-0.2613 -0.2653
JC425	398.85	0.02	0.6638 0.6637	0.0001	0.6637	0.4020 0.4017	0.0002	0.4018	-0.2619 -0.2619
JC426	398.72	0.02	0.6539 0.6537	0.0002	0.6538	0.4138 0.4075	0.0063	0.4106	-0.2401 -0.2462
JC431	392.30	0.02	0.0614 0.0610	0.0004	0.0612	0.0562 0.0582	0.0020	0.0572	-0.0052 -0.0028
JC432	392.81	0.02	0.1309 0.1301	0.0008	0.1305	0.1067 0.1049	0.0019	0.1058	-0.0242 -0.0252
JC433	392.92	0.02	0.1761 0.1763	0.0001	0.1762	0.1425 0.1448	0.0022	0.1437	-0.0336 -0.0315
JC434	393.23	0.02	0.2226 0.2210	0.0016	0.2218	0.1674 0.1669	0.0006	0.1671	-0.0552 -0.0542
JC435	393.67	0.02	0.2786 0.2763	0.0023	0.2774	0.1968 0.1997	0.0029	0.1983	-0.0818 -0.0765
JC436	394.32	0.02	0.3470 0.3435	0.0035	0.3453	0.2358 0.2347	0.0011	0.2353	-0.1112 -0.1088
JC441	395.20	0.02	0.4214 0.4252	0.0039	0.4233	0.2772 0.2767	0.0005	0.2770	-0.1442 -0.1485
JC442	396.00	0.02	0.4896 0.4909	0.0012	0.4903	0.3116 0.3134	0.0017	0.3125	-0.1780 -0.1775
JC443	396.73	0.02	0.5533 0.5529	0.0003	0.5531	0.3424 0.3407	0.0018	0.3416	-0.2108 -0.2123
JC444	398.32	0.02	0.6271 0.6250	0.0021	0.6260	0.3952 0.3949	0.0002	0.3950	-0.2319 -0.2301
JC445	399.15	0.02	0.6686 0.6675	0.0011	0.6680	0.4179 0.4167	0.0012	0.4173	-0.2507 -0.2508
JC451	411.91	0.02	0.9717 0.9718	0.0001	0.9718	0.8761 0.8769	0.0007	0.8765	-0.0956 -0.0949
JC452	409.34	0.02	0.9358 0.9360	0.0002	0.9359	0.7731 0.7748	0.0017	0.7739	-0.1627 -0.1613
JC453	406.98	0.02	0.8890 0.8896	0.0006	0.8893	0.6764 0.6781	0.0017	0.6772	-0.2126 -0.2115

	T	T_{dev}	$X_{n\text{-}Decane}$	ΔX	$X_{Dec,\ avg}$	$Y_{n\text{-}Decane}$	ΔY	$Y_{Dec,\ avg}$	$Y\text{-}X$
JC454	404.19	0.02	0.8344 0.8316	0.0027	0.8330	0.5688 0.5709	0.0020	0.5699	-0.2655 -0.2608
JC455	402.79	0.02	0.7990 0.8000	0.0010	0.7995	0.5251 0.5226	0.0025	0.5238	-0.2739 -0.2774
JC456	401.37	0.02	0.7547 0.7549	0.0002	0.7548	0.4543 0.4547	0.0005	0.4545	-0.3005 -0.3002
JC462	399.32	0.02	0.6718 0.6729	0.0011	0.6724	0.4199 0.4188	0.0011	0.4193	-0.2519 -0.2542
JC463	397.08	0.02	0.5754 0.5746	0.0008	0.5750	0.3541 0.3555	0.0014	0.3548	-0.2213 -0.2191
JC464	396.72	0.02	0.5466 0.5449	0.0018	0.5458	0.3351 0.3343	0.0008	0.3347	-0.2116 -0.2106
JC465	395.90	0.02	0.4832 0.4826	0.0006	0.4829	0.3030 0.3020	0.0010	0.3025	-0.1802 -0.1806
JC471	392.05	0.02	0.0246 0.0221	0.0025	0.0233	0.0244 0.0244	0.0000	0.0244	-0.0002 0.0023
JC472	391.96	0.02	0.0265 0.0271	0.0007	0.0268	0.0285 0.0306	0.0021	0.0295	0.0020 0.0034
JC473	391.79	0.02	0.0340 0.0289	0.0051	0.0315	0.0283 0.0277	0.0006	0.0280	-0.0057 -0.0012
JC474	391.87	0.02	0.0302 0.0323	0.0021	0.0312	0.0287 0.0316	0.0030	0.0301	-0.0015 -0.0007
JC475	391.68	0.02	0.0360 0.0405	0.0044	0.0382	0.0297 0.0310	0.0013	0.0304	-0.0063 -0.0094
JC476	391.82	0.02	0.0501 0.0458	0.0043	0.0480	0.0426 0.0409	0.0018	0.0417	-0.0075 -0.0050
2-Hept	392.54	0.01	0.0000	-	0.0000	0.0000	-	0.0000	0.0000

n-Octane/3-Heptanone

Table D. 5: Vapour – liquid equilibrium experimental results for n-octane/3-heptanone at 40kPa

	T	T_{dev}	$X_{n\text{-}Octane}$	ΔX	$X_{Oct,\ avg}$	$Y_{n\text{-}Octane}$	ΔY	$Y_{Oct,\ avg}$	$Y\text{-}X$
n-Octane	367.97	0.02	1.0000	-	1.0000	1.0000	-	1.0000	0.0000
JC511	386.89	0.02	0.0218 0.0219	0.0000	0.0219	0.0800 0.0801	0.0001	0.0800	0.0582 0.0582
JC512	384.44	0.02	0.0708 0.0703	0.0005	0.0706	0.2228 0.2209	0.0019	0.2218	0.1520 0.1505
JC513	383.79	0.02	0.0856 0.0855	0.0002	0.0856	0.2569 0.2566	0.0003	0.2568	0.1713 0.1711
JC514	382.30	0.02	0.1112 0.1171	0.0059	0.1142	0.3198 0.3180	0.0018	0.3189	0.2086 0.2009
JC515	381.52	0.02	0.1396 0.1395	0.0002	0.1395	0.3578 0.3557	0.0021	0.3567	0.2182 0.2162
JC516	379.45	0.02	0.1959 0.1958	0.0001	0.1958	0.4352 0.4427	0.0075	0.4390	0.2393 0.2470
JC521	377.93	0.02	0.2428 0.2437	0.0009	0.2432	0.5031 0.5050	0.0019	0.5040	0.2603 0.2613
JC522	377.75	0.02	0.2530 0.2533	0.0003	0.2531	0.5041 0.5140	0.0098	0.5091	0.2512 0.2607
JC523	375.65	0.02	0.3194 0.3207	0.0013	0.3201	0.5901 0.5870	0.0031	0.5885	0.2707 0.2662
JC524	375.72	0.02	0.3504 0.3547	0.0043	0.3525	0.5959 0.5914	0.0045	0.5936	0.2455 0.2367
JC526	372.98	0.02	0.4707 0.4678	0.0029	0.4693	0.6705 0.6827	0.0121	0.6766	0.1998 0.2148
JC531	368.37	0.02	0.9184 0.9235	0.0051	0.9209	0.9305 0.9361	0.0056	0.9333	0.0120 0.0126
JC532	368.88	0.02	0.8355 0.8454	0.0098	0.8404	0.8829 0.8842	0.0013	0.8836	0.0474 0.0389
JC533	369.90	0.02	0.6976 0.7009	0.0033	0.6992	0.7862 0.7859	0.0003	0.7861	0.0887 0.0851
JC534	370.77	0.02	0.6197 0.6312	0.0115	0.6255	0.7508 0.7430	0.0078	0.7469	0.1311 0.1118
JC535	371.58	0.02	0.5789 0.5598	0.0191	0.5693	0.7146 0.7264	0.0118	0.7205	0.1357 0.1666
JC536	372.28	0.02	0.5132 0.5126	0.0006	0.5129	0.7169 0.7106	0.0062	0.7137	0.2036 0.1980
JC543	375.95	0.02	0.3194 0.3145	0.0049	0.3170	0.5610 0.5667	0.0057	0.5638	0.2416 0.2521
JC544	376.81	0.02	0.2856 0.2849	0.0007	0.2853	0.5391 0.5524	0.0134	0.5458	0.2535 0.2676
JC545	377.66	0.02	0.2498 0.2513	0.0014	0.2505	0.5067 0.5036	0.0031	0.5051	0.2568 0.2524

	T	T_{dev}	$X_{n\text{-}Octane}$	ΔX	$X_{Oct,\ avg}$	$Y_{n\text{-}Octane}$	ΔY	$Y_{Oct,\ avg}$	$Y\text{-}X$
JC552	385.05	0.02	0.0590 0.0592	0.0002	0.0591	0.1912 0.1916	0.0004	0.1914	0.1323 0.1325
JC553	383.37	0.02	0.0828 0.0829	0.0001	0.0828	0.2560 0.2559	0.0001	0.2559	0.1732 0.1730
JC554	383.00	0.02	0.1022 0.1012	0.0010	0.1017	0.2766 0.2773	0.0007	0.2769	0.1744 0.1761
JC555	380.03	0.02	0.1797 0.1778	0.0019	0.1788	0.3985 0.3974	0.0011	0.3980	0.2188 0.2196
JC562	368.78	0.02	0.8326 0.8396	0.0070	0.8361	0.8767 0.8696	0.0071	0.8731	0.0440 0.0299
JC563	369.47	0.02	0.7586 0.7672	0.0085	0.7629	0.8415 0.8395	0.0020	0.8405	0.0829 0.0723
JC564	370.35	0.02	0.6654 0.6640	0.0014	0.6647	0.7912 0.7922	0.0010	0.7917	0.1258 0.1281
JC565	371.01	0.02	0.6158 0.6063	0.0095	0.6110	0.7622 0.7586	0.0036	0.7604	0.1464 0.1523
3-Hept	388.11	0.01	0.0000	-	0.0000	0.0000	-	0.0000	0.0000

n-Nonane/3-Heptanone

Table D. 6: Vapour – liquid equilibrium experimental results for n-nonane/3-heptanone at 40kPa

	T	T_{dev}	$X_{n\text{-}Nonane}$	ΔX	$X_{Non,\ avg}$	$Y_{n\text{-}Nonane}$	ΔY	$Y_{Non,\ avg}$	$Y\text{-}X$
n-Nonane	391.87	0.02	1.0000	-	1.0000	1.0000	-	1.0000	0.0000
JC611	387.48	0.02	0.0744 0.0749	0.0005	0.0746	0.1169 0.1153	0.0016	0.1161	0.0425 0.0404
JC612	387.25	0.02	0.1140 0.1138	0.0002	0.1139	0.1674 0.1687	0.0013	0.1680	0.0534 0.0549
JC613	386.82	0.02	0.1393 0.1393	0.0000	0.1393	0.1969 0.1970	0.0001	0.1969	0.0576 0.0577
JC614	386.59	0.02	0.1724 0.1730	0.0006	0.1727	0.2356 0.2343	0.0013	0.2349	0.0632 0.0613
JC615	386.33	0.02	0.2236 0.2236	0.0000	0.2236	0.2778 0.2796	0.0018	0.2787	0.0542 0.0560
JC621	386.10	0.02	0.2496 0.2470	0.0026	0.2483	0.3057 0.3054	0.0003	0.3055	0.0561 0.0584
JC622	385.79	0.02	0.3469 0.3475	0.0006	0.3472	0.3754 0.3751	0.0003	0.3752	0.0285 0.0276
JC623	385.72	0.02	0.4286 0.4256	0.0030	0.4271	0.4315 0.4316	0.0001	0.4316	0.0029 0.0061
JC624	385.87	0.02	0.4822 0.4855	0.0033	0.4838	0.4707 0.4701	0.0006	0.4704	-0.0115 -0.0154
JC625	386.02	0.02	0.5319 0.5333	0.0014	0.5326	0.5054 0.5044	0.0010	0.5049	-0.0265 -0.0289
JC626	386.25	0.02	0.5992 0.6013	0.0021	0.6003	0.5453 0.5419	0.0034	0.5436	-0.0539 -0.0594
JC631	390.66	0.02	0.9572 0.9571	0.0001	0.9571	0.9238 0.9242	0.0005	0.9240	-0.0334 -0.0328
JC632	389.71	0.02	0.9203 0.9194	0.0009	0.9199	0.8549 0.8574	0.0024	0.8561	-0.0654 -0.0621
JC633	389.09	0.02	0.8813 0.8850	0.0037	0.8831	0.8079 0.8030	0.0050	0.8054	-0.0733 -0.0820
JC634	388.55	0.02	0.8546 0.8564	0.0018	0.8555	0.7723 0.7664	0.0059	0.7694	-0.0823 -0.0900
JC635	387.93	0.02	0.8148 0.8095	0.0053	0.8122	0.7289 0.7237	0.0052	0.7263	-0.0859 -0.0858
JC636	387.54	0.02	0.7773 0.7748	0.0026	0.7760	0.6846 0.6830	0.0016	0.6838	-0.0927 -0.0918
JC641	386.29	0.02	0.6389 0.6469	0.0080	0.6429	0.5710 0.5693	0.0017	0.5701	-0.0679 -0.0776
JC642	386.15	0.02	0.5763 0.5759	0.0004	0.5761	0.5302 0.5282	0.0020	0.5292	-0.0461 -0.0477
JC643	385.88	0.02	0.5129 0.5098	0.0031	0.5113	0.4902 0.4891	0.0011	0.4896	-0.0227 -0.0207

	T	T_{dev}	$X_{n\text{-}Nonane}$	ΔX	$X_{Non,\ avg}$	$Y_{n\text{-}Nonane}$	ΔY	$Y_{Non,\ avg}$	$Y\text{-}X$
JC644	385.85	0.02	0.4605 0.4580	0.0025	0.4592	0.4534 0.4557	0.0022	0.4546	-0.0071 -0.0023
JC651	387.72	0.02	0.0492 0.0491	0.0001	0.0491	0.0908 0.0897	0.0011	0.0902	0.0416 0.0406
JC652	387.29	0.02	0.1009 0.1012	0.0003	0.1011	0.1512 0.1503	0.0009	0.1508	0.0503 0.0491
JC653	386.57	0.02	0.1661 0.1638	0.0023	0.1650	0.2237 0.2244	0.0007	0.2240	0.0576 0.0605
JC654	386.43	0.02	0.1885 0.1885	0.0001	0.1885	0.2481 0.2512	0.0031	0.2496	0.0595 0.0627
JC655	386.20	0.02	0.2198 0.2196	0.0002	0.2197	0.2787 0.2783	0.0004	0.2785	0.0589 0.0587
JC656	386.07	0.02	0.2875 0.2848	0.0027	0.2861	0.3301 0.3287	0.0014	0.3294	0.0426 0.0439
JC661	390.37	0.02	0.9412 0.9404	0.0009	0.9408	0.8910 0.8879	0.0031	0.8895	-0.0502 -0.0525
JC662	389.11	0.02	0.8887 0.8897	0.0010	0.8892	0.8108 0.8126	0.0017	0.8117	-0.0778 -0.0771
JC663	388.49	0.02	0.8511 0.8517	0.0006	0.8514	0.7679 0.7672	0.0007	0.7675	-0.0832 -0.0845
JC664	387.76	0.02	0.8046 0.8040	0.0006	0.8043	0.7103 0.7100	0.0003	0.7102	-0.0943 -0.0940
JC665	387.13	0.02	0.7442 0.7466	0.0024	0.7454	0.6551 0.6556	0.0005	0.6553	-0.0891 -0.0910
3-Hept	388.36	0.01	0.0000	-	0.0000	0.0000	-	0.0000	0.0000

n-Decane/3-Heptanone

Table D. 7: Vapour – liquid equilibrium experimental results for n-decane/3-heptanone at 40kPa

	T	T_{dev}	$X_{n\text{-}Decane}$	ΔX	$X_{Dec,\ avg}$	$Y_{n\text{-}Decane}$	ΔY	$Y_{Dec,\ avg}$	$Y\text{-}X$
n-Decane	413.88	0.02	1.0000	-	1.0000	1.0000	-	1.0000	0.0000
JC711	388.77	0.02	0.0581 0.0575	0.0007	0.0578	0.0433 0.0431	0.0002	0.0432	-0.0149 -0.0144
JC712	389.40	0.02	0.1215 0.1201	0.0014	0.1208	0.0765 0.0795	0.0031	0.0780	-0.0451 -0.0406
JC713	389.80	0.02	0.1661 0.1673	0.0013	0.1667	0.1111 0.1076	0.0035	0.1093	-0.0550 -0.0597
JC714	390.38	0.02	0.2079 0.2079	0.0001	0.2079	0.1346 0.1337	0.0009	0.1342	-0.0733 -0.0741
JC715	390.93	0.02	0.2538 0.2522	0.0016	0.2530	0.1533 0.1523	0.0011	0.1528	-0.1005 -0.1000
JC721	391.60	0.02	0.3178 0.3175	0.0004	0.3177	0.1782 0.1766	0.0016	0.1774	-0.1397 -0.1408
JC722	392.69	0.02	0.3861 0.3841	0.0020	0.3851	0.2057 0.2068	0.0011	0.2063	-0.1803 -0.1773
JC723	393.48	0.02	0.4478 0.4468	0.0010	0.4473	0.2326 0.2342	0.0016	0.2334	-0.2152 -0.2126
JC724	394.90	0.02	0.5261 0.5260	0.0001	0.5261	0.2747 0.2738	0.0009	0.2743	-0.2514 -0.2521
JC725	396.68	0.02	0.6051 0.6056	0.0005	0.6053	0.3355 0.3337	0.0018	0.3346	-0.2696 -0.2719
JC731	407.06	0.02	0.8967 0.8973	0.0006	0.8970	0.6896 0.6885	0.0011	0.6890	-0.2072 -0.2088
JC732	404.40	0.02	0.8399 0.8396	0.0003	0.8398	0.5736 0.5733	0.0003	0.5734	-0.2663 -0.2663
JC733	402.87	0.02	0.8021 0.8015	0.0006	0.8018	0.5221 0.5211	0.0010	0.5216	-0.2800 -0.2804
JC734	402.20	0.02	0.7848 0.7847	0.0001	0.7848	0.4953 0.4924	0.0029	0.4938	-0.2895 -0.2923
JC735	401.36	0.02	0.7614 0.7629	0.0015	0.7622	0.4262 0.4698	0.0436	0.4480	-0.3353 -0.2931
JC742	399.83	0.02	0.7152 0.7226	0.0074	0.7189	0.4301 0.4282	0.0020	0.4292	-0.2851 -0.2944
JC743	398.57	0.02	0.6776 0.6792	0.0017	0.6784	0.4033 0.4083	0.0050	0.4058	-0.2743 -0.2709
JC744	397.29	0.02	0.6299 0.6312	0.0013	0.6305	0.3591 0.3587	0.0004	0.3589	-0.2708 -0.2724
JC745	396.53	0.02	0.6067 0.6050	0.0017	0.6059	0.3283 0.3316	0.0033	0.3299	-0.2784 -0.2734
JC746	396.26	0.02	0.5919 0.5953	0.0034	0.5936	0.3347 0.3344	0.0003	0.3345	-0.2572 -0.2609

	T	T_{dev}	$X_{n\text{-}Decane}$	ΔX	$X_{Dec,\ avg}$	$Y_{n\text{-}Decane}$	ΔY	$Y_{Dec,\ avg}$	$Y\text{-}X$
JC761	388.93	0.02	0.0224 0.0275	0.0051	0.0250	0.0297 0.0272	0.0025	0.0284	0.0073 -0.0003
JC762	389.05	0.02	0.0692 0.0682	0.0010	0.0687	0.0525 0.0515	0.0011	0.0520	-0.0166 -0.0167
JC763	389.54	0.02	0.1359 0.1366	0.0007	0.1362	0.0928 0.0924	0.0004	0.0926	-0.0430 -0.0442
JC764	390.57	0.02	0.2244 0.2239	0.0005	0.2242	0.1406 0.1403	0.0003	0.1404	-0.0838 -0.0836
JC765	391.15	0.02	0.2689 0.2701	0.0012	0.2695	0.1708 0.1718	0.0011	0.1713	-0.0981 -0.0983
JC782	402.59	0.02	0.7916 0.7918	0.0002	0.7917	0.5166 0.5162	0.0004	0.5164	-0.2751 -0.2757
JC783	398.14	0.02	0.6784 0.6772	0.0013	0.6778	0.3889 0.3877	0.0012	0.3883	-0.2895 -0.2895
JC784	397.83	0.02	0.6523 0.6514	0.0010	0.6519	0.3837 0.3859	0.0022	0.3848	-0.2687 -0.2654
JC785	396.15	0.02	0.5901 0.5900	0.0001	0.5901	0.3388 0.3379	0.0009	0.3384	-0.2513 -0.2521
JC791	413.40	0.02	0.9886 0.9886	0.0000	0.9886	0.9589 0.9582	0.0007	0.9585	-0.0297 -0.0304
JC792	410.11	0.02	0.9403 0.9434	0.0031	0.9418	0.8072 0.8051	0.0021	0.8062	-0.1330 -0.1383
JC793	408.41	0.02	0.9090 0.9126	0.0036	0.9108	0.7406 0.7371	0.0035	0.7389	-0.1684 -0.1754
JC794	406.83	0.02	0.8844 0.8847	0.0003	0.8845	0.6616 0.6573	0.0043	0.6595	-0.2227 -0.2274
JC795	404.85	0.02	0.8415 0.8464	0.0049	0.8439	0.5944 0.5944	0.0000	0.5944	-0.2471 -0.2520
JC796	403.22	0.02	0.8086 0.8100	0.0014	0.8093	0.5140 0.5047	0.0092	0.5094	-0.2946 -0.3053
JC797	400.88	0.02	0.7516 0.7548	0.0033	0.7532	0.4546 0.4562	0.0016	0.4554	-0.2969 -0.2986
3-Hept	388.67	0.01	0.0000	-	0.0000	0.0000	-	0.0000	0.0000

n-Octane/4-Heptanone

Table D. 8: Vapour – liquid equilibrium experimental results for n-octane/4-heptanone at 40kPa

	T	T_{dev}	$X_{n\text{-}Octane}$	ΔX	$X_{Oct,\ avg}$	$Y_{n\text{-}Octane}$	ΔY	$Y_{Oct,\ avg}$	$Y\text{-}X$
n-Octane	368.3	0.02	1.0000	-	1.0000	1.0000	-	1.0000	0.0000
JC811	382.88	0.02	0.0416 0.0418	0.0001	0.0417	0.1230 0.1226	0.0004	0.1228	0.0814 0.0809
JC812	382.13	0.02	0.0672 0.0671	0.0001	0.0671	0.1866 0.1871	0.0005	0.1868	0.1193 0.1200
JC813	380.05	0.02	0.1121 0.1120	0.0001	0.1120	0.2785 0.2755	0.0030	0.2770	0.1664 0.1635
JC814	378.22	0.02	0.1649 0.1640	0.0010	0.1645	0.3550 0.3524	0.0025	0.3537	0.1900 0.1884
JC821	376.94	0.02	0.2061 0.2041	0.0019	0.2051	0.4141 0.4140	0.0001	0.4140	0.2080 0.2098
JC822	376.43	0.02	0.2202 0.2228	0.0026	0.2215	0.4426 0.4498	0.0072	0.4462	0.2224 0.2269
JC823	374.95	0.02	0.2879 0.2874	0.0005	0.2877	0.5022 0.4947	0.0075	0.4984	0.2143 0.2072
JC824	374.30	0.02	0.3166 0.3165	0.0001	0.3165	0.5321 0.5294	0.0027	0.5308	0.2155 0.2129
JC825	373.06	0.02	0.3838 0.3824	0.0014	0.3831	0.5852 0.5826	0.0026	0.5839	0.2014 0.2002
JC826	372.55	0.02	0.4200 0.4158	0.0042	0.4179	0.6091 0.6095	0.0005	0.6093	0.1891 0.1937
JC827	371.25	0.02	0.5056 0.5043	0.0013	0.5050	0.6712 0.6697	0.0015	0.6705	0.1656 0.1654
JC831	368.26	0.02	0.9728 0.9723	0.0005	0.9726	0.9727 0.9723	0.0004	0.9725	-0.0001 0.0000
JC832	368.30	0.02	0.9458 0.9455	0.0003	0.9457	0.9483 0.9482	0.0001	0.9483	0.0025 0.0027
JC833	368.37	0.02	0.9080 0.9074	0.0006	0.9077	0.9195 0.9224	0.0028	0.9210	0.0115 0.0150
JC834	368.77	0.02	0.8206 0.8231	0.0026	0.8219	0.8531 0.8553	0.0022	0.8542	0.0325 0.0322
JC835	369.49	0.02	0.6970 0.6978	0.0009	0.6974	0.7836 0.7901	0.0065	0.7869	0.0867 0.0923
JC836	370.00	0.02	0.6415 0.6415	0.0000	0.6415	0.7527 0.7533	0.0006	0.7530	0.1112 0.1118
JC841	370.72	0.02	0.5655 0.5672	0.0017	0.5664	0.7062 0.7076	0.0014	0.7069	0.1407 0.1404
JC843	371.92	0.02	0.4689 0.4717	0.0028	0.4703	0.6477 0.6495	0.0018	0.6486	0.1788 0.1778
JC844	372.56	0.02	0.4221 0.4234	0.0012	0.4227	0.6253 0.6226	0.0026	0.6240	0.2031 0.1993

	T	T_{dev}	$X_{n\text{-}Octane}$	ΔX	$X_{Oct,\ avg}$	$Y_{n\text{-}Octane}$	ΔY	$Y_{Oct,\ avg}$	$Y\text{-}X$
JC845	373.19	0.02	0.3788 0.3804	0.0017	0.3796	0.5885 0.5877	0.0008	0.5881	0.2098 0.2073
JC846	373.75	0.02	0.3492 0.3454	0.0038	0.3473	0.5777 0.5738	0.0039	0.5757	0.2285 0.2284
JC847	375.15	0.02	0.2868 0.2822	0.0046	0.2845	0.5200 0.5182	0.0017	0.5191	0.2332 0.2361
JC852	382.96	0.02	0.0463 0.0467	0.0003	0.0465	0.1394 0.1395	0.0001	0.1395	0.0931 0.0928
JC853	381.51	0.02	0.0779 0.0780	0.0001	0.0779	0.2058 0.2065	0.0007	0.2062	0.1279 0.1285
JC854	380.61	0.02	0.1023 0.1026	0.0003	0.1025	0.2532 0.2535	0.0004	0.2533	0.1508 0.1509
JC855	379.57	0.02	0.1303 0.1303	0.0000	0.1303	0.3011 0.3001	0.0010	0.3006	0.1708 0.1698
JC856	378.81	0.02	0.1573 0.1538	0.0036	0.1555	0.3451 0.3413	0.0038	0.3432	0.1878 0.1876
JC861	377.50	0.02	0.1978 0.1967	0.0011	0.1972	0.4025 0.3995	0.0030	0.4010	0.2047 0.2028
JC862	377.45	0.02	0.1905 0.1987	0.0081	0.1946	0.3984 0.3938	0.0047	0.3961	0.2079 0.1951
JC863	376.75	0.02	0.2245 0.2236	0.0009	0.2241	0.4399 0.4412	0.0013	0.4405	0.2153 0.2175
JC864	375.74	0.02	0.2666 0.2663	0.0003	0.2665	0.4779 0.4778	0.0001	0.4778	0.2113 0.2114
JC865	374.48	0.02	0.3170 0.3168	0.0002	0.3169	0.5108 0.5264	0.0156	0.5186	0.1938 0.2096
JC866	374.77	0.02	0.3121 0.3117	0.0004	0.3119	0.5252 0.5265	0.0012	0.5259	0.2132 0.2148
JC871	368.34	0.02	0.9806 0.9799	0.0007	0.9802	0.9819 0.9818	0.0001	0.9819	0.0013 0.0019
JC872	368.31	0.02	0.9877 0.9872	0.0005	0.9875	0.9870 0.9872	0.0002	0.9871	-0.0007 -0.0001
JC873	368.48	0.02	0.8819 0.8807	0.0012	0.8813	0.9036 0.9034	0.0001	0.9035	0.0217 0.0227
JC874	368.81	0.02	0.8102 0.8078	0.0024	0.8090	0.8460 0.8537	0.0077	0.8498	0.0358 0.0458
JC875	369.23	0.02	0.7280 0.7350	0.0070	0.7315	0.8109 0.8062	0.0048	0.8086	0.0829 0.0712
JC876	369.87	0.02	0.6577 0.6657	0.0080	0.6617	0.7570 0.7625	0.0055	0.7597	0.0992 0.0967
4-Hept	385.5	0.01	0.0000	-	0.0000	0.0000	-	0.0000	0.0000

n-Nonane/4-Heptanone

Table D. 9: Vapour – liquid equilibrium experimental results for n-nonane/4-heptanone at 40kPa

	T	T_{dev}	$X_{n\text{-}Nonane}$	ΔX	$X_{Non,\ avg}$	$Y_{n\text{-}Nonane}$	ΔY	$Y_{Non,\ avg}$	$Y\text{-}X$
n-Nonane	391.9	0.02	1.0000	-	1.0000	1.0000	-	1.0000	0.0000
JC911	385.08	0.02	0.0568 0.0576	0.0008	0.0572	0.0808 0.0793	0.0015	0.0800	0.0240 0.0217
JC912	384.77	0.02	0.0953 0.0936	0.0016	0.0945	0.1229 0.1239	0.0010	0.1234	0.0276 0.0303
JC913	384.54	0.02	0.1142 0.1128	0.0014	0.1135	0.1434 0.1487	0.0053	0.1460	0.0292 0.0359
JC914	384.42	0.02	0.1411 0.1403	0.0007	0.1407	0.1732 0.1752	0.0020	0.1742	0.0321 0.0349
JC915	384.15	0.02	0.1656 0.1646	0.0010	0.1651	0.1981 0.1994	0.0012	0.1987	0.0325 0.0348
JC916	384.00	0.02	0.2064 0.2047	0.0017	0.2055	0.2307 0.2334	0.0027	0.2320	0.0243 0.0287
JC921	383.79	0.02	0.2347 0.2339	0.0009	0.2343	0.2618 0.2676	0.0057	0.2647	0.0271 0.0337
JC922	383.85	0.02	0.2643 0.2639	0.0004	0.2641	0.2845 0.2848	0.0003	0.2847	0.0202 0.0209
JC923	383.77	0.02	0.3105 0.3092	0.0013	0.3099	0.3153 0.3193	0.0040	0.3173	0.0048 0.0100
JC924	383.82	0.02	0.3550 0.3550	0.0000	0.3550	0.3489 0.3481	0.0008	0.3485	-0.0061 -0.0069
JC925	383.93	0.02	0.4025 0.4064	0.0039	0.4045	0.3810 0.3803	0.0007	0.3807	-0.0215 -0.0261
JC926	383.97	0.02	0.4399 0.4414	0.0015	0.4407	0.4076 0.4095	0.0019	0.4085	-0.0323 -0.0320
JC927	384.26	0.02	0.5043 0.4979	0.0065	0.5011	0.4403 0.4417	0.0013	0.4410	-0.0640 -0.0562
JC931	390.31	0.02	0.9508 0.9506	0.0002	0.9507	0.8872 0.8975	0.0103	0.8923	-0.0636 -0.0531
JC932	389.71	0.02	0.9260 0.9282	0.0022	0.9271	0.8640 0.8641	0.0001	0.8640	-0.0620 -0.0641
JC933	388.63	0.02	0.8795 0.8847	0.0052	0.8821	0.7829 0.7795	0.0034	0.7812	-0.0966 -0.1051
JC934	387.61	0.02	0.8329 0.8389	0.0060	0.8359	0.7203 0.7229	0.0026	0.7216	-0.1127 -0.1161
JC935	387.14	0.02	0.7978 0.8024	0.0045	0.8001	0.6926 0.6943	0.0016	0.6935	-0.1052 -0.1081
JC936	386.59	0.02	0.7669 0.7618	0.0051	0.7644	0.6473 0.6459	0.0014	0.6466	-0.1196 -0.1159
JC941	385.92	0.02	0.7042 0.7152	0.0110	0.7097	0.5949 0.5936	0.0014	0.5942	-0.1092 -0.1216

	T	T_{dev}	$X_{n\text{-}Nonane}$	ΔX	$X_{Non,\ avg}$	$Y_{n\text{-}Nonane}$	ΔY	$Y_{Non,\ avg}$	$Y\text{-}X$
JC942	385.26	0.02	0.6476 0.6482	0.0007	0.6479	0.5465 0.5402	0.0063	0.5434	-0.1010 -0.1080
JC943	384.91	0.02	0.6022 0.6058	0.0036	0.6040	0.5172 0.5218	0.0046	0.5195	-0.0850 -0.0840
JC944	384.60	0.02	0.5682 0.5724	0.0042	0.5703	0.4984 0.4985	0.0001	0.4984	-0.0698 -0.0739
JC945	384.45	0.02	0.5369 0.5368	0.0002	0.5369	0.4727 0.4726	0.0001	0.4726	-0.0642 -0.0642
JC961	390.84	0.02	0.9587 0.9598	0.0011	0.9593	0.8937 0.8996	0.0059	0.8966	-0.0650 -0.0602
JC962	389.03	0.02	0.9013 0.9066	0.0052	0.9040	0.8148 0.8149	0.0000	0.8149	-0.0865 -0.0917
JC963	387.60	0.02	0.8310 0.8342	0.0032	0.8326	0.7241 0.7208	0.0033	0.7225	-0.1069 -0.1134
JC964	386.37	0.02	0.7611 0.7621	0.0010	0.7616	0.6492 0.6476	0.0017	0.6484	-0.1119 -0.1145
JC965	385.63	0.02	0.6938 0.6980	0.0042	0.6959	0.5842 0.5815	0.0027	0.5828	-0.1096 -0.1166
JC966	385.01	0.02	0.6285 0.6302	0.0018	0.6294	0.5332 0.5276	0.0055	0.5304	-0.0953 -0.1026
JC967	384.52	0.02	0.5533 0.5544	0.0011	0.5538	0.4877 0.4853	0.0024	0.4865	-0.0655 -0.0691
JC971	385.28	0.02	0.0381 0.0380	0.0000	0.0380	0.0530 0.0525	0.0005	0.0528	0.0149 0.0145
JC972	384.91	0.02	0.0785 0.0801	0.0016	0.0793	0.1021 0.1045	0.0024	0.1033	0.0235 0.0244
JC973	384.35	0.02	0.1292 0.1296	0.0003	0.1294	0.1617 0.1630	0.0012	0.1624	0.0325 0.0334
JC974	384.05	0.02	0.1763 0.1752	0.0011	0.1757	0.2071 0.2093	0.0022	0.2082	0.0308 0.0341
JC975	383.88	0.02	0.2261 0.2280	0.0019	0.2270	0.2511 0.2521	0.0010	0.2516	0.0251 0.0241
JC977	383.83	0.02	0.3179 0.3211	0.0032	0.3195	0.3238 0.3265	0.0027	0.3251	0.0059 0.0054
4-Hept	385.47	0.01	0.0000	-	0.0000	0.0000	-	0.0000	0.0000

n-Decane/4-Heptanone

Table D. 10: Vapour – liquid equilibrium experimental results for n-decane/4-heptanone at 40kPa

	T	T_{dev}	$X_{n\text{-}Decane}$	ΔX	$X_{Dec,\ avg}$	$Y_{n\text{-}Decane}$	ΔY	$Y_{Dec,\ avg}$	$Y\text{-}X$
n-Decane	413.88	0.02	1.0000	-	1.0000	1.0000	-	1.0000	0.0000
JC011	386.02	0.02	0.0519 0.0545	0.0027	0.0532	0.0419 0.0404	0.0014	0.0411	-0.0100 -0.0141
JC012	386.59	0.02	0.1051 0.1065	0.0014	0.1058	0.0710 0.0689	0.0022	0.0700	-0.0340 -0.0376
JC013	387.31	0.02	0.1710 0.1704	0.0005	0.1707	0.1031 0.1030	0.0001	0.1030	-0.0679 -0.0674
JC014	388.00	0.02	0.2278 0.2309	0.0030	0.2293	0.1221 0.1243	0.0022	0.1232	-0.1057 -0.1065
JC015	388.75	0.02	0.2927 0.2928	0.0001	0.2927	0.1669 0.1646	0.0023	0.1658	-0.1258 -0.1282
JC016	389.70	0.02	0.3498 0.3501	0.0003	0.3499	0.1817 0.1829	0.0011	0.1823	-0.1681 -0.1672
JC021	390.23	0.02	0.3927 0.3904	0.0024	0.3916	0.1966 0.1951	0.0015	0.1958	-0.1962 -0.1953
JC022	391.61	0.02	0.4566 0.4643	0.0078	0.4605	0.2365 0.2321	0.0044	0.2343	-0.2200 -0.2322
JC023	392.23	0.02	0.4980 0.5050	0.0070	0.5015	0.2560 0.2515	0.0045	0.2537	-0.2421 -0.2535
JC024	393.30	0.02	0.5480 0.5558	0.0078	0.5519	0.2834 0.2837	0.0002	0.2836	-0.2646 -0.2721
JC025	394.35	0.02	0.5919 0.5958	0.0039	0.5939	0.2917 0.2909	0.0008	0.2913	-0.3003 -0.3050
JC026	395.65	0.02	0.6402 0.6510	0.0108	0.6456	0.3276 0.3223	0.0053	0.3250	-0.3126 -0.3287
JC031	410.74	0.02	0.9567 0.9597	0.0031	0.9582	0.8191 0.8337	0.0146	0.8264	-0.1376 -0.1260
JC032	408.73	0.02	0.9251 0.9306	0.0055	0.9278	0.7607 0.7569	0.0039	0.7588	-0.1644 -0.1737
JC033	407.10	0.02	0.9011 0.9065	0.0054	0.9038	0.6973 0.6888	0.0085	0.6931	-0.2037 -0.2177
JC035	403.94	0.02	0.8437 0.8481	0.0044	0.8459	0.5962 0.5945	0.0017	0.5953	-0.2475 -0.2536
JC036	400.83	0.02	0.7902 0.7969	0.0067	0.7935	0.4543 0.4433	0.0110	0.4488	-0.3359 -0.3536
JC042	399.62	0.02	0.7594 0.7584	0.0010	0.7589	0.4466 0.4453	0.0013	0.4459	-0.3129 -0.3132
JC043	399.83	0.02	0.7545 0.7605	0.0060	0.7575	0.4688 0.4625	0.0063	0.4656	-0.2857 -0.2980
JC045	397.77	0.02	0.7014 0.7075	0.0061	0.7045	0.4059 0.4045	0.0014	0.4052	-0.2955 -0.3030

	T	T_{dev}	$X_{n\text{-}Decane}$	ΔX	$X_{Dec,\ avg}$	$Y_{n\text{-}Decane}$	ΔY	$Y_{Dec,\ avg}$	$Y\text{-}X$
JC046	393.59	0.02	0.5619 0.5675	0.0055	0.5647	0.3020 0.2985	0.0035	0.3003	-0.2599 -0.2689
JC051	385.45	0.02	0.0214 0.0201	0.0013	0.0208	0.0258 0.0153	0.0105	0.0205	0.0043 -0.0048
JC052	386.00	0.02	0.0429 0.0431	0.0003	0.0430	0.0315 0.0340	0.0025	0.0328	-0.0114 -0.0091
JC053	386.75	0.02	0.0957 0.0973	0.0016	0.0965	0.0652 0.0636	0.0015	0.0644	-0.0305 -0.0336
JC054	387.47	0.02	0.1697 0.1703	0.0005	0.1700	0.1026 0.1036	0.0010	0.1031	-0.0671 -0.0667
JC055	388.48	0.02	0.2610 0.2631	0.0021	0.2620	0.1438 0.1413	0.0025	0.1426	-0.1172 -0.1218
JC056	389.54	0.02	0.3199 0.3243	0.0044	0.3221	0.1830 0.1803	0.0027	0.1817	-0.1369 -0.1440
JC061	412.89	0.02	0.9897 0.9907	0.0011	0.9902	0.9326 0.9481	0.0156	0.9403	-0.0571 -0.0426
JC062	410.24	0.02	0.9539 0.9503	0.0037	0.9521	0.8140 0.8113	0.0027	0.8126	-0.1400 -0.1390
JC063	407.65	0.02	0.9167 0.9167	0.0000	0.9167	0.7135 0.7117	0.0018	0.7126	-0.2033 -0.2051
JC064	405.50	0.02	0.8726 0.8801	0.0075	0.8763	0.6488 0.6384	0.0105	0.6436	-0.2238 -0.2417
JC065	403.84	0.02	0.8440 0.8495	0.0055	0.8468	0.5802 0.5743	0.0060	0.5773	-0.2638 -0.2753
JC067	398.18	0.02	0.7131 0.7213	0.0082	0.7172	0.4175 0.4112	0.0064	0.4144	-0.2956 -0.3101
4-Hept	385.87	0.01	0.0000	-	0.0000	0.0000	-	0.0000	0.0000

Appendix E Thermodynamic Consistency Testing Results

The L/W Consistency Test was performed using *PRO-VLE 2.0* software, making use of the following component specific properties:

Table E. 1: Component parameters used for thermodynamic consistency testing

	2-Heptanone	3-Heptanone	4-Heptanone	n-Octane	n-Nonane	n-Decane	Ethanol	1-Butanol
Antoine A*	6.334	7.019	6.271	6.942	6.562	6.507	7.557	7.329
Antoine B*	-1058.64	-1434.23	-1000.95	-1365.37	-1190.41	-1222.35	-1261.78	-1289.03
Antoine C*	154875	199.498	150.844	210.525	172.783	162.396	191.460	172.217
T_C (K)	611.4	606.6	599.8[a]	568.7	594.6	617.7	514.0	563.1
P_C (atm)	29.016	28.818	28.859[a]	24.574	22.601	20.824	60.567	43.563
V_C ($cm^3.mol^{-1}$)	434	433	430[a]	486	551	617	168	273
T_b (K)	392.75	389.45	386.11	368.44	391.80	414.07	351.52	390.76
ω	0.419	0.4076	0.4248[a]	0.3996	0.4435	0.4923	0.6436	0.5883
V^L ($cm^3.mol^{-1}$)	±155[c]	±155[c]	±155[c]	±180[c]	±200[c]	±220[c]	64.691	100.565
ΔH_V ($cal.mol^{-1}$)	9750	9819	9319[a]	8827	9534	10162	9304	10310
μ (Debye)	2.611[b]	2.809[b]	2.68[c]	0	0	0	1.69	1.66

**Antoine Equation as $\log_{10}P(mmHg) = A-(B/(T(°C) + C))$*
All values taken from Perry's Chemical Engineering Handbook unless otherwise stated
[a] Correlations based on group contribution methods - Perry's Chemical Engineering Handbook
[b] DIPPR Database
[c] Values dependent on max and min T in binary mixture of interest, indicated values are approximate averages

Values for the activity coefficient were generated for each component at each data point within the *PRO-VLE 2.0* software. These values, along with the observable temperature deviations (0.02 °C) and the maximum absolute deviation in reported concentration (0.02 mole fraction) were used to determine D and D_{max} for the McDermott-Ellis Consistency Test. Tables E.1 to E.10 detail the thermodynamic consistency testing results for all experimental data reported here.

Verification: Ethanol/1-Butanol

Table E. 2: Thermodynamic consistency testing results for verification system: ethanol/1-butanol at 1.013bar

			L/W Consistency Test				*McDermott-Ellis Consistency Test*			
T (K)	$X_{ethanol}$	$Y_{ethanol}$	L_i	W_i	L_i/W_i	*D*	$\gamma_{ethanol}$	$\gamma_{t\text{-}butanol}$	*Dev*	Dev_{max}
351.14	1.000	1.000								
354.08	0.835	0.972	3.898	4.147	0.940	3.095	1.056	0.716	0.027	0.723
358.01	0.688	0.935	5.727	6.099	0.939	3.146	1.065	0.738	0.029	0.591
358.73	0.666	0.924	5.87	6.251	0.939	3.143	1.059	0.781	-0.029	0.584
359.00	0.651	0.925	6.188	6.582	0.940	3.085	1.074	0.729	0.039	0.576
359.55	0.637	0.914	6.186	6.583	0.940	3.109	1.063	0.784	-0.020	0.558
360.56	0.600	0.906	6.627	7.04	0.941	3.022	1.079	0.745	0.013	0.545
363.59	0.500	0.870	7.52	7.951	0.946	2.786	1.116	0.725	0.103	0.497
364.78	0.477	0.837	7.233	7.648	0.946	2.789	1.08	0.827	0.093	0.447
367.99	0.382	0.766	7.752	8.145	0.952	2.472	1.106	0.881	0.131	0.412
381.54	0.133	0.378	3.987	4.127	0.966	1.725	1.014	0.992	0.006	0.303
382.25	0.112	0.351	4.103	4.225	0.971	1.465	1.094	0.985	-0.122	0.352
373.93	0.251	0.631	6.958	7.249	0.960	2.048	1.139	0.906	0.000	0.355
374.59	0.248	0.616	6.416	6.692	0.959	2.106	1.101	0.916	-0.085	0.387
369.32	0.355	0.749	7.482	7.855	0.953	2.432	1.112	0.858	0.049	0.398
370.52	0.330	0.714	7.264	7.616	0.954	2.366	1.096	0.897	-0.250	0.991
354.31	0.850	0.974	3.081	3.298	0.934	3.402	1.03	0.723	0.027	0.678
354.58	0.836	0.969	3.359	3.594	0.935	3.380	1.032	0.779	0.026	0.660
357.28	0.729	0.940	4.85	5.184	0.936	3.329	1.038	0.809	0.054	0.570
357.48	0.717	0.930	5.121	5.466	0.937	3.259	1.036	0.896	-0.021	0.556
359.89	0.619	0.905	6.552	6.961	0.941	3.027	1.07	0.814	0.088	0.520
359.90	0.631	0.890	6.072	6.464	0.939	3.127	1.032	0.972	-0.093	0.504
360.89	0.607	0.893	6.023	6.417	0.939	3.167	1.039	0.851	0.047	0.501
361.31	0.592	0.879	6.191	6.59	0.939	3.122	1.033	0.91	-0.039	0.486
363.70	0.515	0.852	6.822	7.234	0.943	2.931	1.057	0.847	0.060	0.464
364.11	0.499	0.834	7.039	7.454	0.944	2.863	1.053	0.904	-0.012	0.451
364.95	0.468	0.823	7.416	7.834	0.947	2.741	1.076	0.876	0.041	0.439
366.00	0.439	0.797	7.504	7.914	0.948	2.659	1.071	0.913		
390.49	0.000	0.000								

n-Octane/2-Heptanone

Table E. 3: Thermodynamic consistency testing results for n-octane/2-heptanone system at 40kPa

			L/W Consistency Test				*McDermott-Ellis Consistency Test*			
T (K)	X_{octane}	Y_{octane}	L_i	W_i	L_i/W_i	*D*	γ_{octane}	$\gamma_{2\text{-}hept}$	*Dev*	Dev_{max}
368.32	1.000	1.000								
388.75	0.038	0.178	3.107	3.088	1.006	0.307	2.533	0.970	-0.030	0.222
386.66	0.063	0.262	4.609	4.599	1.002	0.109	2.386	0.958	-0.062	0.244
382.61	0.131	0.412	7.053	7.091	0.995	0.269	2.029	0.942	-0.045	0.240
382.05	0.146	0.447	7.257	7.307	0.993	0.343	2.008	0.919	-0.012	0.252
379.79	0.201	0.514	8.211	8.3	0.989	0.539	1.794	0.934	0.168	0.310
388.62	0.037	0.171	3.261	3.241	1.006	0.308	2.509	0.982	-0.031	0.218
386.79	0.056	0.247	4.644	4.631	1.003	0.140	2.521	0.966	-0.008	0.223
385.83	0.071	0.281	5.250	5.246	1.001	0.038	2.326	0.967	-0.051	0.234
383.43	0.112	0.378	6.682	6.707	0.996	0.187	2.126	0.949	-0.007	0.235
382.32	0.128	0.413	7.414	7.454	0.995	0.269	2.100	0.947	-0.079	1.906
368.47	0.983	0.984	0.398	0.408	0.975	1.241	1.000	2.189	-0.002	0.259
368.50	0.975	0.974	0.569	0.584	0.974	1.301	0.997	2.416	-0.011	0.298
368.73	0.923	0.934	1.644	1.692	0.972	1.439	1.002	1.973	0.000	0.319
369.70	0.769	0.852	4.511	4.637	0.973	1.377	1.064	1.420	0.032	0.285
370.52	0.663	0.791	6.307	6.472	0.975	1.291	1.116	1.332	-0.003	0.290
372.27	0.520	0.727	8.055	8.245	0.977	1.166	1.237	1.144	-0.013	0.287
374.02	0.406	0.681	9.068	9.253	0.980	1.010	1.404	1.013	-0.008	0.279
374.75	0.365	0.665	9.326	9.504	0.981	0.945	1.491	0.969	0.000	0.278
376.17	0.301	0.630	9.443	9.6	0.984	0.824	1.639	0.924	-0.035	0.275
377.40	0.258	0.613	9.242	9.379	0.985	0.736	1.792	0.871	0.059	0.266
379.92	0.192	0.532	8.295	8.384	0.989	0.534	1.936	0.885	0.053	0.252
381.05	0.166	0.483	7.783	7.85	0.991	0.429	1.966	0.911	-0.227	0.450
368.97	0.795	0.887	4.596	4.715	0.975	1.278	1.097	1.256	0.045	0.304
369.97	0.680	0.830	6.438	6.605	0.975	1.280	1.162	1.165	0.014	0.299
371.42	0.571	0.781	7.661	7.851	0.976	1.225	1.243	1.060	0.037	0.304
374.89	0.369	0.679	9.09	9.267	0.981	0.964	1.499	0.930	0.007	0.284
376.79	0.284	0.632	9.23	9.378	0.984	0.795	1.710	0.877	0.006	1.502
368.31	0.982	0.983	0.583	0.593	0.983	0.850	1.005	2.210	0.004	0.256
368.27	0.980	0.982	0.673	0.685	0.982	0.884	1.008	2.109	-0.003	0.256
368.31	0.978	0.979	0.684	0.696	0.983	0.870	1.005	2.234	0.004	0.272
368.29	0.960	0.967	1.156	1.18	0.980	1.027	1.012	1.932	0.001	0.276
368.42	0.925	0.925	1.904	1.95	0.976	1.194	1.001	2.329		
392.54	0.000	0.000								

n-Nonane/2-Heptanone

Table E. 4: Thermodynamic consistency testing results for n-nonane/2-heptanone system at 40kPa

			L/W Consistency Test				*McDermott-Ellis Consistency Test*			
T (K)	X_{nonane}	Y_{nonane}	L_i	W_i	L_i/W_i	*D*	γ_{nonane}	$\gamma_{2\text{-hept}}$	*Dev*	Dev_{max}
391.78	1.000	1.000								
390.62	0.055	0.110	2.079	2.057	1.011	0.532	2.082	1.007	-0.009	0.231
389.72	0.090	0.169	2.946	2.924	1.008	0.375	2.011	1.005	-0.006	0.232
389.10	0.121	0.211	3.537	3.517	1.006	0.284	1.904	1.008	-0.026	0.239
388.15	0.186	0.294	4.426	4.414	1.003	0.136	1.778	1.005	-0.042	0.244
387.79	0.256	0.361	4.72	4.717	1.001	0.032	1.604	1.007	0.024	0.245
387.29	0.283	0.372	5.195	5.196	1.000	0.010	1.520	1.044	0.230	0.595
390.46	0.956	0.878	1.383	1.391	0.994	0.288	0.958	2.990	-0.059	0.278
388.33	0.835	0.732	3.629	3.652	0.994	0.316	0.979	1.874	-0.003	0.249
387.61	0.751	0.676	4.43	4.458	0.994	0.315	1.029	1.536	-0.009	0.247
387.20	0.685	0.619	4.903	4.933	0.994	0.305	1.047	1.447	0.009	0.255
386.82	0.595	0.578	5.369	5.398	0.995	0.269	1.139	1.262	0.085	0.460
390.56	0.059	0.117	2.135	2.114	1.010	0.494	2.068	1.006	0.017	0.228
389.76	0.079	0.147	2.916	2.893	1.008	0.396	1.990	1.018	-0.021	0.230
389.40	0.106	0.188	3.251	3.23	1.007	0.324	1.918	1.010	-0.003	0.234
388.78	0.140	0.229	3.839	3.821	1.005	0.235	1.804	1.017	-0.014	0.236
388.33	0.176	0.273	4.256	4.242	1.003	0.165	1.735	1.016	-0.056	0.241
387.72	0.239	0.366	4.806	4.802	1.001	0.042	1.746	0.979	0.017	0.247
387.40	0.275	0.370	5.093	5.092	1.000	0.010	1.550	1.032	-0.006	0.247
387.10	0.321	0.403	5.349	5.355	0.999	0.056	1.460	1.054	-0.004	0.250
386.89	0.376	0.434	5.507	5.52	0.998	0.118	1.351	1.095	-0.003	0.249
386.80	0.405	0.454	5.57	5.585	0.997	0.134	1.316	1.111	-0.004	0.250
386.77	0.439	0.473	5.568	5.586	0.997	0.161	1.266	1.139	0.027	0.612
390.96	0.967	0.934	0.872	0.878	0.993	0.343	0.992	2.123	-0.009	0.239
389.79	0.926	0.859	2.082	2.093	0.995	0.263	0.988	2.099	-0.012	0.230
389.65	0.907	0.838	2.24	2.253	0.994	0.289	0.989	1.927	-0.019	0.235
388.73	0.859	0.764	3.206	3.226	0.994	0.311	0.980	1.907	0.010	0.241
388.45	0.828	0.756	3.516	3.538	0.994	0.312	1.015	1.631	-0.018	0.243
387.70	0.755	0.669	4.336	4.364	0.994	0.322	1.010	1.590		
392.54	0.000	0.000								

n-Decane/2-Heptanone

Table E. 5: Thermodynamic consistency testing results for n-decane/2-heptanone system at 40kPa

			L/W Consistency Test				*McDermott-Ellis Consistency Test*			
T (K)	X_{decane}	Y_{decane}	L_i	W_i	L_i/W_i	*D*	γ_{decane}	$\gamma_{2\text{-hept}}$	*Dev*	Dev_{max}
413.88	1.000	1.000								
401.78	0.781	0.494	7.579	7.705	0.984	0.824	0.925	1.759	-0.010	0.257
400.55	0.729	0.455	7.694	7.838	0.982	0.927	0.950	1.587	-0.003	0.256
400.23	0.715	0.444	7.714	7.862	0.981	0.950	0.956	1.554	0.000	0.258
399.68	0.692	0.428	7.771	7.926	0.980	0.987	0.969	1.504	-0.003	0.261
398.85	0.664	0.402	8.002	8.165	0.980	1.008	0.975	1.477	0.027	0.263
398.72	0.654	0.411	7.918	8.081	0.980	1.019	1.016	1.419	0.014	0.572
392.30	0.061	0.057	1.737	1.755	0.990	0.515	1.882	1.018	-0.015	0.279
392.81	0.131	0.106	2.705	2.76	0.980	1.006	1.601	1.027	0.012	0.264
392.92	0.176	0.144	3.547	3.622	0.979	1.046	1.612	1.033	-0.004	0.267
393.23	0.222	0.167	4.211	4.305	0.978	1.104	1.466	1.055	-0.001	0.270
393.67	0.277	0.198	4.937	5.053	0.977	1.161	1.372	1.078	-0.001	0.272
394.32	0.345	0.235	5.73	5.868	0.976	1.190	1.278	1.112	0.000	0.273
395.20	0.423	0.277	6.509	6.666	0.976	1.192	1.192	1.161	0.003	0.272
396.00	0.490	0.312	7.136	7.303	0.977	1.157	1.128	1.220	0.006	0.271
396.73	0.553	0.342	7.749	7.922	0.978	1.104	1.069	1.302	-0.001	0.267
398.32	0.626	0.395	7.719	7.885	0.979	1.064	1.034	1.364	-0.009	0.263
399.15	0.668	0.417	7.787	7.947	0.980	1.017	0.995	1.445	0.145	0.436
411.91	0.972	0.877	1.556	1.563	0.996	0.224	0.962	2.517	-0.032	0.231
409.34	0.936	0.774	3.351	3.378	0.992	0.401	0.953	2.170	-0.040	0.233
406.98	0.889	0.677	4.699	4.757	0.988	0.613	0.944	1.909	-0.043	0.239
404.19	0.833	0.570	6.285	6.379	0.985	0.742	0.927	1.828	-0.012	0.245
402.79	0.799	0.524	6.955	7.069	0.984	0.813	0.929	1.751	-0.072	0.253
401.37	0.755	0.454	7.431	7.567	0.982	0.907	0.892	1.717	0.051	0.267
399.32	0.672	0.419	7.703	7.861	0.980	1.015	0.989	1.450	0.014	0.269
397.08	0.575	0.355	7.869	8.042	0.978	1.087	1.055	1.328	-0.015	0.268
396.72	0.546	0.335	7.61	7.782	0.978	1.117	1.061	1.296	-0.005	0.272
395.90	0.483	0.303	7.086	7.253	0.977	1.165	1.115	1.223	0.056	0.832
392.05	0.023	0.024	1.185	1.182	1.003	0.127	2.121	1.021	0.005	0.247
391.96	0.027	0.030	1.359	1.357	1.001	0.074	2.266	1.022	0.011	0.256
391.79	0.031	0.028	1.614	1.61	1.001	0.062	1.853	1.034	-0.005	0.255
391.87	0.031	0.030	1.534	1.53	1.001	0.033	1.979	1.029	0.012	0.264
391.68	0.038	0.030	1.871	1.87	0.999	0.027	1.625	1.043	-0.004	0.266
391.82	0.048	0.042	1.942	1.95	0.996	0.206	1.793	1.036		
392.54	0.000	0.000								

n-Octane/3-Heptanone

Table E. 6: Thermodynamic consistency testing results for n-octane/3-heptanone system at 40kPa

			L/W Consistency Test				*McDermott-Ellis Consistency Test*			
T (K)	X_{octane}	Y_{octane}	L_i	W_i	L_i/W_i	*D*	γ_{octane}	$\gamma_{3\text{-}hept}$	*Dev*	Dev_{max}
367.97	1.000	1.000								
386.89	0.022	0.080	2.117	2.107	1.005	0.237	2.076	1.022	-0.076	0.247
384.44	0.071	0.222	3.578	3.582	0.999	0.056	1.914	0.986	-0.019	0.223
383.79	0.086	0.257	3.924	3.934	0.997	0.127	1.864	0.978	-0.016	0.228
382.30	0.114	0.319	4.847	4.867	0.996	0.206	1.823	0.972	-0.020	0.233
381.52	0.140	0.357	5.098	5.128	0.994	0.293	1.700	0.971	-0.019	0.241
379.45	0.196	0.439	6.026	6.076	0.992	0.413	1.588	0.973	-0.030	0.248
377.93	0.243	0.504	6.583	6.650	0.990	0.506	1.540	0.963	0.002	0.251
377.75	0.253	0.509	6.557	6.626	0.990	0.523	1.502	0.972	-0.028	0.258
375.65	0.320	0.589	7.276	7.366	0.988	0.615	1.465	0.963	-0.016	0.264
375.72	0.353	0.594	6.523	6.613	0.986	0.685	1.336	0.997	0.024	0.272
372.98	0.469	0.677	6.846	6.951	0.985	0.761	1.249	1.066	0.019	0.449
368.37	0.921	0.933	1.798	1.825	0.985	0.745	1.015	1.764	-0.004	0.285
368.88	0.840	0.884	3.048	3.101	0.983	0.862	1.037	1.479	0.026	0.285
369.90	0.699	0.786	5.060	5.147	0.983	0.852	1.073	1.395	-0.013	0.272
370.77	0.625	0.747	5.767	5.864	0.983	0.834	1.109	1.282	-0.018	0.272
371.58	0.569	0.721	6.143	6.245	0.984	0.823	1.146	1.194	-0.035	0.278
372.28	0.513	0.714	6.623	6.730	0.984	0.801	1.231	1.056	0.052	0.280
375.95	0.317	0.564	7.038	7.124	0.988	0.607	1.403	1.006	-0.021	0.258
376.81	0.285	0.546	6.839	6.917	0.989	0.567	1.472	0.971	0.027	0.253
377.66	0.251	0.505	6.688	6.757	0.990	0.513	1.506	0.981	0.099	0.291
385.05	0.059	0.191	3.211	3.211	1.000	0.000	1.948	0.992	-0.004	0.222
383.37	0.083	0.256	4.405	4.413	0.998	0.091	1.948	0.990	-0.012	0.228
383.00	0.102	0.277	4.390	4.405	0.997	0.171	1.734	0.995	-0.019	0.242
380.03	0.179	0.398	5.793	5.836	0.993	0.370	1.550	1.002	0.040	0.443
368.78	0.836	0.873	3.234	3.289	0.983	0.843	1.033	1.585	-0.018	0.278
369.47	0.763	0.841	4.118	4.192	0.982	0.890	1.066	1.338	0.008	0.283
370.35	0.665	0.792	5.336	5.429	0.983	0.864	1.120	1.199	0.005	0.278
371.01	0.611	0.760	5.824	5.924	0.983	0.851	1.145	1.162		
388.11	0.000	0.000								

n-Nonane/3-Heptanone

Table E. 7: Thermodynamic consistency testing results for n-nonane/3-heptanone system at 40kPa

			L/W Consistency Test				McDermott-Ellis Consistency Test			
T (K)	X_{nonane}	Y_{nonane}	L_i	W_i	L_i/W_i	D	γ_{nonane}	$\gamma_{3\text{-hept}}$	Dev	Dev_{max}
391.87	1.000	1.000								
387.48	0.075	0.116	2.141	2.122	1.009	0.446	1.781	1.018	-0.026	0.238
387.25	0.114	0.168	2.46	2.446	1.006	0.285	1.709	1.008	0.007	0.236
386.82	0.139	0.197	2.947	2.934	1.004	0.221	1.666	1.016	-0.013	0.239
386.59	0.173	0.235	3.255	3.245	1.003	0.154	1.608	1.015	-0.011	0.244
386.33	0.224	0.279	3.632	3.629	1.001	0.041	1.487	1.028	0.000	0.242
386.10	0.248	0.306	3.917	3.917	1.000	0.000	1.483	1.029	-0.008	0.253
385.79	0.347	0.375	4.457	4.47	0.997	0.146	1.312	1.078	-0.002	0.252
385.72	0.427	0.432	4.713	4.736	0.995	0.243	1.231	1.120	-0.009	0.252
385.87	0.484	0.470	4.697	4.725	0.994	0.297	1.175	1.155	-0.004	0.251
386.02	0.533	0.505	4.662	4.694	0.993	0.342	1.141	1.186	-0.003	0.252
386.25	0.600	0.544	4.59	4.627	0.992	0.401	1.083	1.266	0.010	0.425
390.66	0.957	0.924	1.035	1.045	0.990	0.481	1.001	1.707	-0.007	0.237
389.71	0.920	0.856	1.896	1.912	0.992	0.420	0.994	1.791	-0.013	0.233
389.09	0.883	0.805	2.426	2.449	0.991	0.472	0.993	1.691	0.000	0.233
388.55	0.856	0.769	2.901	2.928	0.991	0.463	0.996	1.656	-0.001	0.239
387.93	0.812	0.726	3.415	3.447	0.991	0.466	1.011	1.534	-0.010	0.240
387.54	0.776	0.684	3.719	3.754	0.991	0.468	1.010	1.504	-0.003	0.254
386.29	0.643	0.570	4.652	4.691	0.992	0.417	1.058	1.336	-0.011	0.252
386.15	0.576	0.529	4.633	4.669	0.992	0.387	1.101	1.238	0.007	0.252
385.88	0.511	0.490	4.75	4.781	0.994	0.325	1.160	1.172	-0.002	0.251
385.85	0.459	0.455	4.658	4.684	0.994	0.278	1.200	1.133	0.116	0.432
387.72	0.049	0.090	1.841	1.821	1.011	0.546	2.099	1.012	-0.027	0.246
387.29	0.101	0.151	2.39	2.374	1.007	0.336	1.731	1.013	-0.008	0.243
386.57	0.165	0.224	3.256	3.246	1.003	0.154	1.608	1.020	-0.008	0.239
386.43	0.189	0.250	3.452	3.444	1.002	0.116	1.574	1.020	-0.002	0.242
386.20	0.220	0.278	3.753	3.749	1.001	0.053	1.515	1.029	-0.017	0.248
386.07	0.286	0.329	4.035	4.041	0.999	0.074	1.384	1.049	0.018	0.530
390.37	0.941	0.889	1.287	1.299	0.991	0.464	0.988	1.833	0.002	0.238
389.11	0.889	0.812	2.421	2.442	0.991	0.432	0.995	1.717	-0.004	0.236
388.49	0.851	0.768	2.949	2.976	0.991	0.456	1.002	1.610	-0.006	0.238
387.76	0.804	0.710	3.566	3.599	0.991	0.461	1.004	1.566	-0.007	0.243
387.13	0.745	0.655	4.055	4.092	0.991	0.454	1.020	1.461		
388.36	0.000	0.000								

n-Decane/3-Heptanone

Table E. 8: Thermodynamic consistency testing results for n-decane/3-heptanone system at 40kPa

			L/W Consistency Test				*McDermott-Ellis Consistency Test*			
T (K)	X_{decane}	Y_{decane}	L_i	W_i	L_i/W_i	*D*	γ_{decane}	$\gamma_{3\text{-}hept}$	*Dev*	Dev_{max}
413.88	1.000	1.000								
388.77	0.058	0.043	2.072	2.097	0.988	0.600	1.692	1.038	-0.008	0.297
389.40	0.121	0.078	2.959	3.03	0.977	1.186	1.438	1.050	0.012	0.282
389.80	0.167	0.109	3.67	3.77	0.973	1.344	1.435	1.058	-0.008	0.279
390.38	0.208	0.134	4.082	4.208	0.970	1.520	1.387	1.061	-0.008	0.283
390.93	0.253	0.153	4.624	4.774	0.969	1.596	1.277	1.082	-0.003	0.290
391.60	0.318	0.177	5.536	5.715	0.969	1.591	1.148	1.127	-0.011	0.291
392.69	0.385	0.206	6.082	6.285	0.968	1.641	1.063	1.165	0.010	0.291
393.48	0.447	0.233	6.811	7.03	0.969	1.582	1.007	1.221	0.009	0.290
394.90	0.526	0.274	7.335	7.561	0.970	1.517	0.959	1.290	0.035	0.281
396.68	0.605	0.335	7.506	7.725	0.972	1.438	0.959	1.343	0.125	0.306
407.06	0.897	0.689	4.412	4.474	0.986	0.698	0.950	1.776	-0.072	0.239
404.40	0.840	0.573	5.641	5.748	0.981	0.940	0.918	1.693	-0.018	0.245
402.87	0.802	0.522	6.219	6.353	0.979	1.066	0.919	1.601	-0.021	0.248
402.20	0.785	0.494	6.464	6.609	0.978	1.109	0.908	1.592	-0.058	0.255
401.36	0.762	0.448	6.729	6.89	0.977	1.182	0.872	1.608	0.052	0.263
399.83	0.719	0.429	7.187	7.369	0.975	1.250	0.931	1.474	0.028	0.264
398.57	0.678	0.406	7.427	7.625	0.974	1.315	0.974	1.390	-0.027	0.267
397.29	0.631	0.359	7.54	7.754	0.972	1.399	0.965	1.360	-0.020	0.272
396.53	0.606	0.330	7.681	7.902	0.972	1.418	0.948	1.363	0.030	0.275
396.26	0.594	0.335	7.654	7.875	0.972	1.423	0.991	1.324	0.214	0.911
388.93	0.025	0.028	1.12	1.124	0.996	0.178	2.542	1.014	-0.006	0.294
389.05	0.069	0.052	2.057	2.091	0.984	0.820	1.703	1.031	0.004	0.290
389.54	0.136	0.093	3.181	3.262	0.975	1.257	1.518	1.047	-0.012	0.290
390.57	0.224	0.140	4.28	4.414	0.970	1.541	1.337	1.069	0.006	0.279
391.15	0.270	0.171	4.817	4.975	0.968	1.614	1.327	1.076	-0.032	0.366
402.59	0.792	0.516	6.249	6.388	0.978	1.100	0.929	1.556	-0.014	0.263
398.14	0.678	0.388	7.857	8.06	0.975	1.275	0.944	1.451	0.013	0.268
397.83	0.652	0.385	7.521	7.728	0.973	1.357	0.984	1.362	0.002	0.270
396.15	0.590	0.338	7.665	7.887	0.972	1.427	1.010	1.309	0.110	0.910
413.40	0.989	0.959	0.392	0.394	0.995	0.254	0.989	1.839	-0.051	0.276
410.11	0.942	0.806	2.495	2.523	0.989	0.558	0.964	1.806	-0.016	0.226
408.41	0.911	0.739	3.414	3.464	0.986	0.727	0.962	1.660	-0.053	0.230
406.83	0.885	0.659	4.34	4.412	0.984	0.823	0.928	1.755	-0.011	0.237
404.85	0.844	0.594	5.291	5.393	0.981	0.955	0.933	1.630	-0.086	0.246
403.22	0.809	0.509	6.044	6.175	0.979	1.072	0.879	1.688	0.019	0.256
400.88	0.753	0.455	6.985	7.15	0.977	1.167	0.911	1.552		
388.67	0.000	0.000								

n-Octane/4-Heptanone

Table E. 9: Thermodynamic consistency testing results for n-octane/4-heptanone system at 40kPa

			L/W Consistency Test				*McDermott-Ellis Consistency Test*			
T (K)	X_{octane}	Y_{octane}	L_i	W_i	L_i/W_i	*D*	γ_{octane}	$\gamma_{4\text{-}hept}$	*Dev*	Dev_{max}
368.3	1.000	1.000								
382.88	0.042	0.123	2.493	2.580	0.966	1.715	1.878	1.017	-0.050	0.223
382.13	0.067	0.187	2.804	2.919	0.961	2.009	1.829	0.992	-0.007	0.230
380.05	0.112	0.277	4.094	4.279	0.957	2.209	1.724	0.994	-0.005	0.236
378.22	0.164	0.354	5.010	5.256	0.953	2.396	1.589	1.004	-0.015	0.239
376.94	0.205	0.414	5.569	5.856	0.951	2.512	1.546	1.001	-0.023	0.242
376.43	0.222	0.446	5.780	6.084	0.950	2.562	1.562	0.984	0.011	0.252
374.95	0.288	0.498	6.098	6.437	0.947	2.704	1.407	1.027	-0.012	0.251
374.30	0.317	0.531	6.237	6.590	0.946	2.752	1.391	1.023	-0.005	0.258
373.06	0.383	0.584	6.313	6.683	0.945	2.847	1.316	1.050	-0.005	0.260
372.55	0.418	0.609	6.206	6.575	0.944	2.887	1.278	1.066	-0.006	0.266
371.25	0.505	0.670	5.969	6.329	0.943	2.927	1.212	1.109	0.013	0.763
368.26	0.973	0.972	0.661	0.686	0.964	1.856	1.005	1.930	-0.002	0.266
368.30	0.946	0.948	1.101	1.153	0.955	2.307	1.007	1.789	0.001	0.267
368.37	0.908	0.921	1.707	1.796	0.950	2.541	1.017	1.591	0.002	0.275
368.77	0.822	0.854	2.834	3.001	0.944	2.862	1.028	1.496	0.005	0.280
369.49	0.697	0.787	4.332	4.596	0.943	2.957	1.092	1.248	0.003	0.270
370.00	0.642	0.753	4.796	5.093	0.942	3.003	1.115	1.202	0.010	0.270
370.72	0.566	0.707	5.421	5.756	0.942	2.997	1.161	1.145	0.003	0.270
371.92	0.470	0.649	5.918	6.279	0.943	2.960	1.235	1.075	-0.003	0.265
372.56	0.423	0.624	6.107	6.475	0.943	2.925	1.293	1.033	0.019	0.261
373.19	0.380	0.588	6.236	6.603	0.944	2.858	1.330	1.030	-0.016	0.261
373.75	0.347	0.576	6.258	6.621	0.945	2.819	1.402	0.987	0.011	0.257
375.15	0.284	0.519	5.968	6.304	0.947	2.738	1.478	0.971	0.133	0.329
382.96	0.047	0.139	2.325	2.412	0.964	1.837	1.892	1.001	-0.009	0.225
381.51	0.078	0.206	3.231	3.366	0.960	2.046	1.763	1.001	-0.016	0.226
380.61	0.102	0.253	3.710	3.875	0.957	2.175	1.700	0.996	-0.007	0.230
379.57	0.130	0.301	4.258	4.459	0.955	2.306	1.637	0.997	-0.019	0.233
378.81	0.156	0.343	4.561	4.788	0.953	2.428	1.590	0.991	-0.008	0.238
377.50	0.197	0.401	5.150	5.419	0.950	2.545	1.532	0.994	0.011	0.239
377.45	0.195	0.396	5.235	5.506	0.951	2.523	1.530	1.001	-0.029	0.242
376.75	0.224	0.441	5.425	5.717	0.949	2.621	1.516	0.985	0.004	0.248
375.74	0.266	0.478	5.695	6.014	0.947	2.724	1.427	1.007	0.018	0.252
374.48	0.317	0.519	6.057	6.404	0.946	2.785	1.352	1.043	-0.032	0.253
374.77	0.312	0.526	5.855	6.194	0.945	2.814	1.379	1.010	-0.053	1.332
368.34	0.980	0.982	0.456	0.474	0.962	1.935	1.005	1.670	0.001	0.259
368.31	0.987	0.987	0.361	0.373	0.968	1.635	1.004	1.858	0.009	0.482
368.48	0.881	0.903	2.076	2.191	0.948	2.695	1.024	1.504	0.007	0.271
368.81	0.809	0.850	3.025	3.203	0.944	2.858	1.038	1.430	0.006	0.273
369.23	0.731	0.809	3.989	4.229	0.943	2.920	1.079	1.273	0.007	0.270
369.87	0.662	0.760	4.572	4.856	0.942	3.012	1.096	1.243		
385.50	0.000	0.000								

n-Nonane/4-Heptanone

Table E. 10: Thermodynamic consistency testing results for n-nonane/4-heptanone system at 40kPa

			L/W Consistency Test				*McDermott-Ellis Consistency Test*			
T (K)	X_{nonane}	Y_{nonane}	L_i	W_i	L_i/W_i	*D*	γ_{nonane}	$\gamma_{4\text{-}hept}$	*Dev*	Dev_{max}
391.9	1.000	1.000								
385.08	0.057	0.080	1.357	1.384	0.980	0.985	1.747	1.008	-0.004	0.243
384.77	0.094	0.123	1.879	1.918	0.980	1.027	1.645	1.011	0.002	0.238
384.54	0.113	0.146	2.218	2.265	0.979	1.048	1.636	1.013	-0.005	0.241
384.42	0.141	0.174	2.498	2.552	0.979	1.069	1.569	1.016	0.006	0.242
384.15	0.165	0.199	2.905	2.969	0.978	1.090	1.547	1.022	-0.002	0.246
384.00	0.206	0.232	3.29	3.361	0.979	1.068	1.451	1.036	0.004	0.245
383.79	0.234	0.265	3.66	3.739	0.979	1.068	1.469	1.035	-0.011	0.247
383.85	0.264	0.285	3.771	3.852	0.979	1.063	1.397	1.045	0.002	0.250
383.77	0.310	0.317	4.114	4.2	0.980	1.034	1.327	1.068	-0.004	0.251
383.82	0.355	0.349	4.321	4.408	0.980	0.997	1.273	1.087	-0.003	0.252
383.93	0.404	0.381	4.49	4.578	0.981	0.970	1.217	1.115	0.004	0.251
383.97	0.441	0.409	4.661	4.749	0.981	0.935	1.195	1.134	-0.008	0.254
384.26	0.501	0.441	4.712	4.797	0.982	0.894	1.123	1.19	0.074	0.442
390.31	0.951	0.892	1.213	1.22	0.994	0.288	0.983	1.937	0.006	0.231
389.71	0.927	0.864	1.678	1.688	0.994	0.297	0.996	1.667	-0.026	0.234
388.63	0.882	0.781	2.503	2.523	0.992	0.398	0.979	1.717	-0.003	0.236
387.61	0.836	0.722	3.263	3.294	0.991	0.473	0.987	1.619	-0.001	0.239
387.14	0.800	0.693	3.529	3.566	0.990	0.521	1.005	1.488	-0.012	0.239
386.59	0.764	0.647	3.876	3.92	0.989	0.564	1	1.475	-0.009	0.244
385.92	0.710	0.594	4.239	4.295	0.987	0.656	1.01	1.411	-0.003	0.248
385.26	0.648	0.543	4.548	4.615	0.985	0.731	1.034	1.336	0.005	0.250
384.91	0.604	0.519	4.648	4.721	0.985	0.779	1.073	1.264	0.007	0.250
384.60	0.570	0.498	4.765	4.843	0.984	0.812	1.102	1.227	-0.003	0.250
384.45	0.537	0.473	4.727	4.808	0.983	0.850	1.117	1.202	0.078	0.458
390.84	0.959	0.897	0.729	0.734	0.993	0.342	0.964	2.171	0.010	0.244
389.03	0.904	0.815	2.228	2.243	0.993	0.335	0.984	1.761	-0.014	0.240
387.60	0.833	0.722	3.256	3.287	0.991	0.474	0.991	1.591	0.001	0.243
386.37	0.762	0.648	4.084	4.132	0.988	0.584	1.012	1.469	-0.015	0.245
385.63	0.696	0.583	4.45	4.51	0.987	0.670	1.021	1.395	-0.006	0.249
385.01	0.629	0.530	4.69	4.761	0.985	0.751	1.048	1.314	0.002	0.253
384.52	0.554	0.486	4.754	4.834	0.983	0.834	1.109	1.214	0.004	0.596
385.28	0.038	0.053	1.048	1.068	0.981	0.945	1.725	1.011	-0.005	0.251
384.91	0.079	0.103	1.653	1.687	0.980	1.018	1.632	1.012	0.006	0.245
384.35	0.129	0.162	2.499	2.553	0.979	1.069	1.6	1.018	-0.001	0.245
384.05	0.176	0.208	3.068	3.135	0.979	1.080	1.52	1.027	-0.003	0.247
383.88	0.227	0.252	3.53	3.606	0.979	1.065	1.436	1.04	-0.009	0.253
383.83	0.319	0.325	4.105	4.19	0.980	1.025	1.319	1.067		
385.47	0.000	0.000								

n-Decane/4-Heptanone

Table E. 11: Thermodynamic consistency testing results for n-decane/4-heptanone system at 40kPa

			L/W Consistency Test				*McDermott-Ellis Consistency Test*			
T (K)	X_{decane}	Y_{decane}	L_i	W_i	L_i/W_i	*D*	γ_{decane}	$\gamma_{4\text{-}hept}$	*Dev*	Dev_{max}
413.88	1.000	1.000								
386.02	0.053	0.041	1.595	1.638	0.974	1.330	1.948	1.015	-0.012	0.292
386.59	0.106	0.070	2.528	2.6	0.972	1.404	1.628	1.024	-0.004	0.292
387.31	0.171	0.103	3.648	3.753	0.972	1.419	1.447	1.041	-0.011	0.296
388.00	0.229	0.123	4.596	4.726	0.972	1.395	1.258	1.071	0.033	0.294
388.75	0.293	0.166	5.649	5.805	0.973	1.362	1.292	1.085	-0.030	0.294
389.70	0.350	0.182	6.302	6.471	0.974	1.323	1.146	1.123	-0.001	0.296
390.23	0.392	0.196	6.952	7.132	0.975	1.278	1.082	1.161	0.005	0.295
391.61	0.460	0.234	7.478	7.661	0.976	1.209	1.048	1.194	0.011	0.290
392.23	0.501	0.254	8.005	8.193	0.977	1.161	1.022	1.235	0.009	0.288
393.30	0.552	0.284	8.359	8.544	0.978	1.094	1	1.278	-0.050	0.289
394.35	0.594	0.291	8.481	8.659	0.979	1.039	0.918	1.352	0.016	0.285
395.65	0.646	0.325	8.629	8.796	0.981	0.958	0.902	1.42	0.229	0.388
410.74	0.958	0.826	2.174	2.174	1.000	0.000	0.953	2.024	-0.002	0.227
408.73	0.928	0.759	3.358	3.368	0.997	0.149	0.961	1.725	-0.027	0.225
407.10	0.904	0.693	4.326	4.348	0.995	0.254	0.947	1.722	-0.003	0.239
403.94	0.846	0.595	5.885	5.939	0.991	0.457	0.96	1.544	-0.156	0.256
400.83	0.794	0.449	7.556	7.656	0.987	0.657	0.853	1.714	0.070	0.263
399.62	0.759	0.446	7.797	7.909	0.986	0.713	0.923	1.525	0.035	0.258
399.83	0.757	0.466	7.531	7.639	0.986	0.712	0.96	1.449	-0.016	0.260
397.77	0.704	0.405	8.121	8.257	0.984	0.830	0.96	1.407	0.006	0.281
393.59	0.565	0.300	8.432	8.615	0.979	1.074	1.021	1.275	0.227	1.061
385.45	0.021	0.021	1.257	1.285	0.978	1.101	2.572	1.021	-0.032	0.281
386.00	0.043	0.033	1.332	1.366	0.975	1.260	1.934	1.014	-0.023	0.299
386.75	0.096	0.064	2.085	2.146	0.972	1.442	1.635	1.014	0.003	0.296
387.47	0.170	0.103	3.459	3.56	0.972	1.439	1.447	1.035	0.002	0.299
388.48	0.262	0.143	5.046	5.188	0.973	1.388	1.257	1.077	0.005	0.290
389.54	0.322	0.182	5.675	5.83	0.973	1.347	1.253	1.082	0.328	1.507
412.89	0.990	0.940	0.905	0.898	1.008	0.388	0.983	2.771	-0.071	0.273
410.24	0.952	0.813	2.509	2.51	1.000	0.020	0.958	1.928	-0.034	0.226
407.65	0.917	0.713	4.135	4.151	0.996	0.193	0.944	1.834	-0.006	0.234
405.50	0.876	0.644	5.153	5.19	0.993	0.358	0.955	1.615	-0.038	0.237
403.84	0.847	0.577	6.012	6.068	0.991	0.464	0.933	1.628	-0.026	0.263
398.18	0.717	0.414	8.072	8.203	0.984	0.805	0.951	1.432		
385.87	0.000	0.000								

Appendix F Thermodynamic Modelling Extensive Results

n-Octane/2-Heptanone

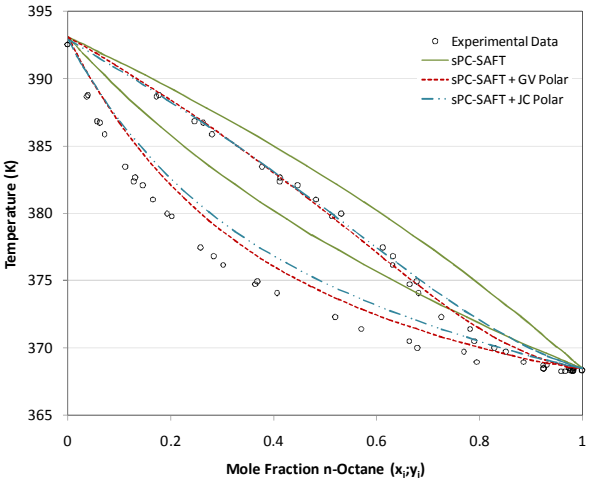

Figure F. 3: Pure predictions for isobaric VLE in n-octane/2-heptanone system at 40kPa. Only pure component data included in parameter regression.

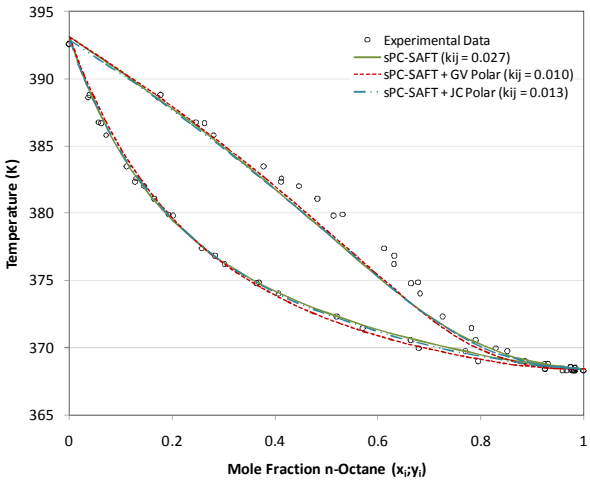

Figure F. 4: Correlations for isobaric VLE in n-octane/2-heptanone system at 40kPa. Only pure component data included in parameter regression.

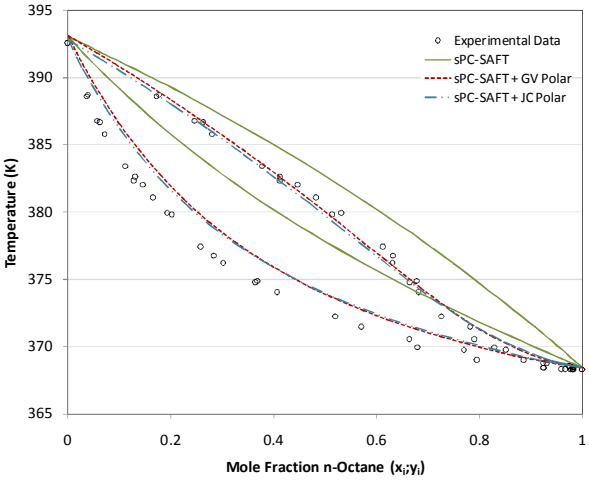

Figure F. 5: Pure predictions for isobaric VLE in n-octane/2-heptanone system at 40kPa. Correlation for polar parameter (x_p/n_p) used with pure component data in parameter regression.

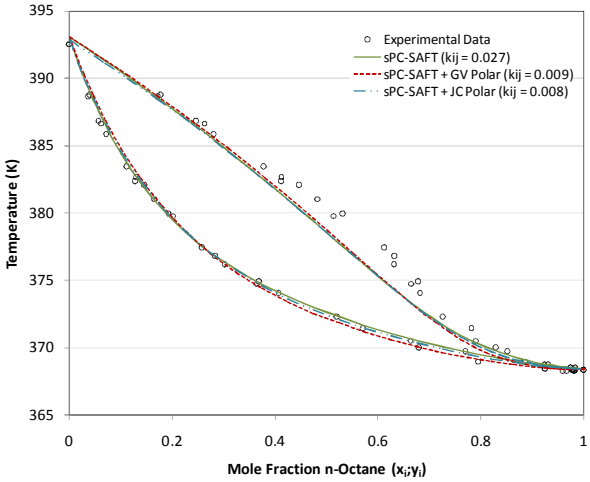

Figure F. 6: Correlations for isobaric VLE in n-octane/2-heptanone system at 40kPa. Correlation for polar parameter (x_p/n_p) used with pure component data in parameter regression.

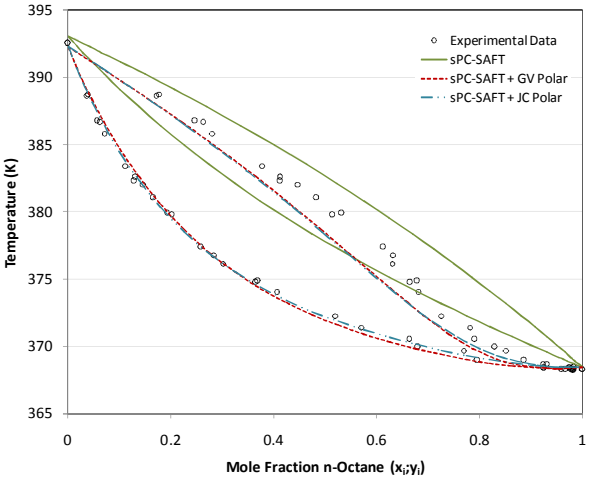

Figure F. 7: Pure predictions for isobaric VLE in n-octane/2-heptanone system at 40kPa. n-Octane/2-heptanone VLE data used with pure component data in parameter regression.

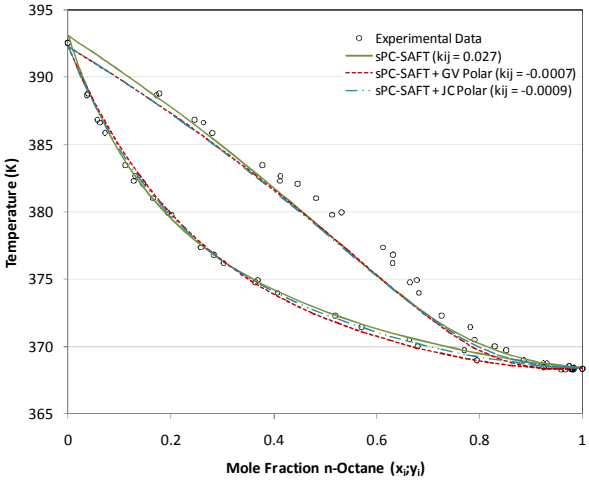

Figure F. 8: Correlations for isobaric VLE in n-octane/2-heptanone system at 40kPa. n-Octane/2-heptanone VLE data used with pure component data in parameter regression.

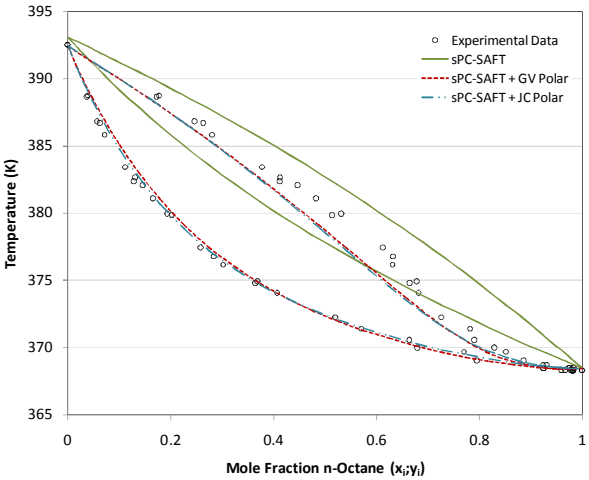

Figure F. 9: Pure predictions for isobaric VLE in n-octane/2-heptanone system at 40kPa. n-Nonane/2-heptanone VLE data used with pure component data in parameter regression.

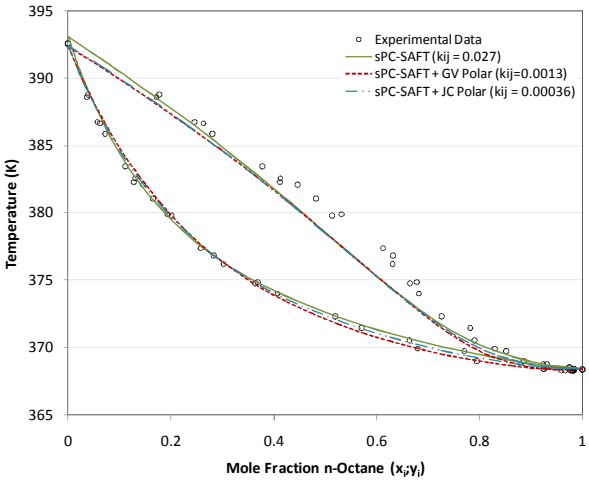

Figure F. 10: Correlations for isobaric VLE in n-octane/2-heptanone system at 40kPa. n-Nonane/2-heptanone VLE data used with pure component data in parameter regression.

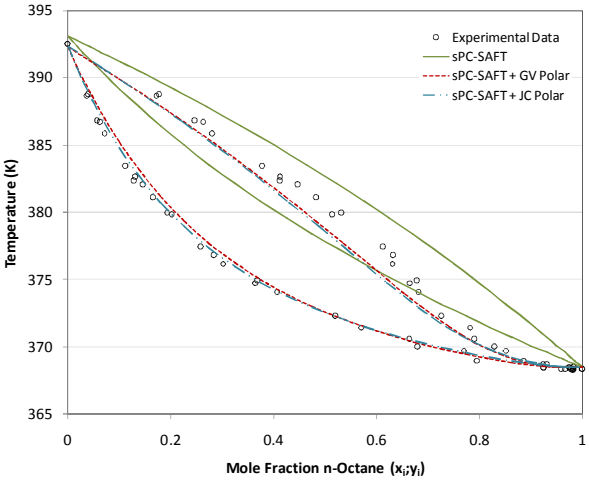

Figure F. 11: Pure predictions for isobaric VLE in n-octane/2-heptanone system at 40kPa. n-Decane/2-heptanone VLE data used with pure component data in parameter regression.

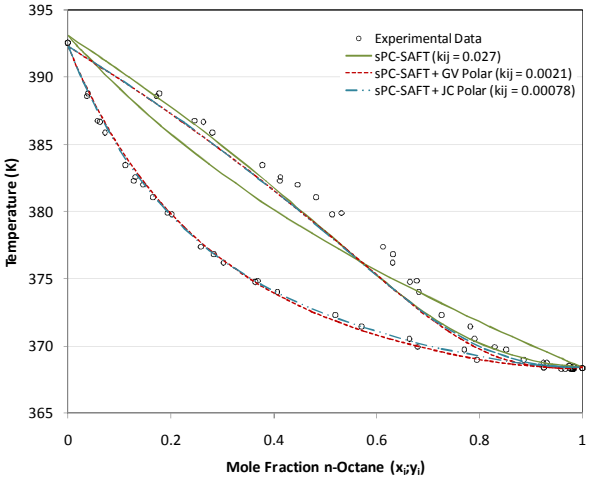

Figure F. 12: Correlations for isobaric VLE in n-octane/2-heptanone system at 40kPa. n-Decane/2-heptanone VLE data used with pure component data in parameter regression.

n-Nonane/2-Heptanone

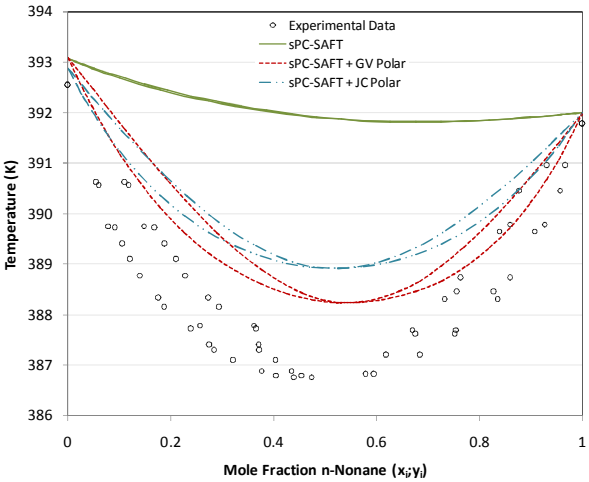

Figure F. 13: Pure predictions for isobaric VLE in n-nonane/2-heptanone system at 40kPa. Only pure component data included in parameter regression.

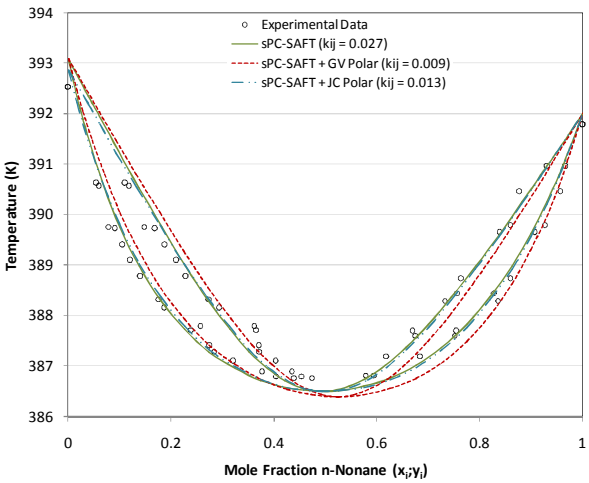

Figure F. 14: Correlations for isobaric VLE in n-nonane/2-heptanone system at 40kPa. Only pure component data included in parameter regression.

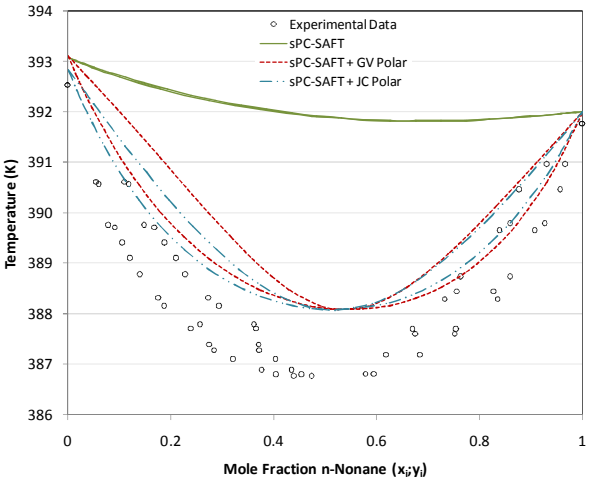

Figure F. 15: Pure predictions for isobaric VLE in n-nonane/2-heptanone system at 40kPa. Correlation for polar parameter (x_p/n_p) used with pure component data in parameter regression.

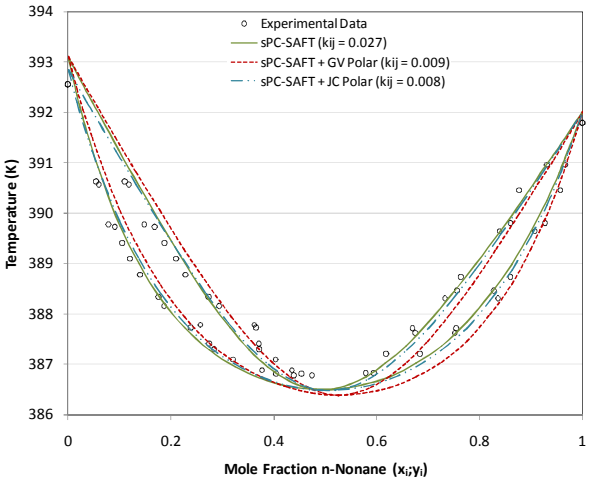

Figure F. 16: Correlations for isobaric VLE in n-nonane/2-heptanone system at 40kPa. Correlation for polar parameter (x_p/n_p) used with pure component data in parameter regression.

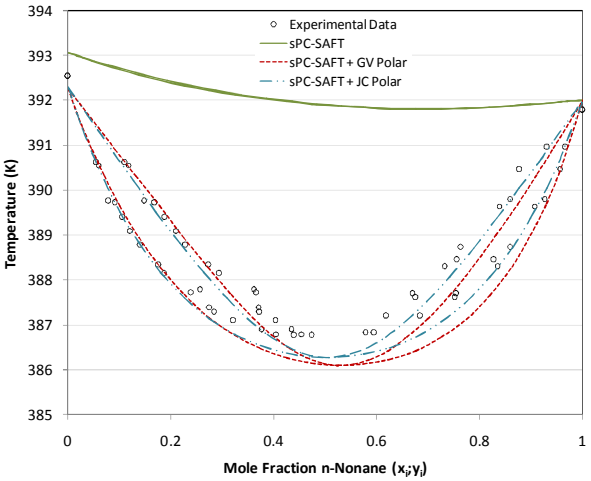

Figure F. 17: Pure predictions for isobaric VLE in n-nonane/2-heptanone system at 40kPa. n-Octane/2-heptanone VLE data used with pure component data in parameter regression.

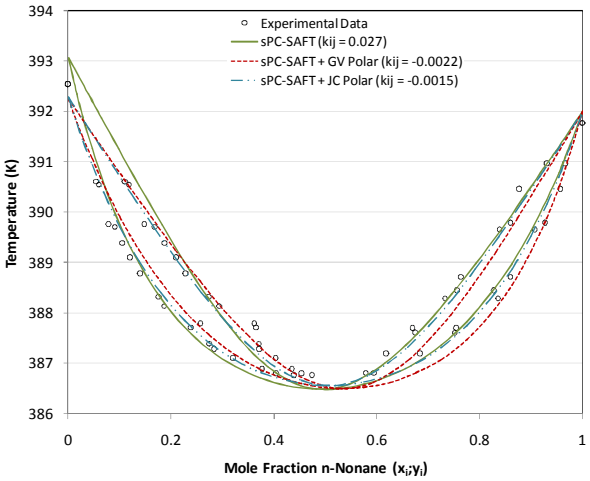

Figure F. 18: Correlations for isobaric VLE in n-nonane/2-heptanone system at 40kPa. n-Octane/2-heptanone VLE data used with pure component data in parameter regression.

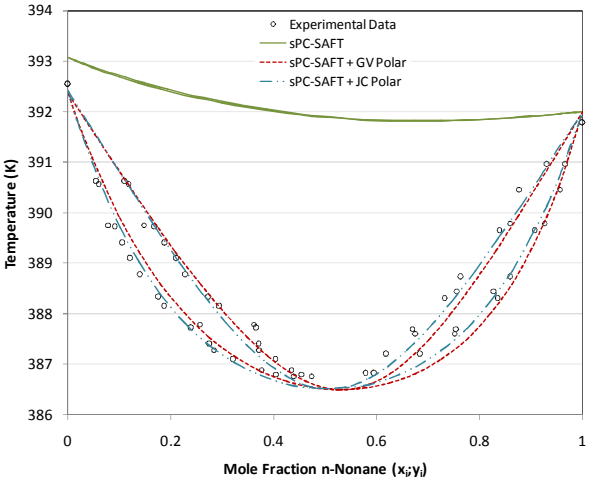

Figure F. 19: Pure predictions for isobaric VLE in n-nonane/2-heptanone system at 40kPa. n-Nonane/2-heptanone VLE data used with pure component data in parameter regression.

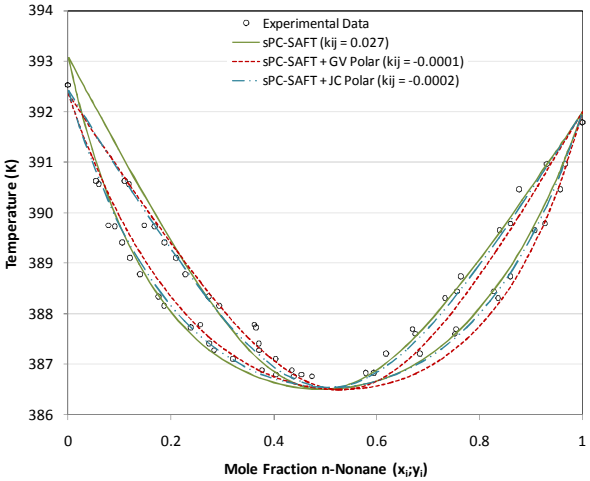

Figure F. 20: Correlations for isobaric VLE in n-nonane/2-heptanone system at 40kPa. n-Nonane/2-heptanone VLE data used with pure component data in parameter regression.

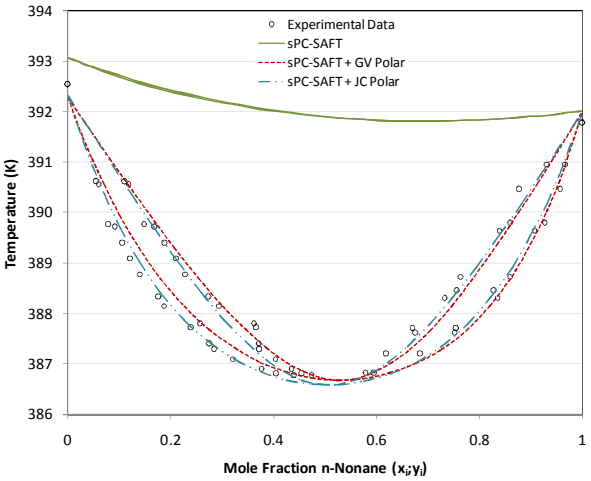

Figure F. 21: Pure predictions for isobaric VLE in n-nonane/2-heptanone system at 40kPa. n-Decane/2-heptanone VLE data used with pure component data in parameter regression.

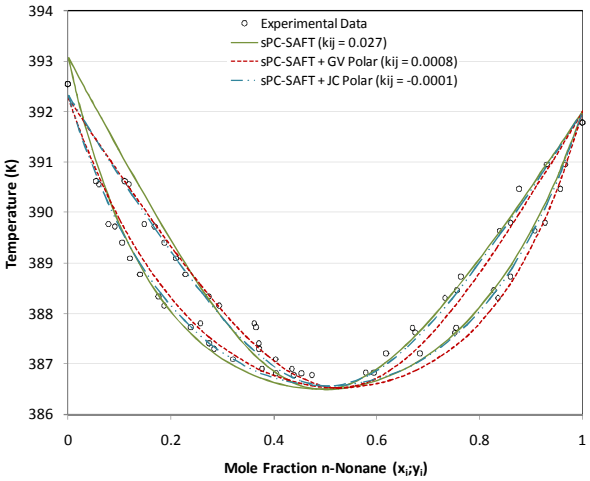

Figure F. 22: Correlations for isobaric VLE in n-nonane/2-heptanone system at 40kPa. n-Decane/2-heptanone VLE data used with pure component data in parameter regression.

n-Decane/2-Heptanone

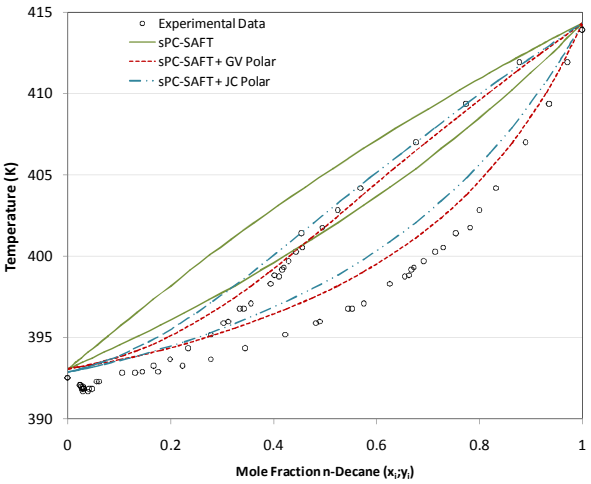

Figure F. 23: Pure predictions for isobaric VLE in n-decane/2-heptanone system at 40kPa. Only pure component data included in parameter regression.

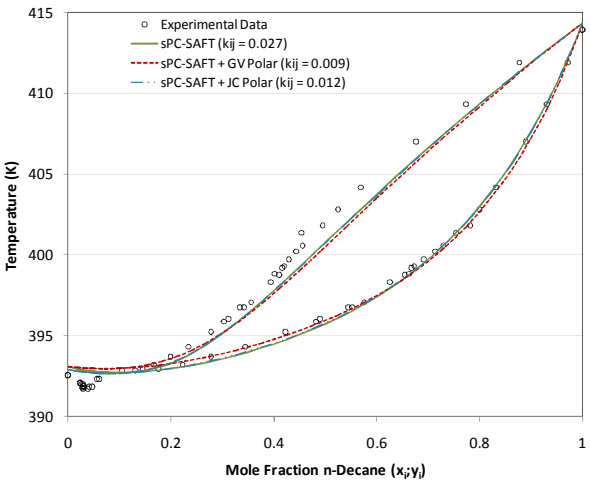

Figure F. 24: Correlations for isobaric VLE in n-decane/2-heptanone system at 40kPa. Only pure component data included in parameter regression.

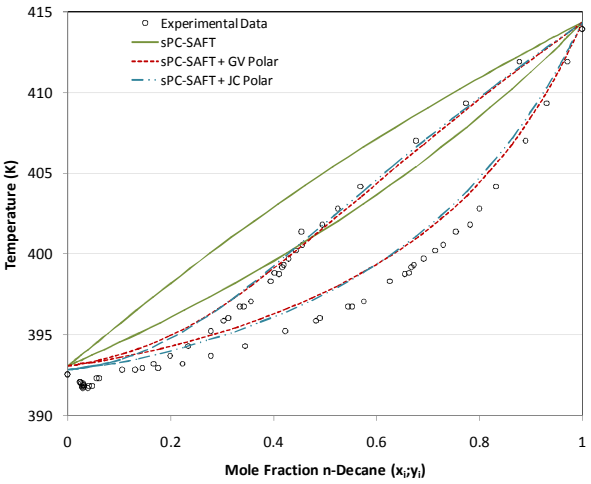

Figure F. 25: Pure predictions for isobaric VLE in n-decane/2-heptanone system at 40kPa. Correlation for polar parameter (x_p/n_p) used with pure component data in parameter regression.

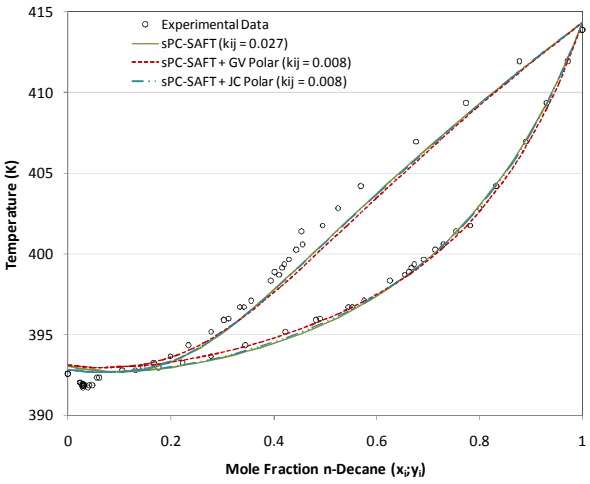

Figure F 26: Correlations for isobaric VLE in n-decane/2-heptanone system at 40kPa. Correlation for polar parameter (x_p/n_p) used with pure component data in parameter regression.

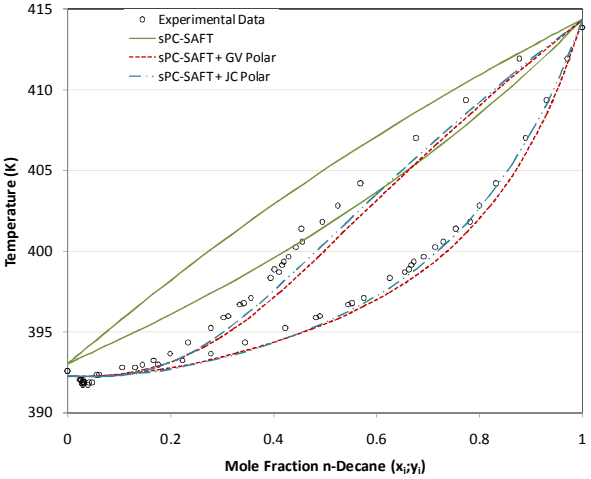

Figure F. 27: Pure predictions for isobaric VLE in n-decane/2-heptanone system at 40kPa. n-Octane/2-heptanone VLE data used with pure component data in parameter regression.

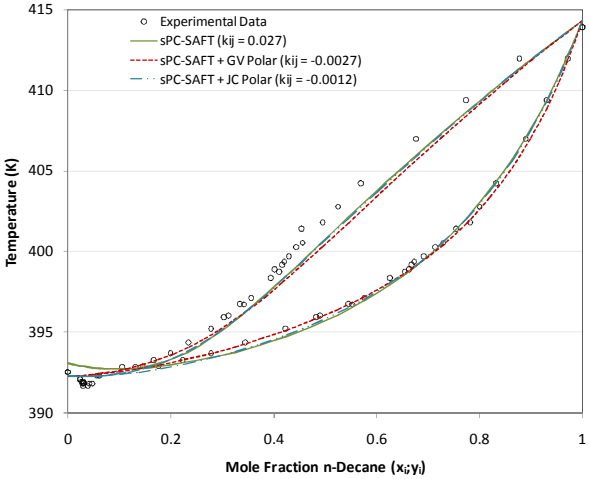

Figure F. 28: Correlations for isobaric VLE in n-decane/2-heptanone system at 40kPa. n-Octane/2-heptanone VLE data used with pure component data in parameter regression.

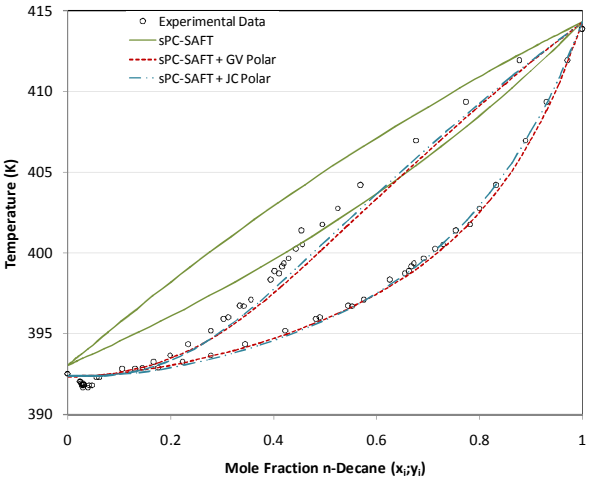

Figure F. 29: Pure predictions for isobaric VLE in n-decane/2-heptanone system at 40kPa. n-Nonane/2-heptanone VLE data used with pure component data in parameter regression.

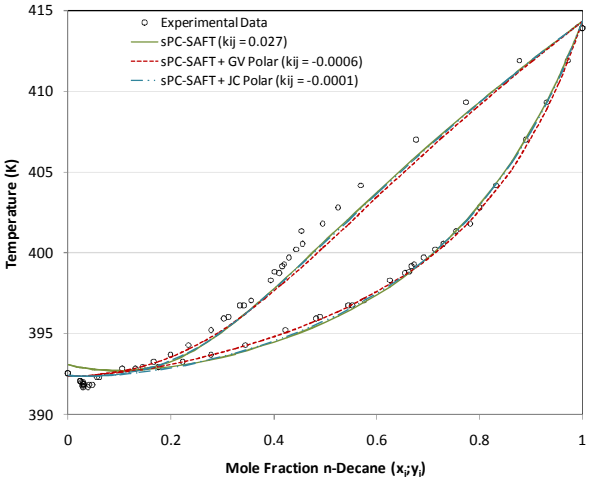

Figure F. 30: Correlations for isobaric VLE in n-decane/2-heptanone system at 40kPa. n-Nonane/2-heptanone VLE data used with pure component data in parameter regression.

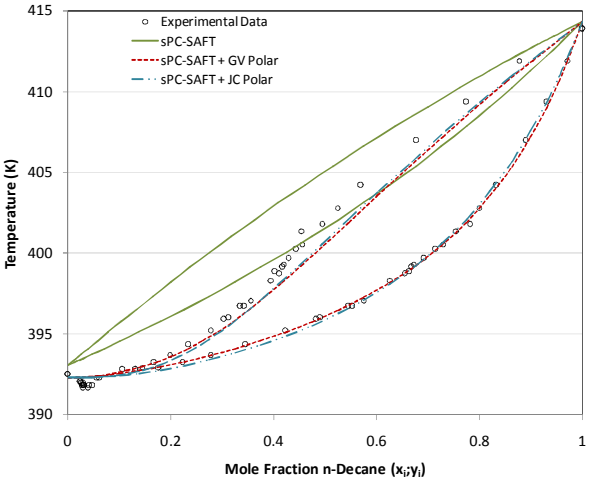

Figure F. 31: Pure predictions for isobaric VLE in n-decane/2-heptanone system at 40kPa. n-Decane/2-heptanone VLE data used with pure component data in parameter regression.

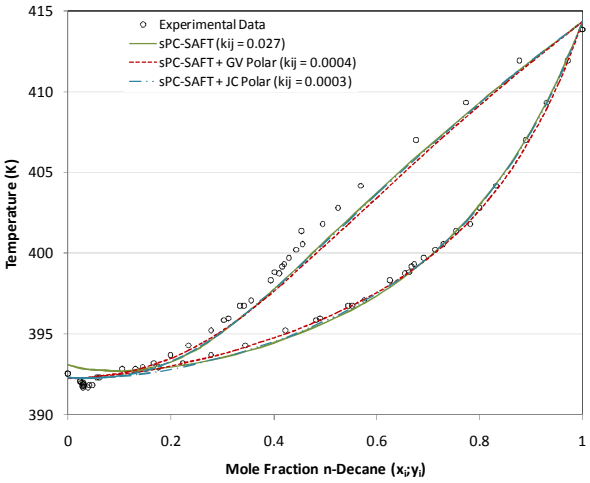

Figure F. 32: Correlations for isobaric VLE in n-decane/2-heptanone system at 40kPa. n-Decane/2-heptanone VLE data used with pure component data in parameter regression.

n-Octane/3-Heptanone

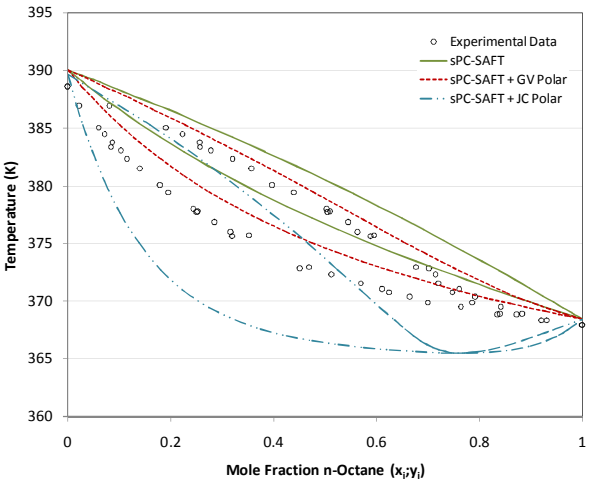

Figure F. 33: Pure predictions for isobaric VLE in n-octane/3-heptanone system at 40kPa. Only pure component data included in parameter regression.

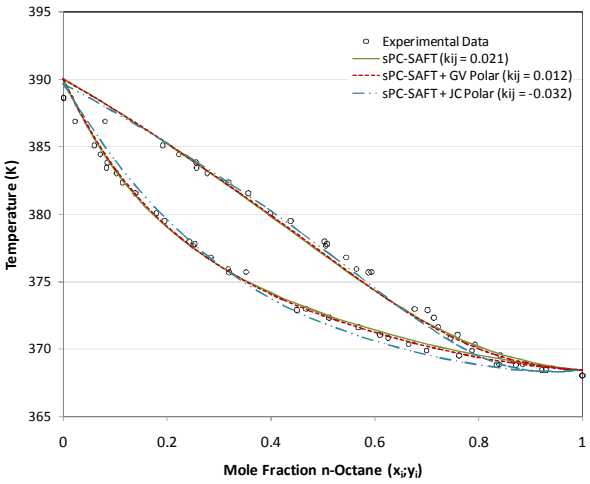

Figure F. 34: Correlations for isobaric VLE in n-octane/3-heptanone system at 40kPa. Only pure component data included in parameter regression.

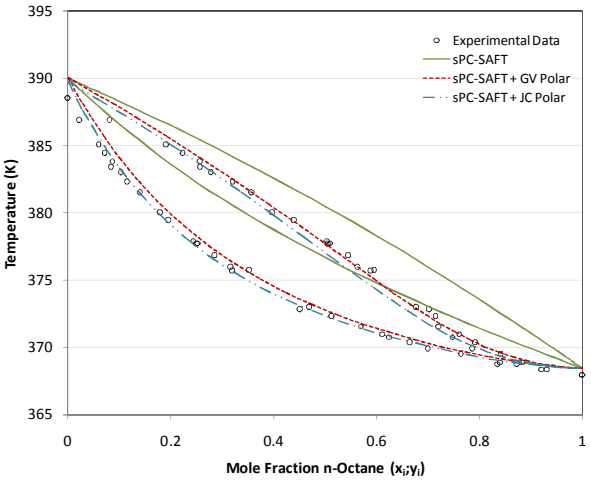

Figure F. 35: Pure predictions for isobaric VLE in n-octane/3-heptanone system at 40kPa. Correlation for polar parameter (x_p/n_p) used with pure component data in parameter regression.

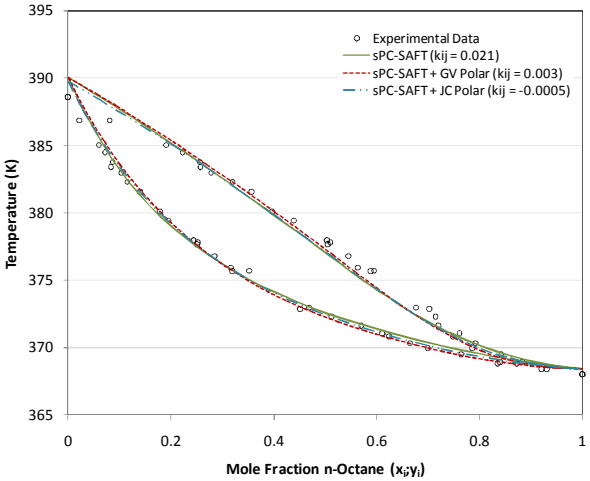

Figure F. 36: correlations for isobaric VLE in n-octane/3-heptanone system at 40kPa. Correlation for polar parameter (x_p/n_p) used with pure component data in parameter regression.

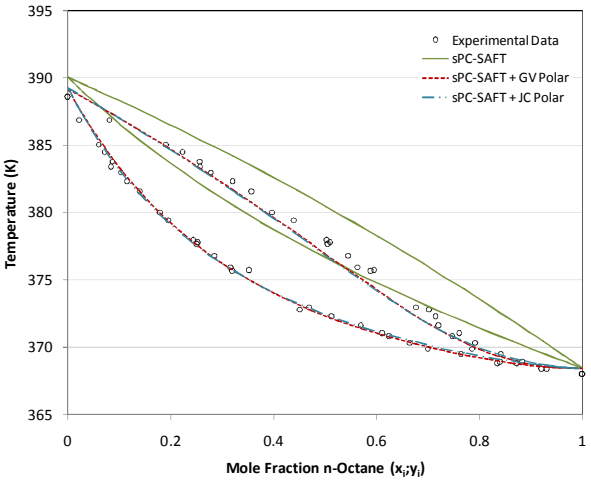

Figure F. 37: Pure predictions for isobaric VLE in n-octane/3-heptanone system at 40kPa. n-Octane/3-heptanone VLE data used with pure component data in parameter regression.

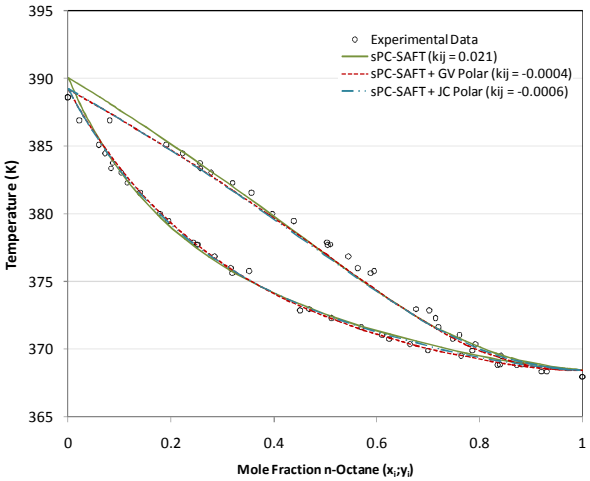

Figure F. 38: Correlations for isobaric VLE in n-octane/3-heptanone system at 40kPa. n-Octane/3-heptanone VLE data used with pure component data in parameter regression.

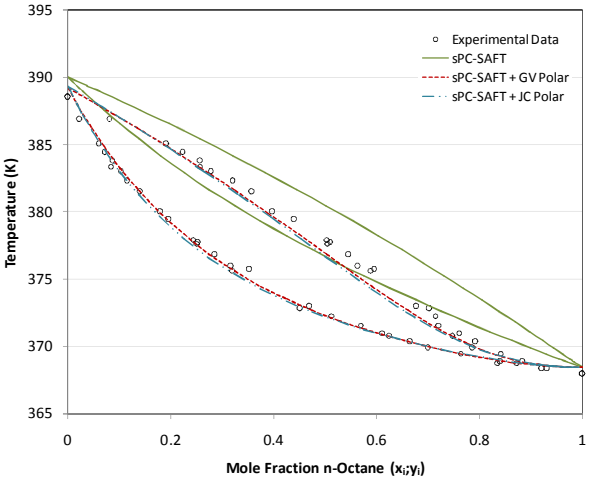

Figure F. 39: Pure predictions for isobaric VLE in n-octane/3-heptanone system at 40kPa. n-Nonane/3-heptanone VLE data used with pure component data in parameter regression.

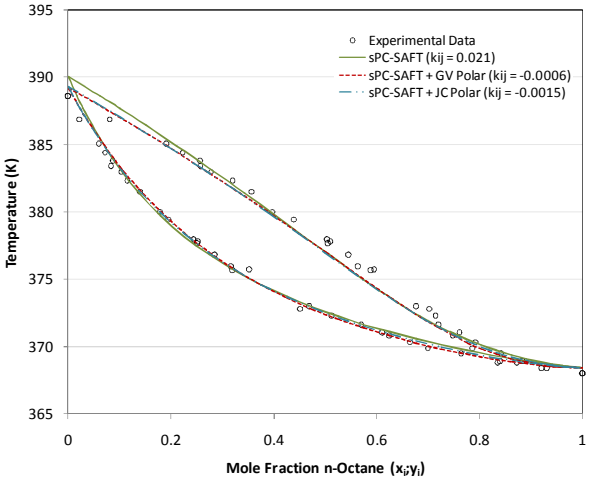

Figure F. 40: Correlations for isobaric VLE in n-octane/3-heptanone system at 40kPa. n-Nonane/3-heptanone VLE data used with pure component data in parameter regression.

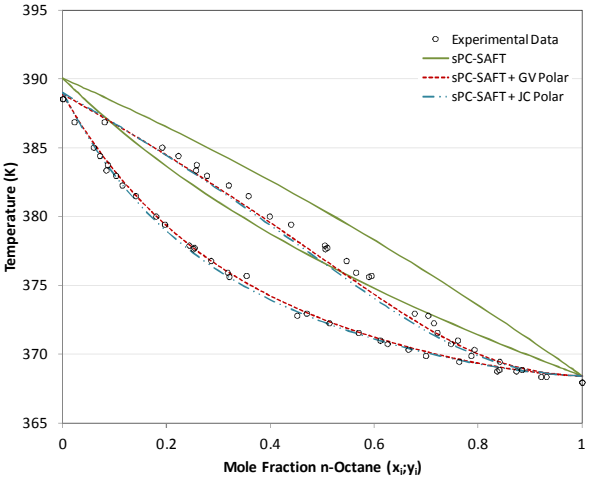

Figure F. 41: Pure predictions for isobaric VLE in n-octane/3-heptanone system at 40kPa. n-Decane/3-heptanone VLE data used with pure component data in parameter regression.

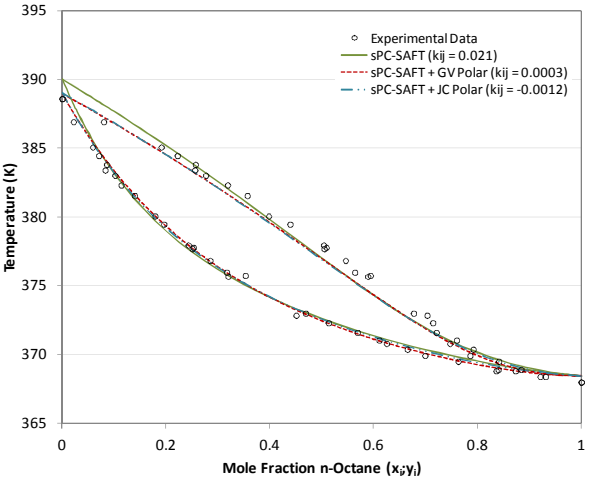

Figure F. 42: Correlations for isobaric VLE in n-octane/3-heptanone system at 40kPa. n-Decane/3-heptanone VLE data used with pure component data in parameter regression.

n-Nonane/3-Heptanone

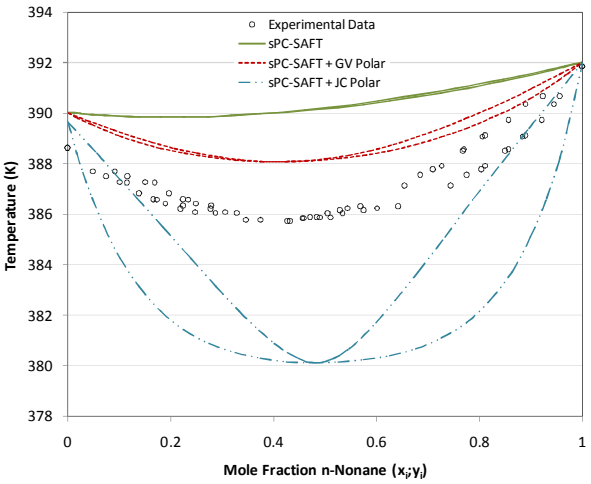

Figure F. 43: Pure predictions for isobaric VLE in n-nonane/3-heptanone system at 40kPa. Only pure component data included in parameter regression.

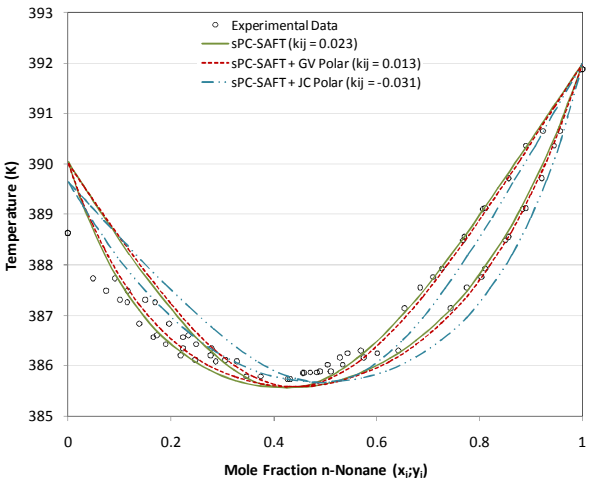

Figure F. 44: Correlations for isobaric VLE in n-nonane/3-heptanone system at 40kPa. Only pure component data included in parameter regression.

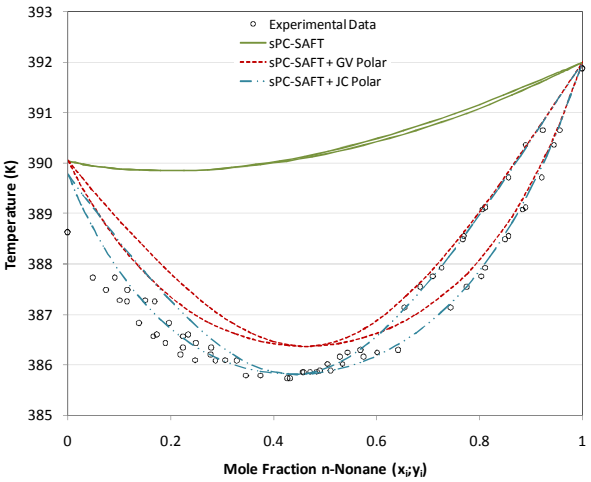

Figure F 45: Pure predictions for isobaric VLE in n-nonane/3-heptanone system at 40kPa. Correlation for polar parameter (x_p/n_p) used with pure component data in parameter regression.

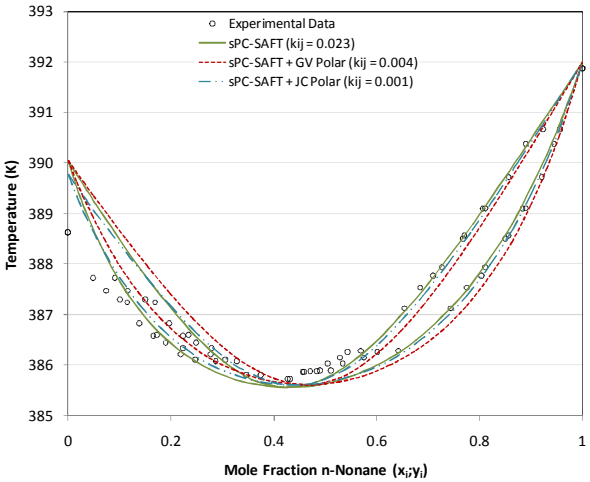

Figure F. 46: Correlations for isobaric VLE in n-nonane/3-heptanone system at 40kPa. Correlation for polar parameter (x_p/n_p) used with pure component data in parameter regression.

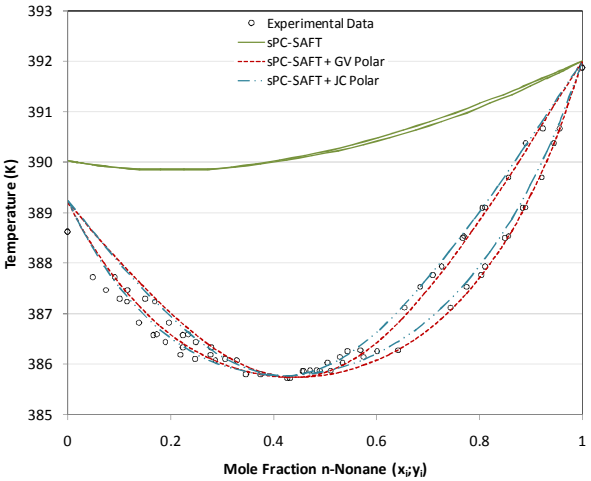

Figure F. 47: Pure predictions for isobaric VLE in n-nonane/3-heptanone system at 40kPa. n-Octane/3-heptanone VLE data used with pure component data in parameter regression.

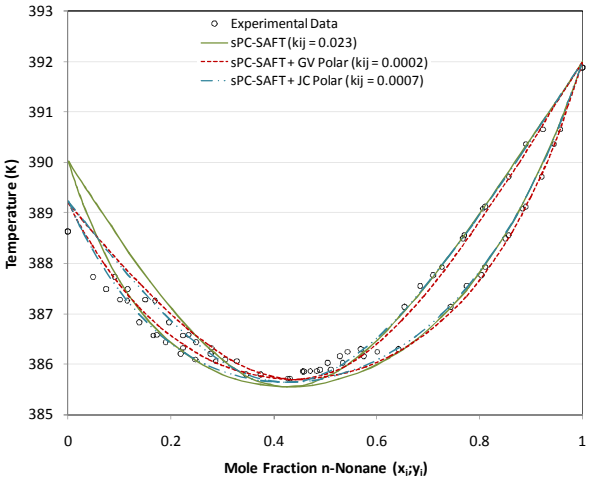

Figure F. 48: Correlations for isobaric VLE in n-nonane/3-heptanone system at 40kPa. n-Octane/3-heptanone VLE data used with pure component data in parameter regression.

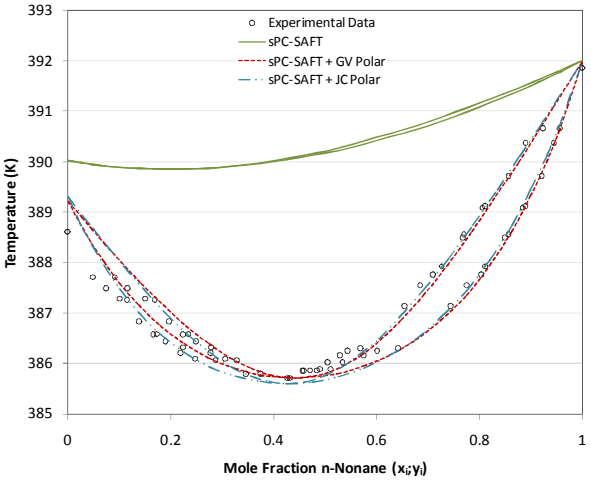

Figure F. 49: Pure predictions for isobaric VLE in n-nonane/3-heptanone system at 40kPa. n-Nonane/3-heptanone VLE data used with pure component data in parameter regression.

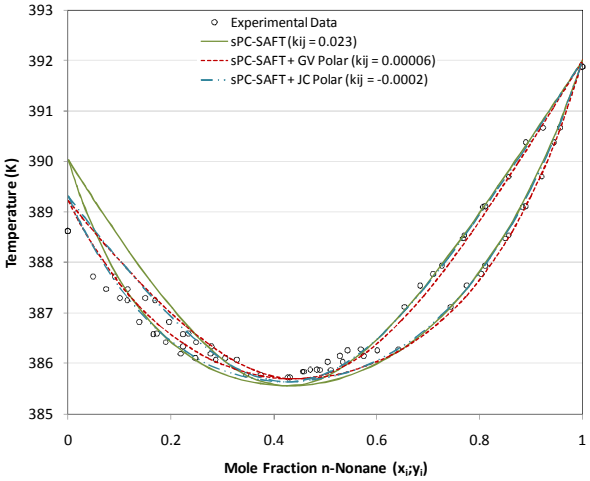

Figure F. 50: Correlations for isobaric VLE in n-nonane/3-heptanone system at 40kPa. n-Nonane/3-heptanone VLE data used with pure component data in parameter regression.

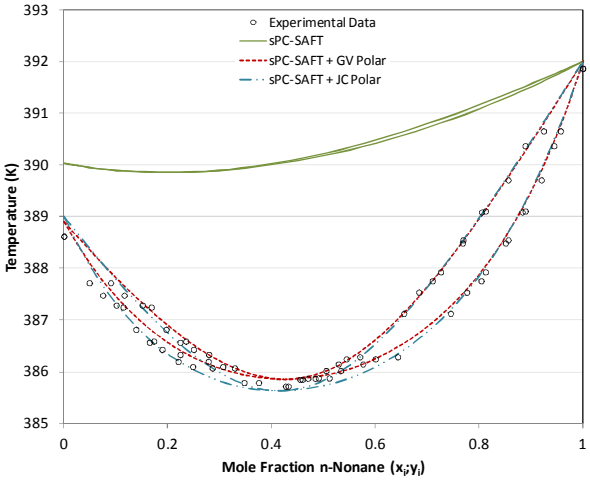

Figure F. 51: Pure predictions for isobaric VLE in n-nonane/3-heptanone system at 40kPa. n-Decane/3-heptanone VLE data used with pure component data in parameter regression.

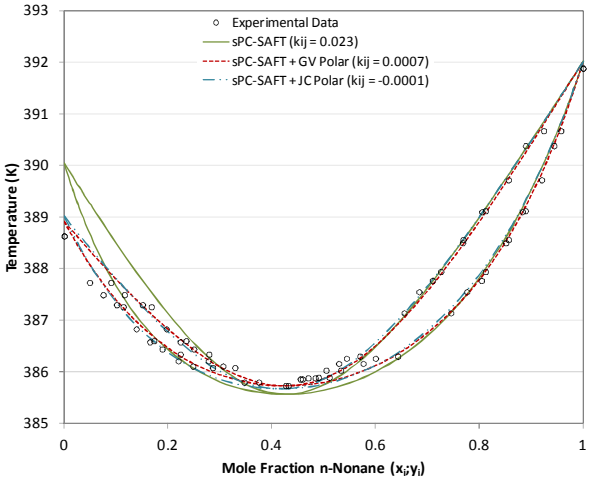

Figure F. 52: Correlations for isobaric VLE in n-nonane/3-heptanone system at 40kPa. n-Decane/3-heptanone VLE data used with pure component data in parameter regression.

n-Decane/3-Heptanone

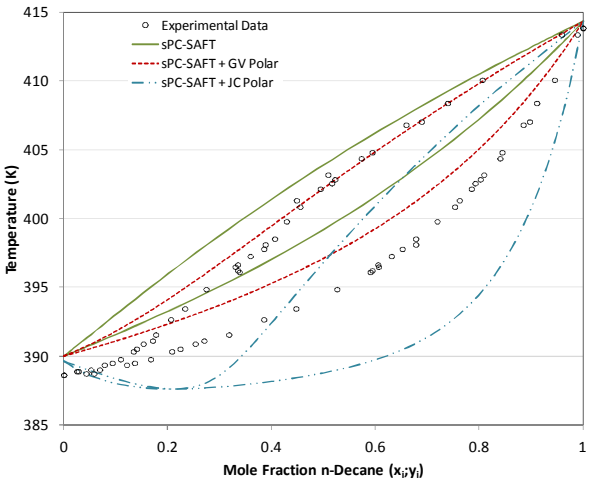

Figure F. 53: Pure predictions for isobaric VLE in n-decane/3-heptanone system at 40kPa. Only pure component data included in parameter regression.

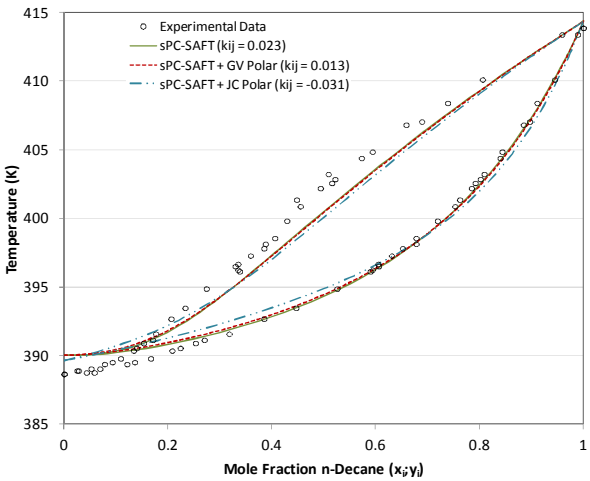

Figure F. 54: Correlations for isobaric VLE in n-decane/3-heptanone system at 40kPa. Only pure component data included in parameter regression.

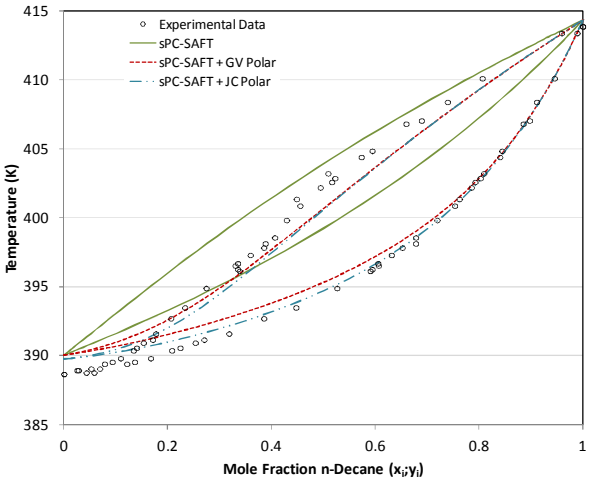

Figure F. 55: Pure predictions for isobaric VLE in n-decane/3-heptanone system at 40kPa. Correlation for polar parameter (x_p/n_p) used with pure component data in parameter regression.

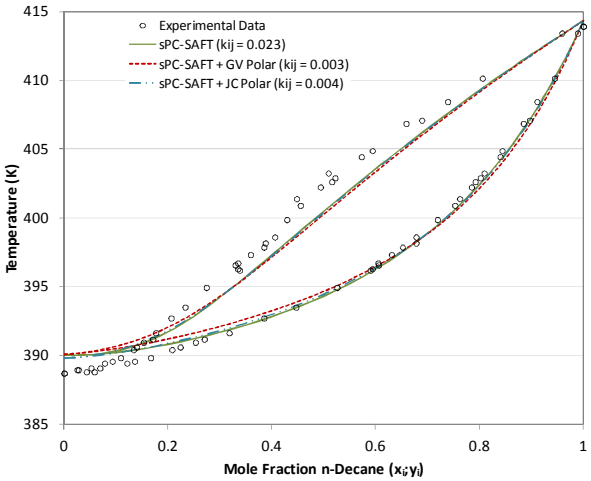

Figure F. 56: Correlations for isobaric VLE in n-decane/3-heptanone system at 40kPa. Correlation for polar parameter (x_p/n_p) used with pure component data in parameter regression.

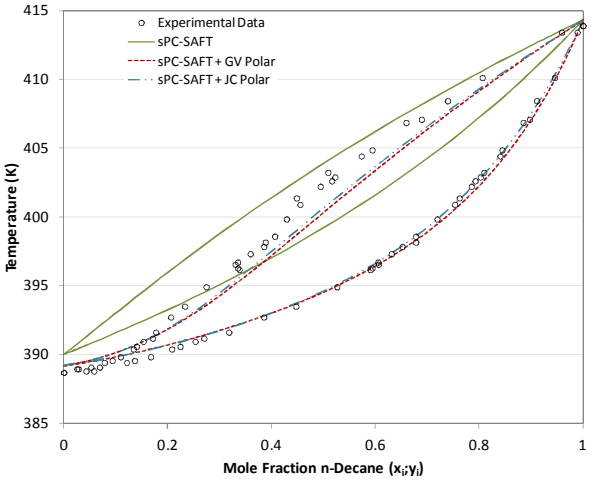

Figure F. 57: Pure predictions for isobaric VLE in n-decane/3-heptanone system at 40kPa. n-Octane/3-heptanone VLE data used with pure component data in parameter regression.

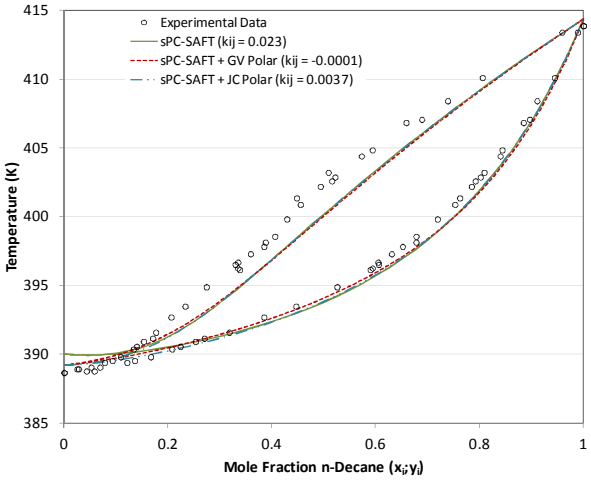

Figure F. 58: Correlations for isobaric VLE in n-decane/3-heptanone system at 40kPa. n-Octane/3-heptanone VLE data used with pure component data in parameter regression.

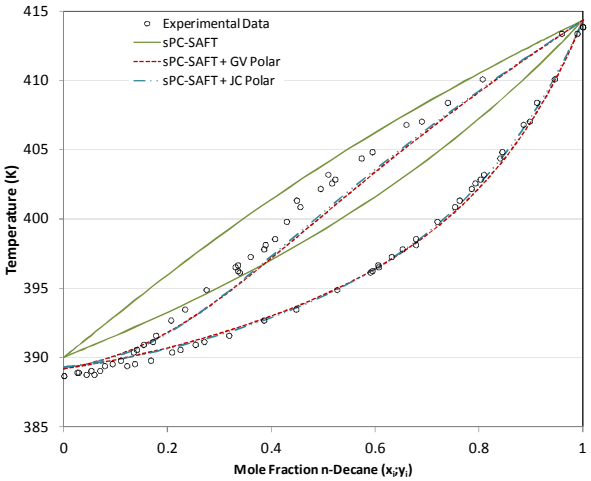

Figure F. 59: Pure predictions for isobaric VLE in n-decane/3-heptanone system at 40kPa. n-Nonane/3-heptanone VLE data used with pure component data in parameter regression.

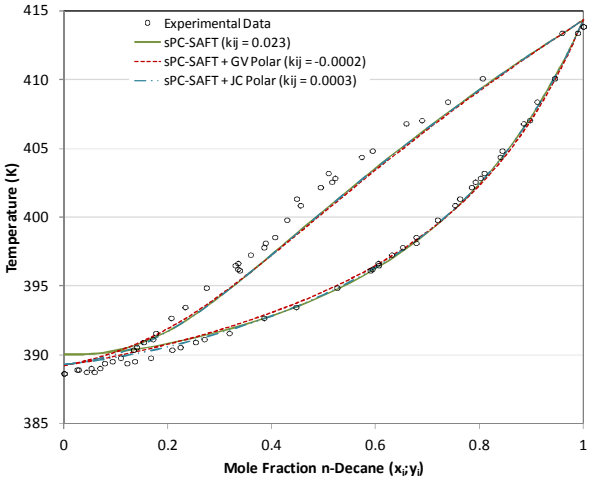

Figure F. 60: Correlations for isobaric VLE in n-decane/3-heptanone system at 40kPa. n-Nonane/3-heptanone VLE data used with pure component data in parameter regression.

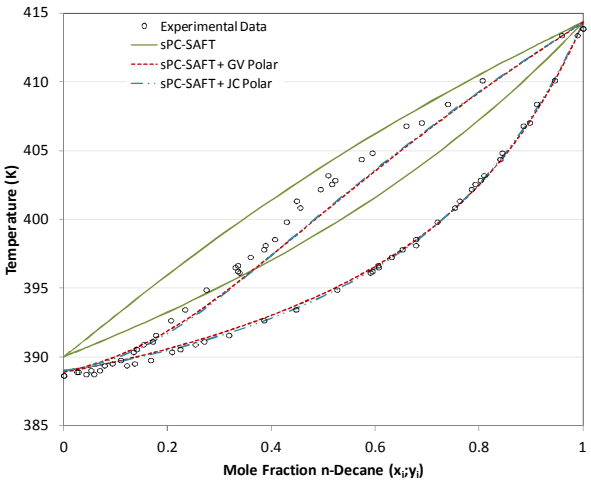

Figure F. 61: Pure predictions for isobaric VLE in n-decane/3-heptanone system at 40kPa. n-Decane/3-heptanone VLE data used with pure component data in parameter regression.

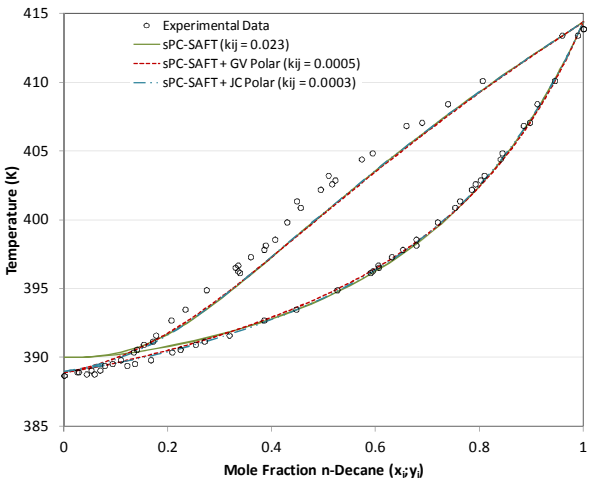

Figure F. 62: Correlations for isobaric VLE in n-decane/3-heptanone system at 40kPa. n-Decane/3-heptanone VLE data used with pure component data in parameter regression.

n-Octane/4-Heptanone

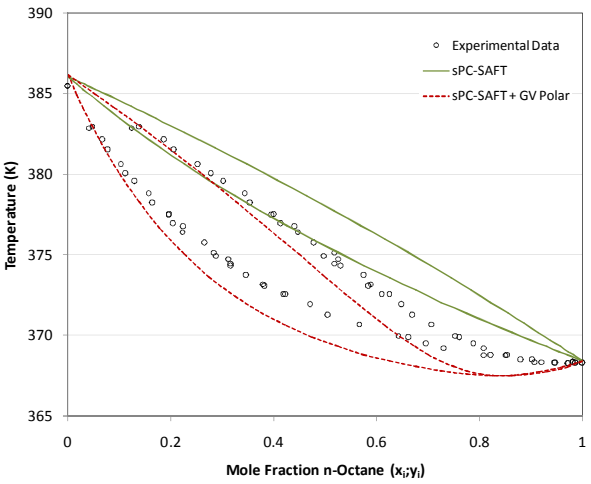

Figure F. 63: Pure predictions for isobaric VLE in n-octane/4-heptanone system at 40kPa. Only pure component data included in parameter regression. Parameters for 4-heptanone in sPC-SAFT + JC polar could not be determined, hence this model's omission.

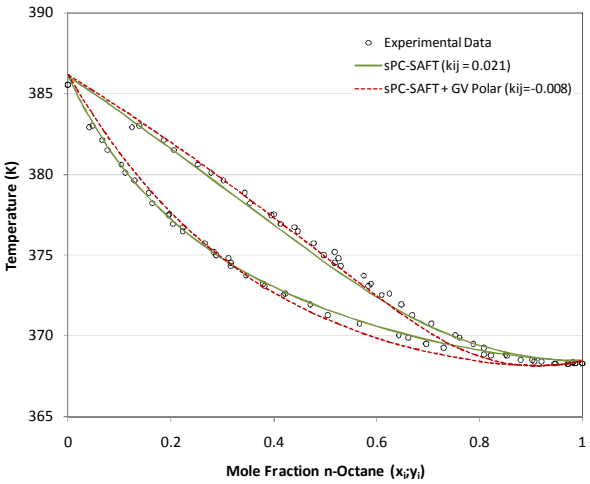

Figure F. 64: Correlations for isobaric VLE in n-octane/4-heptanone system at 40kPa. Only pure component data included in parameter regression. Parameters for 4-heptanone in sPC-SAFT + JC polar could not be determined, hence this model's omission.

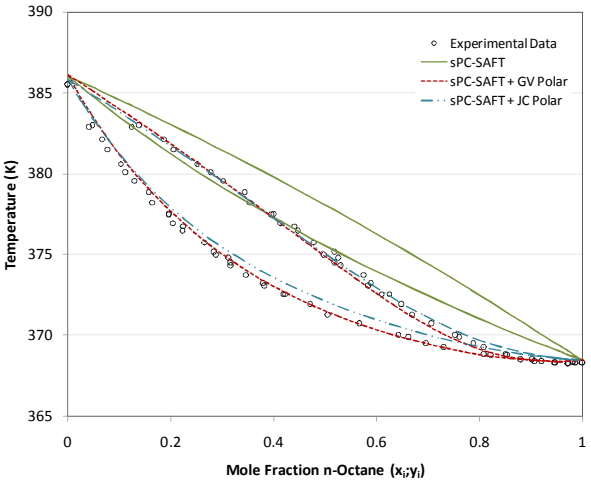

Figure F. 65: Pure predictions for isobaric VLE in n-octane/4-heptanone system at 40kPa. Correlation for polar parameter (x_p/n_p) used with pure component data in parameter regression.

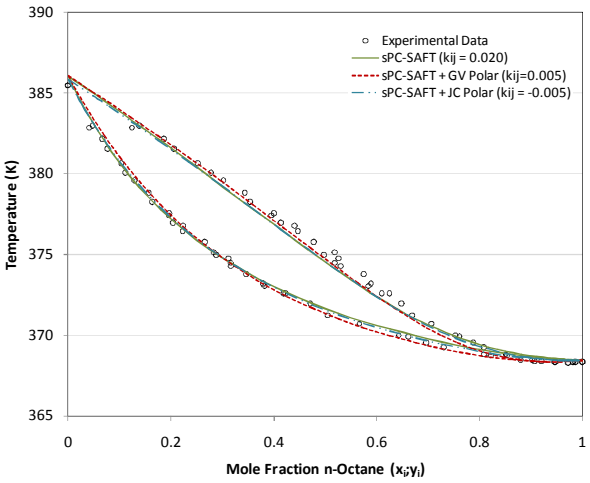

Figure F. 66: Correlations for isobaric VLE in n-octane/4-heptanone system at 40kPa. Correlation for polar parameter (x_p/n_p) used with pure component data in parameter regression.

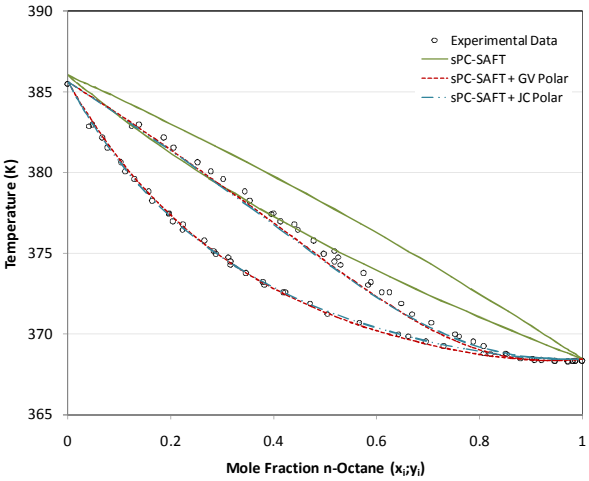

Figure F. 67: Pure predictions for isobaric VLE in n-octane/4-heptanone system at 40kPa. n-Octane/4-heptanone VLE data used with pure component data in parameter regression.

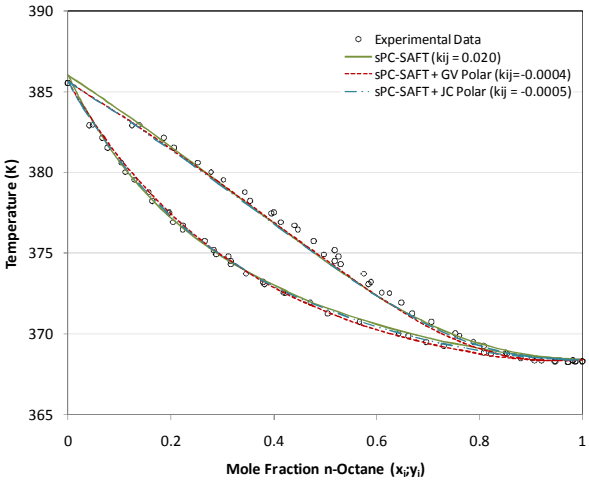

Figure F. 68: Correlations for isobaric VLE in n-octane/4-heptanone system at 40kPa. n-Octane/4-heptanone VLE data used with pure component data in parameter regression.

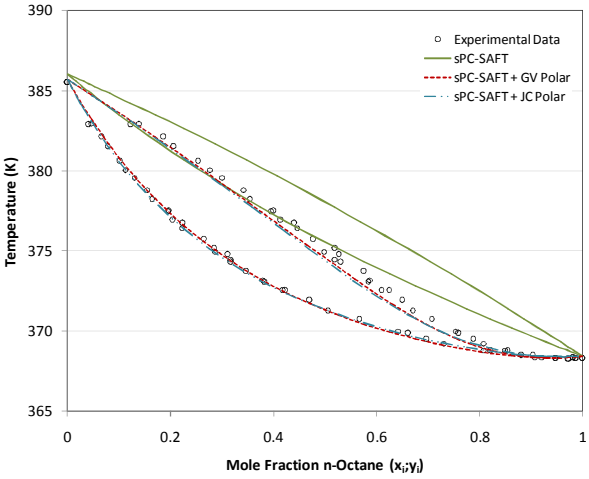

Figure F. 69: Pure predictions for isobaric VLE in n-octane/4-heptanone system at 40kPa. n-Nonane/4-heptanone VLE data used with pure component data in parameter regression.

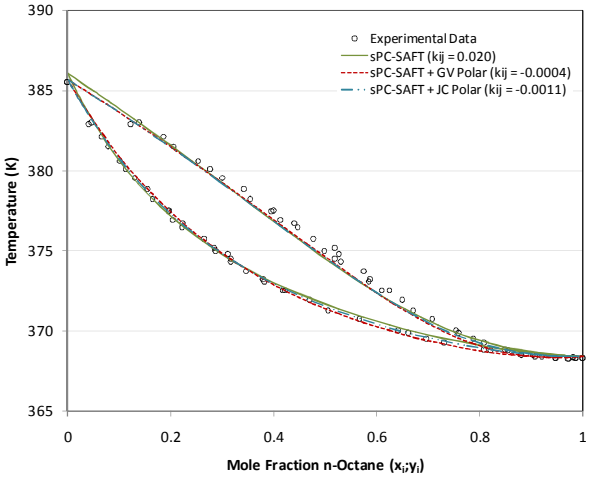

Figure F. 70: Correlations for isobaric VLE in n-octane/4-heptanone system at 40kPa. n-Nonane/4-heptanone VLE data used with pure component data in parameter regression.

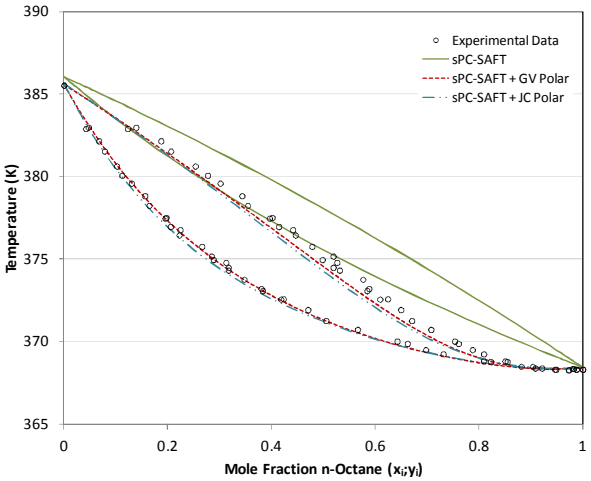

Figure F. 71: Pure predictions for isobaric VLE in n-octane/4-heptanone system at 40kPa. n-Decane/4-heptanone VLE data used with pure component data in parameter regression.

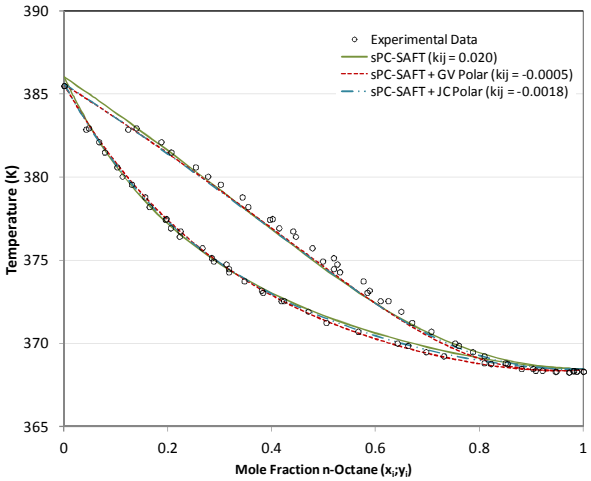

Figure F. 72: Correlations for isobaric VLE in n-octane/4-heptanone system at 40kPa. n-Decane/4-heptanone VLE data used with pure component data in parameter regression.

.

n-Nonane/4-Heptanone

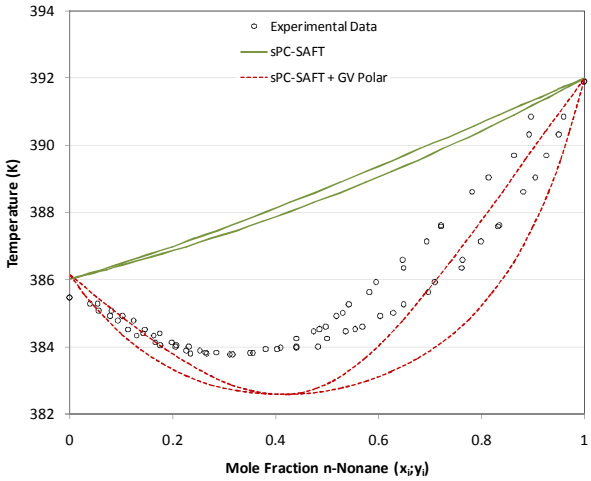

Figure F. 73: Pure predictions for isobaric VLE in n-nonane/4-heptanone system at 40kPa. Only pure component data included in parameter regression. Parameters for 4-heptanone in sPC-SAFT + JC polar could not be determined, hence this model's omission.

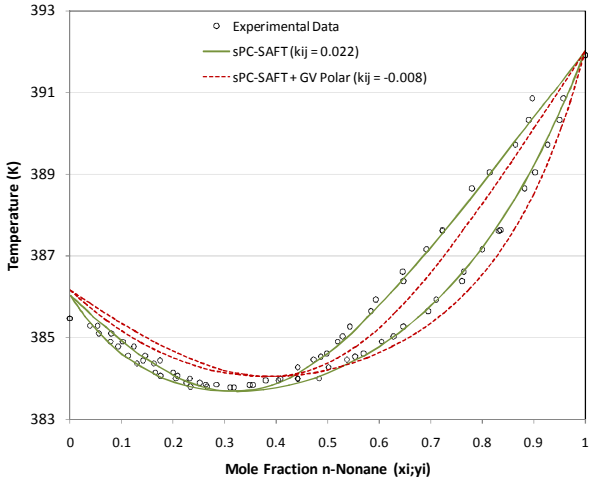

Figure F. 74: Correlations for isobaric VLE in n-nonane/4-heptanone system at 40kPa. Only pure component data included in parameter regression. Parameters for 4-heptanone in sPC-SAFT + JC polar could not be determined, hence this model's omission.

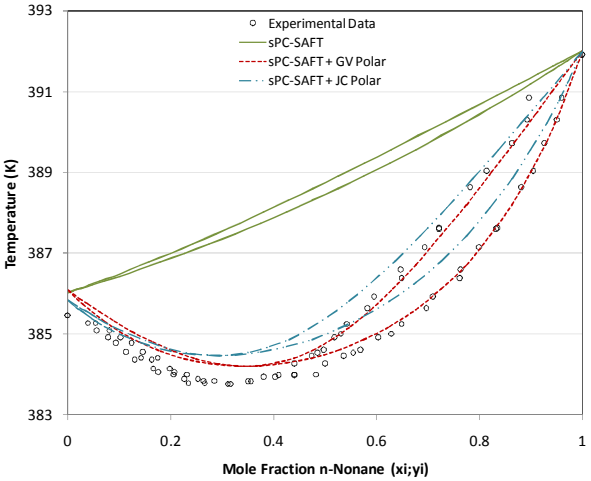

Figure F. 75: Pure predictions for isobaric VLE in n-nonane/4-heptanone system at 40kPa. Correlation for polar parameter (x_p/n_p) used with pure component data in parameter regression.

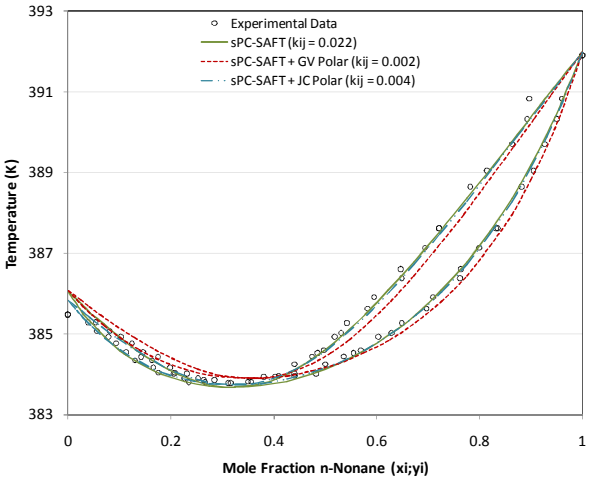

Figure F. 76: Correlations for isobaric VLE in n-nonane/4-heptanone system at 40kPa. Correlation for polar parameter (x_p/n_p) used with pure component data in parameter regression.

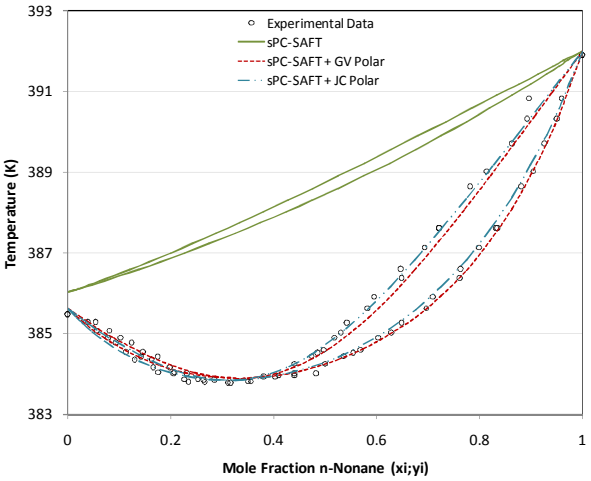

Figure F. 77: Pure predictions for isobaric VLE in n-nonane/4-heptanone system at 40kPa. n-Octane/4-heptanone VLE data used with pure component data in parameter regression.

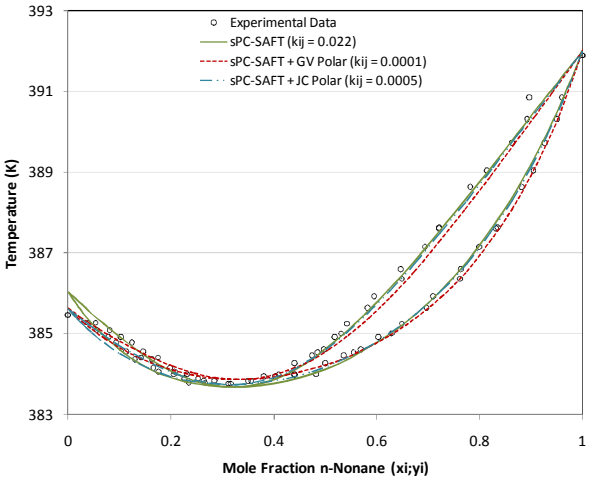

Figure F. 78: Correlations for isobaric VLE in n-nonane/4-heptanone system at 40kPa. n-Octane/4-heptanone VLE data used with pure component data in parameter regression.

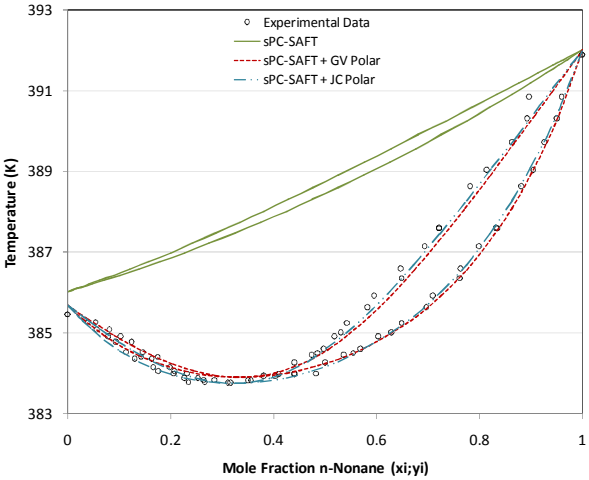

Figure F. 79: Pure predictions for isobaric VLE in n-nonane/4-heptanone system at 40kPa. n-Nonane/4-heptanone VLE data used with pure component data in parameter regression.

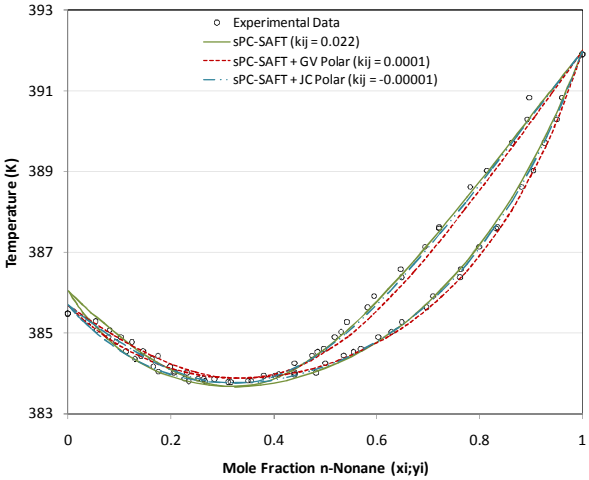

Figure F. 80: Correlations for isobaric VLE in n-nonane/4-heptanone system at 40kPa. n-Nonane/4-heptanone VLE data used with pure component data in parameter regression.

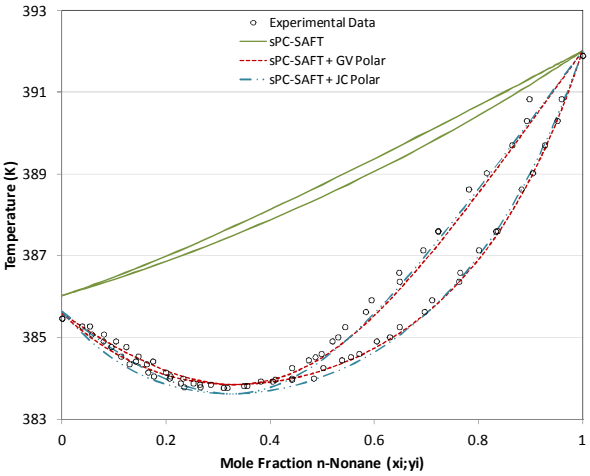

Figure F. 81: Pure predictions for isobaric VLE in n-nonane/4-heptanone system at 40kPa. n-Decane/4-heptanone VLE data used with pure component data in parameter regression.

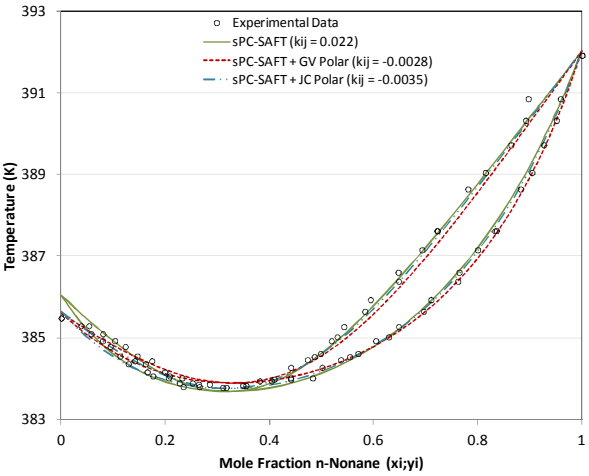

Figure F. 82: Correlations for isobaric VLE in n-nonane/4-heptanone system at 40kPa. n-Decane/4-heptanone VLE data used with pure component data in parameter regression.

n-Decane/4-Heptanone

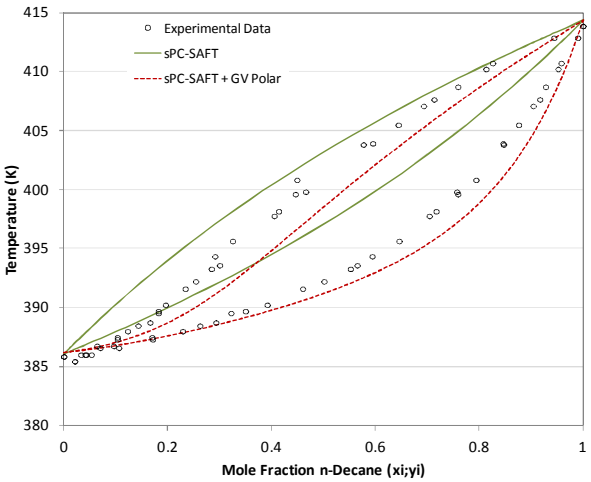

Figure F. 83: Pure predictions for isobaric VLE in n-decane/4-heptanone system at 40kPa. Only pure component data included in parameter regression. Parameters for 4-heptanone in sPC-SAFT + JC polar could not be determined, hence this model's omission.

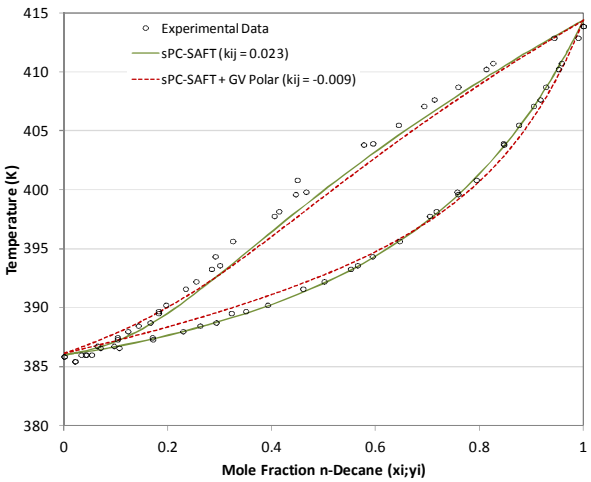

Figure F. 84: Correlations for isobaric VLE in n-decane/4-heptanone system at 40kPa. Only pure component data included in parameter regression. Parameters for 4-heptanone in sPC-SAFT + JC polar could not be determined, hence this model's omission.

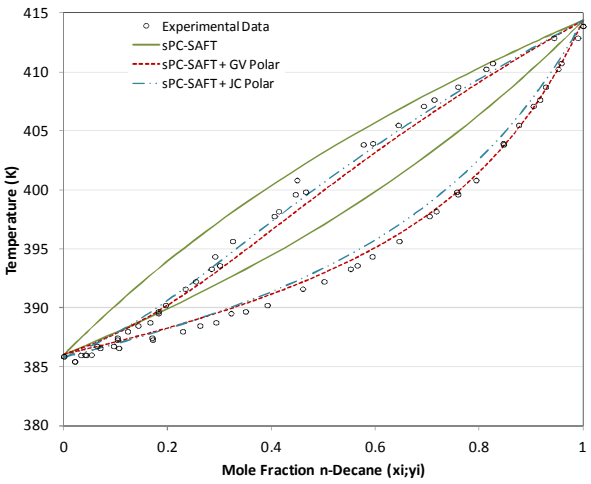

Figure F. 85: Pure predictions for isobaric VLE in n-decane/4-heptanone system at 40kPa. Correlation for polar parameter (x_p/n_p) used with pure component data in parameter regression.

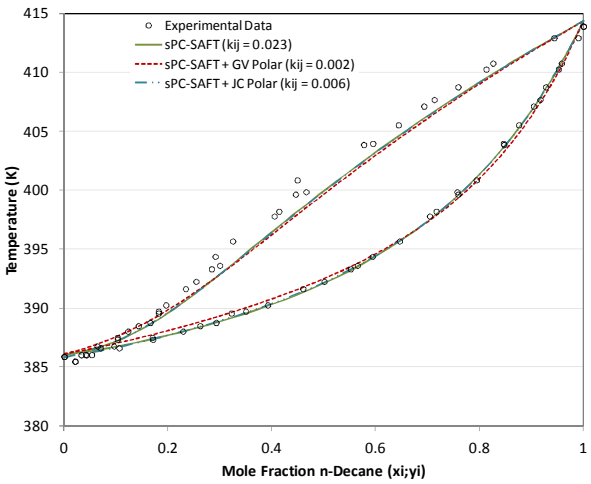

Figure F. 86: Correlations for isobaric VLE in n-decane/4-heptanone system at 40kPa. Correlation for polar parameter (x_p/n_p) used with pure component data in parameter regression.

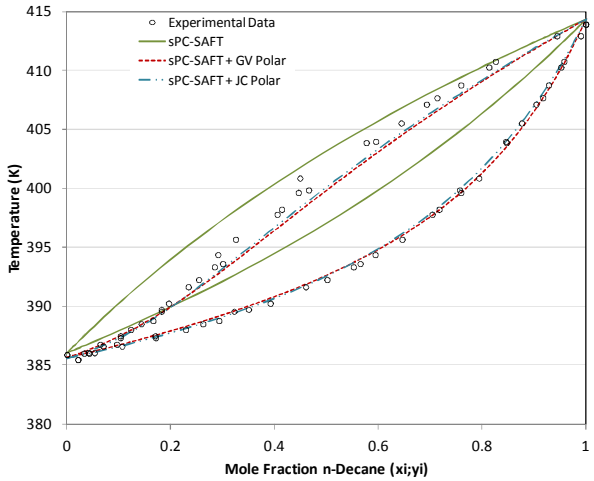

Figure F. 87: Pure predictions for isobaric VLE in n-decane/4-heptanone system at 40kPa. n-Octane/4-heptanone VLE data used with pure component data in parameter regression.

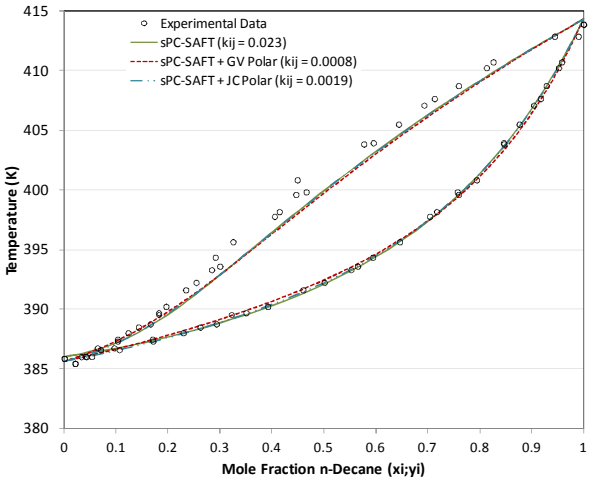

Figure F. 88: Correlations for isobaric VLE in n-decane/4-heptanone system at 40kPa. n-Octane/4-heptanone VLE data used with pure component data in parameter regression.

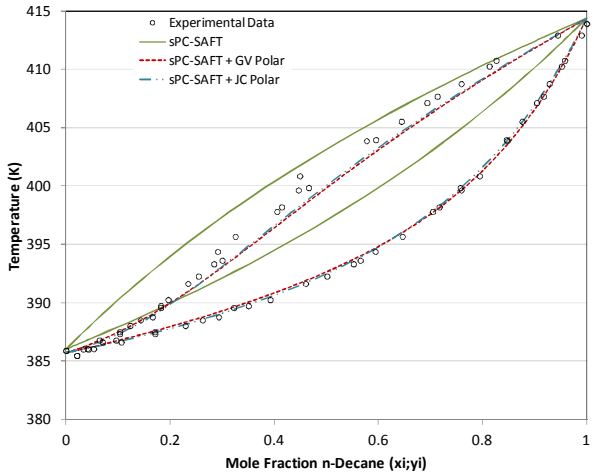

Figure F. 89: Pure predictions for isobaric VLE in n-decane/4-heptanone system at 40kPa. n-Nonane/4-heptanone VLE data used with pure component data in parameter regression.

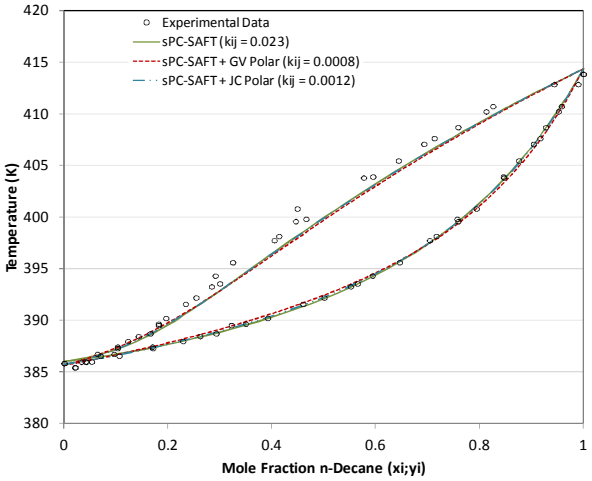

Figure F. 90: Correlations for isobaric VLE in n-decane/4-heptanone system at 40kPa. n-Nonane/4-heptanone VLE data used with pure component data in parameter regression.

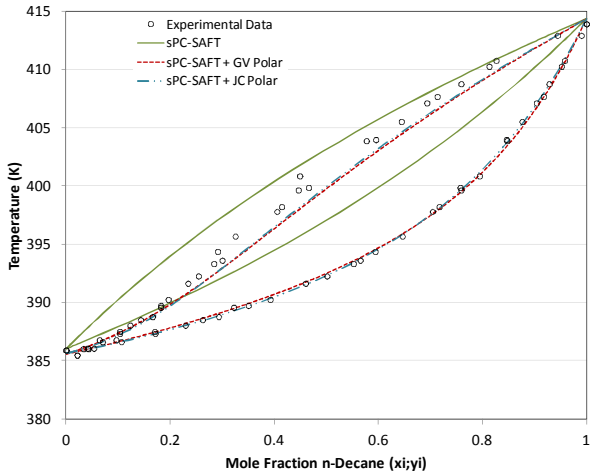

Figure F. 91: Pure predictions for isobaric VLE in n-decane/4-heptanone system at 40kPa. n-Decane/4-heptanone VLE data used with pure component data in parameter regression.

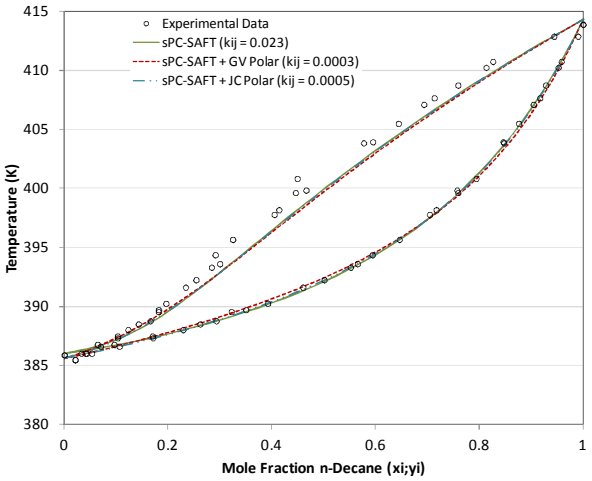

Figure F. 92: Correlations for isobaric VLE in n-decane/4-heptanone system at 40kPa. n-Decane/4-heptanone VLE data used with pure component data in parameter regression.

n-Hexane/4-Heptanone

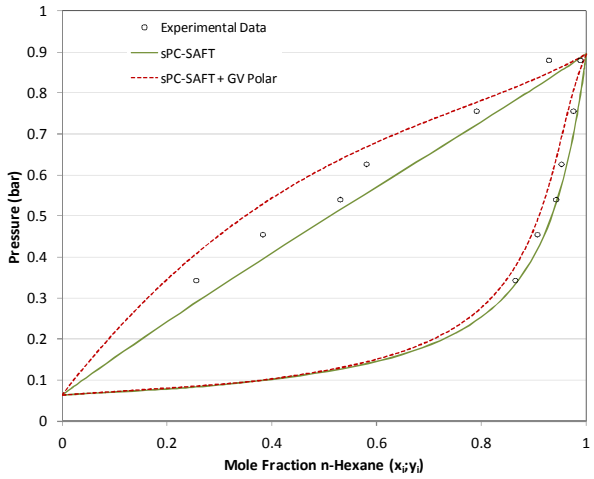

Figure F. 93: Pure predictions for isothermal VLE in n-hexane/4-heptanone system at 338.15 K. Only pure component data included in parameter regression. Parameters for 4-heptanone in sPC-SAFT + JC polar could not be determined, hence this model's omission.

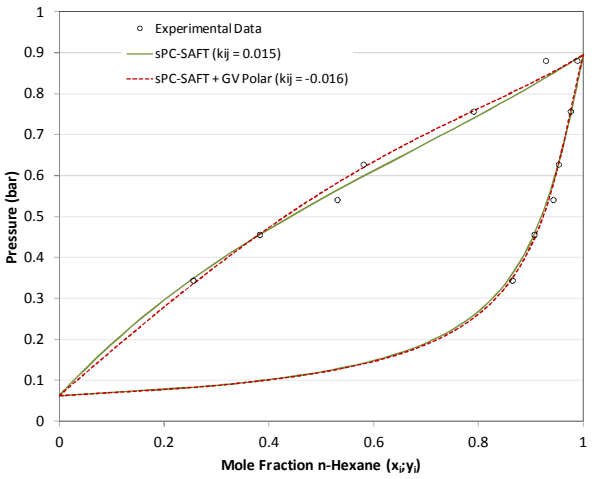

Figure F. 94: Correlations for isothermal VLE in n-hexane/4-heptanone system at 338.15 K. Only pure component data included in parameter regression. Parameters for 4-heptanone in sPC-SAFT + JC polar could not be determined, hence this model's omission.

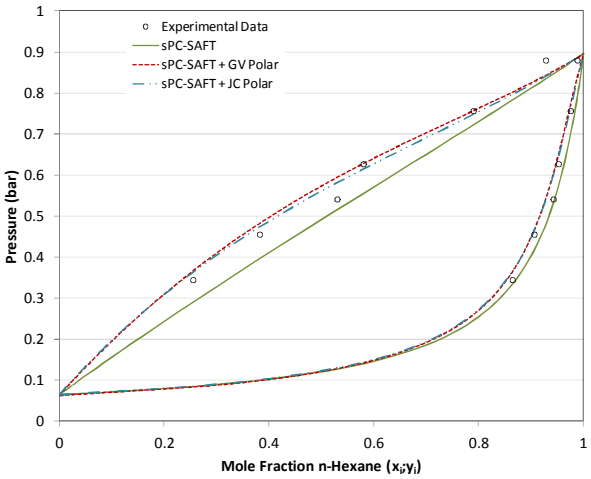

Figure F. 95: Pure predictions for isothermal VLE in n-hexane/4-heptanone system at 338.15 K. Correlation for polar parameter (x_p/n_p) used with pure component data in parameter regression.

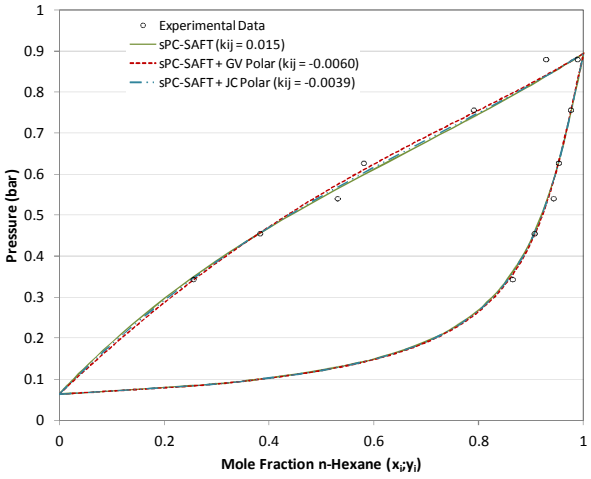

Figure F. 96: Correlations for isothermal VLE in n-hexane/4-heptanone system at 338.15 K. Correlation for polar parameter (x_p/n_p) used with pure component data in parameter regression.

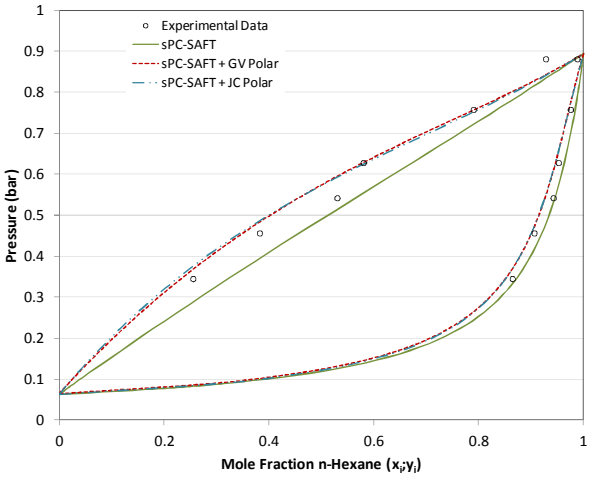

Figure F. 97: Pure predictions for isothermal VLE in n-hexane/4-heptanone system at 338.15 K. n-Octane/4-heptanone VLE data used with pure component data in parameter regression.

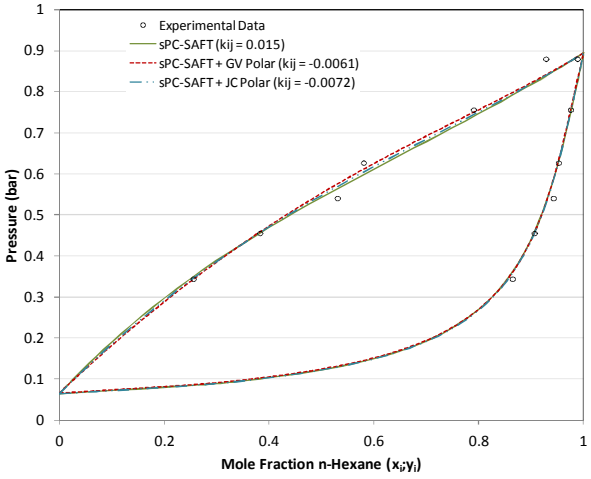

Figure F. 98: Correlations for isothermal VLE in n-hexane/4-heptanone system at 338.15 K. n-Octane/4-heptanone VLE data used with pure component data in parameter regression.

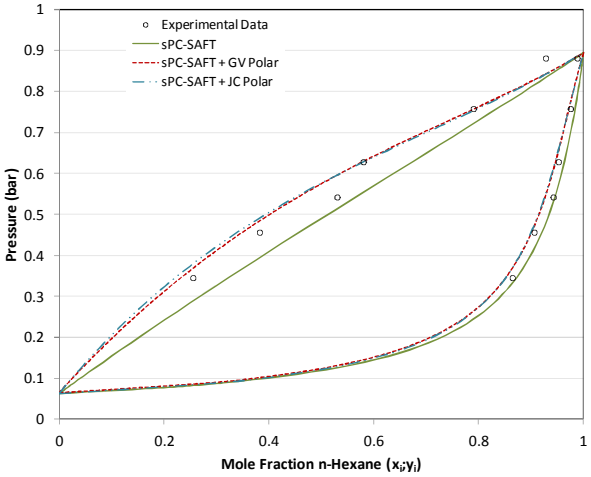

Figure F. 99: Pure predictions for isothermal VLE in n-hexane/4-heptanone system at 338.15 K. n-Nonane/4-heptanone VLE data used with pure component data in parameter regression.

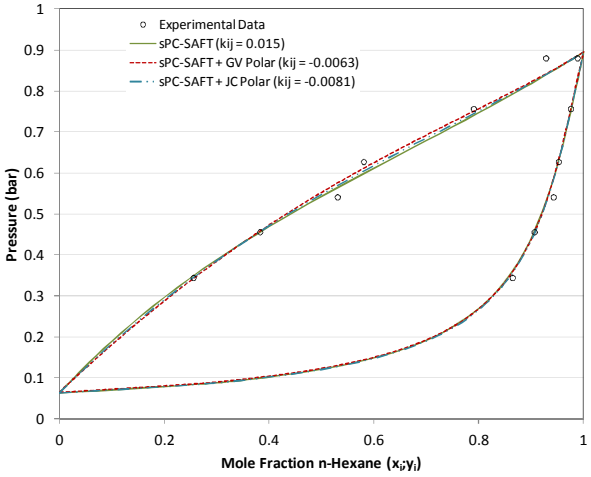

Figure F. 100: Correlations for isothermal VLE in n-hexane/4-heptanone system at 338.15 K. n-Nonane/4-heptanone VLE data used with pure component data in parameter regression.

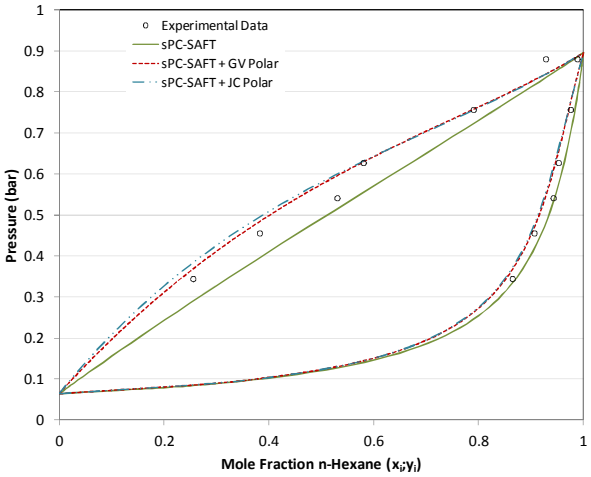

Figure F. 101: Pure predictions for isothermal VLE in n-hexane/4-heptanone system at 338.15 K. n-Decane/4-heptanone VLE data used with pure component data in parameter regression.

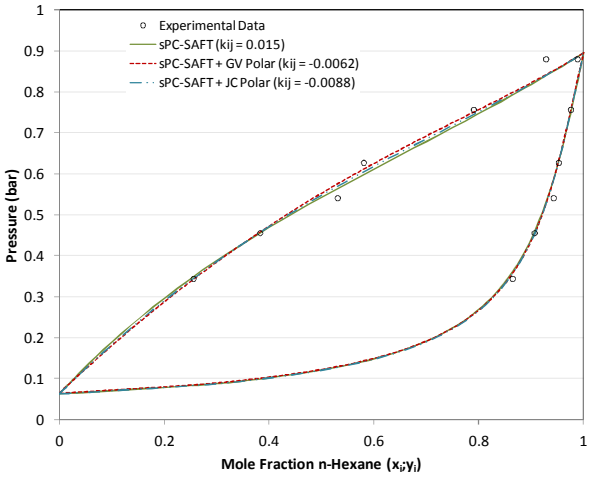

Figure F. 102: Correlations for isothermal VLE in n-hexane/4-heptanone system at 338.15 K. n-Decane/4-heptanone VLE data used with pure component data in parameter regression.